NASA Contractor Report 3738

Control Definition Study for Advanced Vehicles

Maris Lapins, R. Paul Martorella, Robert W. Klein, Rudolph C. Meyer, and Michael J. Sturm

CONTRACT NAS1-16636
NOVEMBER 1983

25th Anniversary
1958-1983

NASA

NASA Contractor Report 3738

Control Definition Study for Advanced Vehicles

Maris Lapins, R. Paul Martorella, Robert W. Klein, Rudolph C. Meyer, and Michael J. Sturm
Grumman Aerospace Corporation
Bethpage, New York

Prepared for
Langley Research Center
under Contract NAS1-16636

National Aeronautics
and Space Administration

Scientific and Technical
Information Branch

1983

CONTENTS

CONTENTS (contd)

ILLUSTRATIONS

ILLUSTRATIONS (contd)

ILLUSTRATIONS (contd)

ILLUSTRATIONS (contd)

ILLUSTRATIONS (contd)

TABLES

CONTROL DEFINITION STUDY FOR ADVANCED VEHICLES

Maris Lapins, R. Paul Martorella, Robert W. Klein,
Rudolph C. Meyer, and Michael J. Sturm
Grumman Aerospace Corporation

1 - SUMMARY

The results of a generic investigation into control requirements for a canard-configured, Relaxed Static Stability Supersonic Strike Fighter Aircraft at high angle-of-attack are reported. The study aircraft is the Grumman Aerospace Corporation Supersonic Tactical Aircraft Configuration. Two longitudinal control laws are developed: "G" command and α command systems. The lateral/directional laws are designed to roll the aircraft about the stability axes and to provide direct rudder command. Model-following algorithms, intended to ensure desired handling qualities, are developed for a full-authority digital fly-by-wire control system. These algorithms permit control system gain variations with flight condition and changes in plant dynamics.

Part of this study was devoted to determining canard actuator rate requirements for this class of aircraft. Simple linear analytical expressions for maximum canard rates/deflections are verified with empirical data acquired in nonlinear engineering simulations at low angle-of-attack.

A major emphasis of this investigation was development of command limiters that prevent aircraft departure. Particular attention was given to suppressing inertia and kinematic coupling. Limiters were implemented in all three aircraft angular axes: $\Delta n_z/\alpha$ (α/α_c), roll rate, and rudder command limiters in the pitch, roll, and yaw axes, respectively. The resulting augmented aircraft was shown to be departure-resistant with realistic canard actuator rates (100 deg/sec). The control structure is amenable to a systematic piloted handling qualities simulation/evaluation.

This report also includes a summary discussion of the study aircraft design evolution, wind-tunnel test program, and simulation math model. Appendices are included detailing the simulation propulsion and aerodynamic math models and tabulated results of the canard deflection/rate requirement study. A separate appendix, by R. Paul Martorella, discusses the control law design philosophy. Conclusions regarding stability and control issues that impact the design of Relaxed Static Stability aircraft are presented.

2 - INTRODUCTION

The NASA Langley Research Center is engaged in a stall/spin research program on military airplane configurations. Two broad objectives of this research are to provide reliable predictions of the stall/spin characteristics of specific airplanes and to develop the technology required to improve the departure and spin resistance of current and future high-performance fighter designs. In accomplishing this latter objective, efforts in recent years have been focused on both the airframe design and the automatic control system design since, for currently evolving fighters, both play a critical role in determining the airplane high angle-of-attack characteristics. An important aspect of this research is the investigation of proposed advanced combat aircraft configurations early in the design cycle to provide timely prediction of expected stall/spin characteristics and identification of airframe and flight control system features which will provide satisfactory characteristics. Of particular interest currently are advanced canard configured fighter designs being developed to provide increased maneuverability and efficient supersonic cruise performance. Most of these designs incorporate moderate to high levels of Relaxed Static Stability (RSS) to achieve these performance objectives. As discussed in Ref. 1 and 2, use of RSS can significantly impact control system requirements during aggressive maneuvering at high angles-of-attack.

The Grumman Aerospace Corporation has developed a number of advanced fighter configurations that feature close-coupled canard aerodynamics and Relaxed Static Stability (RSS). These development programs have been carried out under both in-house and USAF funding. One of these designs, the Supersonic Tactical Aircraft Configuration (STAC), provides an excellent study vehicle for a generic investigation of the stability and control issues of RSS aircraft. This design also incorporates many of the technology elements that will be required to meet the demanding mission requirements of a future USAF Advanced Tactical Fighter (ATF). Extensive STAC wind-tunnel testing has provided a substantial performance, stability, and control data base, thus making possible a realistic generic investigation into the flight mechanics of this class of aircraft.

For these reasons, the NASA Langley Research Center contracted the Grumman Aerospace Corporation to conduct the "Control Definition Study for Advanced Vehicles" during May 1981 through April 1982 (Contract No. NAS1-16636). The contract called for an in-depth study of the high angle-of-attack flight mechanics of a canard-configured, supersonic fighter designed to operate at moderate to high levels of longitudinal RSS. The objectives of the study were to determine

- Control power requirements
- Control actuation rate requirements
- Control augmentation requirements
- Control system maneuver limiting functions
- RSS - unique aircraft handling qualities requirements for automatic control system concepts designed to meet realistic Air Combat Maneuvering (ACM) requirements.

The approach taken was to develop generic control laws that permit maximum maneuverability while protecting the aircraft from loss of control and spin entry. The primary objectives were to develop an understanding of the high angle-of-attack flight dynamics of the canard fighter design and establish design criteria for ensuring competent levels of ACM capability for this class of aircraft at the preliminary design stage.

This study was accomplished in three major phases: Longitudinal Control System Development, Lateral/Directional Control System Development, and Complete Control System Evaluation and Modification for ACM. The results of these phases are reported in Sections 7, 8 and 9, respectively. In addition, this report includes a summary discussion of the STAC design evolution (Section 4), STAC wind tunnel test program (Section 5), and simulation math model (Section 6).

From the outset of the study, it was clear that many of the issues regarding RSS aircraft flight mechanics can only be resolved by piloted simulation. This is, in part, due to a lack of control system design guidelines for this class of aircraft. The developed control laws were therefore designed to permit a systematic variation of critical control system parameters during a subsequent piloted handling qualities evaluation. The developed control laws do, nevertheless, represent a realistic RSS fighter control system that is adequate for the demands of Air Combat Maneuvering. Furthermore, sufficient insight was gained to provide design guidelines for future RSS aircraft development.

3 - NOMENCLATURE

3.1 SYMBOLS

A_y	lateral acceleration, positive along positive y body axis, g units
AR	aspect ratio, b^2/S_w
a_o, a_1, a_2	regression coefficients (Tables 7-1 and 7-2)
b	wing span, ft
C_D	drag coefficient, Drag/$\bar{q}S_w$
C_{D_i}	induced drag coefficient
C_{D_o}	zero-lift drag coefficient
C_L	lift coefficient, Lift/$\bar{q}S_w$
C_l	rolling moment coefficient, Rolling Moment/$\bar{q}S_w b$
C_m	pitching moment coefficient, Pitching Moment/$\bar{q}S_w \bar{c}_w$
C_N	normal force coefficient, Normal Force/$\bar{q}S_w$
C_n	yawing moment coefficient, Yawing Moment/$\bar{q}S_w b$
C_T	thrust coefficient, Thrust/$\bar{q}S_w$
C_Y	side force coefficient, Side Force/$\bar{q}S_w$
CAP	Control Anticipation Parameter (Equation 7.17)
CANTRM	canard bias (trim) signal (Section 7.3.2)
$\bar{c}_w$	wing mean aerodynamic chord, ft
F_x, F_y, F_z	total forces acting along x,y,z body axes, lb
G,G'	generalized gain
G	rudder-differential canard deflection command gearing ratio

G_{DCAI}	differential canard-aileron interconnect (crossfeed) control system gain
G_{LSRI}	lateral stick-rudder interconnect control system gain
g	acceleration due to gravity, ft/sec^2
h	altitude, ft
I_x, I_y, I_z	moments of inertia about x,y,z body axes, slug-ft^2
I_{xz}	product of inertia with respect to x and z axes, slug-ft^2
j	$\sqrt{-1}$
K	drag-due-to-lift factor
K_F, K_I, K_q, K_{n_z}	forward loop, integrator, pitch rate, normal acceleration longitudinal control system gains
K_P, K_{pI}	forward loop, integrator roll control system gains
K_r	yaw rate feedback directional control system gain
K_α	angle-of-attack feedback longitudinal control system gain
K_1, K_2	rudder/differential canard blending functions
L/D	lift-to-drag ratio
L,M,N	total moments acting about the x,y,z body axes, ft-lb
M	Mach number
m	aircraft mass, slugs
n_z	normal load factor at aircraft cg, g units
n_{z_c}	pilot commanded load factor, g units
n_{z_L}	limited load factor command, g units
$n_{z_{ss}}$	steady-state normal load factor, g units
n_{z_α}	change in load factor per unit change in angle-of-attack, g units

p,q,r	body axis angular rates about x,y,z axes, deg/sec (or rad/sec)
p_c	pilot commanded body axis roll rate, deg/sec
p_L	limited roll rate command, deg/sec
p_s, r_s	stability axis angular rates, deg/sec (or rad/sec)
$\bar{q}$	dynamic pressure, psf
R^2	multiple regression correlation coefficient
R_N	Reynolds Number
S_w	wing reference area, ft^2
S_c	canard reference area, ft^2
S_v	vertical tail(s) reference area, ft^2
s	LaPlace variable, sec^{-1}
t	time, sec
U	body x axis component of total velocity, ft/sec
u,v,w	perturbation components of aircraft velocity along x,y,z body axes, ft/sec
u_g, v_g, w_g	gust velocity components along x,y,z body axes, ft/sec
V, V_T, V_o	aircraft resultant (total) velocity, ft/sec or KEAS
W_1, W_2	cruise/maneuver wing designations
X,Y,Z	aerodynamic forces acting along body x,y,z axes, lbs
x,y,z	aircraft body axes
X_{cg}	aircraft center of gravity location along x axis
XSTAB	yaw rate feedback function (Figure 8-5)
α	angle-of-attack, deg
α_c	pilot commanded angle-of-attack, deg
α_{c_L}	limited angle-of-attack command, deg

β	angle-of-sideslip, deg
γ	flight path angle, deg
Δ	increment
$\Delta\delta_c$	differential canard deflection angle $\left(\delta_{c_l} - \delta_{c_r}\right)$, deg
δ_a	aileron deflection angle, positive for right roll, deg
$\delta_{a_l}, \delta_{a_r}$	port and starboard aileron deflection angle, deg
δ_c	symmetric canard deflection angle, positive for nose-up pitch, deg
$\delta_{c_i}, \delta_{c_r}$	peak canard deflection for motion initiation and recovery, deg
$\delta_{c_l}, \delta_{c_r}$	port and starboard canard deflection angle, deg
δ_f	flap deflection angle, deg
δ_j	thrust vector angle, deg
δ_{LE}	leading edge flap deflection angle, positive up, deg
δ_r	rudder deflection angle, positive for nose right yaw, deg
δ_{r_L}	limited rudder deflection angle command, deg
δ_{rp}	pilot (pedal) commanded rudder deflection angle, deg
δ_{TH}	throttle (power) setting, % of maximum
ε	error, %
ζ	damping ratio for second order dynamic system
ζ_a, ζ_{sp}	open-loop, closed-loop short period damping ratio
ζ_l, ζ_d	open-loop, closed-loop dutch roll mode damping ratio
θ, ϕ, ψ	Euler angles, deg
Λ	white noise

Λ_{LE} leading edge sweep angle, deg

λ taper ratio

ρ atmospheric density, slug/ft^3

σ real part of complex root

σ root-mean-square value

τ time delay, sec

τ_a actuator time constant, sec

τ_c longitudinal stick input prefilter time constant, sec

τ_e effective lag, sec

τ_L lag filter time constant, sec

τ_p lateral stick input prefilter time constant, sec

τ_R roll mode time constant, sec

τ_{R_o} desired roll mode time constant at M = 0.4, sea level, sec

τ_r rudder pedal input prefilter time constant, sec

τ_w washout filter time constant, sec

Φ power spectral density function

ω frequency, rad/sec (or deg/sec)

ω_a, ω_{sp} open-loop, closed-loop short period frequency, rad/sec

ω_l, ω_d open-loop, closed-loop dutch roll mode frequency, rad/sec

$$Z_w = \frac{1}{m}\frac{\partial Z}{\partial w}, \frac{1}{sec} \qquad C_{N_\alpha} = \frac{\partial C_N}{\partial \alpha} \qquad L'_i = \frac{L_i + (I_{xz}/I_x)N_i}{1 - (I_{xz}^2/I_x I_z)}$$

$$Z_\delta = \frac{1}{m}\frac{\partial Z}{\partial \delta_c}, \frac{ft}{rad\text{-}sec^2} \qquad C_{N_{\dot{\delta}_c}} = \frac{\partial C_N}{\partial \dot{\delta}_c} \qquad N'_i = \frac{N_i + (I_{xz}/I_z)L_i}{1 - (I_{xz}^2/I_x I_z)}$$

$$M_q = \frac{1}{I_y}\frac{\partial M}{\partial q}, \frac{1}{\text{sec}} \qquad C_{m_q} = \frac{\partial C_m}{\partial \frac{\bar{q}\bar{c}_w}{2V}}$$

$$M_w = \frac{1}{I_y}\frac{\partial M}{\partial w}, \frac{1}{\text{ft-sec}} \qquad C_{m_\alpha} = \frac{\partial C_m}{\partial \alpha}$$

$$M_\delta = \frac{1}{I_y}\frac{\partial M}{\partial \delta_c}, \frac{1}{\text{rad-sec}^2} \qquad C_{m_{\delta_c}} = \frac{\partial C_m}{\partial \delta_c}$$

$$Y_v = \frac{1}{mU}\frac{\partial Y}{\partial \beta}, \frac{1}{\text{sec}} \qquad C_{Y_\beta} = \frac{\partial C_y}{\partial \beta}$$

$$C_{l_\beta} = \frac{\partial C_l}{\partial \beta}$$

$$L_p = \frac{1}{I_x}\frac{\partial L}{\partial p}, \frac{1}{\text{sec}} \qquad C_{l_p} = \frac{\partial C_l}{\partial \frac{pb}{2V}}$$

$$L_{\delta_a} = \frac{1}{I_x}\frac{\partial L}{\partial \delta_a}, \frac{1}{\text{rad-sec}^2} \qquad C_{l_{\delta_a}} = \frac{\partial C_l}{\partial \delta_a}$$

$$C_{n_\beta} = \frac{\partial C_n}{\partial \beta}$$

$$N_r = \frac{1}{I_z}\frac{\partial N}{\partial r}, \frac{1}{\text{sec}} \qquad C_{n_r} = \frac{\partial C_n}{\partial \frac{rb}{2V}}$$

$$N_{\delta_r} = \frac{1}{I_z}\frac{\partial N}{\partial \delta_r}, \frac{1}{\text{rad-sec}^2} \qquad C_{n_{\delta_r}} = \frac{\partial C_n}{\partial \delta_r}$$

$$N_{\Delta\delta_c} = \frac{1}{I_z}\frac{\partial N}{\partial \Delta\delta_c}, \frac{1}{\text{rad-sec}^2} \qquad C_{n_{\Delta\delta_c}} = \frac{\partial C_n}{\partial \Delta\delta_c}$$

$$C_{n_{\beta,dyn}} = C_{n_\beta}\cos\alpha + \frac{I_z}{I_x} C_{\ell_\beta} \sin\alpha$$

3.2 SUBSCRIPTS

A	actual measured (achieved) value
DRY	dry power (non-afterburning) setting
c	commanded input
sym	symmetric
Max	maximum
min	minimum
trim	trim value
$(\ )_g$	gain appropriate to "G" command control system
$(\ )_\alpha$	gain appropriate to α command control sytem

3.3 SUPERSCRIPTS

$(\dot{})$	indicates time derivative

3.4 ABBREVIATIONS AND ACRONYMS

ACM	Air Combat Maneuvering
AEDC	Arnold Engineering Development Center
AEDC PWT-4T	AEDC Propulsion Wind Tunnel, 4T, Test Facility
AEDC VKF-A	AEDC Von Karmen Facility - A
AEDC 16T	AEDC 16-Foot Transonic Test Facility
AFCS	Automatic Flight Control System
ATF	Advanced Tactical Fighter
A/B	Afterburner
A/C	Aircraft
BL	Butt Line
$B_3N_1C_1^*W_1V_2$	Configuration Designations
cg	Center of Gravity
CAP	Control Anticipation Parameter
EAI	Electronic Associates, Inc.
FDL	Flight Dynamics Laboratory (USAF)
FTGTF	Fixed Turbine Geometry Turbofan
FTGTJ	Fixed Turbine Geometry Turbojet
FS	Fuselage Station
"G"	Maneuver command (as in "G" command) system
I/O	Input/Output
KEAS	Knots Equivalent Air Speed
LCDP	Lateral Control Divergence Parameter
LSRI	Lateral Stick-Rudder Interconnect
LSWT	Grumman Low-Speed Wind Tunnel
OPR	Overall Pressure Ratio
PSD	Power Spectral Density
RSS	Relaxed Static Stability
SFC	Specific Fuel Consumption
SM	Static Margin
SRAM	Short Range Attack Missile
STAC	Supersonic Tactical Aircraft Configuration
STOL	Short Takeoff/Landing
TOGW	Takeoff Gross Weight
VCE	Variable Cycle Engine
VTGTJ	Variable Turbine Geometry Turbojet

4 - STUDY AIRCRAFT: SUPERSONIC TACTICAL AIRCRAFT CONFIGURATION (STAC)

4.1 BACKGROUND

Grumman's STAC configuration was developed during 1977-78 in response to USAF Advanced Tactical Fighter (ATF) requirements. The primary goals for this program were to demonstrate:

- Efficient supersonic cruise;

$$\frac{M(L/D)}{SFC} = 8.0$$

- A competent level of sustained transonic maneuverability; 3.5 to 4.0 g's at M = 0.9, 30,000 ft altitude

- An advanced level of supersonic maneuverability.

These requirements are listed in order of importance relative to their impact on the configuration design. The target supersonic cruise efficiency is approximately twice that of contemporary tactical aircraft and was to be accomplished in a realistic design context. Maneuver requirements were to be achieved by developing a variable-camber supercritical wing that would be equally effective at transonic and supersonic speeds.

Extensive design studies at Grumman indicated that USAF/FDL technology goals related to tactical supersonic cruise aircraft could be achieved by pursuing a dedicated high-technology configuration development effort. The full meaning and implications of these words can best be realized by tracing the configuration development. As will be shown, it takes a combination of advanced technology and extraordinary coordination of the propulsion, aerodynamic, and functional configuration design (including the aggressive use of advanced control concepts) to achieve the targeted performance. Based on these findings, a USAF/Grumman program was initiated to develop the technology and demonstrate the performance capability for a candidate strike-fighter design concept.

The importance of dedicating the design effort to minimum zero-lift drag becomes apparent when one realizes the effort required to achieve the supersonic performance goal. Figure 4-1A shows the variation in airframe cruise efficiency, L/D_{Max}, with Mach number for a nominal advanced tactical aircraft. The L/D_{Max} of 6.0 at M = 2.0 is respectable for this class of aircraft and commensurate with designing a supersonic transport for L/D_{Max} near 9.0. As expected, the airframe lift-drag ratio falls abruptly at transonic speeds due to the buildup in zero-lift wave drag. The continuing decline in lift-drag ratio beyond M = 1.2 is due to increased wave drag associated with lift.

The corresponding trend in propulsion efficiency at intermediate or maximum dry power is indicated in Figure 4-1B. For low-to-moderate bypass

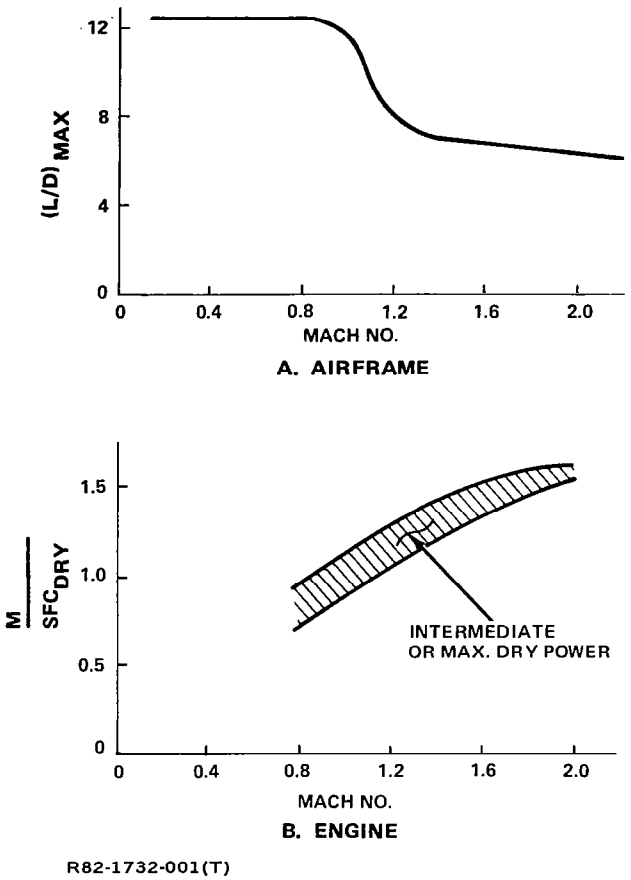

Figure 4-1. - Representative efficiencies for airframe and engine.

ratio fighter-type engines, M/SFC improves steadily with Mach number due to the ram effect on cycle pressure ratio.

Combining the individual airframe and propulsion trends, Figure 4-2, suggests that supersonic cruise efficiencies competitive with subsonic levels are possible. This is indeed the case if the aircraft cruises at or near L/D_{Max} at non-afterburning power settings. This ideal engine-airframe match typically prevails at subsonic cruise but not at supersonic conditions, with the result that high-speed cruise efficiency is severely degraded.

An indication of the thrust-required/thrust-available mismatch that can occur at supersonic cruise is evident in Figure 4-3. Here, the zero-lift drag and drag at L/D_{Max} very nearly double between M = 0.9 and M = 1.6. Thrust available, however, is determined by the engine size needed to meet the dominant maneuver requirement at M = 0.9 and the thrust lapse with Mach number. The severe decay in engine thrust coefficient for the fixed-geometry turbofan engine in Figure 4-3 results in maximum afterburning being required for L/D_{Max}

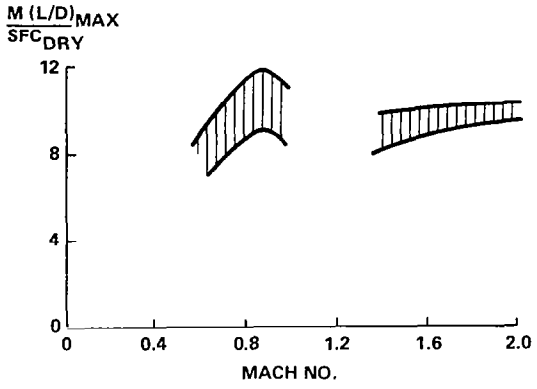

Figure 4-2. - Supersonic cruise efficiency for ideal engine - airframe match.

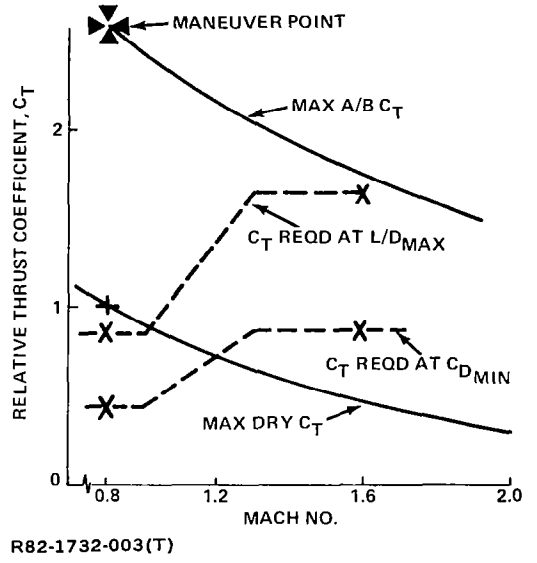

Figure 4-3. - Thrust lapse/drag rise with flight Mach No.

cruise at M = 1.6. Although airframe efficiency is maximum at this flight condition, the corresponding SFC is nearly twice that at dry power and cruise efficiency is marginal. Cruising at lower altitudes, or lift coefficients well below that for best L/D, allows the engine to be throttled back to partial afterburning for improved SFC but excessively degrades airframe efficiency. Best cruise altitude lies somewhere between these extremes; yet, for today's tactical aircraft, best cruise efficiency is less than one half that targeted for the ATF.

Although the current-technology engine-airframe combination used above to illustrate the cruise-match problem is dated, the broad conclusions are valid, i.e., solving the engine-airframe cruise match problem is the key to tactical supersonic cruise. It was first thought that advanced engines, especially variable-cycle engines, could resolve the problem, but this was not the case. The results of a parametric engine study assuming 1985 plus technology are summarized in Figure 4-4. Four generic engines, all sized to the same maximum A/B thrust at M = 0.9, h = 30,000 ft were considered. The SFC versus thrust coefficient and maximum thrust at M = 2.0 for three of the four engines (FTGTF, FTGTJ, VCE, VTGTJ) are seen to be similar. Based on available thrust, the FTGTF is not a good choice although this disadvantage is partly offset by its low weight. For the STAC design mission, which emphasizes supersonic cruise efficiency, the FTGTJ is best. An overall pressure ratio (OPR) near 20 provides reasonable subsonic cruise SFC.

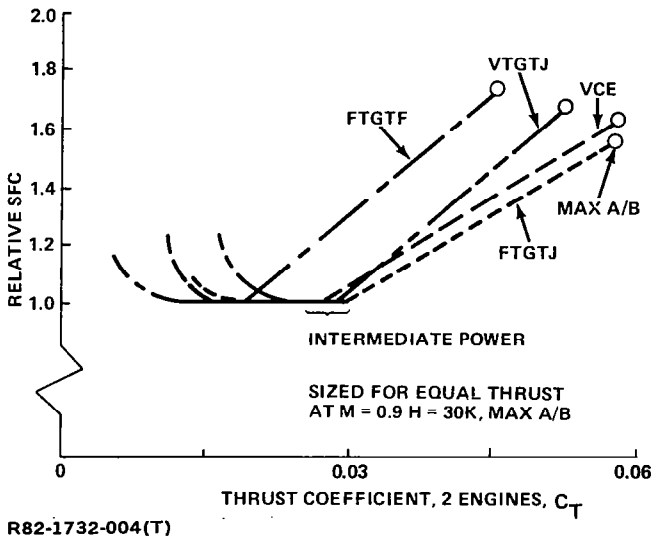

Figure 4-4. - Candidate engine characteristics at Mach 2.0.

It is apparent, then, that a satisfactory supersonic cruise-match can only be achieved by minimizing aircraft drag. Cruise drag, in turn, is largely determined by aircraft zero-lift drag. Figure 4-5 notes that cruise drag at L/D_{Max} is only dependent on C_{D_o} (although aircraft L/D_{Max} is equally dependent on zero-lift drag, C_{D_o}, and drag-due-to-lift, K). Required thrust can be substantially reduced by cruising at a lift coefficient somewhat less than that for best L/D, with little loss in cruise L/D. The critical supersonic design requirement, therefore, is to minimize zero-lift drag to improve cruise L/D and avoid afterburner operation.

CRUISE DRAG

$$C_D = C_{D_o} + KC_L^2,\ K = C_{D_i}/C_L^2$$

- **AIRFRAME EFFICIENCY DEPENDS ON BOTH C_{D_o} AND K**

$$(L/D)_{MAX} = \left[\frac{1}{4KC_{D_o}}\right]^{1/2}$$

- **CRUISE DRAG AT $(L/D)_{MAX}$ DEPENDS ONLY ON C_{D_o}**

$$C_D \text{ AT } (L/D)_{MAX} = 2C_{D_o}$$

- **SUPERCRUISE ENGINE-AIRFRAME MATCHING DRIVES CRUISE ALTITUDE DOWN**

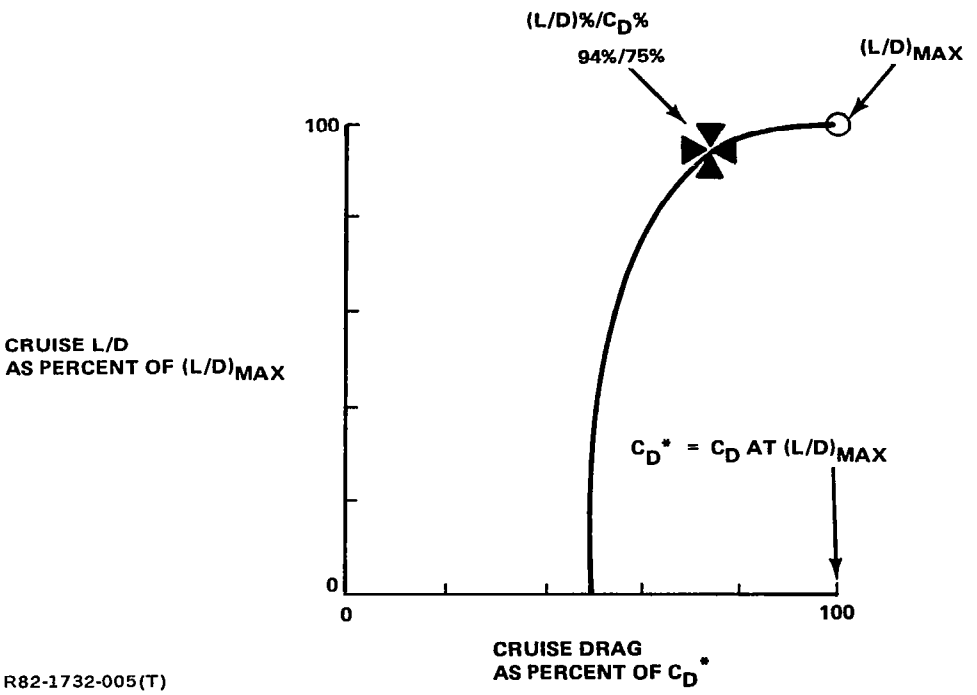

Figure 4-5. - Supercruise drag considerations.

The dramatic reduction in zero-lift-drag needed to achieve an acceptable cruise match at M = 2.0 is illustrated in Figure 4-6. The "current aircraft" referred to are operational tactical aircraft having supersonic dash capability but not designed for supersonic cruise. Given the need, a new aircraft based on existing engines and technology could be designed for approximately 25% less drag at M = 2.0. The proposed STAC strike-fighter configuration, however, had to be designed for less than half the drag of current aircraft and that issue defined the prerequisite technology needs.

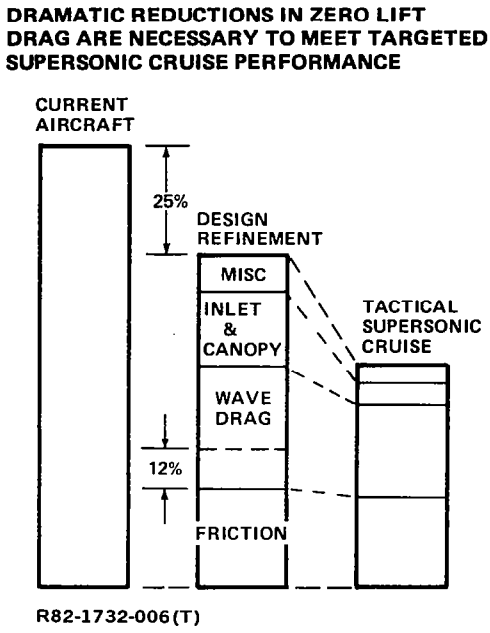

Figure 4-6. - Zero Lift Drag Comparisons at Mach 2.0.

It is clear from the drag breakdown in Figure 4-6 that substantial improvements in detail design and wave drag were required. The wing wave drag (~ 12%) was certainly a significant but not overwhelming part of the problem. The very low drag of the proposed aircraft, which ensures non-afterburning M = 2.0 cruise, in itself posed a problem since the small jet exit area at these power settings would normally result in excessive nozzle boattail drag. These penalties, however, can be eliminated with advanced nonaxisymmetric nozzles that fully expand the engine throughflow for improved thrust/reduced boattail drag. A variable-geometry inlet, low profile or variable-geometry cockpit, tandem recessed weapon carriage, and compact, high thrust-to-weight engines round out the enabling technology complement.

4.2 DESIGN EVOLUTION

The mission/payload requirements for the STAC Strike-Fighter design effort were:

- 350 n mi/200 n mi subsonic/supersonic radius, 550 n mi total radius
- M = 2.0 cruise
- 3.5 g sustained maneuver capability, stores-on, 50% fuel, at M = 0.9, h = 30,000 ft
- Crew: one
- Weapon load: Two 2500-lb SRAM-type missiles
- Avionics: 1250 lb.

No explicit provision for overload stores, gun and ammunition, electronic countermeasures suite, or separate air-to-air missiles was mandated at that

stage of the design effort. The governing philosophy was to concentrate on solving the fundamental air-vehicle design problems first and then modifying the design to accommodate these items as required. This configuration would, in fact, be the baseline for addressing these design considerations.

Preliminary studies indicated that the desired dry power supersonic cruise requirement could be achieved with an advanced configuration concept. Parametric studies showed that a minimum takeoff gross weight (TOGW) design would have the following characteristics:

- TOGW: 40,000 lb
- Fuel fraction: 0.30
- Takeoff wing loading: 90 lb/ft^2
- Takeoff thrust-to-weight: 0.80
- Wing: Aspect Ratio = 2.6
  Leading edge sweep = 57 deg
  Taper ratio = 0.2
  Thickness ratio = 0.035
- Engine: Advanced Fixed Turbine Geometry Afterburning Turbojet.

It is worth noting that the above optimum thrust and wing loading are such that the summed engine plus wing weight are a minimum for the specified M = 0.9 maneuver requirement. The parametrics are telling us that the maneuver requirement sizes both the wing and engine, and that the configuration is sensitive to structural weight implications. An interesting corollary is that, had the STAC maneuver requirement been 4.5 g or 5.0 g instead of the stipulated 3.5 g, both the optimum wing size and installed thrust would be increased proportionately such that the maneuver lift coefficient would remain the same. In this respect, then, the specified maneuver level is simply a sizing issue and not a technology issue.

The selection of a tandem centerline weapon installation led quite naturally to a twin-engine arrangement. A relatively short duct, podded configuration was selected to minimize structural weight and internal/external wetted area. The resulting configuration, a canard layout, is shown in Figure 4-7A and a general arrangement drawing is provided in Figure 4-7B. Study results indicated that canard wake ingestion by the inlet would be a rare occurrence confined to non-critical flight conditions. Subsequent wind tunnel tests (Ref. 3) confirmed these findings.

The choice between a conventional aft-tail arrangement or a canard configuration was based on trim considerations and development potential. The historical advantage of a canard configuration for supersonic cruise is evident from Figure 4-8. If the aircraft (canard or aft-tail) is required to be longitudinally stable at low speed, then stability at M = 2.0 is excessive and a substantial trim drag penalty is incurred. This is particularly true for aft-tail configurations, where a tail down-load is needed to trim. As the required longitudinal stability is relaxed, the trim drag at supersonic cruise will decrease for either arrangement although the canard maintains an advantage throughout the parametric range shown. These results are based on lifting-surface theory calculations for planar wing/canard/aft-tail configurations; the percentages cited are relative to the untrimmed isolated wing drag (the

- **WING**

REFERENCE AREA	S_W	=	444 FT^2
ASPECT RATIO	AR	=	2.6
LEADING EDGE SWEEP	Λ_{LE}	=	57°
TAPER RATIO	λ	=	0.2

- **CANARD**

REFERENCE AREA (TOTAL)	S_C	=	70 FT^2
ASPECT RATIO (PER PANEL)	AR	=	1.27
LEADING EDGE SWEEP	Λ_{LE}	=	57°
TAPER RATIO	λ	=	0.223

- **VERTICAL TAILS**

REFERENCE AREA (TOTAL)	S_V	=	84 FT^2
ASPECT RATIO (PER SURFACE)	AR	=	0.955
LEADING EDGE SWEEP	Λ_{LE}	=	60°
TAPER RATIO	λ	=	0.233

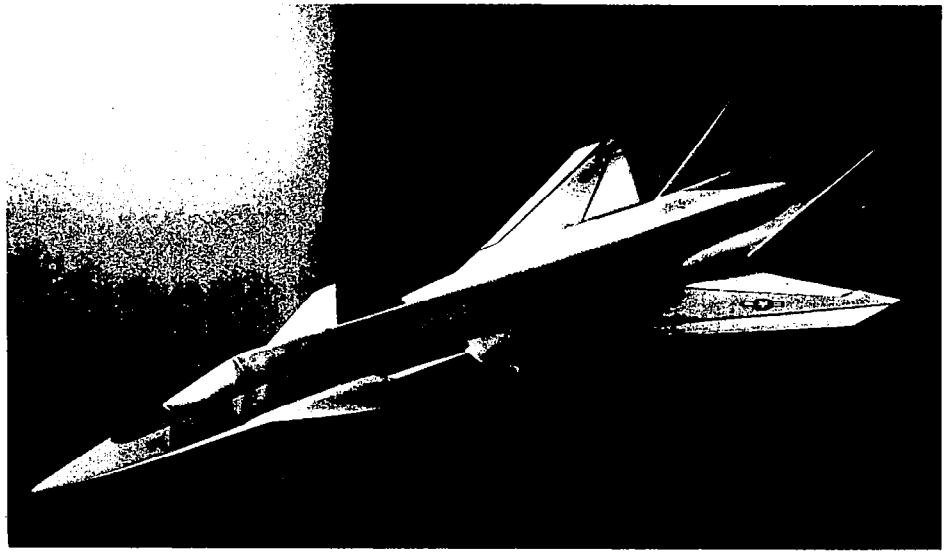

A. BASELINE STAC

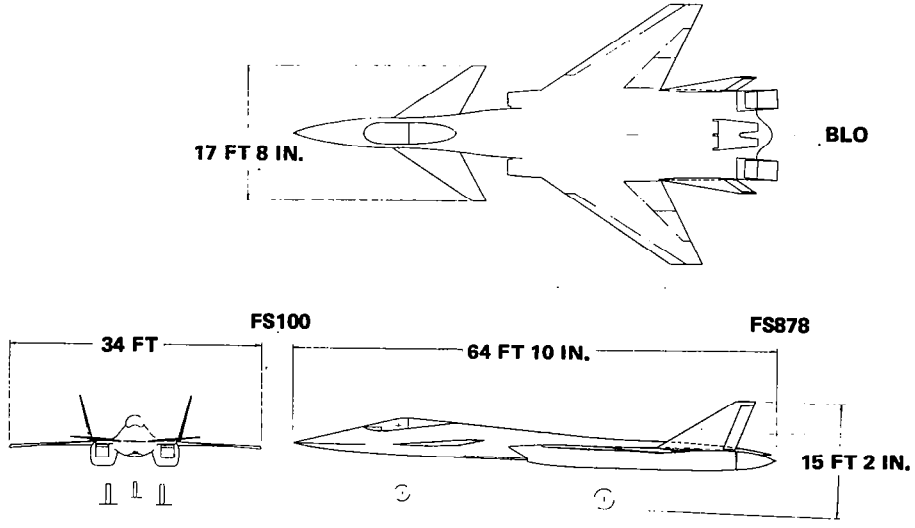

B. STAC 3-VIEW

R82-1732-007(T)

Figure 4-7. - Supersonic Tactical Aircraft Configuration (STAC)

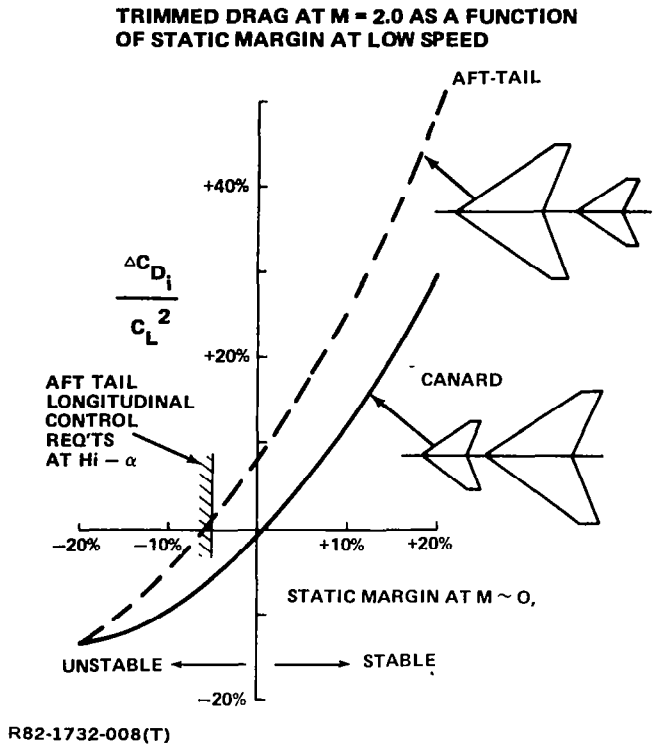

Figure 4-8. - Trimmed Drag-Due-To-Lift at Mach 2.0.

theoretical trends shown were subsequently confirmed by wind tunnel data). Although specific high-angle-of-attack data are required to make firm statements, it appears that the maximum permissible instability of aft-tail configurations is more limited than that for canard configurations. The aft-tail longitudinal control boundary shown is a rough estimate of how this consideration could limit supersonic cruise/maneuver performance. Additional discussion is provided in Ref. 3.

Similar trim drag issues arise at transonic speeds, although in this case the situation is more complex. In general, however, given the substantial nose-down moments produced by variable-camber maneuver wings, the aft-tail configuration must be trimmed with a tail down-load which additionally burdens the wing. The corresponding trim load for a canard is positive and the comparison favors the canard arrangement.

The strike-fighter cruise-maneuver design conflict was resolved by designing the basic wing to minimize supersonic cruise drag and using internal actuators to modify the wing shape for maximum transonic maneuver performance as shown in Figure 4-9. For simplicity, the variable-camber mechanization is limited to single curvature or cylindrical camber changes with geometrical generators parallel to the front and rear beam, respectively. The substantial washout/wing twist introduced when cambering the inversely-tapered leading edge

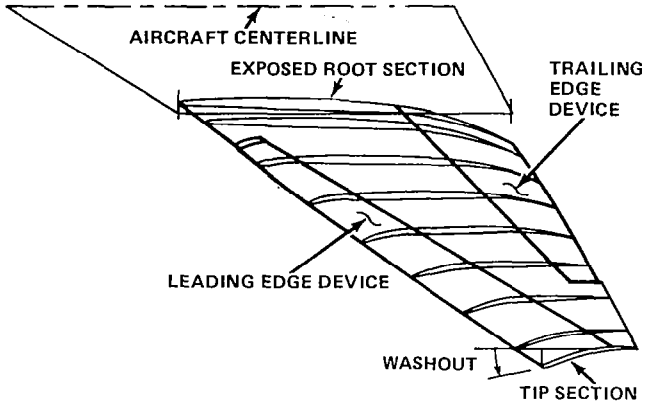

Figure 4-9. - Variable-twist/variable-camber transonic maneuver wing configuration.

flap gives the variable-twist/variable-camber wing its name. In effect, the overswept leading and trailing edge hinge lines permit control over both the spanwise and chordwise load distribution on the wing at all flight conditions. A simple yet effective means for accomplishing this was mandatory since the transonic maneuver wing design calls for nearly 20 degrees of wing twist.

Supersonic cruise tactical aircraft will also display significant levels of supersonic maneuverability. Available thrust at maximum A/B permits sustained maneuvering at C_L levels well beyond the current state-of-the-art in supersonic wing design. The potential drag reductions that could be realized by developing an improved supersonic maneuver wing are indicated in Figure 4-10. The conventional-design maneuver drag noted is for a planar wing with zero leading-edge suction. A much lower drag level is possible if the wing is shaped to realize 100% leading edge suction, as indicated by the low drag curve. The development of such a supercritical maneuver wing concept was successfully accomplished under a separate NASA contract (Ref. 4).

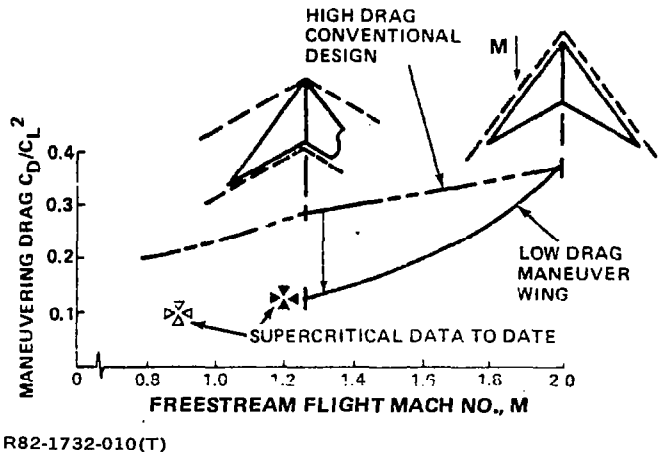

Figure 4-10. - Potential improvements in supersonic maneuvering capability.

4.3 SUMMARY OF AIRCRAFT CHARACTERISTICS

The STAC wind tunnel test program was designed to provide basic data on:

- Aircraft performance
- Stability and control characteristics
- Maneuver wing performance
- Propulsion-Airframe integration
- Weapon separation.

These objectives were successfully accomplished during some 300 hours of high-speed wind tunnel testing at the USAF/AEDC during 1977-78. Additional high-angle-of-attack data were acquired in January 1979 in the AEDC 16-ft Transonic Wind Tunnel facility.

Representative data from this test series appear in Figure 4-11. The data show (Ref. 5) that the targeted supersonic zero-lift drag and supersonic cruise efficiency goals were achieved during the STAC development program. Figure 4-12 highlights these results by comparison to contemporary zero-lift drag and supersonic cruise efficiency standards.

Figure 4-13 summarizes the variation in STAC trimmed drag with aircraft static margin at M = 0.9, C_L = 0.71, the aircraft maneuver design point. The vertical scale gives the measured configuration drag at C_L = 0.71 for each of three wing configurations at canard deflections of 0, -4, and -8 degrees. The horizontal scale gives the center-of-gravity location at which each configura-

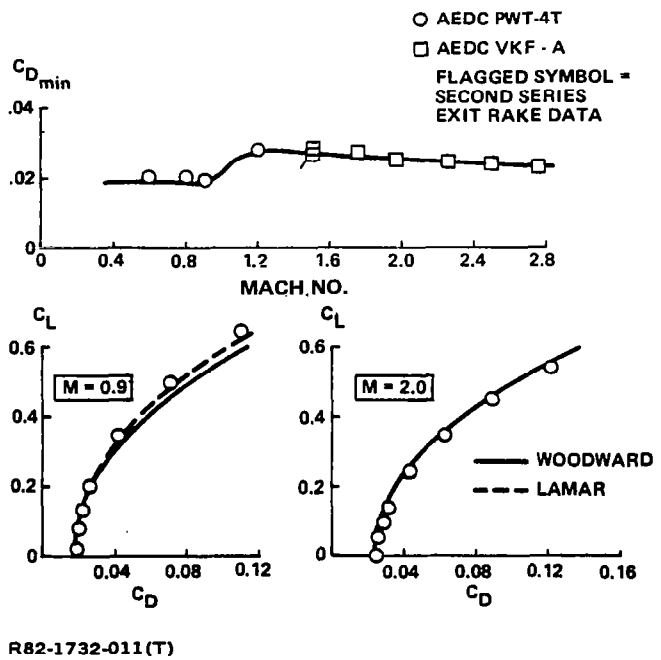

Figure 4-11. - Data correlation - model drag

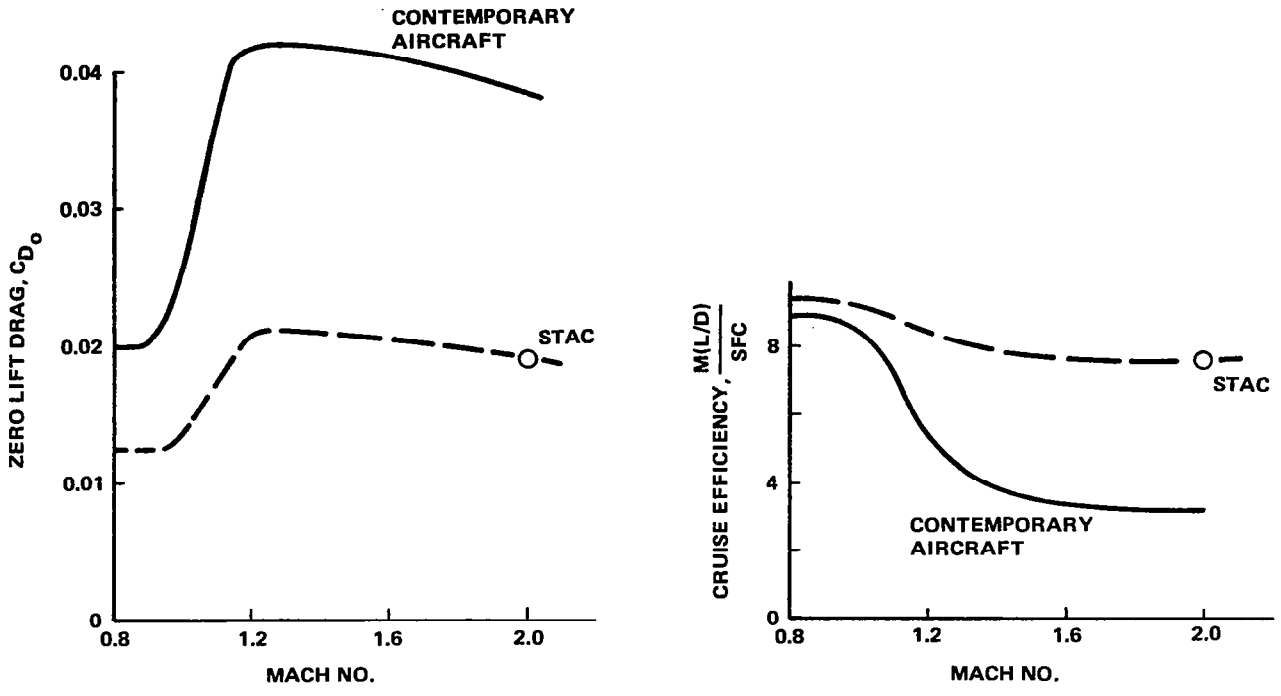

Figure 4-12. - Aircraft efficiency.

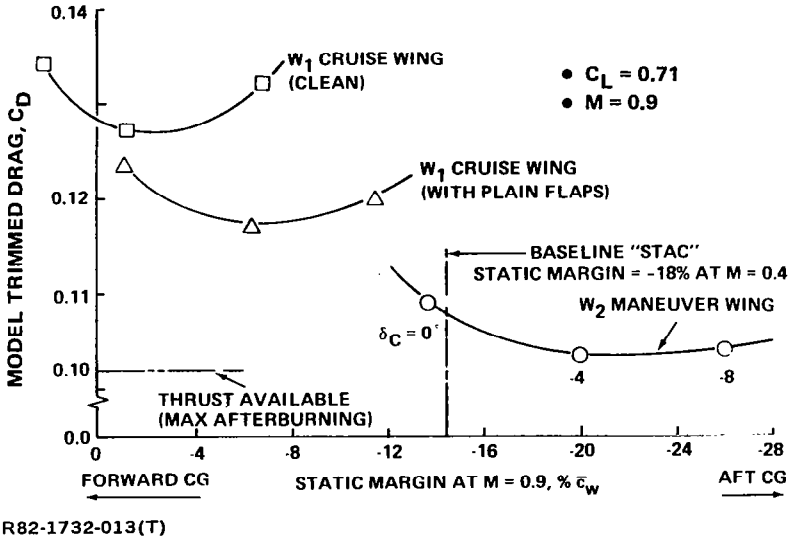

Figure 4-13. - STAC trimmed drag vs static margin.

tion trims, denoted in terms of the aircraft static margin (SM) corresponding to that center-of-gravity. The W_1 wing shown is the baseline supersonic cruise wing designed for C_L = 0.16, M = 2.0. This wing is characterized by mild twist and camber; approximately 4 degrees of washout, and 1% camber. The

very low zero-lift moment of this wing means that this configuration will trim at or near the aerodynamic center for reasonable canard settings, Figure 4-13.

Test data for the same wing with simple leading edge/trailing edge flap deflections show a significant reduction in maneuver drag and a corresponding increase in zero-lift moment and rearward shift in the center-of-gravity for trim.

The same pattern is repeated as one progresses to the STAC W_2 wing, a highly cambered supercritical maneuver wing designed specifically for this flight condition. For the range of wing configurations shown, the trimmed drag varies from a high of $C_D = 0.1270$ (if the aircraft is balanced neutrally stable) to a low of $C_D = 0.1030$ (if the aircraft is balanced 20% unstable). The overall variation, some 240 drag counts, corresponds to approximately 25% of the maximum afterburning thrust available at this flight condition. If the present aircraft were to be balanced neutrally stable and the installed thrust up-sized so that performance is comparable to that obtained with the W_2 maneuver wing at a SM = -20% $\bar{c}_w$, then, with an aircraft growth factor of near 4.0 and engine thrust-to-weight between 8 and 10, the aircraft TOGW would increase by 8% to 10%. Avoiding this penalty by balancing the aircraft unstable is just one example of the substantial benefits achievable by aggressive exploitation of advanced control concepts in fighter aircraft design.

As might be expected, there are limits to the level of longitudinal instability that can be introduced to minimize trim drag. The STAC pitching moment characteristics in Figure 4-14 show that the baseline aircraft, SM = -18% $\bar{c}_w$ (canard neutral) at M = 0.4 (SM = -15% $\bar{c}_w$ at M = 0.9), can be trimmed to angles-of-attack in excess of 80 degrees. The aircraft does not exhibit deep stall at this cg; however, the nose-down moment available beyond α = 20 degrees is limited. Whether this aerodynamic margin is sufficient is a complex issue that ultimately comes down to determining the point at which the related AFCS maneuver limiting requirement seriously degrades aircraft mission capability. The excellent vortex flow characteristics exhibited by the present configuration (Figure 4-15), with $C_{L_{Max}}$ occurring at $\alpha \approx 40$ degrees, suggests that this class of aircraft should be designed with due consideration to high-angle-of-attack issues.

The importance of achieving good high-angle-of-attack stability and control characteristics was recognized early in the STAC concept development. Figure 4-16 summarizes some of the requirements and issues considered at that time. "Best judgement" and earlier reentry vehicle/YF-16/YF-17 experience were used as design guidelines since quantitative requirements were not available. The present study, in fact, provides some of the required information.

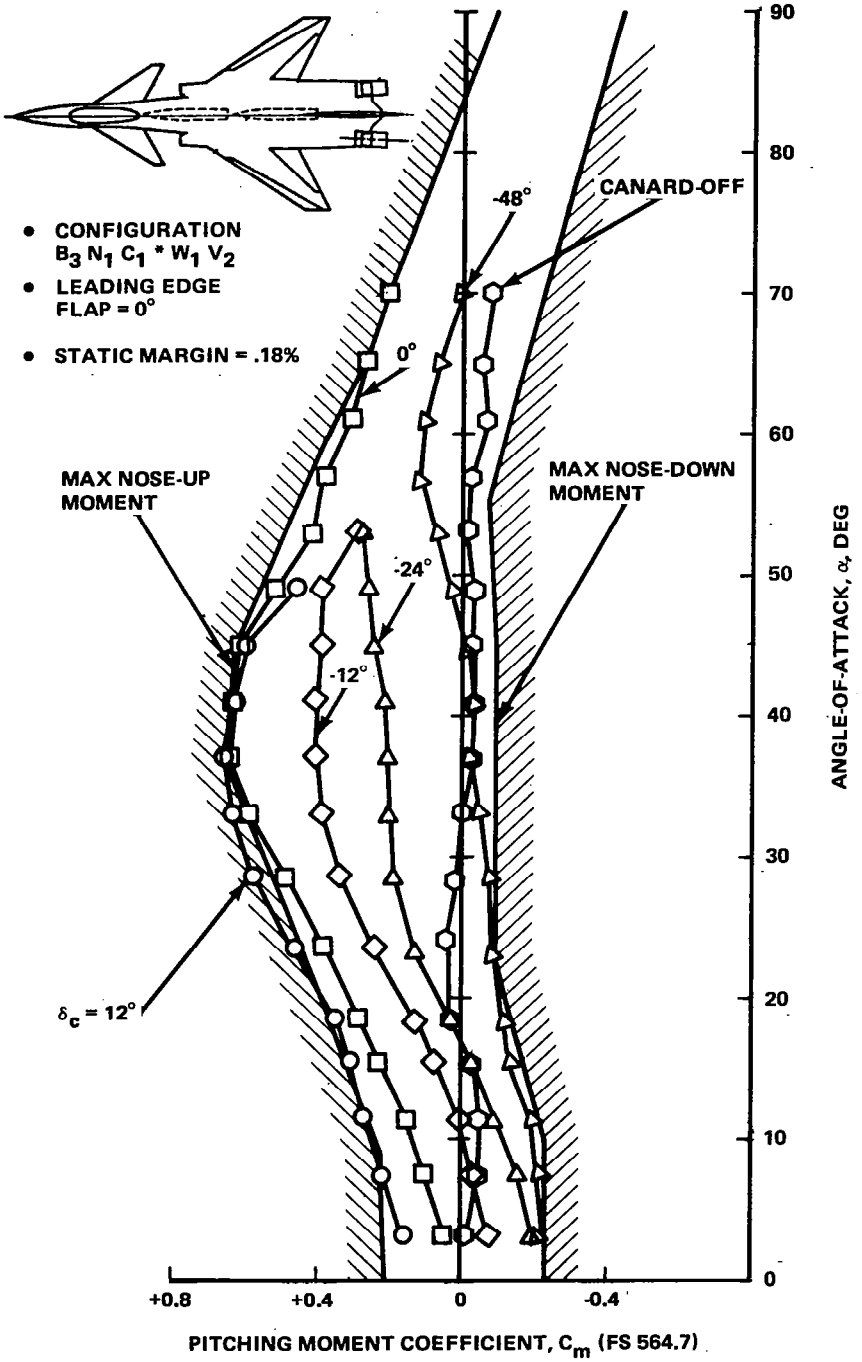

Figure 4-14. - STAC pitching moment characteristics, M = 0.17

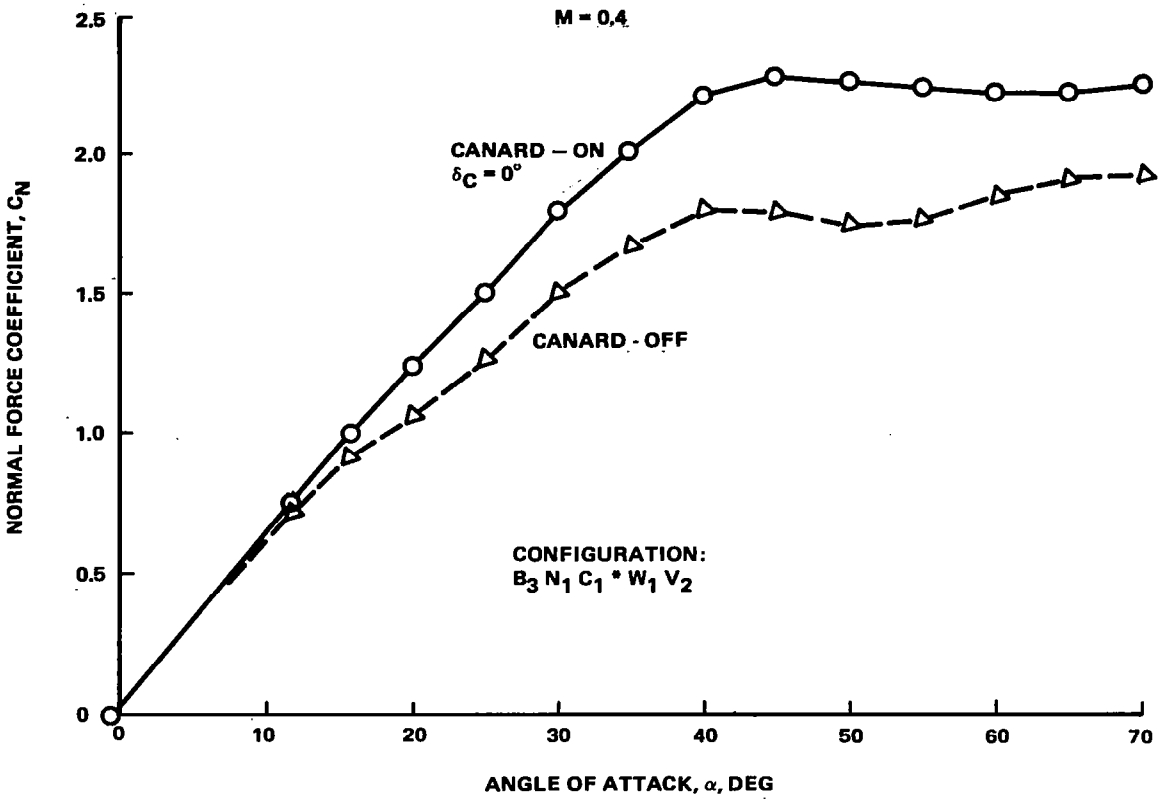

Figure 4-15. - STAC normal force characteristics.

- **LONGITUDINAL**
  - STABLE C_m BREAK AT HIGH α
  - NO DEEP STALL
  - ADEQUATE CONTROL FOR DEPARTURE PREVENTION
  - ADEQUATE CONTROL FOR STOL OPERATION
- **LATERAL/DIRECTIONAL**
  - STABLE $C_{n_{\beta_{DYN}}}$ – MANDATORY
  - STABLE C_{ℓ_β} – MANDATORY
  - STABLE C_{n_β} – DESIREABLE → MANDATORY
  - POSITIVE ROLL CONTROL TO $\alpha = 90°$
  - POSITIVE YAW CONTROL TO $\alpha = 90°$

R82-1732-016(T)

Figure 4-16. - Target high-angle-of-attack stability and control requirements.

5 - STAC WIND TUNNEL EVALUATION

5.1 DESCRIPTION OF THE MODEL AND TEST PROGRAM

Table 5-1 summarizes the STAC wind tunnel test program. The Transonic I and Supersonic I series tests established basic aircraft performance, stability, and control characteristics for angles-of-attack from 0 to 16°, M = 0.6 to M = 2.75. Test results generally confirmed published pretest estimates and no "surprises" were encountered. Note that theoretical predictions for the transonic maneuver wing at M = 0.9 were not generated due to state-of-the-art computer code limitations at the time. Engineering estimates, based on extrapolating Ferris' data, Ref. 6, however, compared favorably with test results. Documentation of the STAC high-angle-of-attack aerodynamic characteristics was accomplished during two subsonic wind tunnel entries. The modular 1/27 scale wind tunnel model used in all testing is shown in Figure 5-1.

TABLE 5-1. - USAF/GRUMMAN STAC PROGRAM MILESTONES.

• PRELIMINARY DESIGN STUDIES		JAN. 1977
• GO-AHEAD FOR CO-OP EFFORT		JUNE 1977
• STAC DESIGN & MODEL FAB'N (GRUMMAN)		NOV. 1977
• WIND TUNNEL TESTS (USAF/AEDC)		
TRANSONIC I	BASIC A/C TRANSONIC MANEUVER WING	DEC. 1977
SUPERSONIC I	BASIC A/C PROPULSION/AIRFRAME INTEGRATION	APR.-MAY 1978
SUPERSONIC II	SUPERSONIC MANEUVER WING STORES CARRIAGE & SEP'N	JULY & SEPT. 1978
TRANSONIC II	BASIC A/C INVEST'N TO $\alpha = 70°$	JAN. 1979
• GRUMMAN LSWT HIGH-α DOCUMENTATION		SEPT. 1980

R82-1732-017(T)

The first high-angle-of-attack test was conducted in the AEDC Propulsion Wind Tunnel Facility, Tunnel 16T, during January 1979. The M = 0.4 test angle-of-attack range extended from -6° to +70° with yaw sweeps at every 5° of α covering the sideslip range -3° to +16°. Additional data at angles-of-attack to 35° were obtained at M = 0.9 and M = 1.2.

The baseline configuration, $B_3N_1C_1^*W_1V_2$, consisted of the following modular components:

B_3 - basic model fuselage

N_1 - reference nacelle

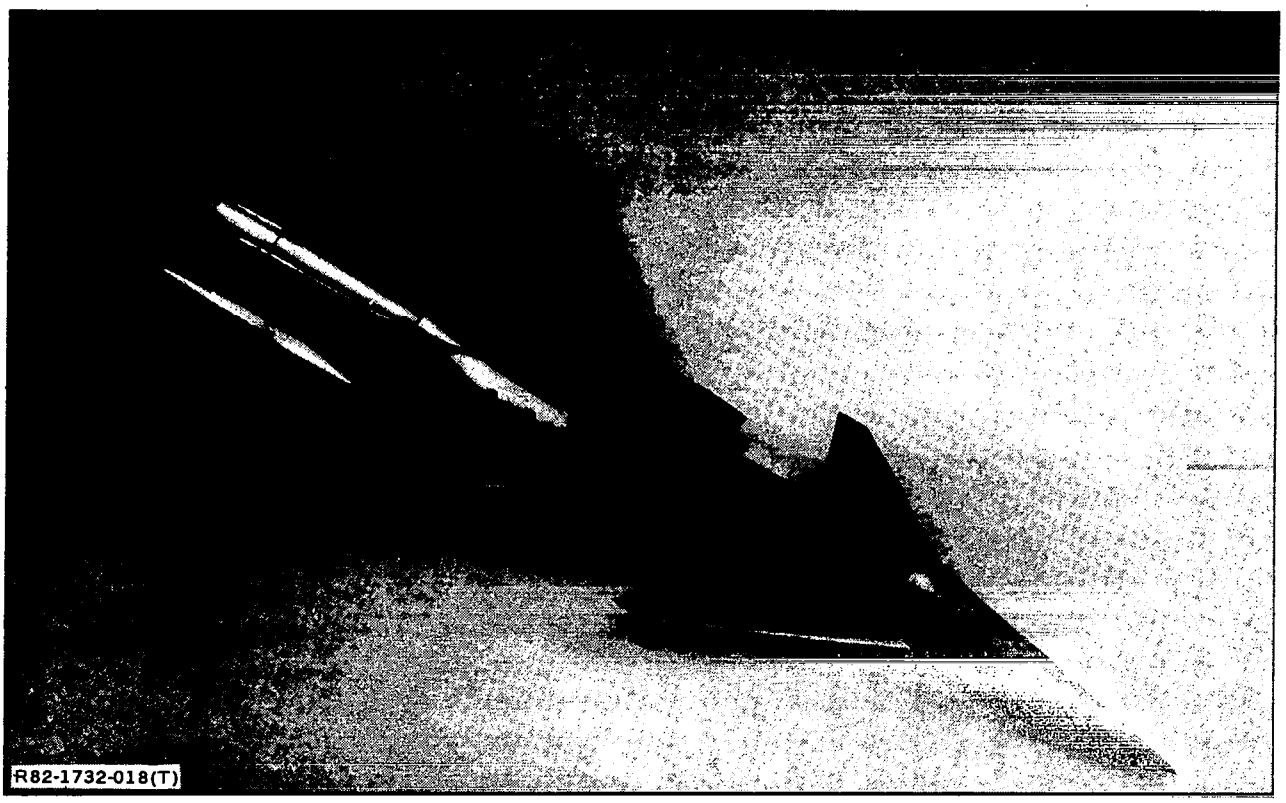

Figure 5-1. - 1/27-scale STAC wind-tunnel model.

C_1^* - canard, 70 ft^2, zero dihedral

W_1 - supersonic cruise wing

V_2 - twin nacelle-mounted vertical tails.

The 16T test schedule is presented in Table 5-2. Some data were also acquired for a configuration consisting of a semi-conic inlet in combination with a single centerline vertical tail.

The next STAC subsonic high-angle-of-attack wind tunnel test was conducted in the Grumman 7 x 10-ft Low-Speed Wind Tunnel (LSWT) during September 1980. A total of 536 runs were made to document the longitudinal stability, lateral/directional stability, and control characteristics. This testing was accomplished in three angle-of-attack ranges using various sting-offsets as noted below.

Sting Offset	Angle-of-Attack, Deg	Yaw Sweeps, Deg
Low	-1 to 25	α = 2,8,12,16,20,25
Mid	28 to 53	α = 30,35,40,45,50
High	55 to 70	α = 55,60,65,70

The sideslip range extended from -4° to +20°.

TABLE 5-2. - AEDC PWT-16T WIND-TUNNEL TEST.

α	β	CONTROL SURFACES (DEG)				COMMENTS
		δ_c	δ_{LE}	δ_{TE}	δ_r	
X	X	0	0	0	0	BASELINE
X	X	-12	↓	↓	↓	
X	X	-24				
X	X	OFF		↓		CANARD OFF
X		↓		14		T.E. FLAP
X	X	-48		0		BASELINE
X	X	OFF		↓		SEMI-CONIC INLET/SINGLE VERT TAIL
X	X	-24				
X	X	↓	↓		-10	RUDDER
X	X	-12	-30		0	BASELINE
X	X	-24	0	↓	-10	RUDDER
X	X	↓	↓	14/OFF	0	AILERON
	X	0/OFF		0	↓	DIFFERENTIAL CANARD
	X	-24	↓	↓	OFF	VERT TAIL OFF

R82-1732-019(T)

The test schedule is presented in Table 5-3. The baseline $B_3N_1C_1^*W_1V_2$ configuration was employed throughout this test. Configuration comments are noted in the far right column.

Test data for the maneuver wing configuration, $B_3N_1C_1^*W_2V_2$, were acquired at AEDC in December 1977 and were limited to the conventional 0° to 20° angle-of-attack range.

5.2 SUMMARY OF TEST DATA

The STAC configuration exhibits excellent vortex flow characteristics up to an angle-of-attack of 40°, after which vortex breakdown and transition to fully separated flow occurs (see Figure 4-15). A favorable "canard effect" is evident; the canard vortices tending to suppress wing separation.

A baseline configuration was defined with the cg located at FS564.7, resulting in a configuration static margin at low-angle-of-attack, M = 0.4, 16% $\bar{c}_w$ unstable (based on a 180-in. reference chord). The pitching moment data in Figure 5-2 indicate a mild wing-body pitch-up beyond α = 10° as shown by the canard-off data. This figure also compares the AEDC 16T and Grumman LWST data for the canard-off and zero canard incidence configurations. In general, good agreement was noted between test data from both facilities although detail differences were observed. The pitching moment discrepancies in Figure 5-2 were the most significant departures observed.

With the exception of a mild directional instability near α = 20°, the STAC configuration exhibits positive lateral/directional static stability

TABLE 5-3. - GRUMMAN LOW-SPEED WIND-TUNNEL TEST.

STING OFFSET						CONTROL SURFACES (DEG)				COMMENTS
LOW		MID		HIGH						
α	β	α	β	α	β	δ_c	δ_{LE}	δ_{TE}	δ_r	
X	X	X	X	X	X	0	0	0	0	BASELINE
X	X	X	X	X	X	OFF	↓	↓	↓	CANARD OFF
X	X	X	X			-24				BASELINE
X	X	X	X	X	X	-48				
X	X	X	X			-12				
X	X	X	X			12				
X	X	X	X			24				
		X				-24			-10	RUDDER
		X				↓		14/0	0	AILERON
		X						14/OFF	↓	
		X					-30	↓		
		X	X				↓	0		
X	X	X	X			-12		↓		BASELINE
		X				-24			-10	RUDDER
		X	X			↓			0	TRANSONIC CANOPY
		X	X						↓	NOSE STRAKE
		X	X			0				BASELINE
		X	X			OFF				CANARD OFF
		X	X			12/-48				DIFFERENTIAL CANARD
		X	X			0/-48				
		X	X			-12/-48				
		X	X			-48/12				
		X	X			-48/0				
		X	X			-48/-12				
		X	X			0/OFF				
		X	X			OFF/0				
		X	X	X	X	-48				BASELINE
		X	X			-24			OFF	VERT TAIL OFF
		X	X			↓			↓	LEFT TAIL OFF
		X	X							RIGHT TAIL OFF
		X					0/-30		0	DIFFERENTIAL L.E.
				X		-48	↓		↓	
				X	X	↓	-30			TRANSONIC CANOPY
				X					-10	RUDDER
				X	X				OFF	VERT TAIL OFF
				X				14/OFF	0	AILERON
				X	X	-24/-48		0		DIFFERENTIAL CANARD
				X	X	-12/-48				
				X	X	0/-48				
				X	X	-48/0				
				X	X	-48/-12				
				X	X	-48/-24	↓	↓	↓	
X						-12	0		-10	RUDDER
X	X					↓	↓		OFF	VERT TAIL OFF
X	X								↓	RIGHT TAIL OFF
X	X									LEFT TAIL OFF
X	X								0	TRANSONIC CANOPY
X	X							↓	↓	SAWTOOTH L.E.
X		X				↓	↓	14		T.E. FLAP
		X	X			-24	↓	0		SAWTOOTH L.E.
		X	X			↓	-30	↓		ASYMMETRIC NOSE STRAKE (LEFT)
		X	X				↓			RIGHT
X	X					-24/0	0			DIFFERENTIAL CANARD
X	X					0/-24	↓	↓		
X						-12		14/OFF	↓	AILERON

R82-1732-020(T)

(body axes) throughout the angle-of-attack range 0° to 70°. The configuration also exhibits positive lateral/directional control over the same angle-of-attack range. Wing trailing edge ailerons, geared to provide large upward deflections at high-angle-of-attack, provide near-constant rolling moment to $\alpha = 70°$. Twin vertical-tail rudders are effective to 30° angle-of-attack, and differential canard deflection provides effective yaw control throughout the remaining angle-of-attack range.

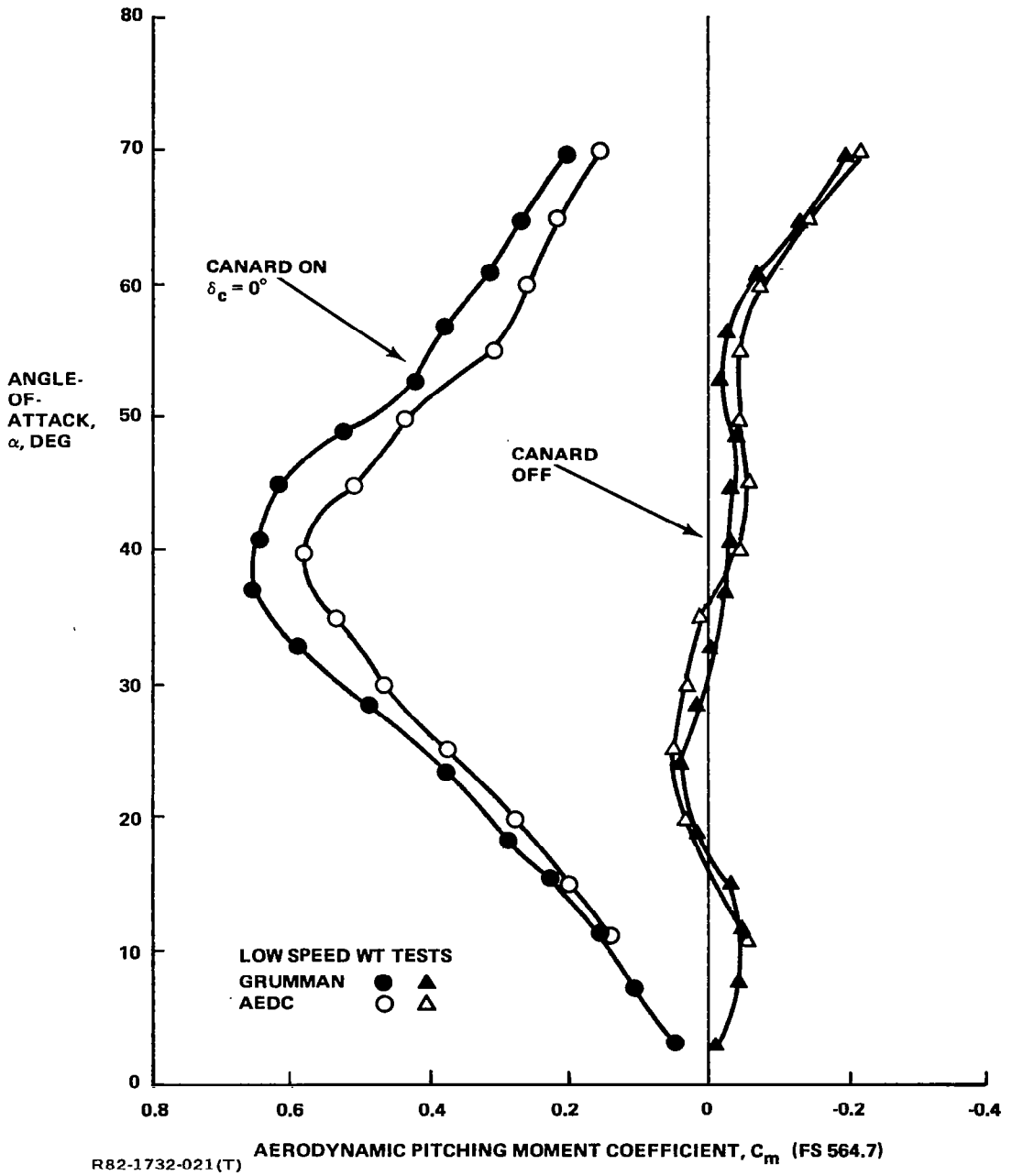

Figure 5-2. - STAC pitching moment characteristics.

6 - STAC ENGINEERING SIMULATION

6.1 SIMULATION MECHANIZATION

Most of this study was conducted using an EAI HYSHARE 2000 hybrid computer. The HYSHARE 2000 system consists of a general-purpose digital processor and three parallel analog processors. The full six-degree-of-freedom equations of motion and aerodynamic, propulsion, and control system math models were programmed for digital computation. The analog capability of the system served to interface with various I/O devices, including a fixed-base simulation cockpit.

An all-digital aircraft simulation mode was selected for flexibility in accomplishing modifications to the math models. For engineering simulation, the computer was operated in non-real time at a rate equivalent to as many as 200 passes/second in real time. The entire simulation code was executed during each pass. All control system filters were modeled using first-order Tustin approximations. Atmospheric turbulence was generated using two random-noise generators. Their outputs were shaped using analog filters before being sampled and summed with the aerodynamic velocities and rates in the math model.

6.2 STAC SIMULATION MATH MODEL

Mass and dimensional properties of the simulated STAC aircraft are presented in Table 6-1. Appendix A lists the gross thrust and ram drag characteristics of the simulated STAC powerplants and describes the engine dynamic

TABLE 6-1. - STAC MASS AND DIMENSIONAL CHARACTERISTICS

• WEIGHT	35,876 LB
• MOMENTS OF INERTIA:	
I_x	22,000 SLUG-FT^2
I_y	209,000 SLUG-FT^2
I_z	231,000 SLUG-FT^2
I_{xz}	0
• WING DIMENSIONS:	
SPAN	34 FT
AREA	444 FT^2
MEAN AERODYNAMIC CHORD	15.01 FT
• NOMINAL CENTER OF GRAVITY LOCATION (FUSELAGE STATION)	564.7 IN.
• NOMINAL SURFACE DEFLECTION LIMITS:	
CANARD (LEFT & RIGHT)	-90° → +90°
FLAPERONS/AILERONS	-90° → +90°
RUDDER	-20° → +20°
LEADING EDGE FLAPS	-50° → 0°
NOZZLES	-30° → +90°

R82-1732-024(T)

model. The programmed aerodynamic data used in the simulation are listed in Appendix B, which also describes the analytic synthesis of the aerodynamic math model. A brief summary of the programmed STAC aerodynamic characteristics follows.

6.2.1 Longitudinal Aerodynamic Model

The configuration static margin at low-angles-of-attack is -16% $\bar{c}_w$ at the nominal center-of-gravity position (FS564.7) with the canard in its trim setting. A moderate pitch up is indicated at $\alpha = 10°$ as shown by the canard-off pitching moment characteristics in Figure 6-1. Note the high degree of fidelity that was maintained between the aerodynamic math model and the test data. Figure 6-1 also gives the maximum nose-up and nose-down canard power boundaries. The angle-of-attack range from 25° to 55° is the region of least available nose-down moment. A positive 33° canard setting provides the maximum nose-up moment at $\alpha = 0°$. The aerodynamically most effective canard deflection decreases with angle-of-attack to $\alpha = 40°$, beyond which a 0° canard setting forms the nose-up boundary.

As noted, the pitching moment data shown in Figure 6-1 are for the basic $B_3N_1C_1^*W_1V_2$ configuration. The effects of wing maneuver devices and flap deflections were accounted for incrementally to facilitate future parametric studies. Maneuver device deflection for the STAC W_2 wing entails a smooth, cylindrical, variable-camber shape change throughout the leading edge and trailing edge device areas. The resulting camber and twist substantially reduce configuration drag at sustained maneuver levels. Full deployment would give the "transonic wing normal force, pitching moment, and axial force increments." Since no aerodynamic test data were available for maneuver device deflections beyond 18° angle-of-attack, it was conservatively assumed that the maneuver device increments decayed linearly beyond 16° angle-of-attack to zero at 24° angle-of-attack. The present study, however, did not assume use of the W_2 wing, since the emphasis of the investigation was the subsonic, rather than transonic flight regime.

Leading-edge and trailing-edge flap deflections in the form of simple rotations about front and rear beam hinge lines were also available (i.e., W_1 wing with plain flap deflection). Trailing-edge flap deflections were employed symmetrically for augmented longitudinal response or differentially for roll control. Leading-edge flap deflection had a beneficial effect on linearizing the rolling moment variation with sideslip at high-angle-of-attack but also introduced an unwelcome nose-up moment. The improvement in lateral/directional characteristics was, however, considered sufficiently desirable to warrant the use of the leading edge devices, and the leading-edge flap was scheduled with angle-of-attack as shown in Figure 6-2. Flap deflection test data are available to angle-of-attack of 70 degrees and are summarized in Appendix B.

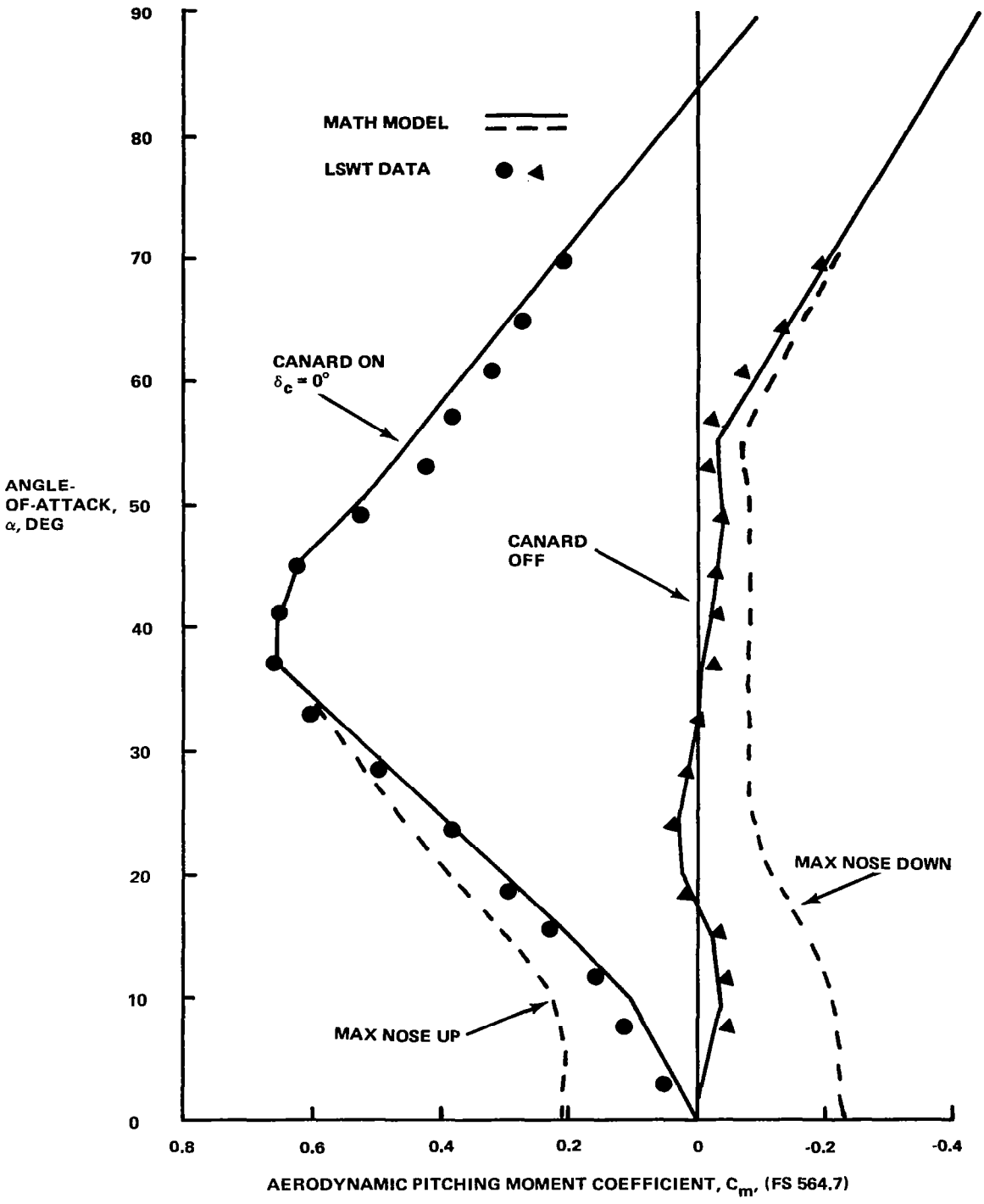

R82-1732-022(T)

Figure 6-1. - STAC pitching moment characteristics (simulated).

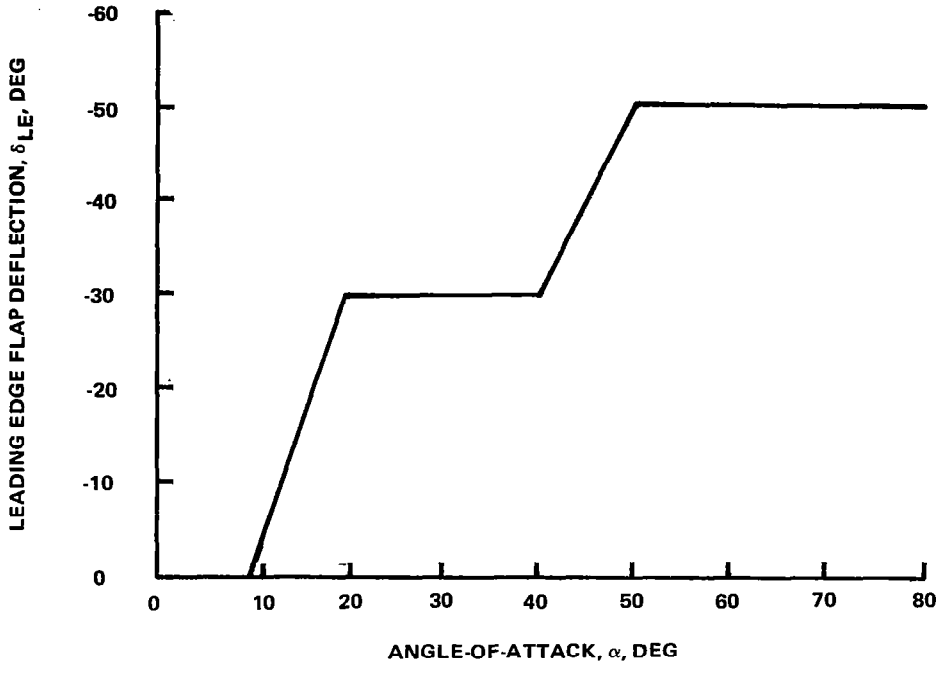

R82-1732-023(T)

Figure 6-2. - Leading edge flap deflection schedule with angle-of-attack.

6.2.2 Lateral/Directional Aerodynamic Model

Figure 6-3 shows a representative variation in STAC body axis yawing moment with angle-of-attack for $\beta = 8°$. There is the usual break in directional stability in the $\alpha = 10°$ to $15°$ region, yielding a slightly unstable value at $\alpha \simeq 20°$. At $\alpha = 25°$ there is a sharp increase in directional stability, followed by flow breakdown and the onset of fully separated flow beyond

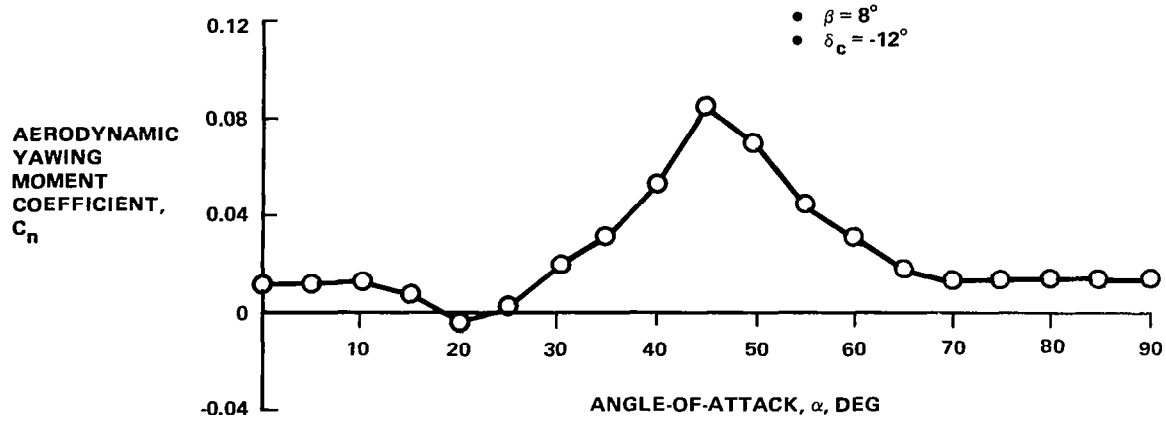

R82-1732-025(T)

Figure 6-3. - Yawing moment characteristics of simulated STAC configuration.

α = 45°. This sharp increase in stability is attributed to the "lens-shaped" forebody cross-section. Figure 6-4 depicts the STAC forebody lines and the associated cross-flow phenomenon.

Wing leading edge droop was found to stabilize the vortex flow, producing more favorable lateral stability characteristics. This effect is shown in Figure 6-5, where 30° of droop significantly "smooths out" the C_{l_β} variation at small sideslip angles.

Lateral/directional control is accomplished by ailerons for roll and rudder/differential canard for yaw. The maximum available control power versus angle-of-attack for each is presented in Figure 6-6. Good aileron control is maintained across the angle-of-attack range by providing large up-aileron deflection capability. Rudder power starts decaying at $\alpha \simeq 25°$ and is completely lost by α = 35°. Differential canard works well across the angle-of-attack range, being least effective when $\alpha \simeq 25°$ to 55°, and is blended with rudder by the AFCS. Maximum available differential canard effectiveness is dependent on the mean canard incidence for trim; the case shown is for the baseline cg location, FS 564.7.

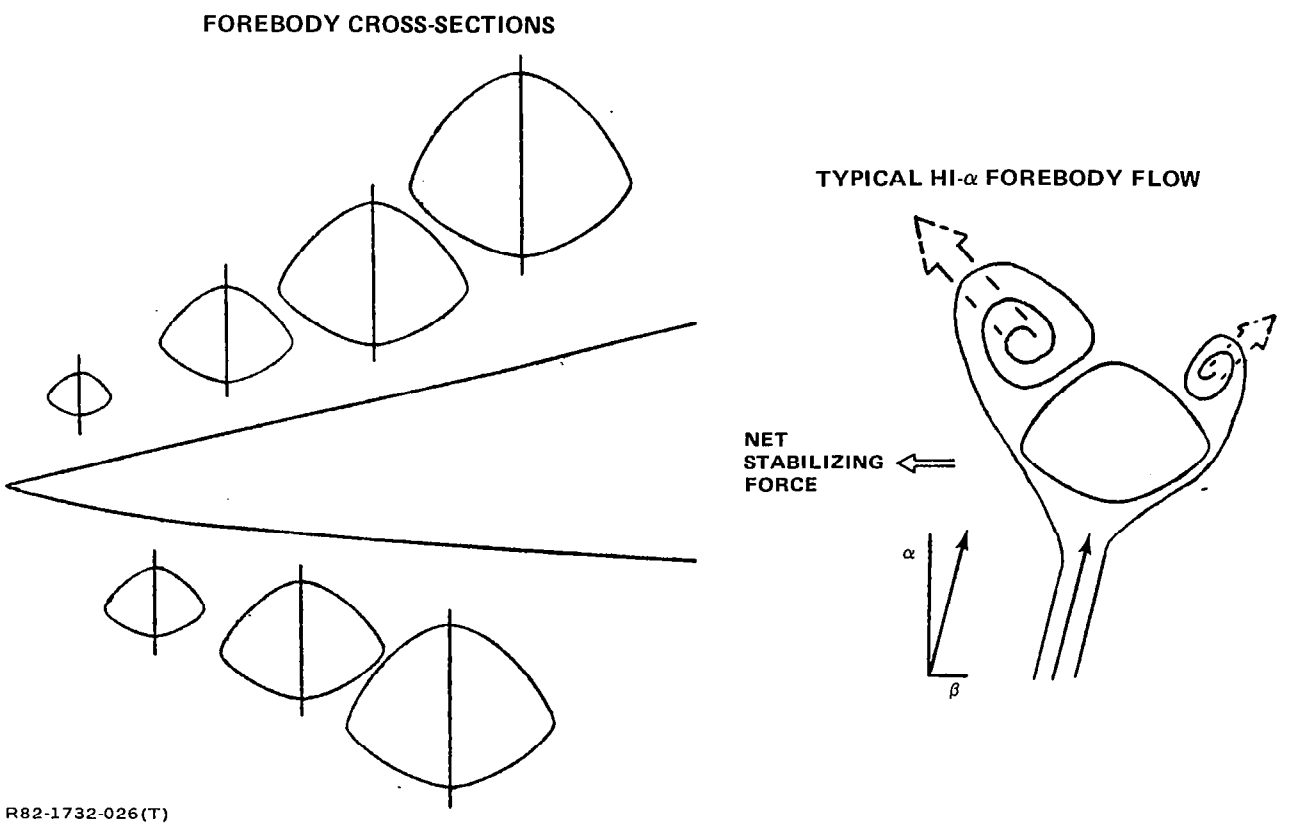

Figure 6-4. - STAC forebody flow phenomenon.

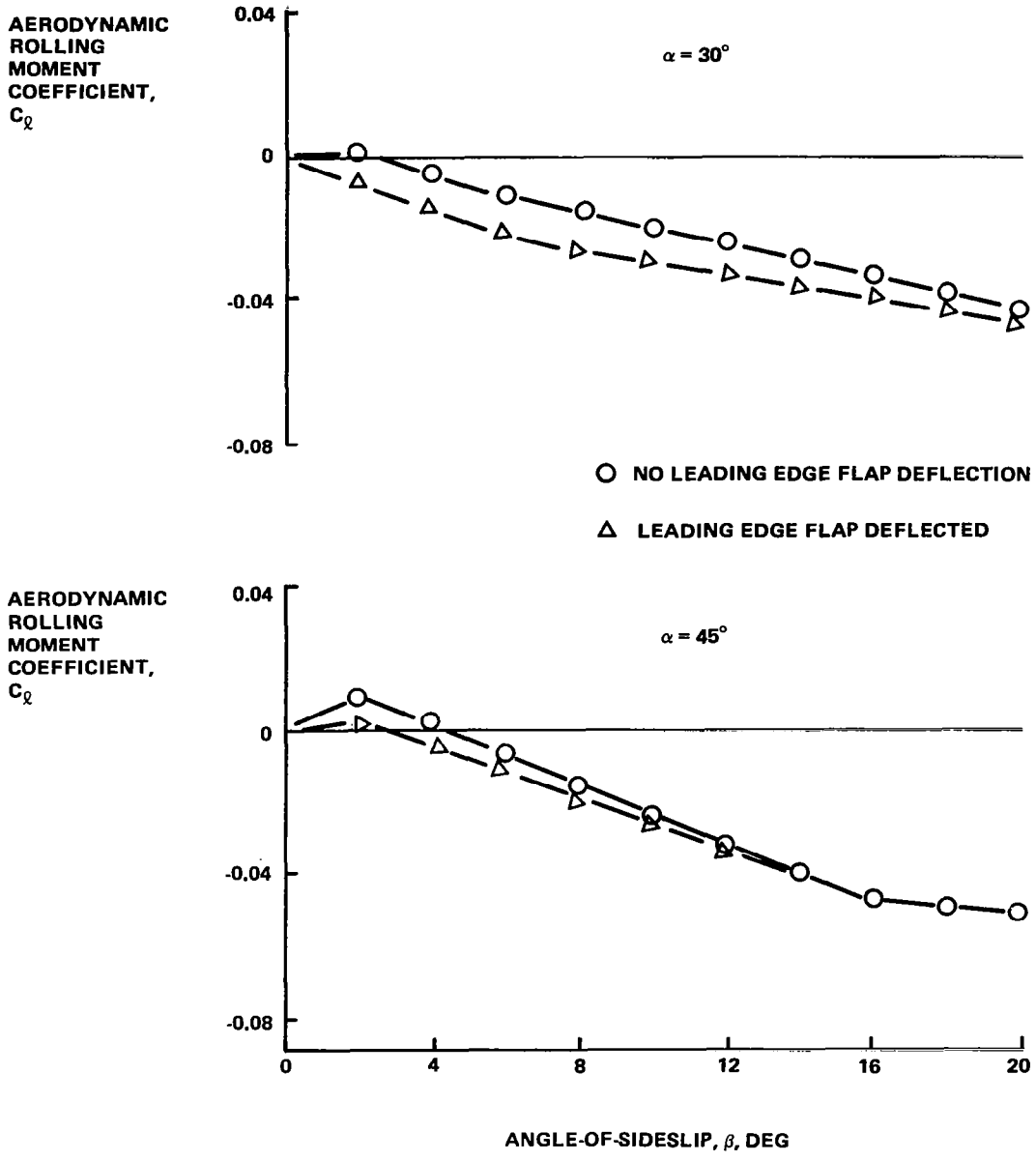

Figure 6-5. - Leading edge droop effect on rolling moment characteristics.

R82-1732-027(T)

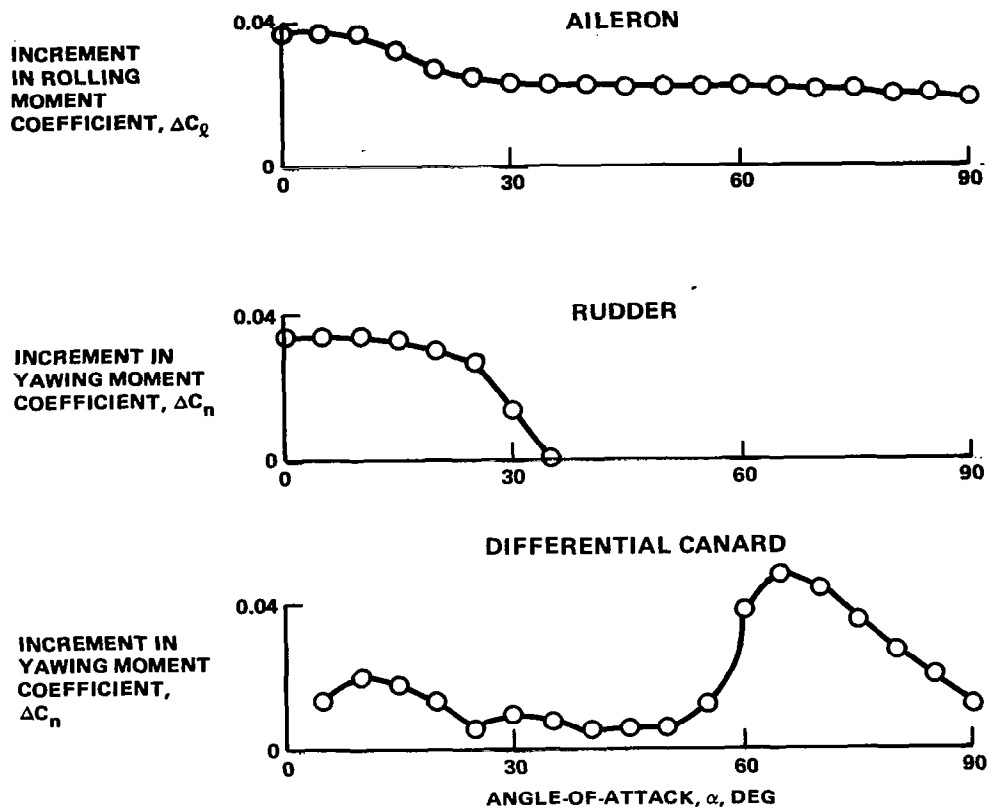

Figure 6-6. - Lateral/directional control characteristics.

7 - BASIC LONGITUDINAL CONTROL SYSTEM DESIGN AND EVALUATION

7.1 DESIGN PHILOSOPHY

The overall objective of the Control Definition Study for Advanced Vehicles was to investigate generic flight mechanics issues pertinent to a representative Relaxed Static Stability (RSS), canarded, tactical aircraft configuration. Specific concerns included:

- Aerodynamic control power requirements
- Control actuation rate requirements
- Control power augmentation requirements
- Control input limiting requirements.

Control laws were to be defined that would yield predictable flying qualities throughout the aircraft's flight envelope. Furthermore, since it was recognized that maintaining control in high-angle-of-attack flight at low speed would present the greatest challenge to control system design, a major emphasis was placed on the development of control laws that would permit aggressive Air Combat Maneuvering (ACM) to very low airspeeds while providing departure resistance.

A full authority, digital, fly-by-wire control system was assumed from the outset. The design problem was simplified by assuming the availability of noise/error-free sensors. Aircraft structural modes were also neglected. Even with these simplifications, control synthesis by design methodologies such as modern control theory was expected to yield a highly augmented airframe exhibiting "higher-order" response characteristics to control inputs. Interpreting "higher-order" responses in the context of established handling qualities criteria is, at present, an unresolved but active research problem. Although some progress has been made (e.g., "equivalent-systems" approach), these investigations have so far mostly addressed statically stable, aft-tail configurations. The extension of such response matching methods to RSS, canard configured aircraft may not be straightforward. In order to avoid these interpretive issues, a classical design approach was used to design a control law that yielded, in the pitch axis, a classical second-order response for the closed-loop short-period mode. The well-established modal parameter ranges set forth in the Military Specification for Flying Qualities of Piloted Airplanes (MIL-F-8750C, Ref. 7) were then used to establish the desired closed-loop characteristics. Residual misgivings regarding applicability of the specification made it desirable to maintain a level of flexibility in gain selection to permit substantial adjustment of the response characteristics during piloted simulations.

These considerations led to the concept of control algorithms that would compute system gains in real-time as a function of pre-computed plant characteristics, flight condition, and desired handling qualities metrics. This control law design approach is discussed in greater detail in Appendix C.

In keeping with the generic nature of this investigation, it was decided to study two fundamentally different longitudinal control laws: incremental load factor ("G") command and angle-of-attack (α) command systems. The major

emphasis, however, was on the "G" system; primarily because of its self-trimming features with the stick in detent. Whereas a "G" command system is relatively novel, the α system has historically been the more common. The differences between the two systems are described later in this report.

With the foregoing caveats in mind, it is worth returning to a discussion of the control issue concerns listed previously. In retrospect, it is clear that providing adequate longitudinal control power and sufficient actuator rates are the key issues in preventing control-induced departures of RSS aircraft. In this study, the only pitch control device investigated was the all-moving slab canard surface. Pitching moment characteristics about the reference cg for the baseline STAC aircraft were presented in Figure 6-1. (In passing, it might be noted that the pitching moment curves shown are qualitatively similar to F-16 characteristics.) Note that the STAC nose-down pitch control margin available from the canard at low α degrades with increasing angle-of-attack until the wing-body configuration breaks stable at $\alpha \simeq 55^\circ$. For $5^\circ \leq \alpha \leq 70^\circ$ the nose-up acceleration that can be imparted to the aircraft far exceeds the available nose-down recovery moment. In the $30^\circ \leq \alpha \leq 55^\circ$ range the canard nose-down capability is at a minimum. Since the intent was to develop control laws that would permit the aircraft to operate to near stall ($\alpha \simeq 35^\circ$), it was clear that this high-angle-of-attack trim condition would have to be approached at a rate commensurate with the pitch control margin available to prevent command overshoot or departure.

Given the severely limited control power available at high-angle-of-attack, canard rate restrictions were expected to have an adverse impact on departure prevention. Prior to this study, it was unclear what impact high levels of RSS might have on canard actuator rate requirements. The planned canard rate study, described below, provided added impetus to the development of a control law mechanization that would permit an evaluation of actuator rates as a function of closed-loop control system performance metrics and configuration static margin.

Control power augmentation and/or control (command) input limiting were to be considered if adequate agility/departure resistance could not be achieved within the baseline airframe/control system constraints. The possibility that one or both of these methods would become necessary required a feedback control law structure that would be unaffected by such subsequent "outer-loop" modifications.

Finally, it was recognized that aircraft such as STAC are characterized by aerodynamics which are highly nonlinear with respect to angle-of-attack (Figures 7-1 and 7-2). The data shown are for the nominal STAC configuration and were computed from the aero math model perturbed about a trim point. The canard derivatives (Figure 7-2) are particularly interesting. Note that, at $\alpha = 0^\circ$, deflection of the canard results in a pure moment about the pitch axis. Any lift produced by the canard is cancelled by downwash on the wing. Beyond $\alpha = 16^\circ$, the wing and canard are effectively uncoupled.

An approximate locus of open-loop "short period" roots with angle-of-attack is depicted in Figure 7-3. The data show that, if the designer intended to maintain uniform handling qualities, control system gains would have

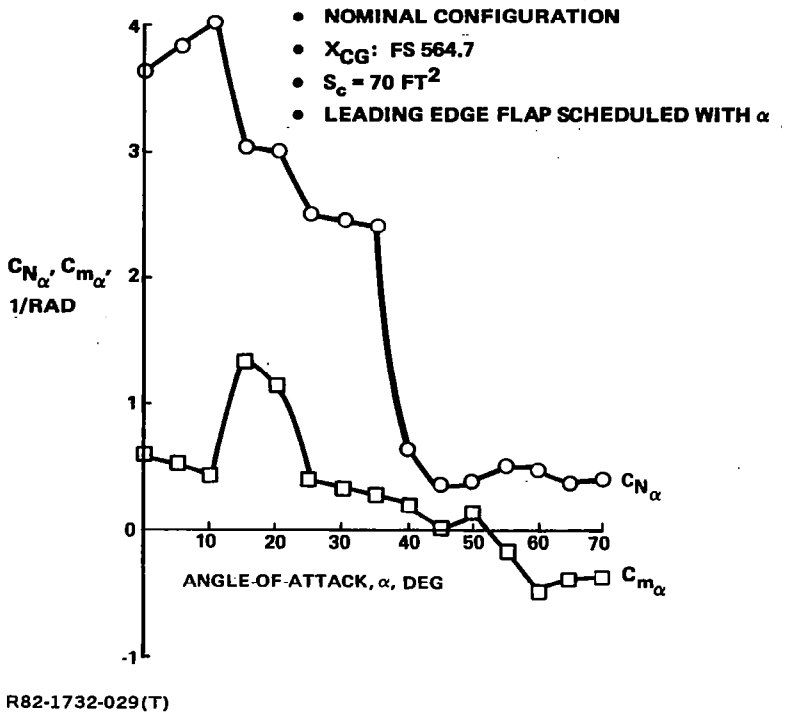

Figure 7-1. - STAC airframe normal force and pitching moment derivatives about trim vs angle-of-attack.

to be made a function of angle-of-attack. Although this approach was in fact adopted for this study, it is recognized that it may not be desirable to do so in practice.

7.2 LONGITUDINAL CONTROL LAW SYNTHESIS

A block diagram of the "G" command longitudinal control system is shown in Figure 7-4. With this system a pilot stick command results in a change in the aircraft load factor. For the stick in detent, the aircraft will, in principle, maintain 1-g flight independent of airspeed (up to the stall angle-of-attack). The throttle is used to command airspeed. At constant airspeed, a step stick input will result in a constant time rate of change of flight path angle ($\dot{\gamma}$); a pulse will result in an incremental change in flight path angle ($\Delta\gamma$). Note that the essential feedback (n_z) is biased by the term ($\cos\theta \cos\phi$). Inclusion of this bias term eliminates the need to retrim the aircraft with attitude changes. Pitch rate feedback (q) provides system damping. An integrator in the forward loop was initially included to eliminate steady state error. Its ultimate effect, however, was more complex, as described below. The bias signal labeled "CANTRM" was included to provide desired system characteristics during the canard rate study (see below). The canard actuator was modelled as a pure first-order lag with a nominal time constant τ_a = 0.05 sec. A variable canard deflection limit was programmed

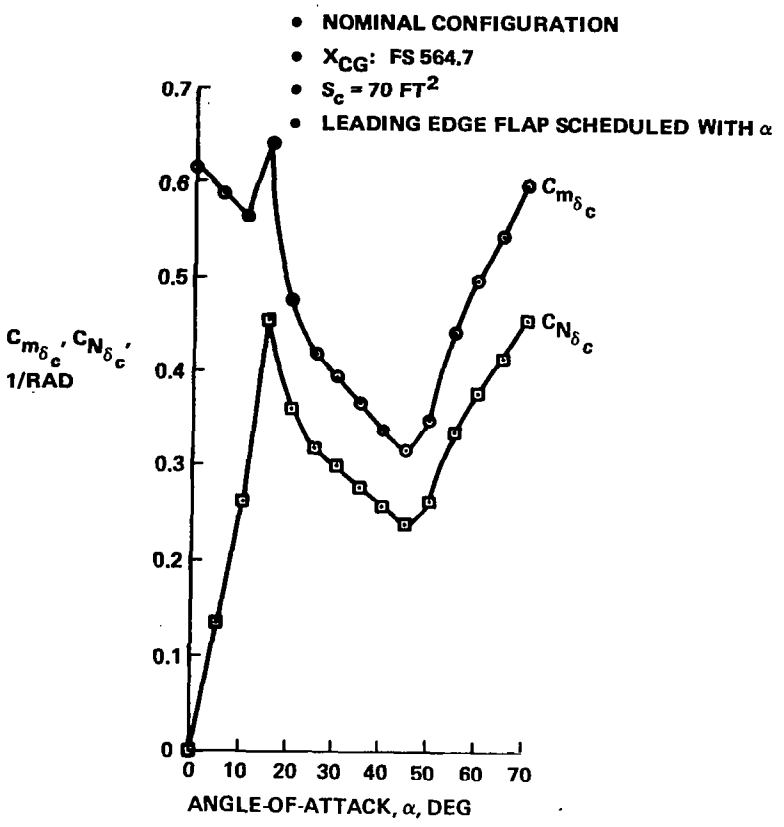

Figure 7-2. - STAC canard normal force and pitching moment derivatives about trim vs angle-of-attack.

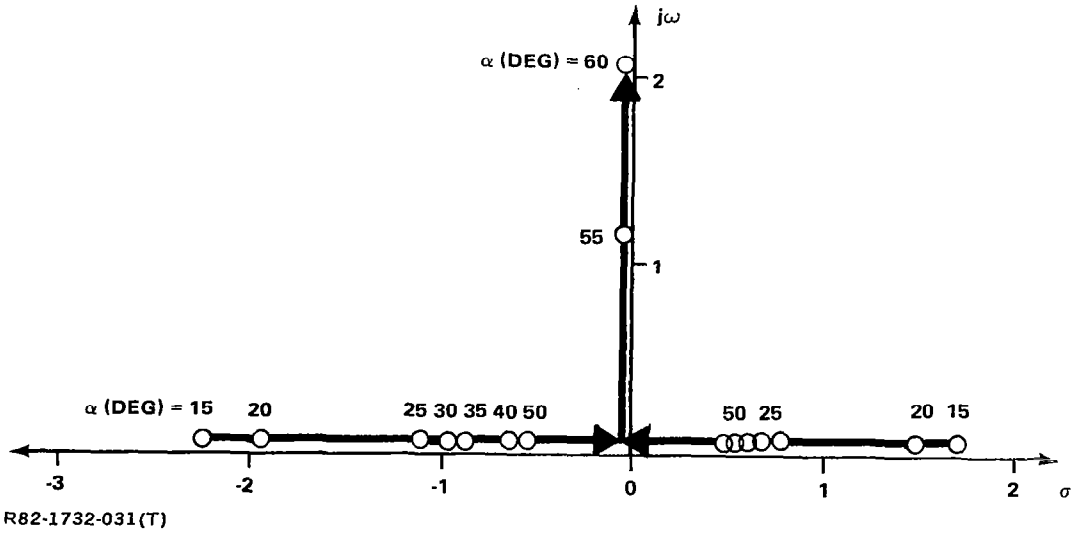

Figure 7-3. - Locus of open-loop short-period roots as a function of angle-of-attack (α) (1-G flight).

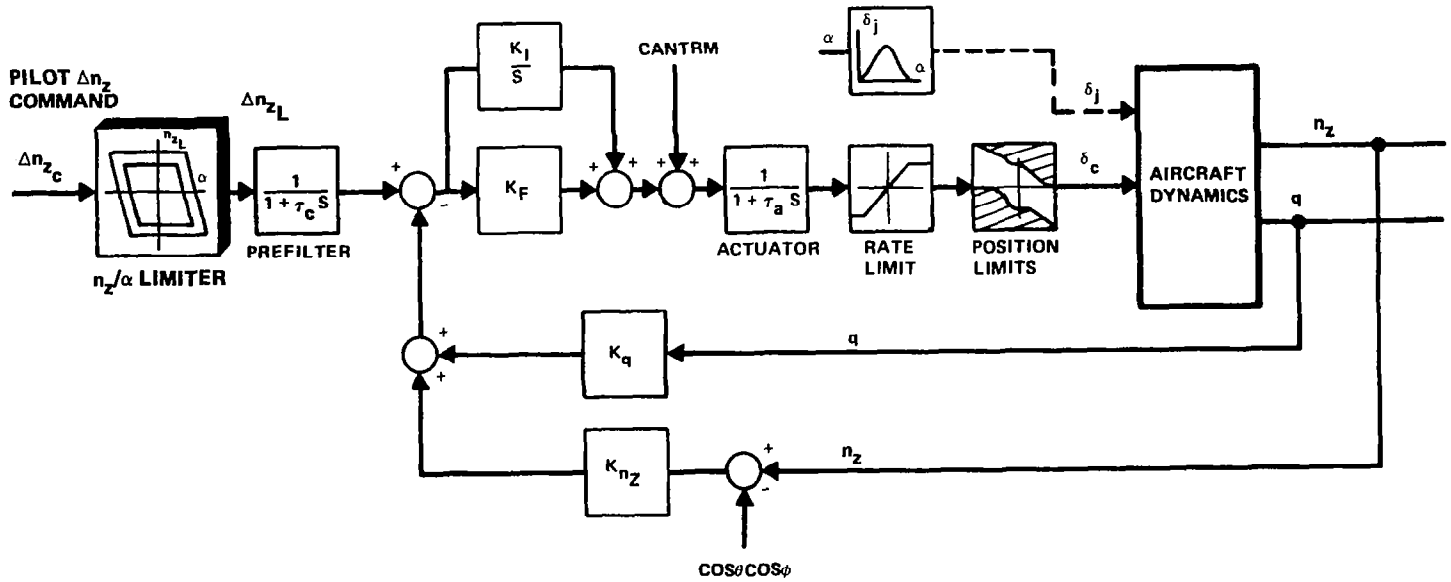

R82-1732-032(T)

Figure 7-4. - "G" command longitudinal control system.

with α in order to limit the canard deflection to its most aerodynamically effective angle (Figure 7-5). The possibility of using thrust vectoring for pitch control power augmentation was recognized as shown by the command labeled δ_j. The pilot stick command input is modified by two functions. The command $(\Delta n_z/\alpha)$ limiter is discussed in Section 9. The command prefilter, a first-order lag with variable time constant τ_c, serves to reduce canard rates for abrupt control inputs.

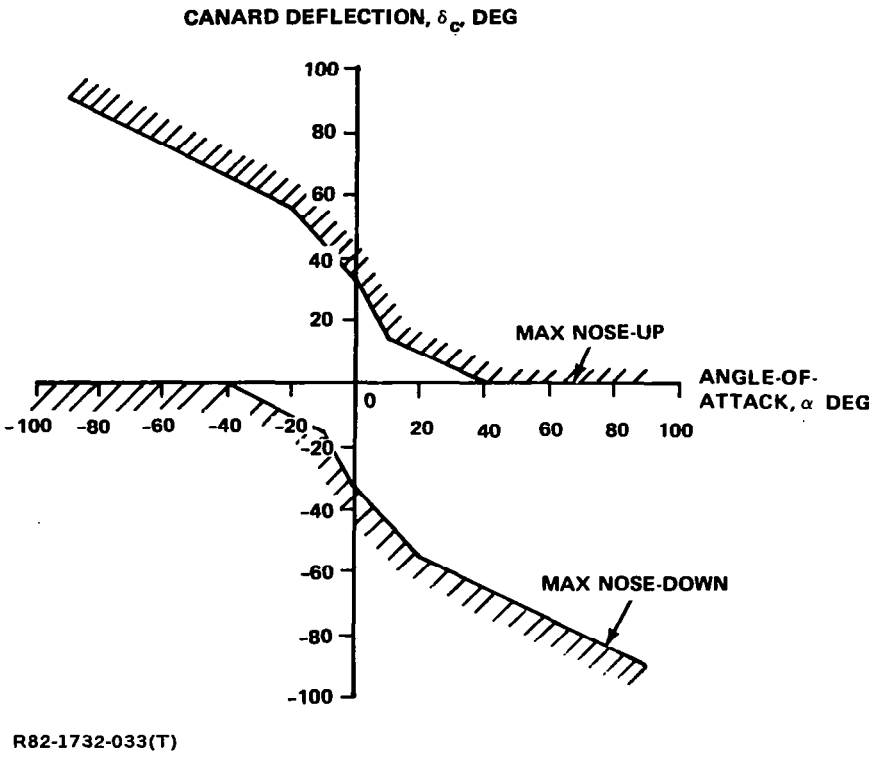

Figure 7-5. - Canard deflection limit schedule.

If the actuator, prefilter, and limiter are neglected, the approximate short-period closed-loop transfer function for this system is of the form:

$$\frac{\Delta n_z(s)}{\Delta n_{z_c}(s)} = \frac{b_3 s^3 + b_2 s^2 + b_1 s^1 + b_0 s^0}{s^3 + a_2 s^2 + a_1 s^1 + a_0 s^0} \quad . \tag{7.1}$$

One of the numerator roots is $(s + K_I/K_F)$; the other two are a conjugate pair of weakly damped, high-frequency zeros. If the denominator is factored such that one root is also $(s + K_I/K_F)$, and the high-frequency zeros are neglected, the previous transfer function is reduced to the form:

$$\frac{\Delta n_z(s)}{\Delta n_{z_c}(s)} = \frac{G'(s + K_I/K_F)(s^2 + 2\zeta\ \omega\ s + \omega^2)}{(s + K_I/K_F)(s^2 + 2\zeta_{sp}\omega_{sp}\ s + \omega_{sp}^2)}, \tag{7.2}$$

$$= \frac{G}{s^2 + 2\zeta_{sp}\omega_{sp}\ s + \omega_{sp}^2}, \tag{7.3}$$

where G, ω_{sp}, ζ_{sp} are functions of the plant characteristics, the control system gains K_F, K_I, K_{n_z}, K_q, and airspeed. If ζ_{sp} and ω_{sp} (closed-loop short period damping and frequency) are treated as parameters, and the gain G is constrained so as to yield zero steady state error, expressions can be derived for the control system gains required to yield the desired pure second-order short-period response:

$$(K_F)_g = \frac{-\omega_{sp}^2}{\left(\frac{V_0 Z_w M_\delta}{g}\right)}\left\{\frac{1 + (Z_\delta/V_0M_\delta)(K_I/K_F - 2\zeta_a\omega_a - M_q)}{1+(Z_\delta/V_0M_\delta)\left[(M_q + 2\zeta_{sp}\omega_{sp})\left(\frac{M_w Z_\delta}{M_\delta Z_w} - 1\right) - \left(\frac{V_0 M_w}{Z_\delta}\right) - \left(\frac{\omega_{sp}^2}{Z_w}\right)\right]}\right\} \tag{7.4}$$

$$(K_q)_g = \frac{2\zeta_{sp}\omega_{sp} - 2\zeta_a\omega_a + K_I/K_F - Z_\delta\left(\frac{(K_F)_g}{g}\right)\left(M_q + 2\zeta_{sp}\omega_{sp}\right)}{(K_F)_g M_\delta\left[1 - (Z_\delta/V_0M_\delta)(M_q + 2\zeta_{sp}\omega_{sp})\right]} \tag{7.5}$$

$$K_{n_z} = 1 - (K_q)_g\ (g/V_0) \tag{7.6}$$

and

$$\left(\frac{K_I}{K_F}\right)^2 - 2\zeta_a\omega_a\left(\frac{K_I}{K_F}\right) + \omega_a^2 = 0 \tag{7.7}$$

Here the quantities ω_a^2 and $2\zeta_a\omega_a$ represent the open-loop short period as approximated by:

$$2\zeta_a\omega_a \simeq -Z_w - M_q, \tag{7.8}$$

$$\omega_a^2 \simeq Z_w M_q - V_0 M_w\ . \tag{7.9}$$

Several points regarding these expressions should be noted. Only the positive root of the quadratic in (K_I/K_F) is meaningful, since the forward-loop gains must be positive. In implementing a digital gain computing algorithm, (K_I/K_F) is determined first; the computation of K_F, K_q, K_{n_z}, and K_I follow in sequence. The algorithm is highly generalized. Depending on the desired fidelity of the second-order short period response, the stability derivatives that appear can either be held as constants or stored and used as a function of angle-of-attack, aircraft loading, Mach Number, etc. For this investigation, non-dimensional stability derivatives were stored in tables as a function of angle-of-attack (e.g., Figure 7-1 and 7-2), and the dimensional derivatives were computed continuously as flight conditions changed. Note also that the canard normal force contribution (Z_δ) is included in the gain expressions - this effect was determined to be important to achieving high fidelity short period model-following even at moderate angles-of-attack.

The angle-of-attack (α) command longitudinal control system shown in Figure 7-6 is functionally identical to the "G" command system. Note, however, that the bias term $\frac{g}{V_0}(\cos\theta\cos\phi)$ is applied to the pitch rate, yielding, in effect, a "washed-out" pitch rate feedback. The α system gains are computed as for the "G" system:

$$(K_F)_\alpha = \frac{\omega_{sp}^2 V_0}{(V_0 M_\delta - Z_\delta M_q)} , \tag{7.10}$$

$$(K_q)_\alpha = \frac{2\zeta_{sp}\omega_{sp} - 2\zeta_a\omega_a + K_I/K_F - Z_\delta \left(\frac{(K_F)_\alpha}{V_0}\right)}{(K_F)_\alpha M_\delta \left[1 - \frac{Z_\delta \left(M_w Z_\delta - Z_w M_\delta\right)}{M_\delta \left(V_0 M_\delta - Z_\delta M_q\right)}\right]} , \tag{7.11}$$

$$K_\alpha = 1 + (K_q)_\alpha V_0 \frac{M_w Z_\delta - Z_w M_\delta}{V_0 M_\delta - Z_\delta M_q} . \tag{7.12}$$

The computation of (K_I/K_F) is as above (Eq 7.7).

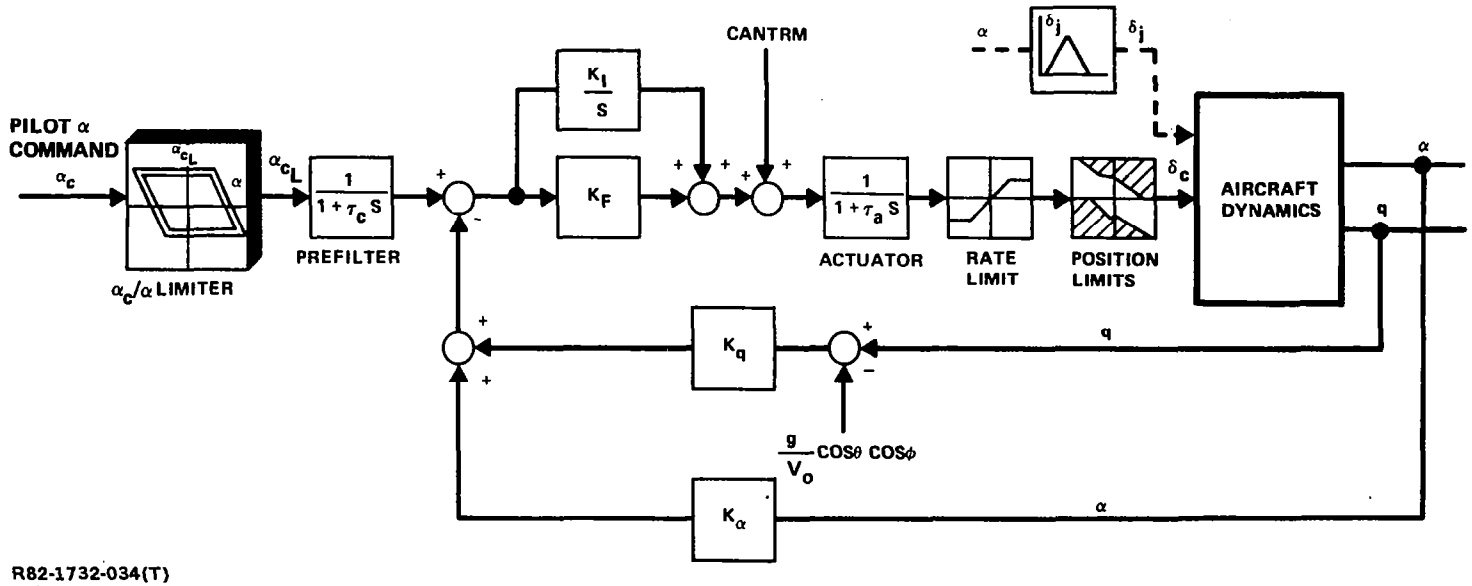

Figure 7-6. - "α" command longitudinal control system.

Although the angle-of-attack system differs from the "G" command insofar as the effect of pilot commands (airspeed controlled by the stick; rate-of-climb, by throttle), the control loop structure is similar. Note that, to first order,

$$(K_F)_\alpha \simeq n_{z_\alpha} (K_F)_g, \tag{7.13}$$

$$(K_q)_\alpha \simeq (K_q)_g / n_{z_\alpha} \quad , \tag{7.14}$$

and

$$K_\alpha \simeq K_{n_z}, \tag{7.15}$$

where

$$n_{z_\alpha} \equiv \frac{-Z_w V_0}{g}. \tag{7.16}$$

Thus, the essential feedbacks carry the same gain, and the forward loop and pitch rate gains differ by n_{z_α}, as might be expected.

7.3 LONGITUDINAL CONTROL LAW EVALUATION

7.3.1 Basic Response

A typical time history of the STAC aircraft response for a positive step stick input with the "G" command longitudinal control system is shown in Figure 7-7. The simulation was for a constant-speed case (M = 0.4, sea level). Note the cyclic response of the canard, typical of statically unstable vehicles. Following the initial trailing-edge-down excursion required to initiate motion for a positive incremental load factor command, the canard drives to a recovery trim deflection more negative (trailing edge up) than that required to trim the initial (lower) angle-of-attack.

The same characteristic canard deflection signature is apparent if a step command is applied to the α system. Typical responses of the two systems are compared in Figure 7-8. Of particular note is the long-term aircraft response following removal of the step command. Whereas the aircraft with the α system enters a classical Phugoid oscillation, there is an absence of speed stability with the "G" system. Angle-of-attack diverges as the control system attempts to maintain 1-g flight with the aircraft decelerating in a climb. Early in this study a limited authority autothrottle was mechanized to mask the speed divergence of the "G" system. This modification was abandoned when adverse pilot comments were noted during preliminary piloted simulation. The evaluation pilots were particularly reluctant to accept automatic power reduction during diving maneuvers in ACM.

In the discussion that follows, the Control Anticipation Parameter (CAP) is used as a response metric in lieu of the short-period frequency (ω_{sp}). CAP is classically defined as the ratio of the initial aircraft pitch accel-

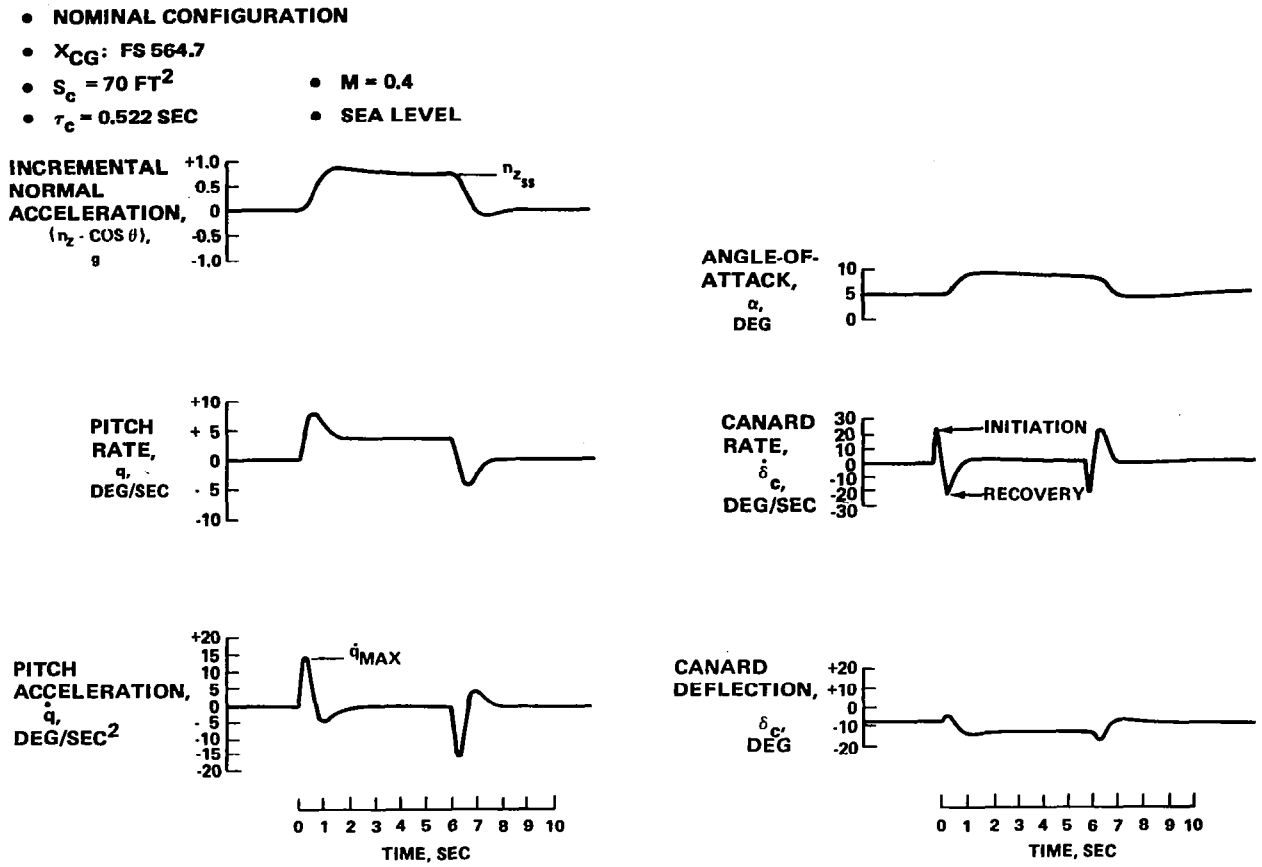

R82-1732-035(T)

Figure 7-7. - Typical "G" command system response to a step command input.

eration to the steady-state load factor following a step input at the elevator. For a stable aircraft it can be shown that CAP is a measure of the short-period frequency:

$$\omega_{sp} \simeq \sqrt{CAP \cdot n_{z_\alpha}} \tag{7.17}$$

For a statically unstable aircraft a step input at the elevator (or canard) would, of course, result in divergence. For this study, therefore, the classical definition of CAP was modified; CAP is defined herein as the ratio of the maximum pitch acceleration to steady-state incremental load factor for a step stick input. Note that the maximum pitch acceleration shown in Figure 7-7 occurs not at t = 0 (as in the classical case) but some time Δt after the command. This additional time delay introduces another handling qualities parameter.

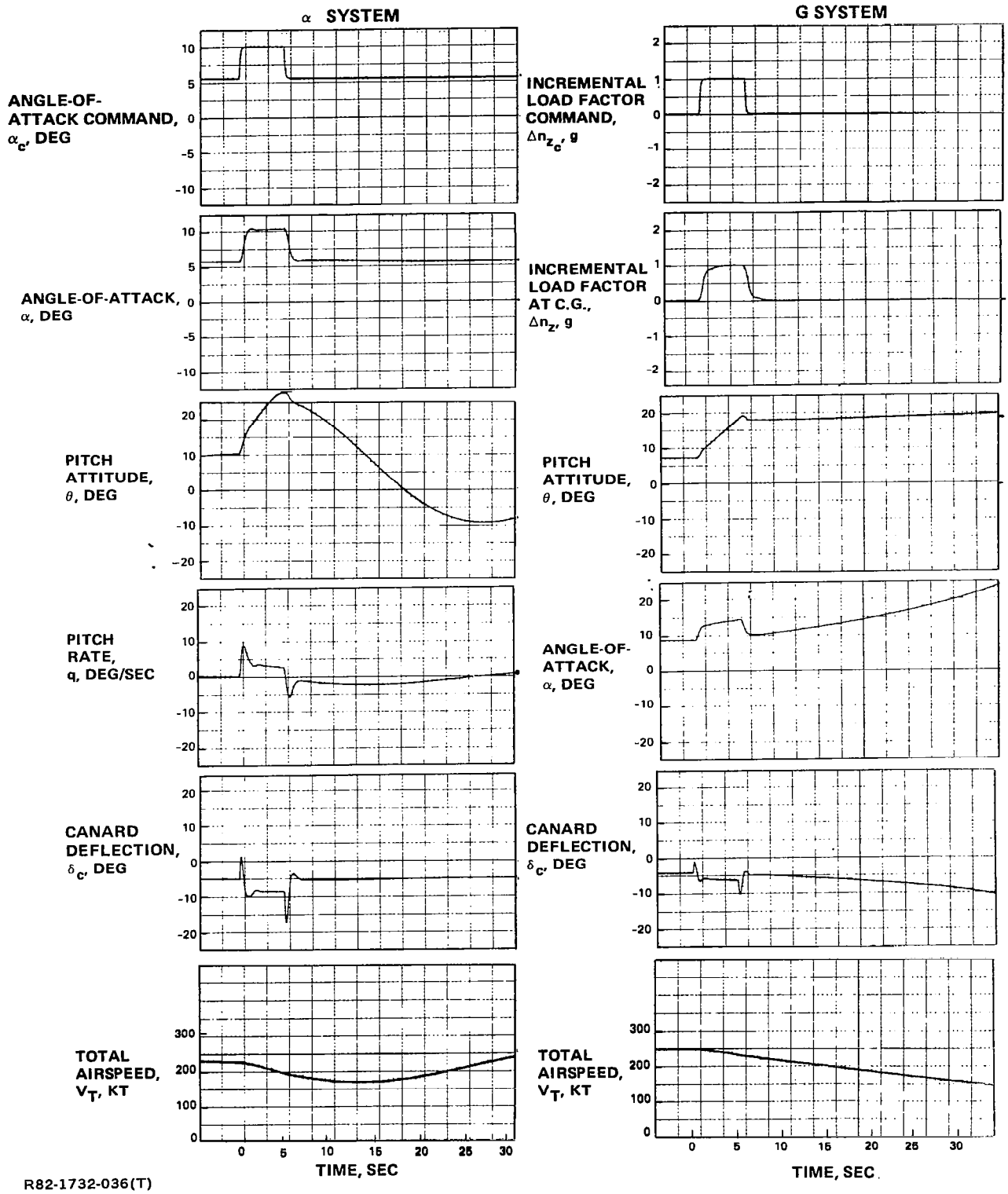

Figure 7-8. - Comparison of angle-of-attack (α) and "G" command longitudinal control laws.

7.3.2 Canard Rate and Deflection Requirement Study

For a statically stable vehicle saturation of the primary pitch control surface either in position or rate will, at worst, lead to a sluggish but convergent response to a pitch command. For a statically unstable vehicle sustained saturation during "recovery" (as defined in Figure 7-7) can lead to departure in pitch. These considerations prompted the canard rate requirement study. The question was: How are canard rates affected by aircraft static margin, canard power, and closed-loop short period frequency and damping levels?

Total aircraft static margin can be varied by:

1. A cg shift, which changes the aircraft static margin and, to some extent, canard pitch power;

2. A change in canard area, which changes canard power and aircraft static margin but not wing-body static margin.

Note that the increase in canard control power associated with an aft cg shift (Method 1) is not proportional to the increase in geometric arm since the wing and canard are aerodynamically close-coupled. Recall that, for the STAC configuration, the downwash on the wing at $\alpha = 0°$ exactly offsets the normal force increment due to canard deflection. Care must be exercised in formulating the aerodynamic math model if this effect is to be properly simulated in parametric static margin studies.

The canard rate requirement study was conducted with a modified "G" command law. The major modification was elimination of the forward loop integrator (the $\Delta n_z/\alpha$ limiter had not yet been developed). The integrator was removed in order to eliminate as many system lags as possible. For the same reason, the canard actuator time constant was set for a very rapid response ($\tau_a = .005$ sec). Since the forward-loop gain was not readjusted, removal of the integrator caused a steady-state error to remain following the transient. This error was removed by including the bias term "CANTRM" (see Figure 7-4), a precomputed approximate canard trim deflection angle programmed with angle-of-attack. The control system was tested to ensure that, with the prefilter time constant $\tau_c = 0$, the gain algorithm would permit independent control of closed-loop frequency and damping. Time history results of this verification exercise are presented in Figure 7-9. The gain algorithm input (commanded) values of CAP_c (implying ω_{sp}) were varied from 0.4 to 1.0 (within the Level 1 range of MIL-F-8785C), and the desired closed-loop short period damping ratio was set to $\zeta_{sp} = 0.3$ and $\zeta_{sp} = 0.7$. Figure 7-10 presents additional data in reduced form. As can be seen, the desired performance was achieved.

In the canard rate requirement study the following levels of the control system performance metrics were used as inputs to the gain computing algo-

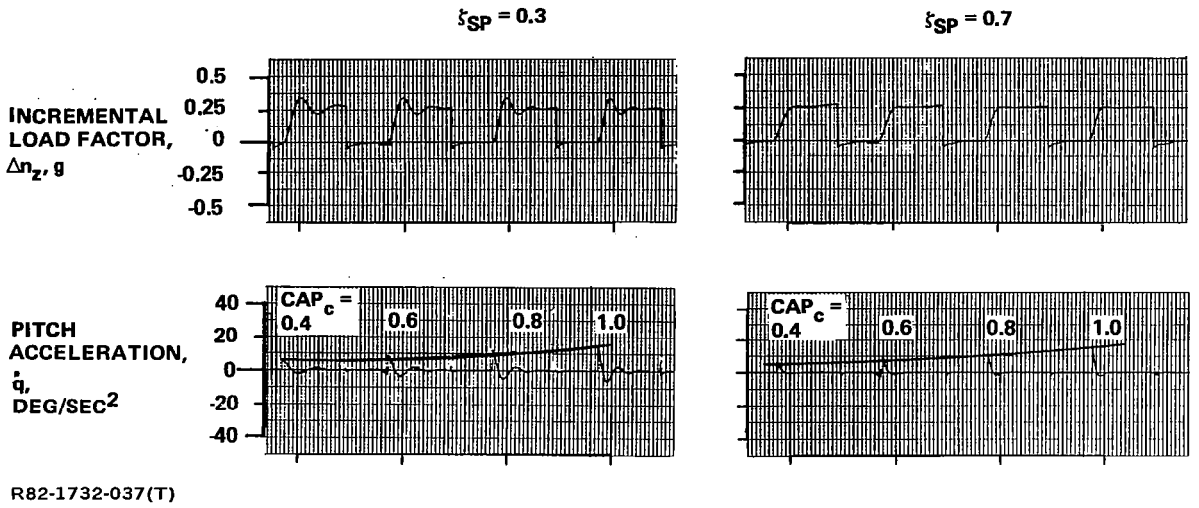

Figure 7-9. - Implicit model following: "G" command longitudinal control system.

rithms: ζ_{sp} = 0.3, 0.5, 0.7; CAP_c = 0.4, 0.6, 0.8, 1.0, 1.5, 2.0. Aircraft wing-body static margin and canard size were varied as shown (see Figure 7-11) by the matrix of simulation test points (and the resulting low-angle-of-attack aircraft static margin). The fifth study parameter, the prefilter time constant, was set to values of τ_c = 0, 0.05, 0.1, 0.25 sec. All runs were made for M = 0.4, sea-level initial conditions. The command was a 0.25 g step stick input. The study results are thus applicable to the linear, low-angle-of-attack range; significant extrapolation to higher angles-of-attack (input step magnitudes) is not valid. Complete results of the canard rate requirement study are presented in Appendix D.

Canard rates for initiation with τ_c = 0 are plotted in Figure 7-12. Measured values of CAP are on the abscissa (CAP_A), and actual peak canard rates at initiation, $\dot{\delta}_{c_i}$, are on the ordinate. Note that the impressed damping ratio ζ_{sp} has negligible effect on initiation rates. Similarly, peak canard deflection during initiation is insensitive to ζ_{sp}, but appears linear in CAP_A (Figure 7-13). These conclusions are supported by multiple linear regression analyses (Tables 7-1 and 7-2).

If the integrator gain is set at K_I = 0, and the normal force contribution of the canard is neglected (Z_δ = 0), the following transfer function for the canard rate due to a stick command input can be derived:

$$\frac{\dot{\delta}_c(s)}{\Delta n_{z_c}(s)} = \frac{K_F s\,(s^2 + 2\zeta_a\omega_a\, s + \omega_a{}^2)}{s^3(\tau_a) + s^2(\tau_a 2\zeta_a\omega_a + 1) + s(\tau_a\omega_a{}^2 + 2\zeta_{sp}\omega_{sp}) + (\omega_a{}^2 + \omega_{sp}{}^2)} \quad (7.17)$$

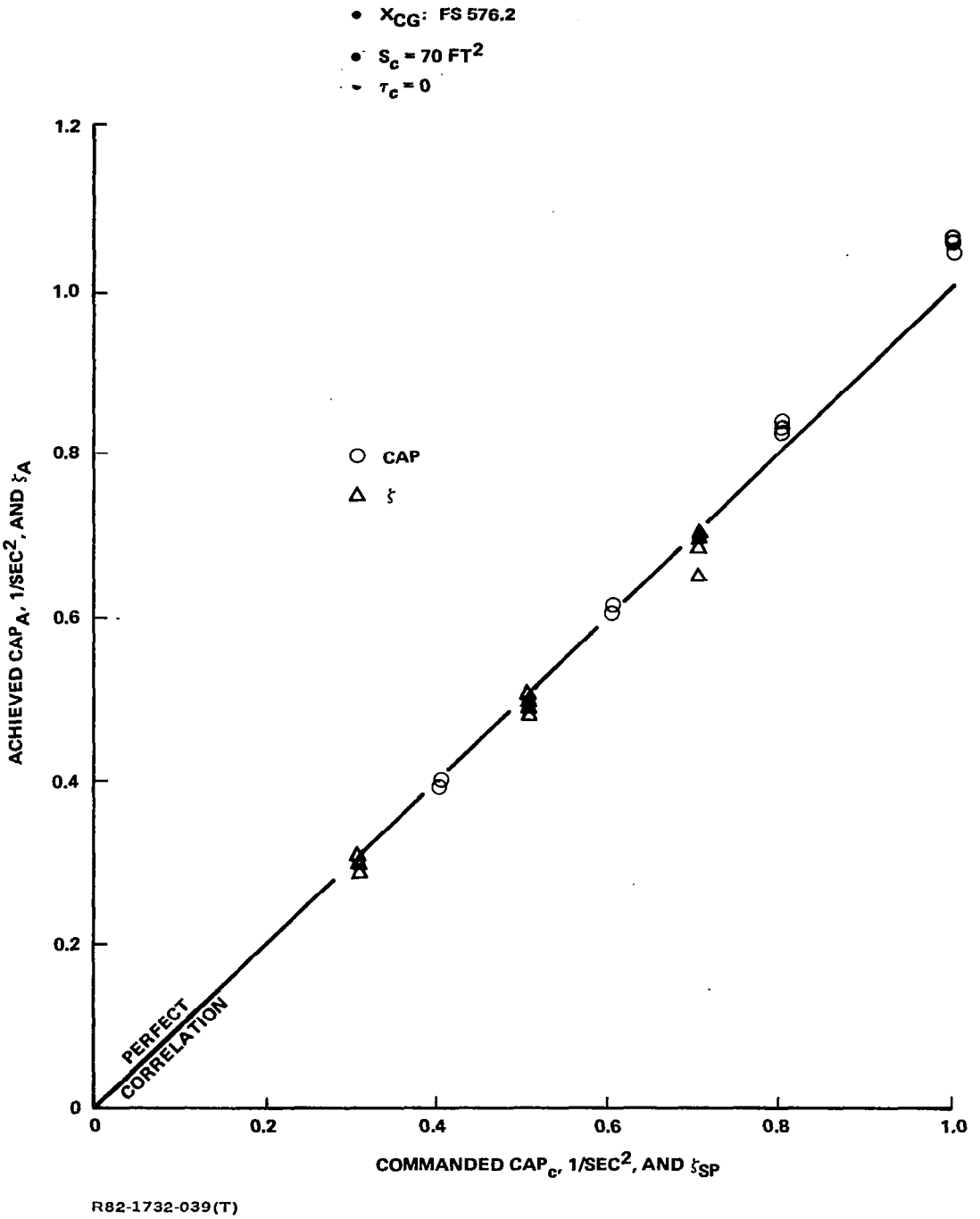

Figure 7-10. - CAP_A and ζ_A (achieved) vs CAP_c and ζ_{sp} (commanded).

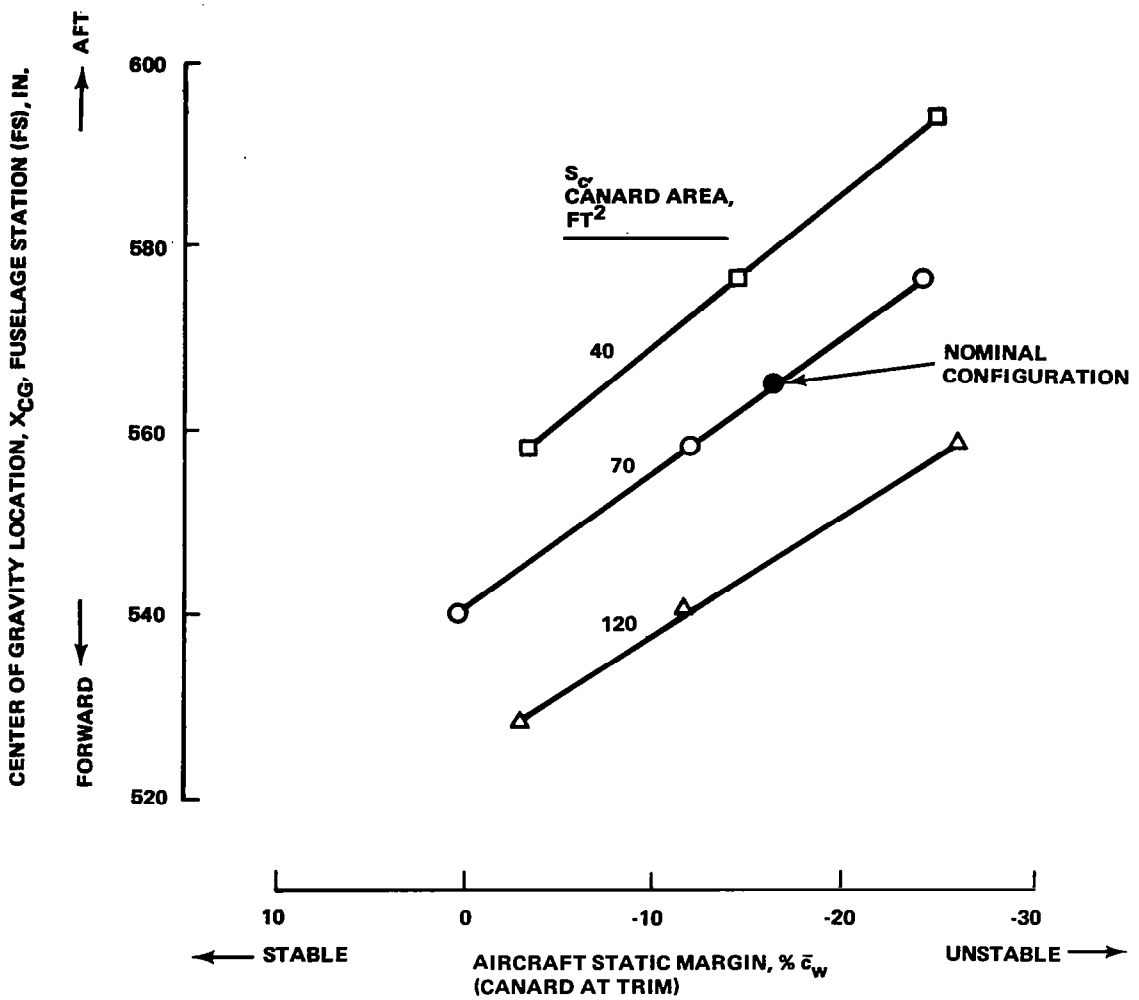

R82-1732-040(T)

Figure 7-11. - Center of gravity location/canard surface area matrix for canard deflection/rate requirements study.

For a pure step input, the initial value theorem yields:

$$\dot{\delta}_c(t = 0^+)_{1g\ step} = \frac{K_F}{\tau_a} = \frac{-\omega_{sp}^2}{\left(\frac{V_o Z_w M_\delta \tau_a}{g}\right)} = \frac{\omega_{sp}^2}{n_{z_\alpha} M_\delta \tau_a} = \frac{CAP_c}{M_\delta \tau_a} \quad . \tag{7.18}$$

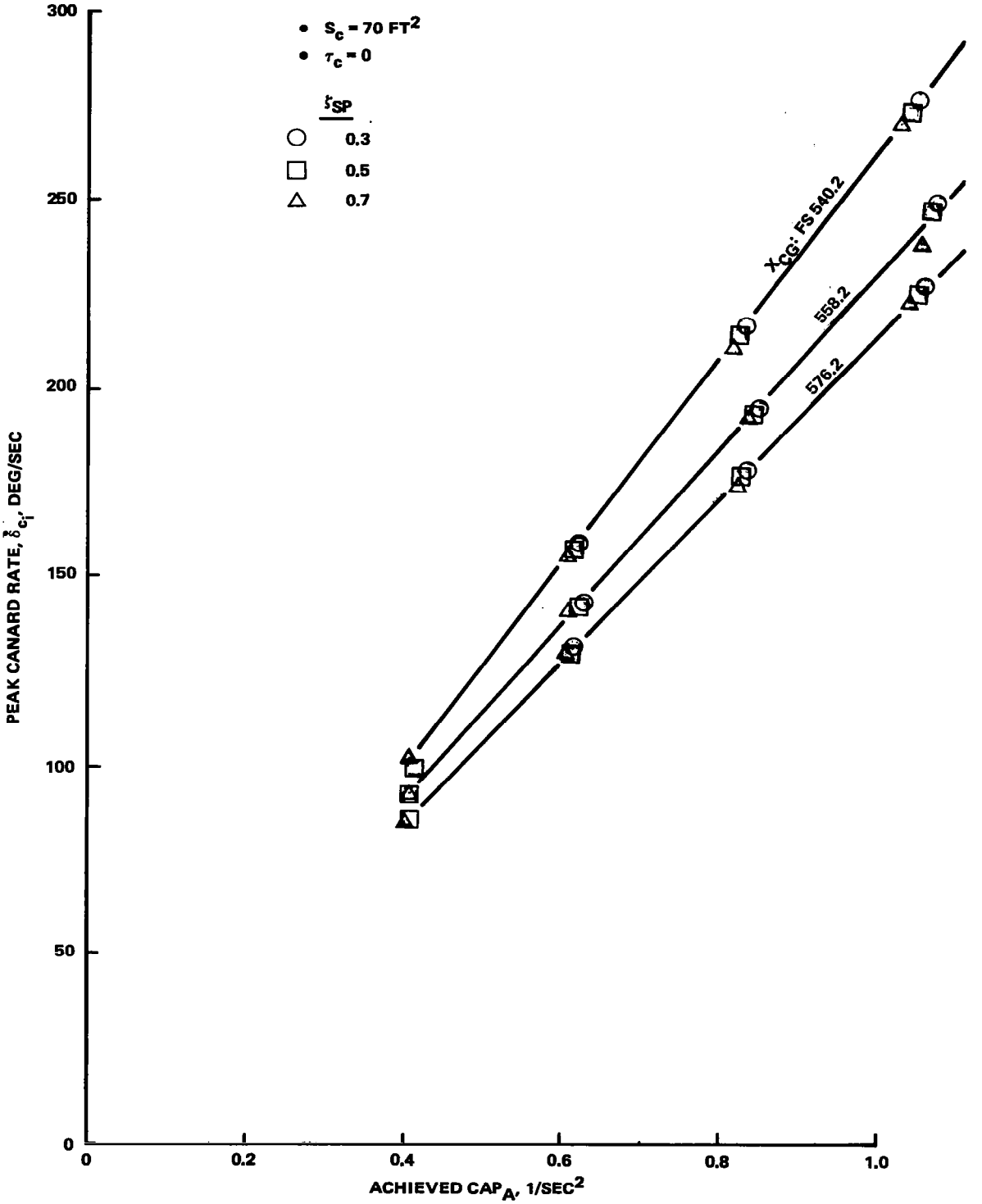

R82-1732-038(T)

Figure 7-12. - Peak canard rate for motion initiation, $\dot{\delta}_{c_i}$, vs achieved CAP$_A$.

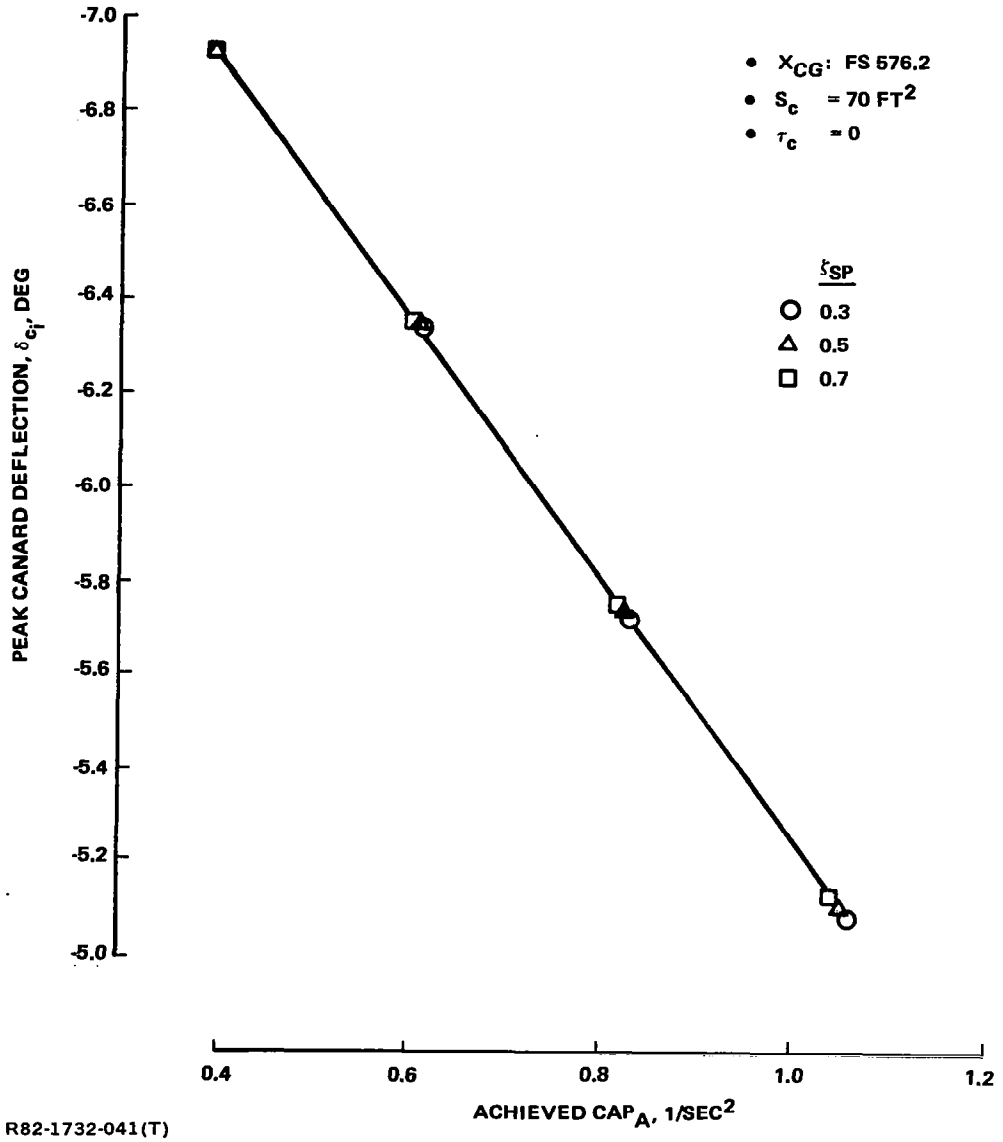

Figure 7-13. - Peak canard deflection for motion initiation, δ_{c_i} vs achieved CAP$_A$.

TABLE 7-1. - PEAK CANARD RATE FOR MOTION INITIATION.

$$\dot{\delta}_{c_i} = a_o + a_1 \zeta_{SP} + a_2 CAP_A \text{ (DEG/SEC)}$$

$$\tau_c = 0$$

S_c, FT^2	X_{CG}, FS (IN.)	X_{CG} % $\bar{c}_w$	SM, % $\bar{c}_w$	a_o	a_1	a_2	R^2
40	558.2	23	- 3.3	-15.44	7.78	416.33	0.9998
40	576.2	33	-14.6	- 1.43	2.04	371.62	1.0000
40	594.2	43	-25.0	- 0.41	6.79	358.02	0.9995
70	540.2	13	0.5	-10.62	1.03	271.92	1.0000
70	558.2	23	-11.8	2.08	-4.84	229.72	0.9997
70	576.2	33	-24.2	- 1.32	0.19	215.32	1.0000
120	528.2	6	- 2.9	- 3.16	-1.74	166.50	0.9997
120	540.2	13	-11.8	- 2.14	0.40	152.31	1.0000
120	558.2	23	-26.4	- 1.26	-0.23	138.22	1.0000

R82-1732-042(T)

TABLE 7-2. - PEAK CANARD DEFLECTION FOR MOTION INITIATION.

$$\delta_{c_i} = a_o + a_1 \zeta_{SP} + a_2 CAP_A \text{ (DEG)}$$

$$\tau_c = 0$$

S_c, FT^2	X_{CG}, FS (IN.)	X_{CG}, % $\bar{c}_w$	SM, % $\bar{c}_w$	a_o	a_1	a_2	R^2
40	558.2	23	- 3.3	- 2.96	0.01	5.49	0.9999
40	576.2	33	-14.6	- 8.37	0.01	4.90	1.000
40	594.2	43	-25.0	-13.47	0.03	4.67	1.000
70	540.2	13	0.5	- 1.11	0.00	3.53	1.000
70	558.2	23	-11.8	- 4.78	0.00	3.05	1.000
70	576.2	33	-24.2	- 8.08	0.02	2.81	1.000
120	528.2	6	- 2.9	- 1.89	0.00	2.17	1.000
120	540.2	13	-11.8	- 3.60	0.00	2.00	1.000
120	558.2	23	-26.4	- 5.91	0.00	1.82	1.000

R82-1732-043(T)

If the time constant of the actuator (τ_a) in this expression is taken to be an effective lag, say τ_e, of the simulated system (including the lags associated with digital sampling),

$$\dot{\delta}_c\ (t = 0^+)_{1g\ step} = \frac{CAP_c}{M_\delta \tau_e} \cdot \tag{7.19}$$

Thus, for $\tau_c = 0$, the canard initiation rates should depend only on the short period frequency, the pitch control power of the canard, and the equivalent lag of the simulated system (the lag time constant should be a system invariant).

This premise was examined by computing τ_e for all simulated cases (matrix of X_{cg} and S_c) using values of M_δ computed from the aerodynamic math model at initial trim. Results of the computation are presented in Table 7-3. The linear regression constant a_2 from Table 7-1 was used to represent $(\dot{\delta}_{c_i}/CAP_c)$. (For $\tau_c = 0$, the data show that $CAP_A \approx CAP_c$).

TABLE 7-3. - DETERMINATION OF EQUIVALENT SYSTEM LAG τ_e.

$\tau_c = 0$
$\Delta n_{z_c} = 0.25$ g

S_c, FT^2	X_{CG}, FS (IN.)	$(\dot{\delta}_{c_i}/CAP_c)$, DEG-SEC	M_δ, 1/SEC^2	$1/\tau_e$, 1/SEC
40	558.2	416	2.39	17.35
40	576.2	372	2.54	16.49
40	594.2	358	2.61	16.31
70	540.2	272	3.55	16.85
70	558.2	230	4.08	16.38
70	576.2	215	4.44	16.66
120	528.2	167	5.81	16.93
120	540.2	152	6.31	16.74
120	558.2	138	6.95	16.74
			AVERAGE:	16.72
			$\therefore \tau_e \cong 0.0598$ SEC FOR $\Delta n_{z_c} = 0.25$ g	

R82-1732-044(T)

If the canard rate response is assumed linear with respect to the magnitude of the command, an expression for the initial peak rate is given by:

$$\dot{\delta}_{c_i} = \frac{CAP_c \, \Delta n_{z_c} \quad (57.3)}{M_\delta \tau_e} \quad \text{(deg/sec)}. \qquad (7.20)$$

where $\tau_e = 0.015$ sec for this simulation. Using this model to predict canard initiation rates results in the correlation shown in Figure 7-14. Note that the simplified expression is accurate within ±5%.

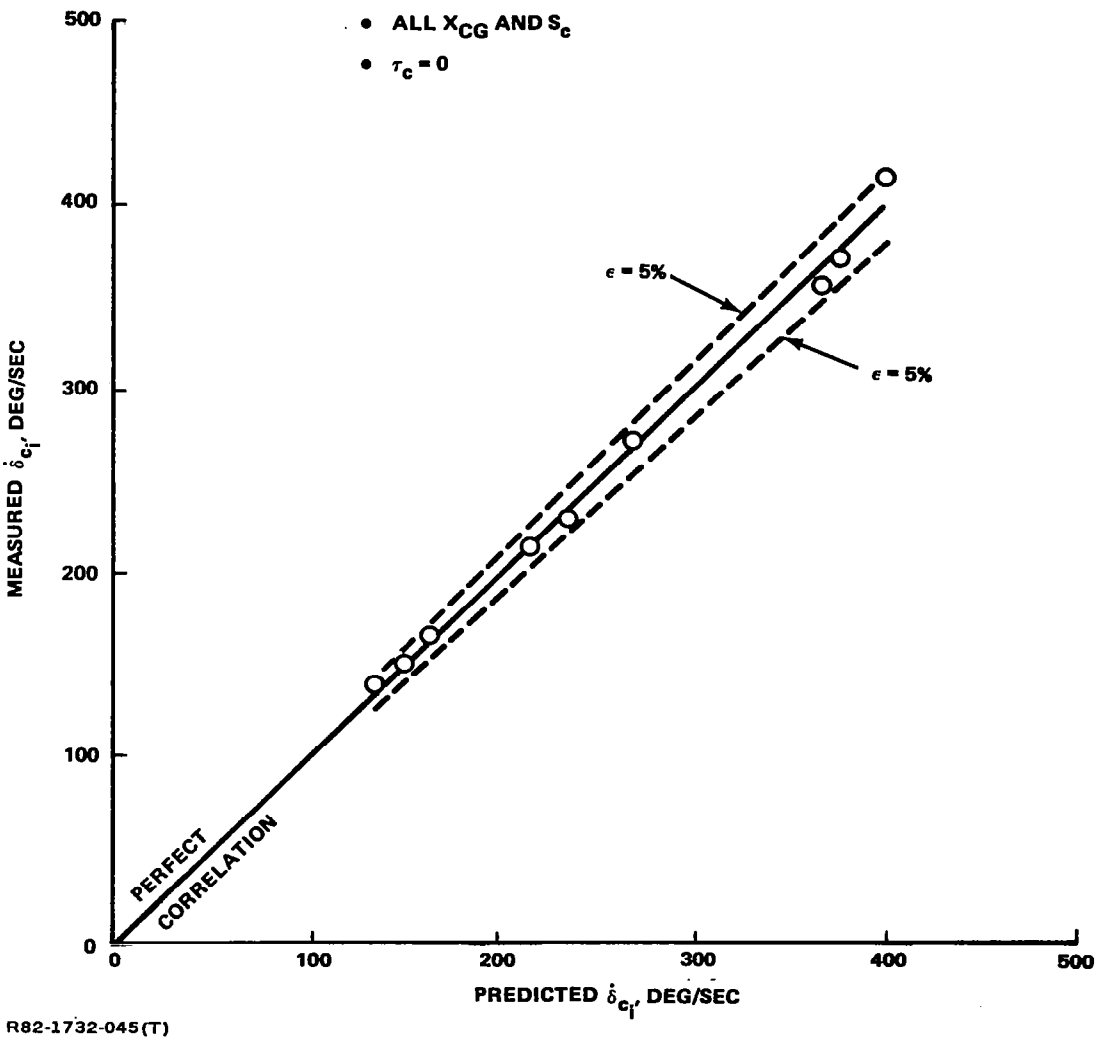

Figure 7-14. - Correlation of actual and predicted peak canard rate for motion initiation.

As the prefilter time constant is increased from $\tau_c = 0$, achieved CAP_A levels fall below the CAP_c values input to the gain computing algorithm. The initial canard rates, however, remain linearly correlated with CAP_c, with the slope $\dot{\delta}_{c_i}$ CAP_c a function of cg position and τ_c but nearly independent of the impressed closed-loop damping ratio ζ_{sp}. Two examples are shown (for $S_c = 70$ ft^2) in Figure 7-15.

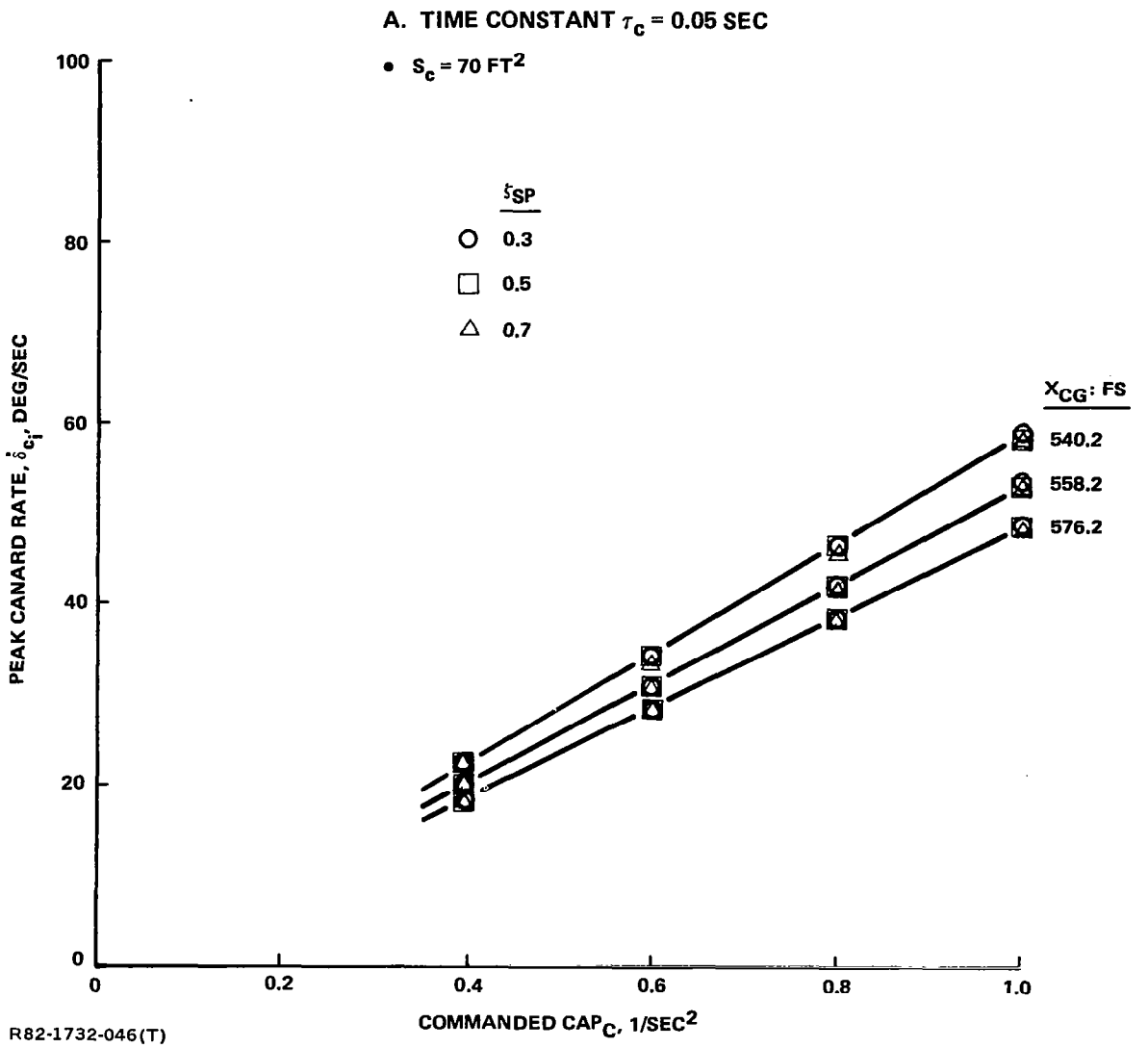

Figure 7-15. - Peak canard rate for motion initiation, $\dot{\delta}_{c_i}$, vs commanded CAP_c with prefilter.

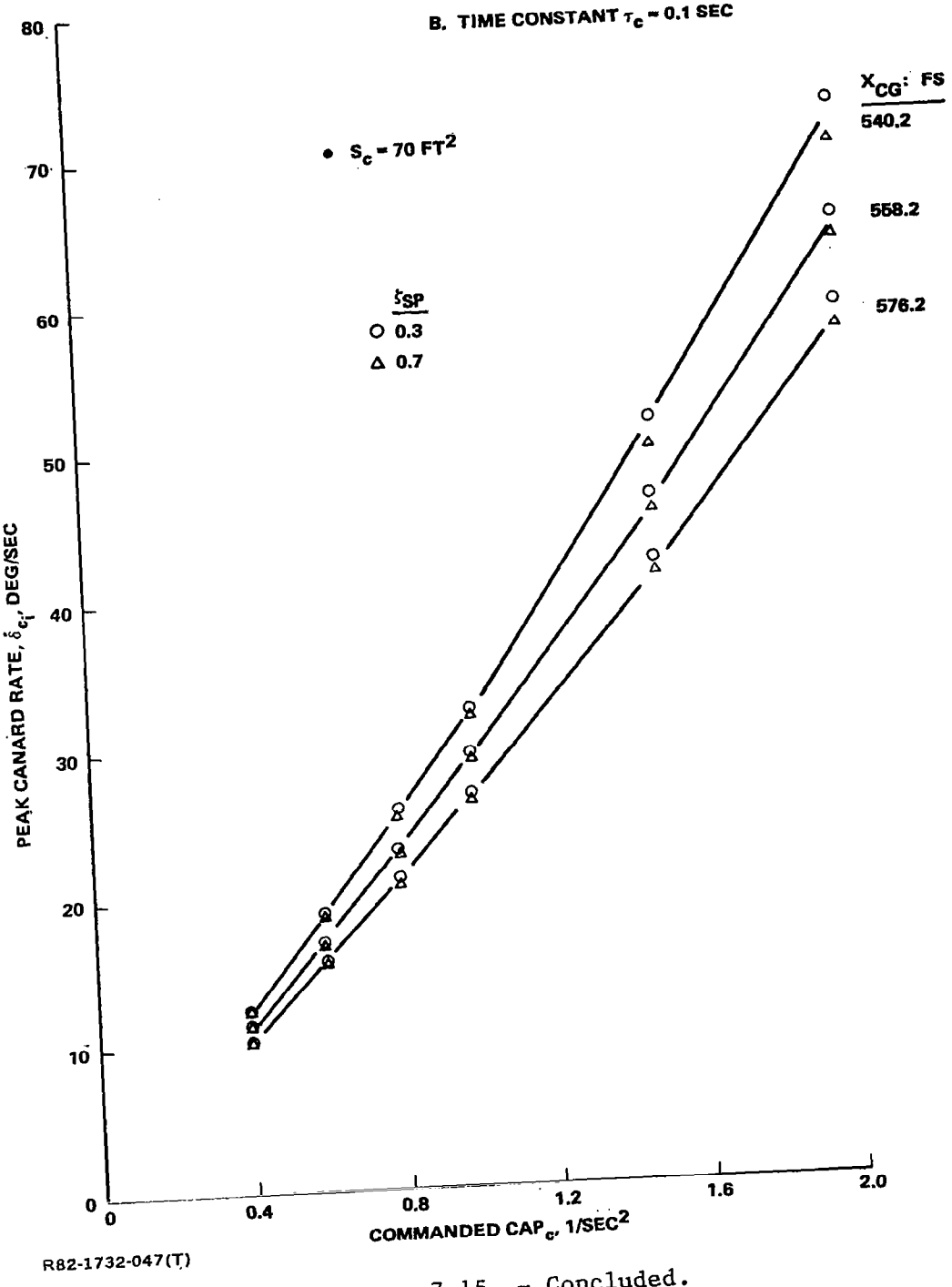

Figure 7-15. - Concluded.

A similarly derived theoretical approximation for canard rate in response to a lagged step input (neglecting the actuator) is given by:

$$\dot{\delta}_{c_i}(t = 0^+)_{\substack{1\ g\ \text{lagged} \\ \text{step}}} = \frac{CAP_c}{M_\delta \tau_c} \qquad (7.21)$$

This relationship is of the same form as Eq (7.19), suggesting that the variation in canard initiation rates (assuming $\tau_c \tau_a \ll 1$) could be explained by:

$$\dot{\delta}_{c_i}(t = 0^+) = \frac{CAP_c\ \Delta n_{z_c}\ (57.3)}{M_\delta\ (\tau_e + \tau_c)} \quad \text{(deg/sec)}; \qquad (7.22)$$

i.e., by replacing the equivalent time constant by its sum with the prefilter time constant. The measured data are well predicted by this simple relationship - as shown for two extreme cases in Figures 7-16 and 7-17.

The reduction in measured CAP_A with increasing τ_c appears linear in CAP_c, independent of canard area S_c and the cg location (static margin), but varying with input values of the closed-loop damping ratio ζ_{sp} (Figures 7-18, 7-19). Note that, for a given non-zero value of τ_c, an equivalent CAP_A level can be achieved with an initial canard rate lower than that if $\tau_c = 0$. For instance, if $M_\delta = 4.08\ 1/sec^2$ ($S_c = 70\ ft^2$, X_{cg} at FS 558.2), for $CAP_A = 0.5$, $\zeta_{sp} = 0.7$, and $\Delta n_{z_c} = 0.25g$:

$\dot{\delta}_{c_i} = 117°/sec$ ($\tau_c = 0$),

$\dot{\delta}_{c_i} = 26°/sec$ ($\tau_c = 0.1$ sec);

since the required $CAP_c \simeq 1.72\ CAP_A$ for $\tau_c = 0.1$ sec.

Thus, it is clear that the prefilter can effectively be used to reduce canard rate requirements. This decrease in rates with τ_c is, however, accompanied by an increasing delay from the instant the command is input, to the time at which the maximum pitch acceleration is achieved. This "transport" lag can be expected to impact a pilot's perception of the responsiveness of the aircraft. Figure 7-20 presents empirical data from the study for the transport lag time delay. In addition to relative time to $\dot{q}_{max}$, the time to achieve a $\Delta n_z = 0.1\ \Delta n_{z_{ss}}$ is also shown. Ultimately, an acceptable upper limit on τ_c must be established in piloted motion base (or in-flight) simulation.

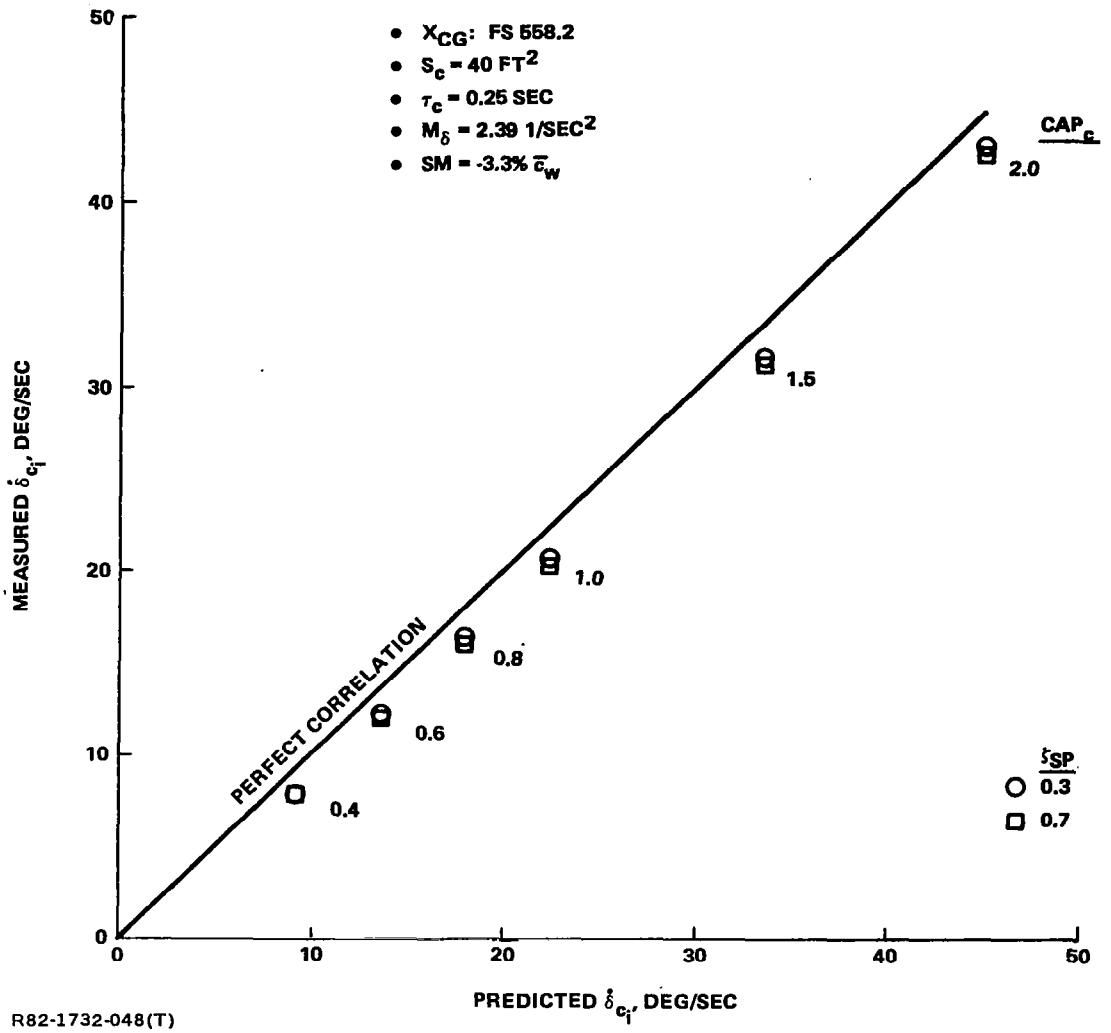

Figure 7-16. - Correlation of actual and predicted peak canard rate for motion initiation, S_c = 40 ft^2.

Examination of the simulation data for peak canard deflection during motion initiation showed that the incremental canard angle from trim can be predicted, for all ζ, by the expression:

$$\Delta(\delta_{c_i}) \cong \frac{CAP_c}{M_\delta} \Delta n_{z_c} \quad (57.3) \quad \text{(deg)}. \tag{7.23}$$

The correlation with empirical data is shown in Figures 7-21 and 7-22 for two extreme cases. The relationship between CAP_A and CAP_c can be inferred from Figures 7-18 and 7-19.

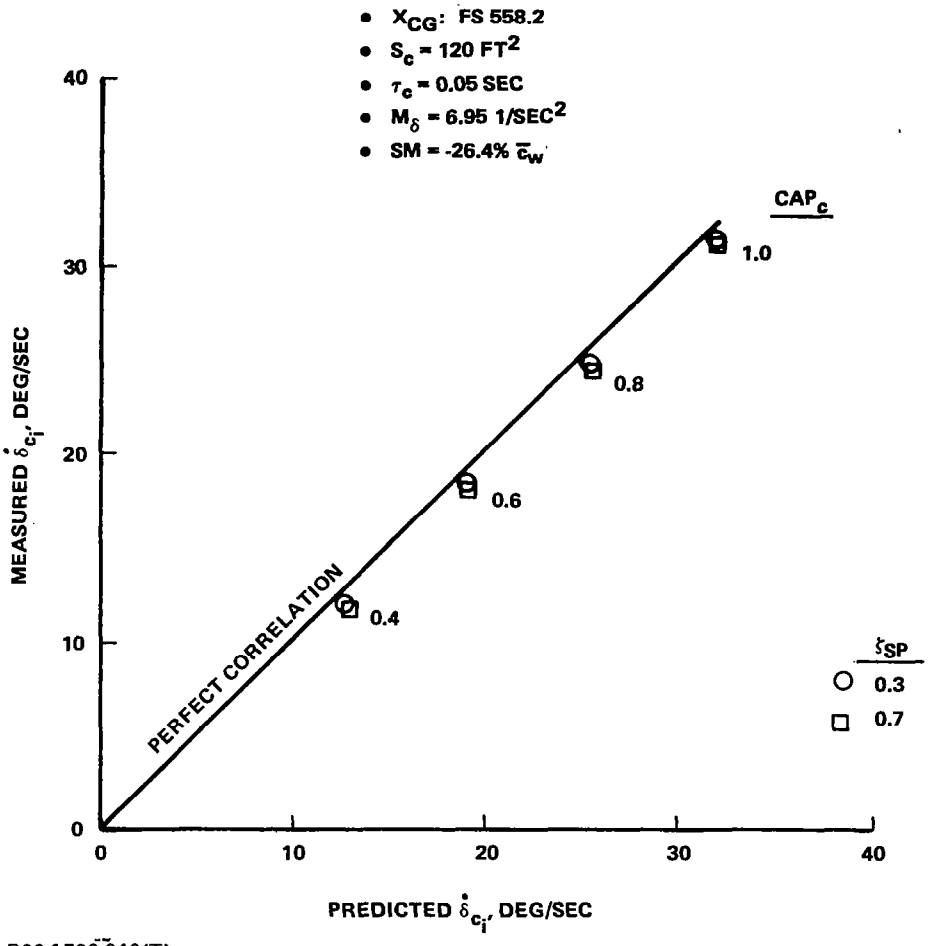

Figure 7-17. - Correlation of actual and predicted peak canard rate for motion initiation, S_c = 120 ft^2.

The prediction of canard recovery rates (second peak in $\dot{\delta}_c$ due to a step input) does not lend itself to simple analytical analysis, especially if $\tau_c \neq 0$. The response is affected by two exponential quantities in τ_c and $\zeta_{sp}\omega_{sp}$. The rates do tend, however, to become linear in CAP$_c$ as τ_c is increased. Selected results of the rate study are presented in Figure 7-23. Note that, if $\tau_c = 0$, the rates associated with $\zeta_{sp} = 0.7$ are higher than for $\zeta_{sp} = 0.3$; the converse is true if $\tau_c \neq 0$. The raw data can be reduced to a more rational form if the recovery canard rates are normalized by M_δ/CAP_c (Figures 7-24 through 7-27). For all cases, these normalized rates increase linearly with increasingly negative aircraft static margin. For a given static margin, the normalized recovery rates are reduced as the prefilter time constant is increased.

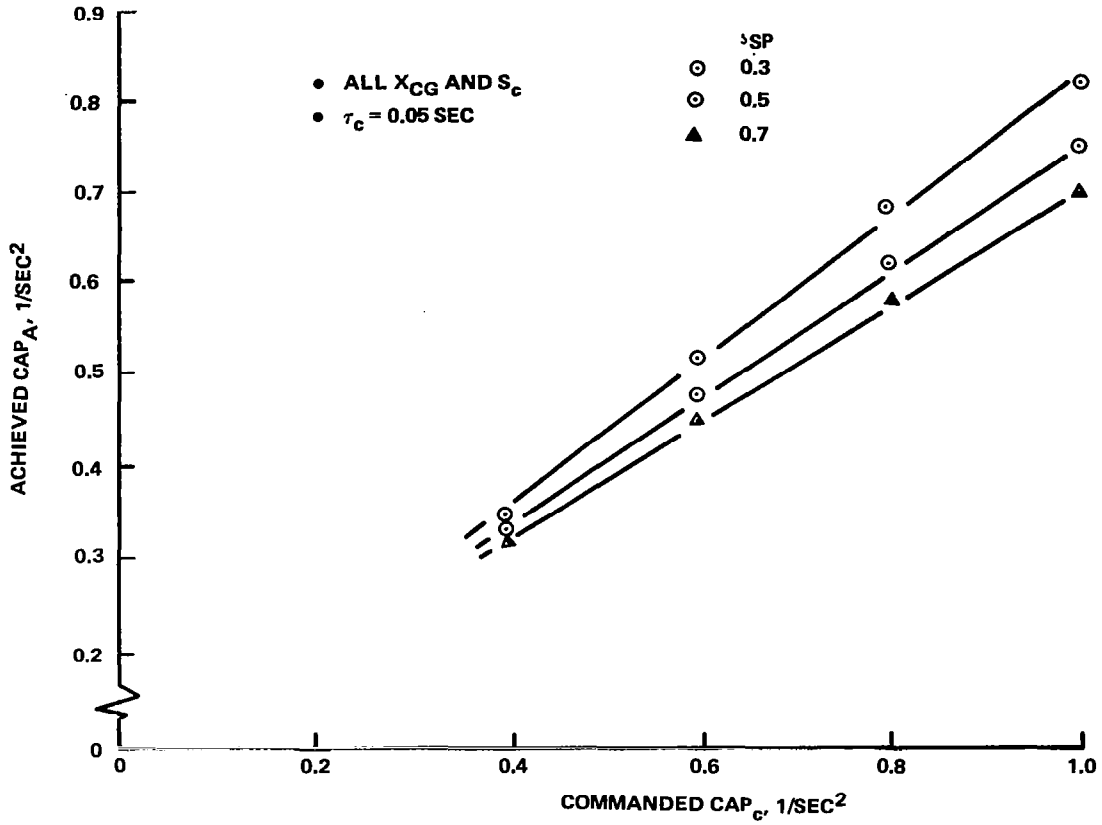

R82-1732-050(T)

Figure 7-18. - Achieved CAP_A vs commanded CAP_c, τ_c = 0.05 sec.

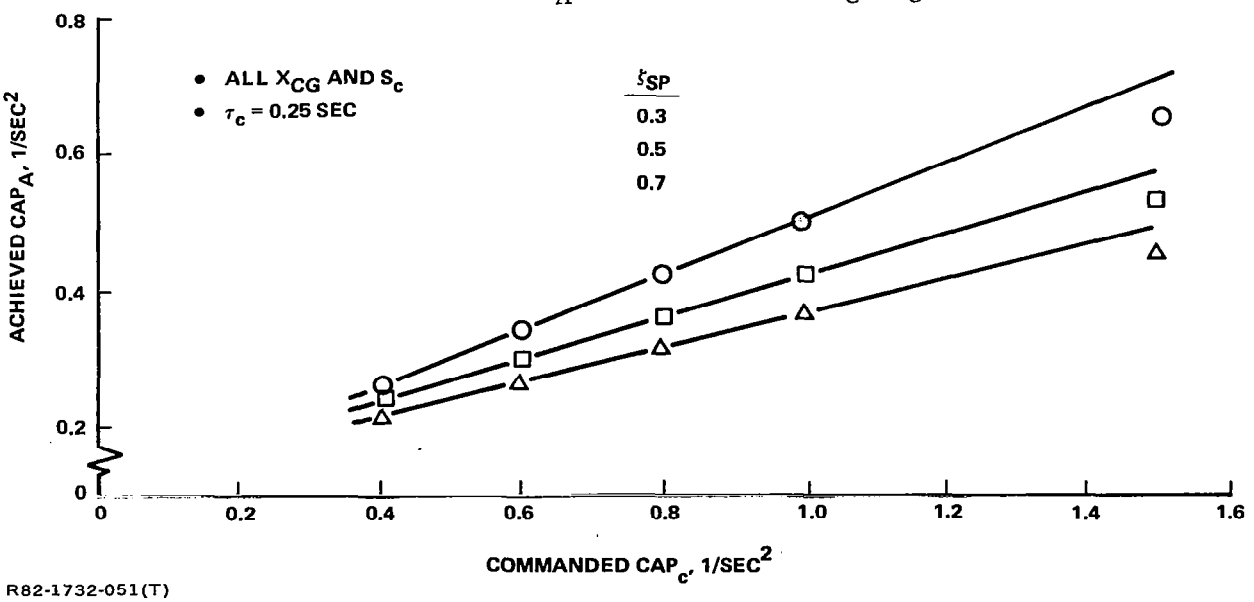

R82-1732-051(T)

Figure 7-19. - Achieved CAP_A vs commanded CAP_c, τ_c = 0.25 sec.

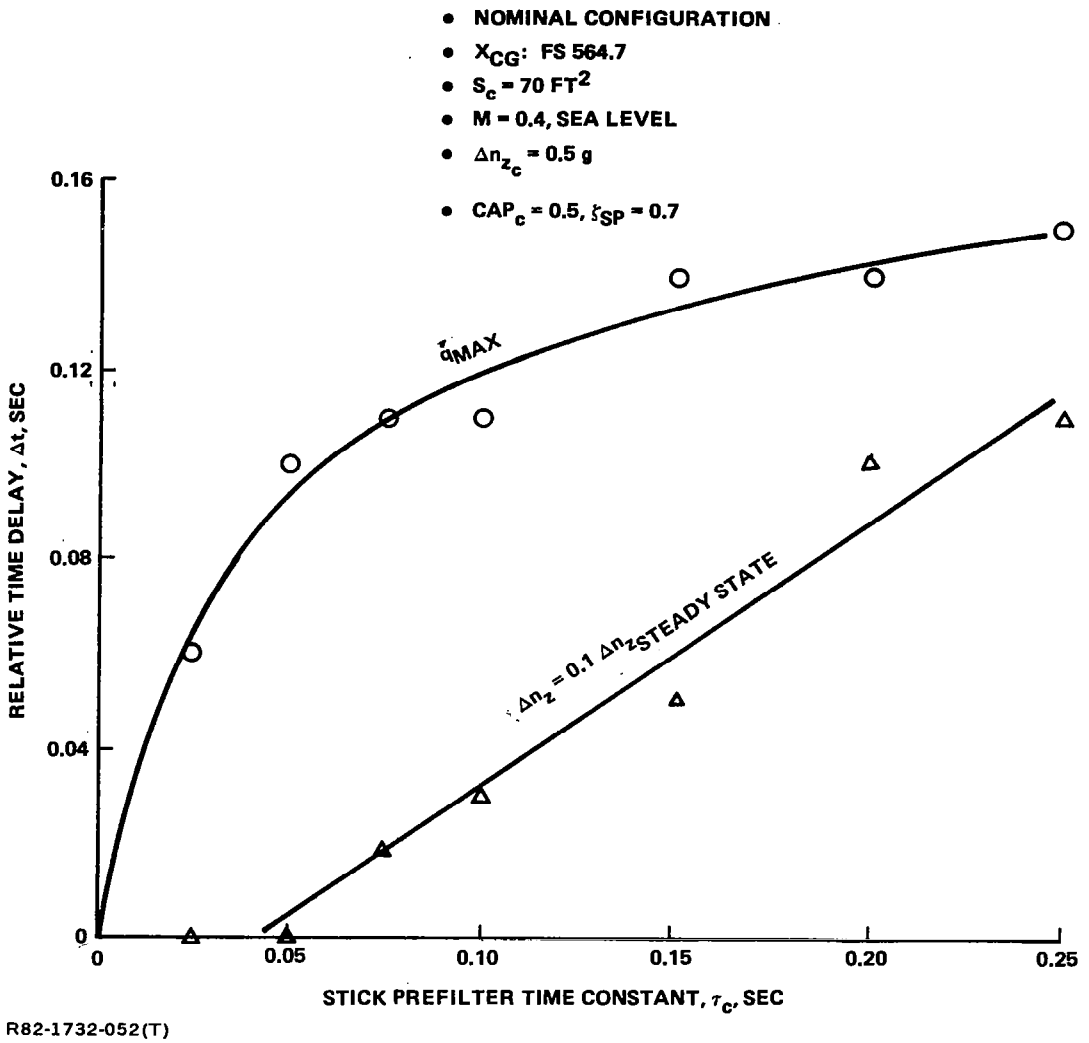

Figure 7-20. - "Transport Lag" vs stick prefilter time constant.

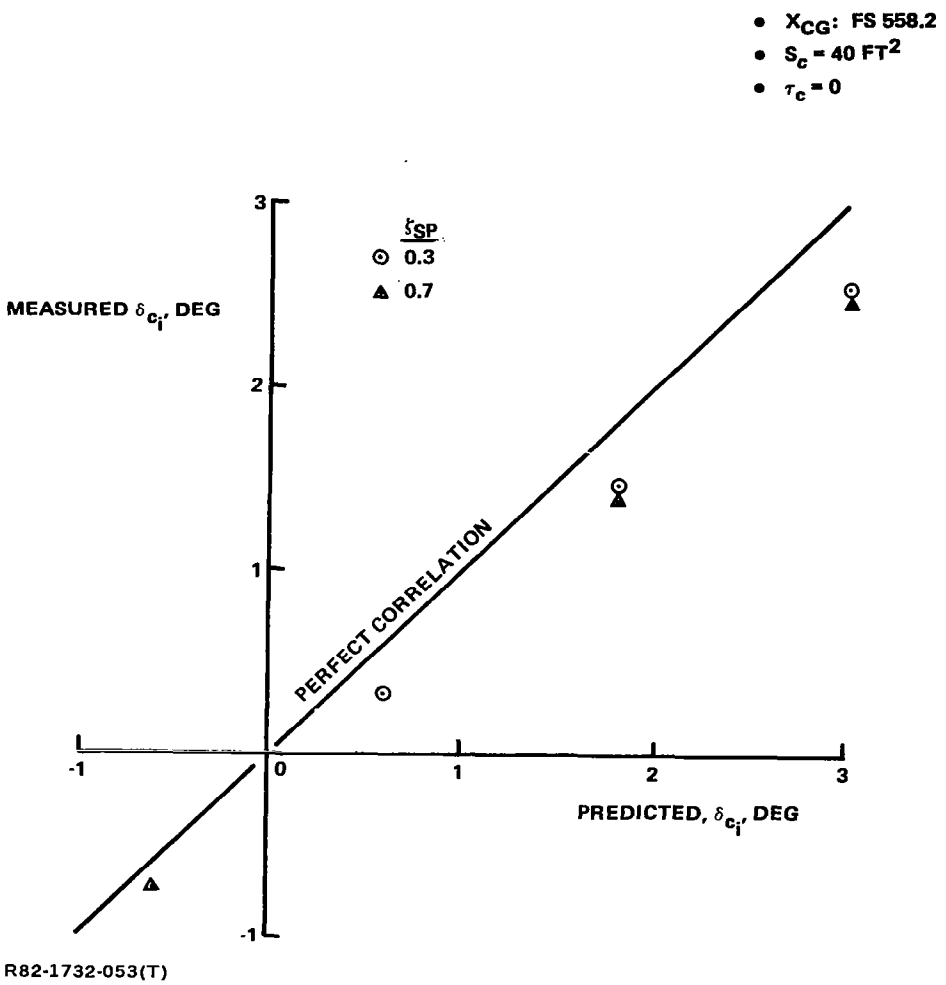

Figure 7-21. - Correlation of actual and predicted peak canard deflection on motion initiation.

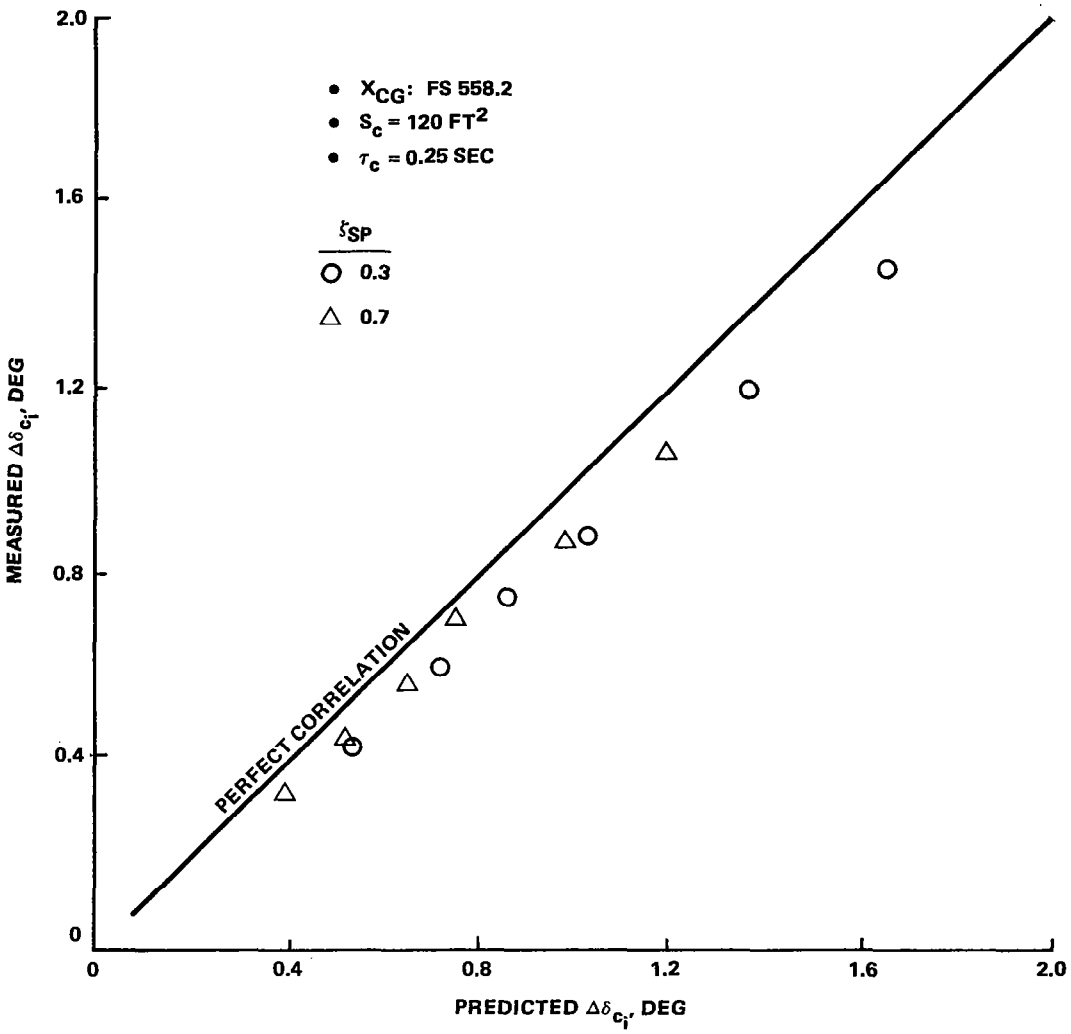

R82-1732-054(T)

Figure 7-22. - Correlation of actual and predicted peak canard deflection on motion initiation (from trim δ_c).

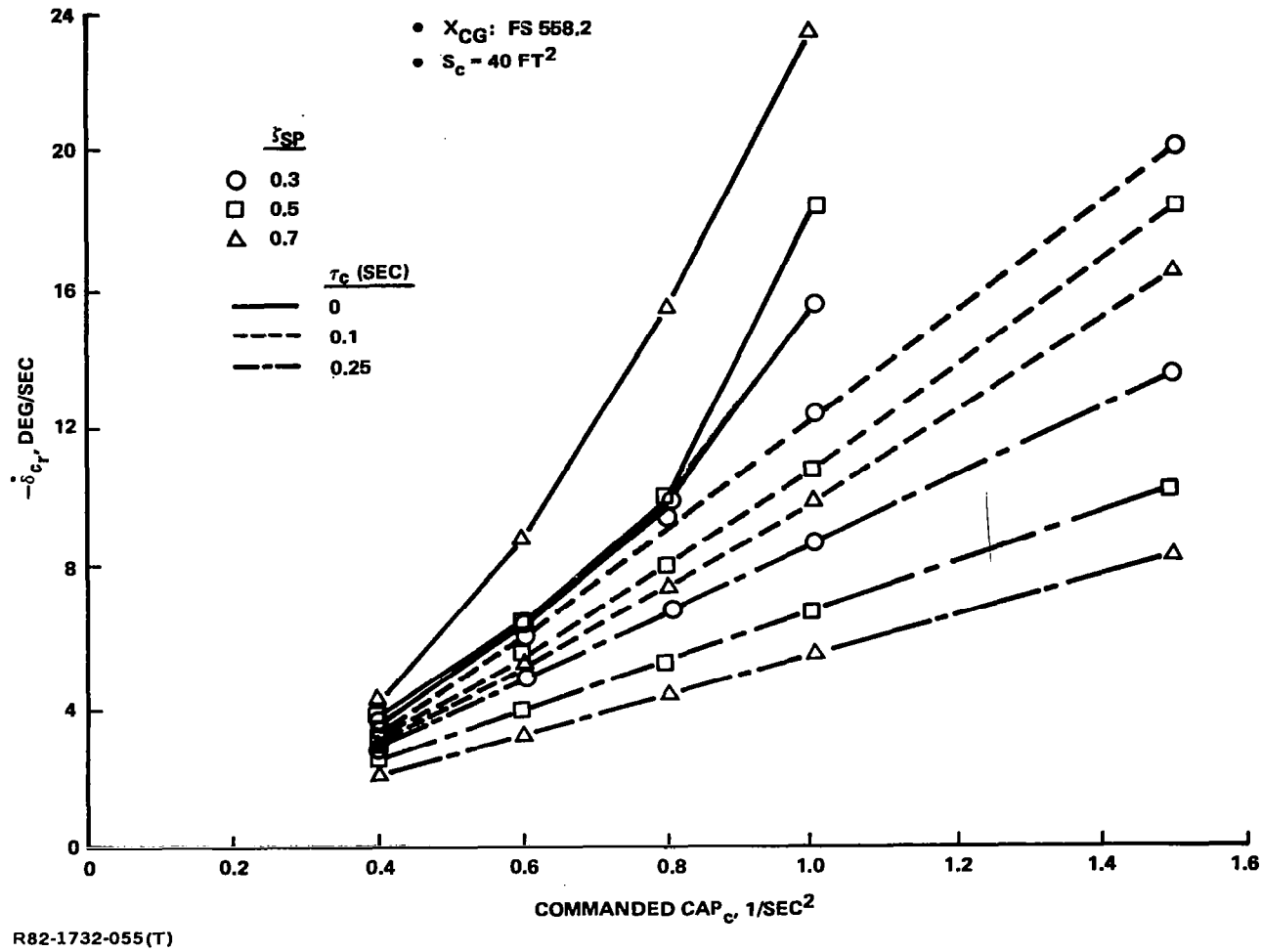

R82-1732-055(T)

Figure 7-23. - Typical variation of peak canard rate on recovery with commanded CAP_c.

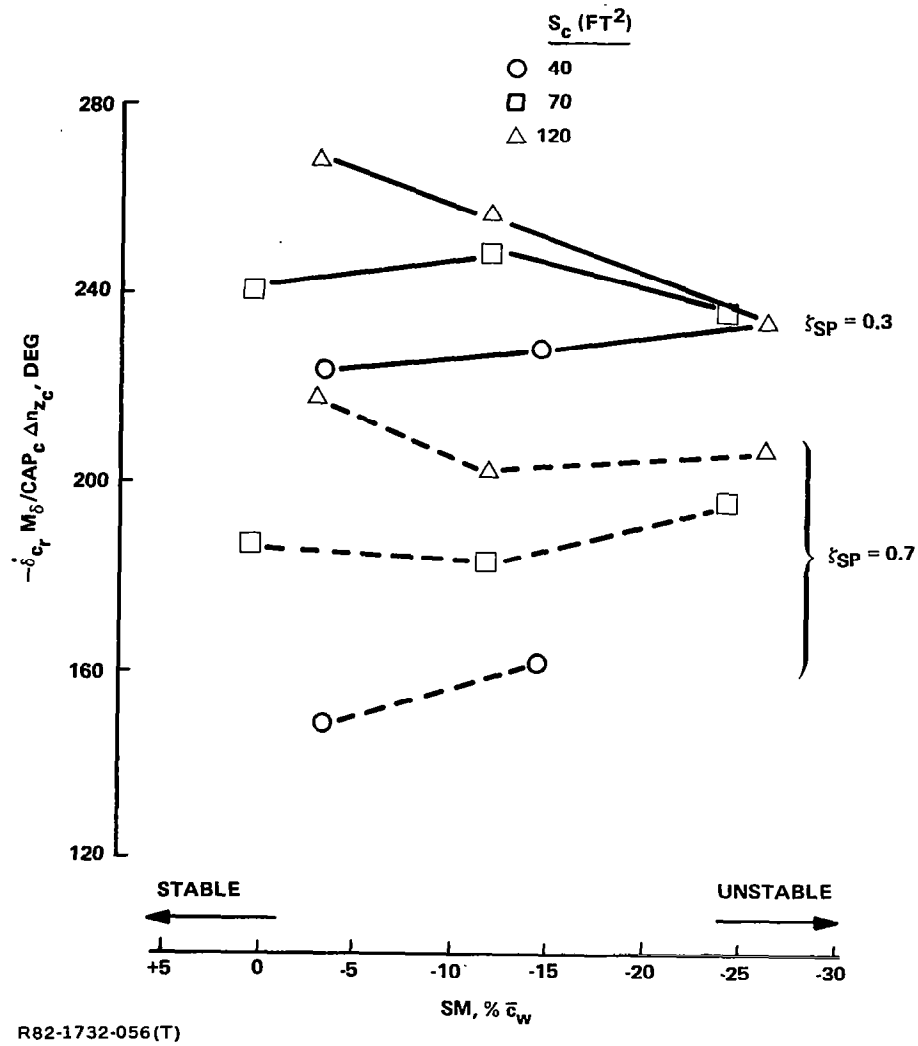

R82-1732-056(T)

Figure 7-24. - Normalized peak canard recovery rates vs aircraft static margin with $\tau_c = 0$.

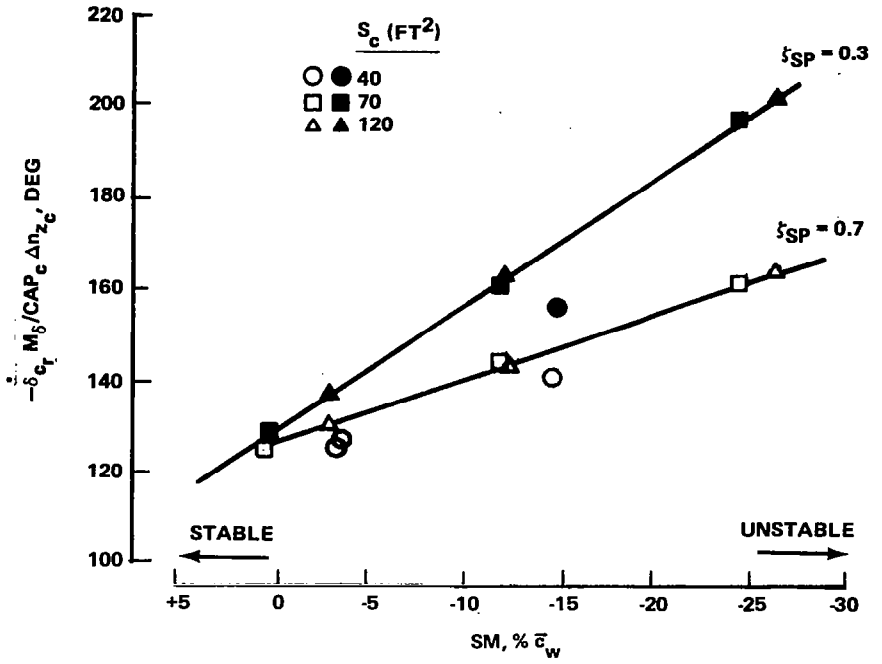

Figure 7-25. Normalized peak canard recovery rates vs aircraft static margin with τ_c =0.05 sec.

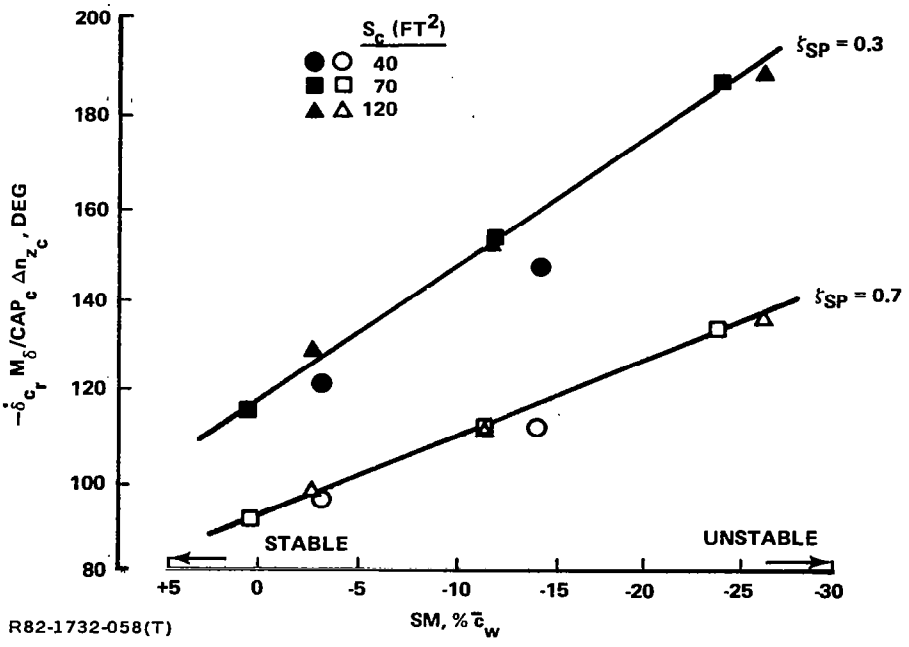

Figure 7-26. Normalized peak canard recovery rates vs aircraft static margin with τ_c = 0.1 sec.

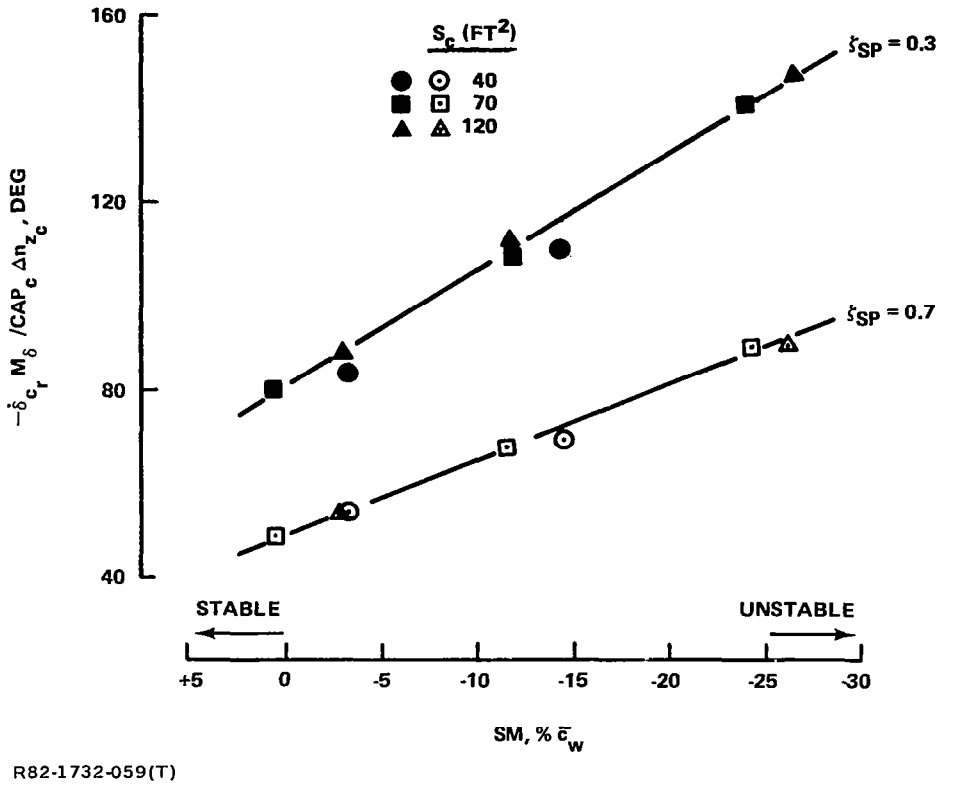

Figure 7-27. Normalized peak canard recovery rates vs aircraft static margin with τ_c = 0.25 sec.

A more useful reduced form is possible if one notes that the canard rates on recovery are consistently lower than those required for motion initiation. If the ratio of canard recovery rate to initiation rate is computed for a given value of CAP_c, these data appear linear in static margin, varying only with ζ_{sp} and τ_c. An example, for CAP_c = 1, is shown in Figures 7-28 and 7-29 for ζ_{sp} = 0.3 and 0.7, respectively. Note that if τ_c = 0, the rate ratio is invariant with static margin, but increases with increasing instability in some proportion to τ_c if $\tau_c \neq 0$ (Figure 7-30). In any case, the peak rate for motion initiation is the determining factor for actuator requirements at low-angle-of-attack and this rate is easily predicted.

Canard deflection angles on recovery are very nearly those required to trim the aircraft at the commanded incremental load factor. Overshoots of the trim deflection are small and correlate with commanded damping ratio, ζ_{sp}.

Although the preceding analysis yields some insight into the functional dependence of canard actuation rates, these study results do not determine actuator rate requirements for the study aircraft configuration. In order to achieve the desired level of performance (CAP_A = 1) with the nominal canard

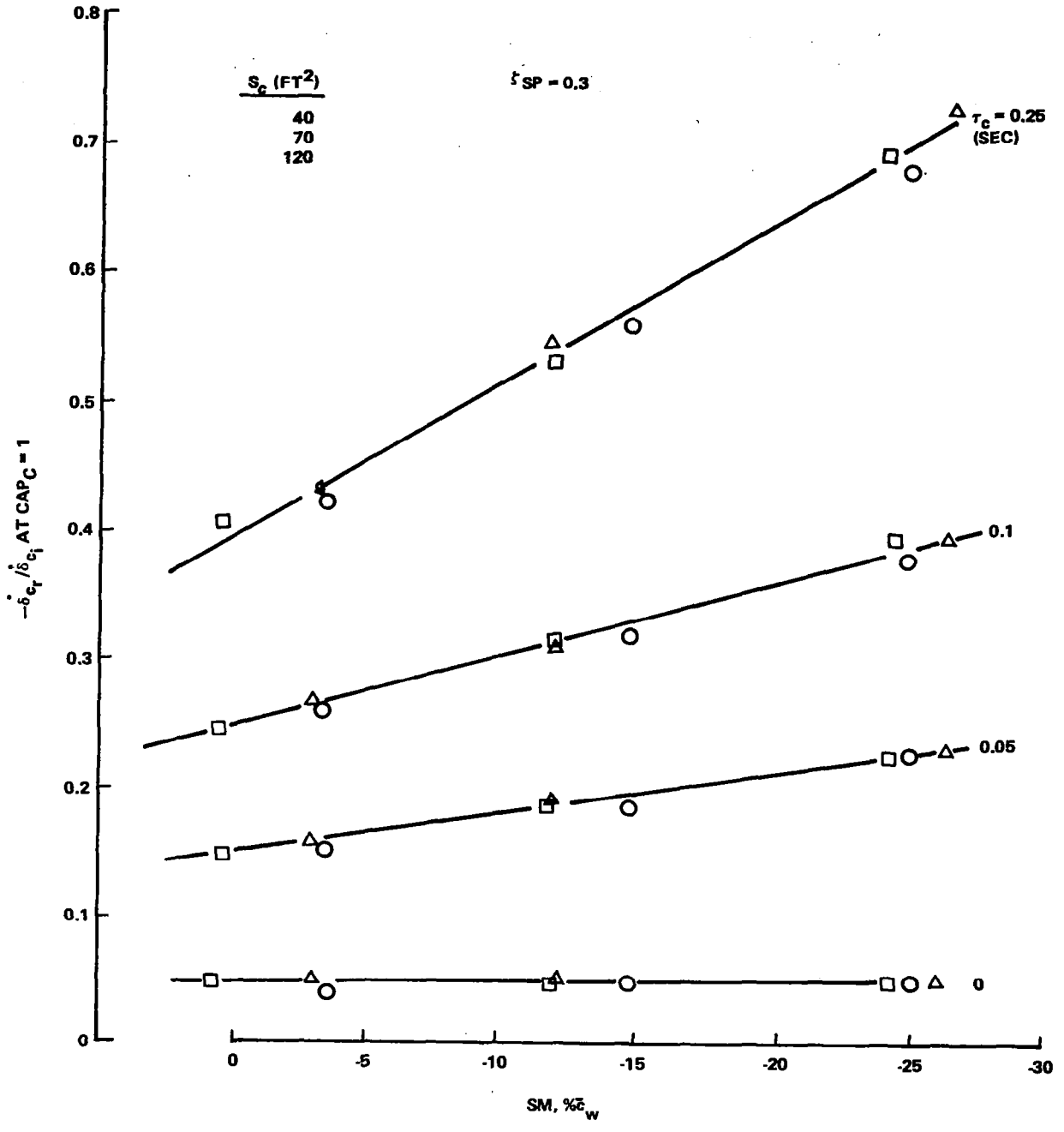

R82-1732-060(T)

Figure 7-28. Ratio of peak canard recovery to initiation rate at CAP_c = 1 vs aircraft static margin, ζ_{sp} = 0.3.

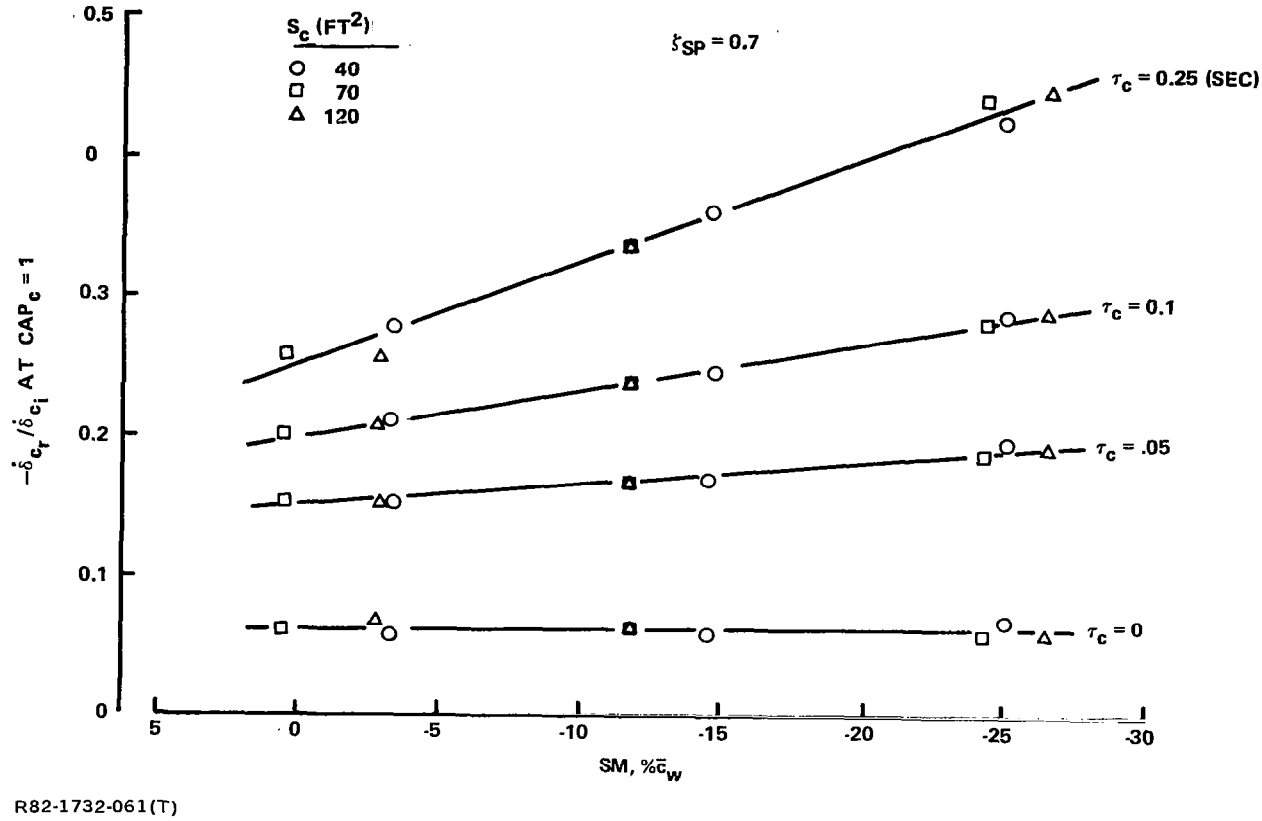

Figure 7-29. Ratio of peak canard recovery to initiation rate at $CAP_c = 1$ vs aircraft static margin, $\zeta_{sp} = 0.7$.

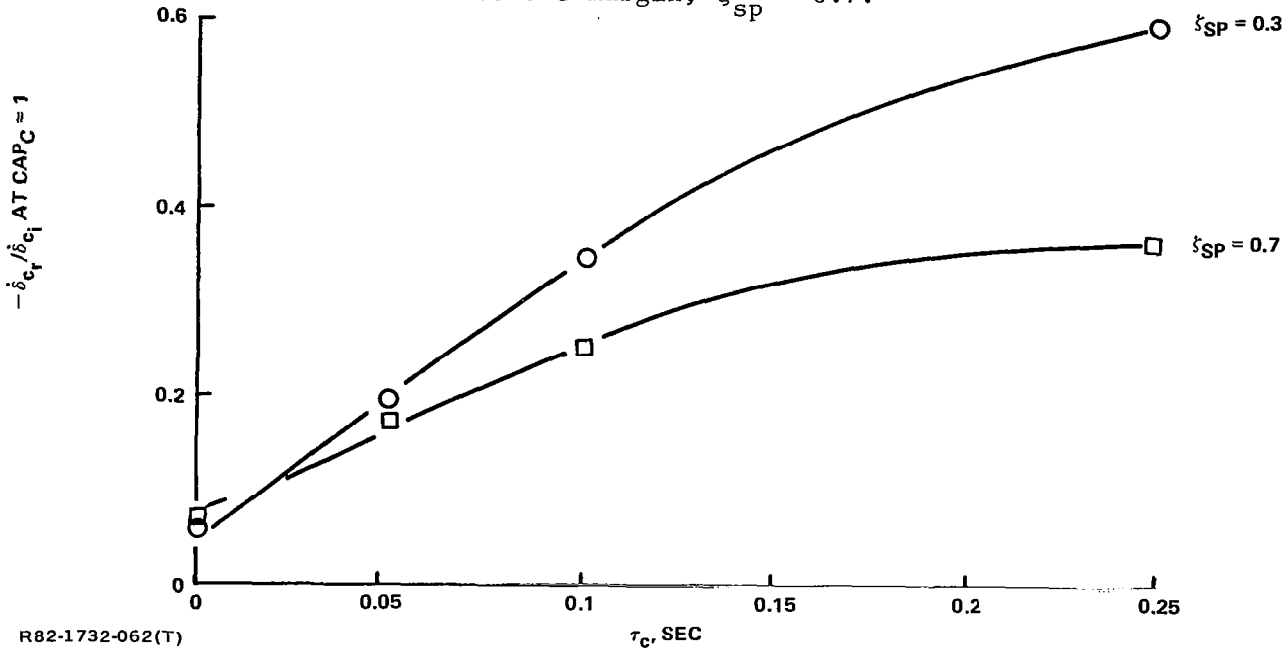

Figure 7-30. Ratio of peak canard recovery to initiation rate at $CAP_c = 1$ and with aircraft SM = 16% c_w vs stick prefilter time constant τ_c.

size (S_c = 70 ft^2) would have required actuator rates of approximately 200 deg/sec/g at M = 0.4, sea level. These rates were considered to be excessive given the large assumed canard deflection requirements ($-90° \leq \delta_c \leq 90°$) and the resultant actuator size, weight, and engine horsepower extraction penalties. Hence, the achievable rates were determined by hardware considerations, and were assumed to be 100 deg/sec. The problem then became one of determining the impact of restricted actuator rates on handling qualities and, as is discussed below, on departure prevention during aggressive maneuvering.

7.3.3 Effect of Forward-Loop Integrator

Whereas for the canard rate/deflection requirement study the forward-loop integrator was removed from the "G" command system, in practice a forward-loop integrator is useful in ensuring zero steady-state error. Although the gain computing algorithm appears to compensate the gains for arbitrary K_I/K_F ratios, mathematically a pure second-order response is possible only for a unique K_I/K_F ratio (the positive root of the quadratic, Eq 7.7). This effect is illustrated in Figure 7-31. The responses shown were computed for the baseline configuration at M = 0.4, sea level, and a 0.25 g step input. The bias term CANTRM was removed. The values CAP_c = 1.0 and ζ_{sp} = 0.7 were input to the model-following algorithm. The prefilter time constant was set to τ_c = 0. The frequency domain equivalent to Figure 7-31 is shown in Figure 7-32. It is clear that the integrator in the simulated "G" command law generates significant numerator dynamics in addition to serving its primary intended purpose - elimination of steady-state error in the presence of plant uncertainties. Note that increasing K_I/K_F not only affects settling time, but also impacts the initial overshoot in the Δn_z response.

With the integrator gain set to the value computed by the algorithm, the effect of increasing τ_c is the same as noted previously; namely, a reduction in the short period frequency and a slight increase in the effective damping ratio (Figure 7-33). For the remainder of this study a level of τ_c = 0.1 sec was selected as a baseline, reflecting a compromise between canard rate demands and the effective transport lag that was thought acceptable. The canard rate study results (for K_I = 0) would predict that, for τ_c = 0.1 sec and ζ_{sp} = 0.7, the ratio $CAP_A/CAP_c \simeq 0.55$. The presence of the integrator, however, results in $CAP_A/CAP_c \cong 0.82$ (Figure 7-34). The canard rates, nevertheless, were still observed to scale with CAP_c.

Thus, if a forward-loop integrator is included, the aircraft response is altered from that with no integrator. The developed gain algorithm can still, however, be used effectively by adjusting the inputs CAP_c or ζ_{sp} to alter the response and compensate for the presence of the integrator. A typical "tuned" response for the nominal aircraft configuration is presented in Figure

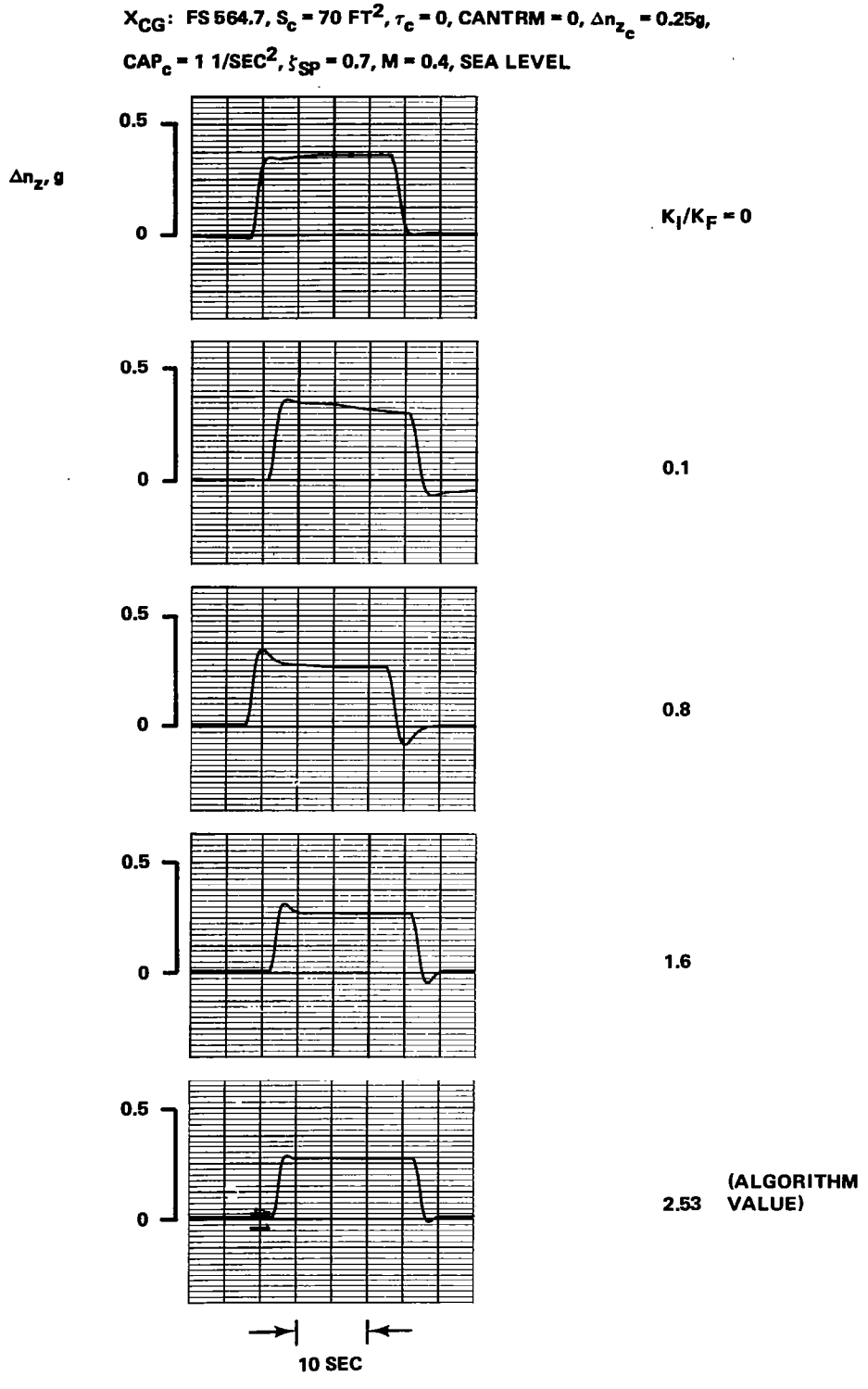

Figure 7-31. Effect of K_I/K_F ratio on incremental load factor response (time domain).

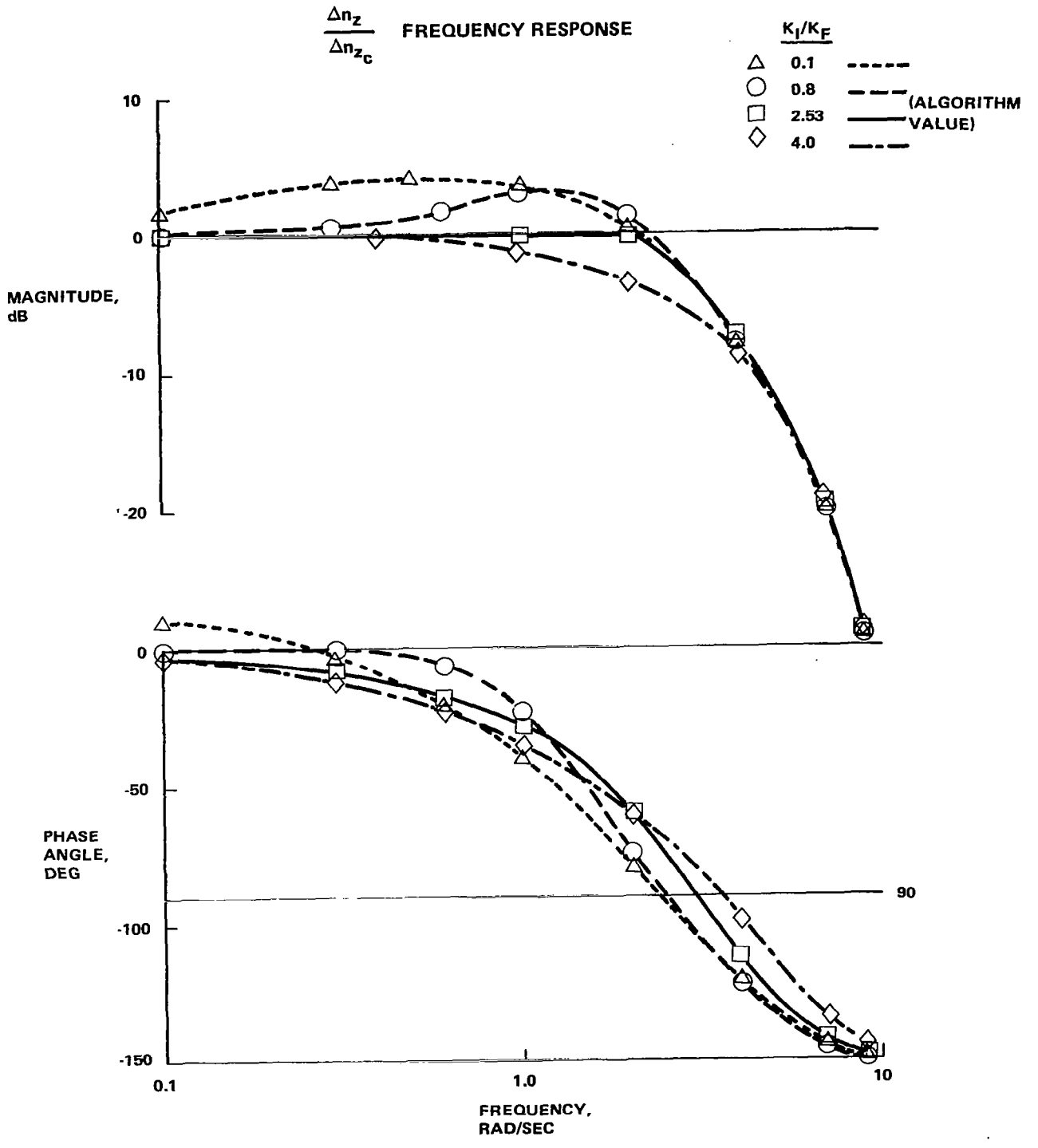

Figure 7-32. Effect of K_I/K_F ratio on incremental load factor response (frequency domain).

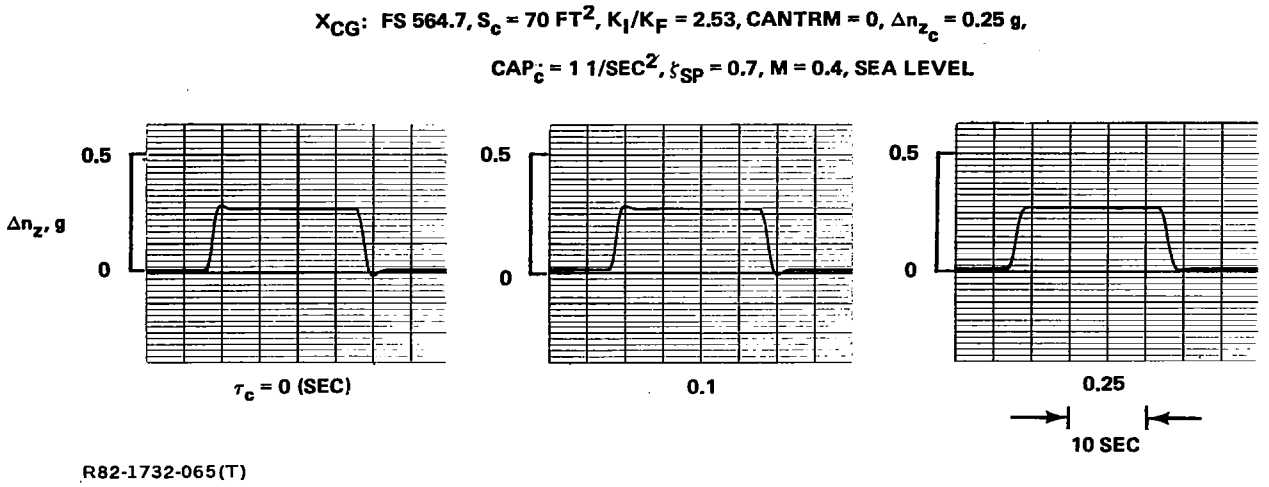

Figure 7-33. - Effect of prefilter time constant on incremental load factor response.

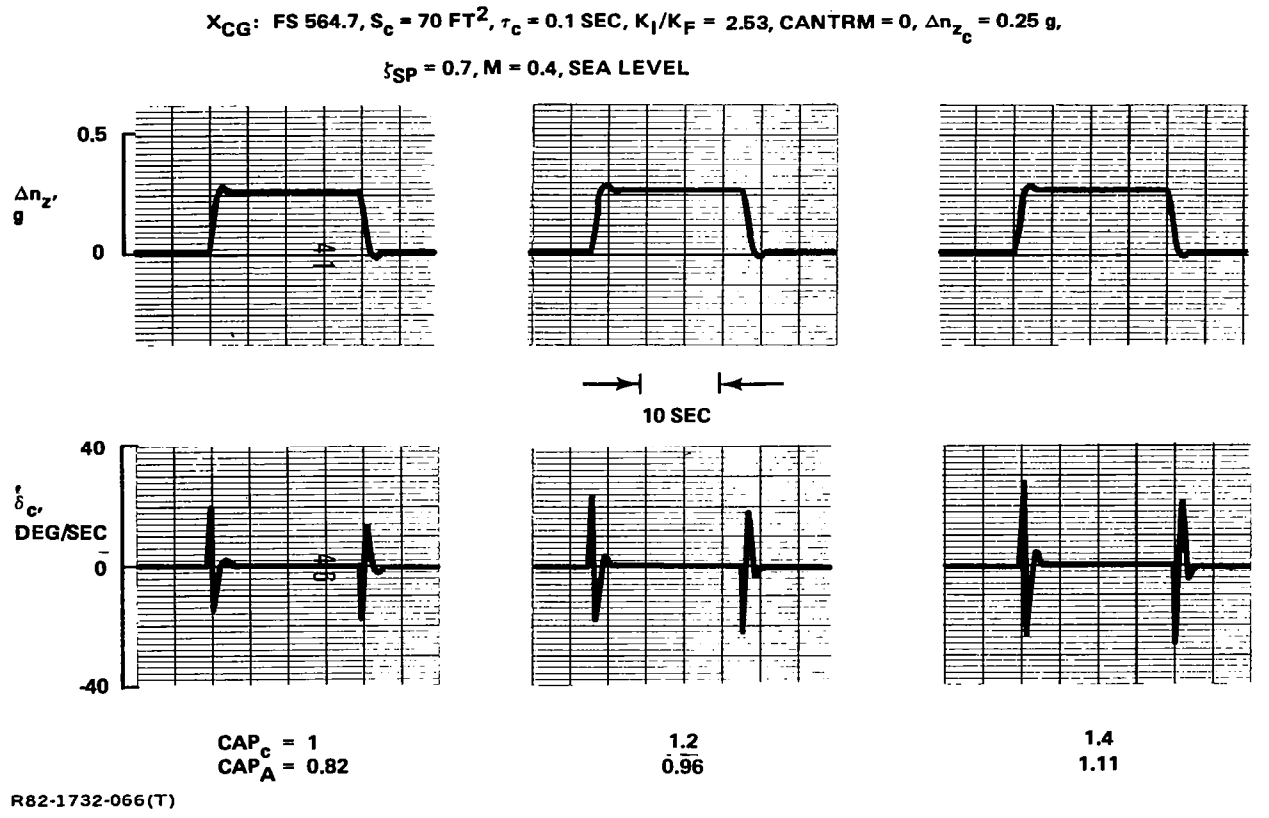

Figure 7-34. - Effect of commanded CAP_c on incremental load factor and canard rate response.

7-35. Here the desired $CAP_A \simeq 1$, $\zeta_A = 0.7$ was achieved for $\tau_c = 0.1$ by setting $CAP_c = 1.3$, $\zeta_{sp} = 0.7$. The flexibility afforded by the gain computing algorithm in adjusting aircraft response is considered a very desirable feature for future piloted handling qualities simulations.

7.3.4 Sensitivity of the "G" Command Law to Plant Variations

The sensitivity of the "G" command law to aerodynamic plant variations was assessed emphasizing the aerodynamic parameters with the highest uncertainty levels. Figure 7-36 shows the results of this study. Aircraft static margin and pitch damping C_{m_q} were varied to determine the sensitivity of the 0.5 g command response at M = 0.4, sea level. Note that the incremental load factor response is essentially unchanged despite a 5% $\bar{c}_w$ change (fore and aft) in cg location. (Normally, prior to flight test, an aircraft's balance is known to within ±3% $\bar{c}_w$). The load factor response is also shown to be insensitive to C_{m_q}, usually a difficult parameter to estimate. Thus the "G" command law proved to be relatively insensitive to major aerodynamic plant variations.

7.3.5 Effects of Atmospheric Turbulence on the "G" Command System

The effect of atmospheric disturbances (both continous turbulence and discrete gusts) on "G" command system performance was also assessed. Continuous atmospheric turbulence was simulated by filtering white noise. The characteristics of the white-noise source are documented in Figure 7-37. The white-noise generator output was autocorrelated and its power spectral density (PSD) function computed. The characteristic impulse of the autocorrelation function at $\tau = 0$ and the flat distribution of the PSD over the frequency range of interest verified proper operation of the generators.

Aerodynamic u and w gust velocity components were introduced in the simulation by sampling the output of analog Dryden filters driven with the white-noise source. The medium-high altitude isotropic Dryden model specified in MIL-F-8785C (Ref. 7) was used to determine the filter parameters. Operation of these analog filters was verified by determining their PSD functions; these PSD's with Dryden asymptotes superimposed are shown in Figure 7-38. Figure 7-39 is a time history of the simulated gust velocities.

Figure 7-40 shows the impact of severe turbulence (σ = 22 ft/sec) on the operation of the "G" system at M = 0.4. Incremental normal acceleration levels peak at ± 1g and canard rates are within ±50°/sec. Angle-of-attack, pitch rate, and canard deflection also show low levels of activity.

The effect of discrete gusts on "G" control system operation was also assessed. In accordance with MIL-F-8785C specifications, a "1-cosine" shape was input to the aircraft and tuned to the closed-loop short-period mode frequency.

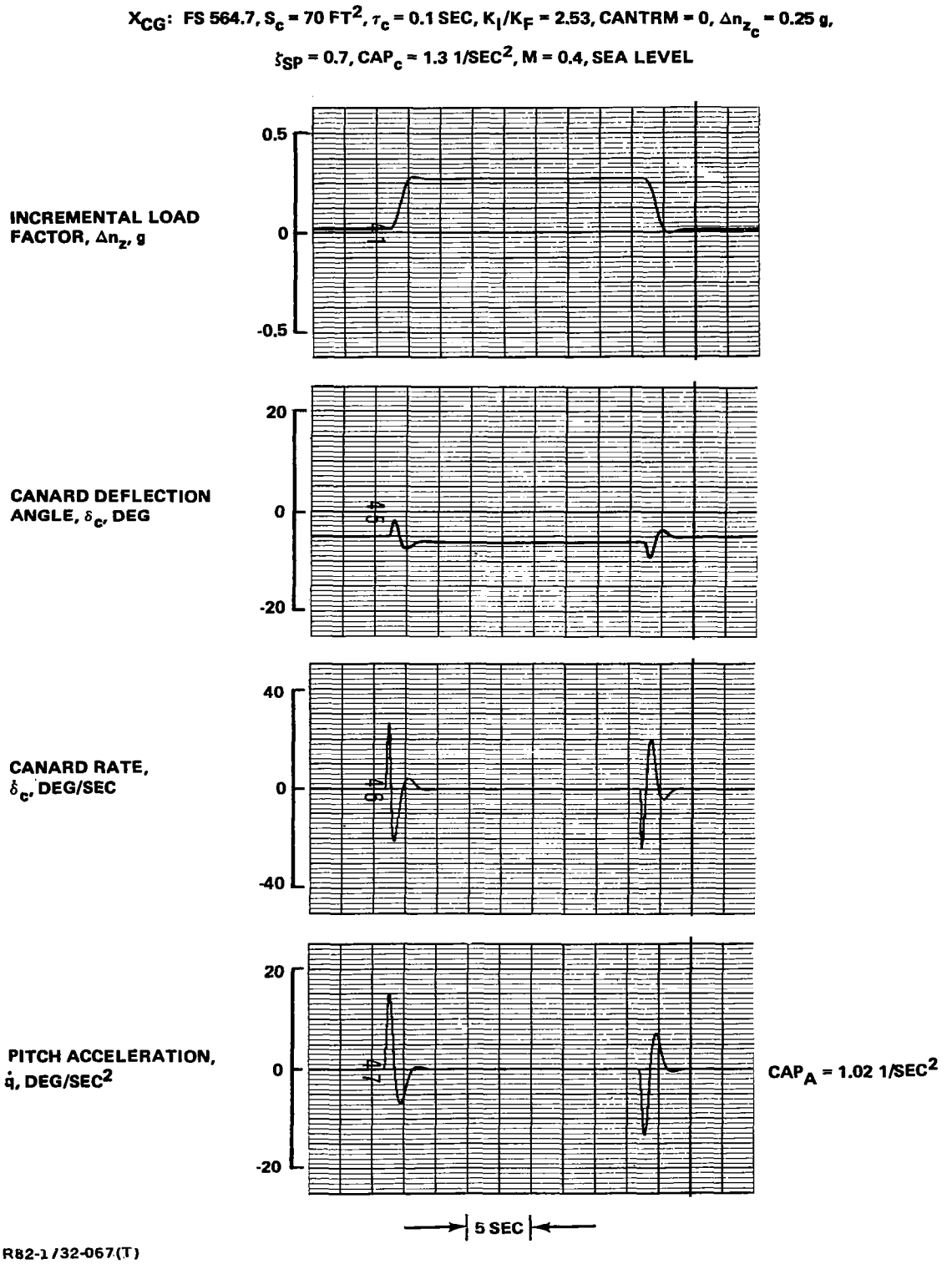

Figure 7-35. - "G" command longitudinal control system final adjusted response.

Figure 7-41 shows the aircraft response when subjected to a vertical gust of "severe" intensity (σ = 22 ft/sec). The aircraft penetrates the gust with minimal canard rate demands (8°/sec) and minimal transients in normal acceleration, angle-of-attack, and canard deflection. Figure 7-42 shows the aircraft transient in response to an equivalent longitudinal gust. Hence, it was concluded that the severe conditions simulated caused no control difficulties at this flight condition.

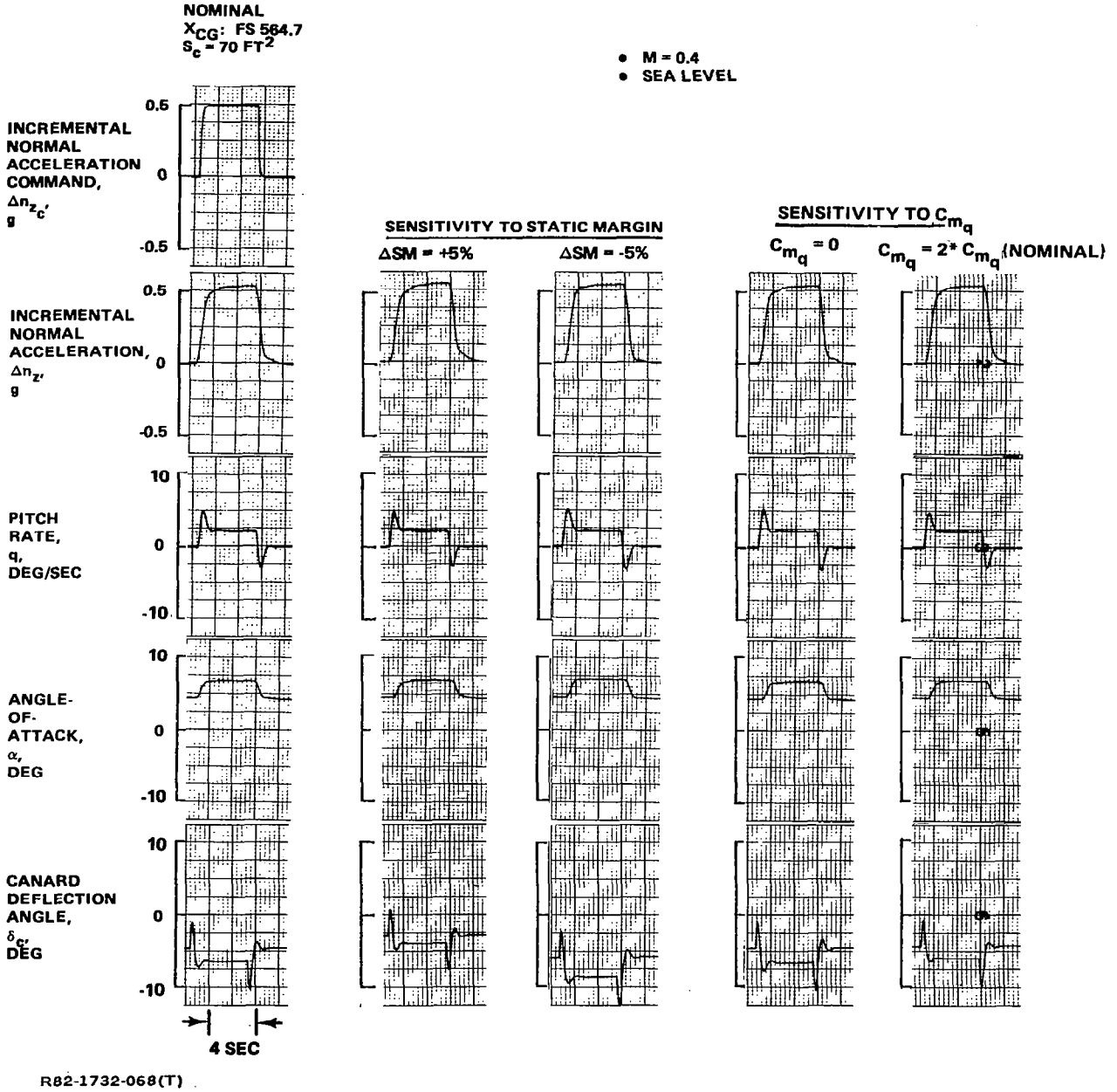

Figure 7-36. - Longitudinal control system sensitivity to aerodynamic plant variations.

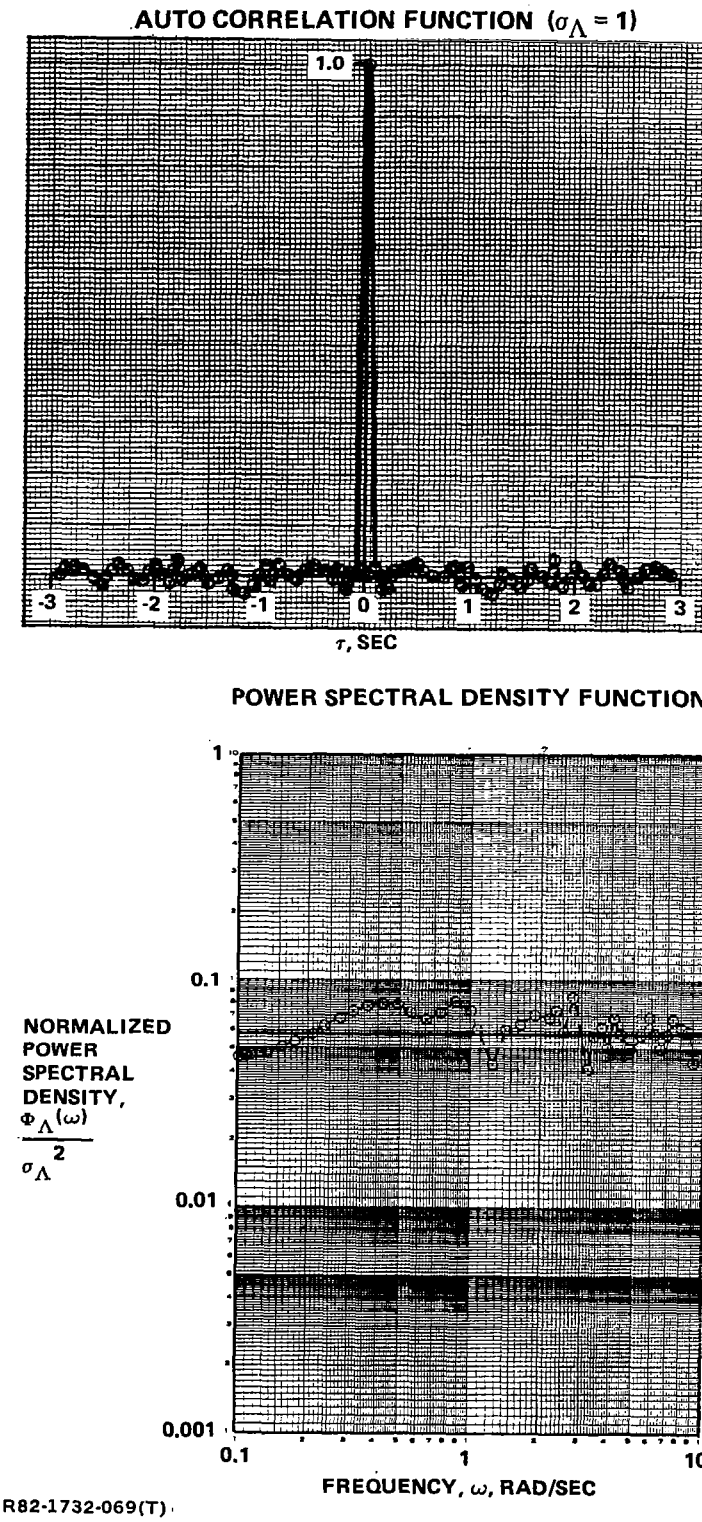

Figure 7-37. - White noise generator autocorrelation, power spectral density functions.

$$\Phi_{u_g}(\omega) = \frac{2.532\,\sigma_u^2}{[1 + (\omega/.2514)^2]}$$

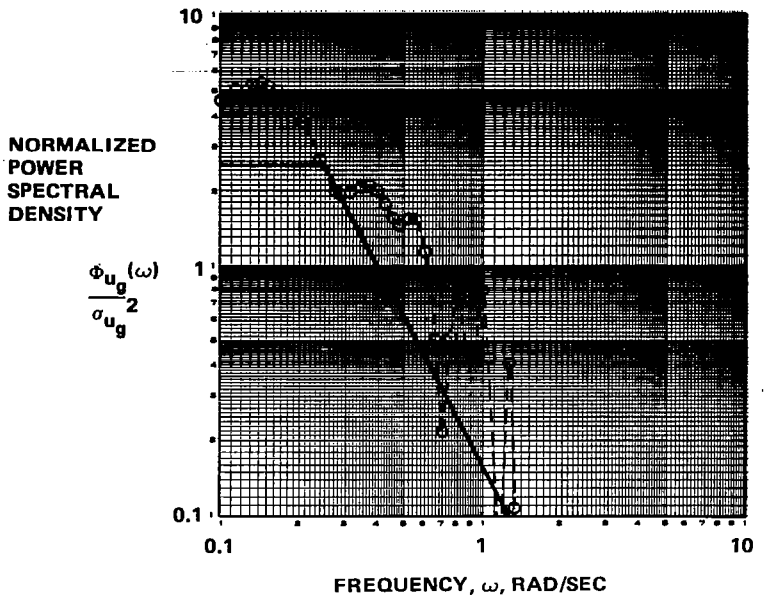

$$\Phi_{v_g}(\omega) = \Phi_{w_g}(\omega) = \frac{1.266\,\sigma_w^2\,[1 + (\omega/.1452)^2]}{[1 + (\omega/.2514)^2]^2}$$

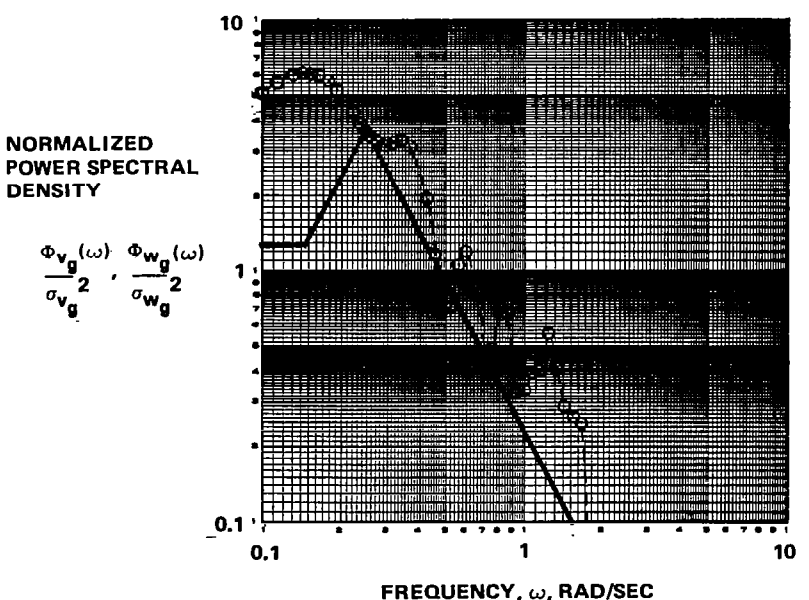

R82-1732-070(T)

Figure 7-38. - Dryden filters for turbulence simulation.

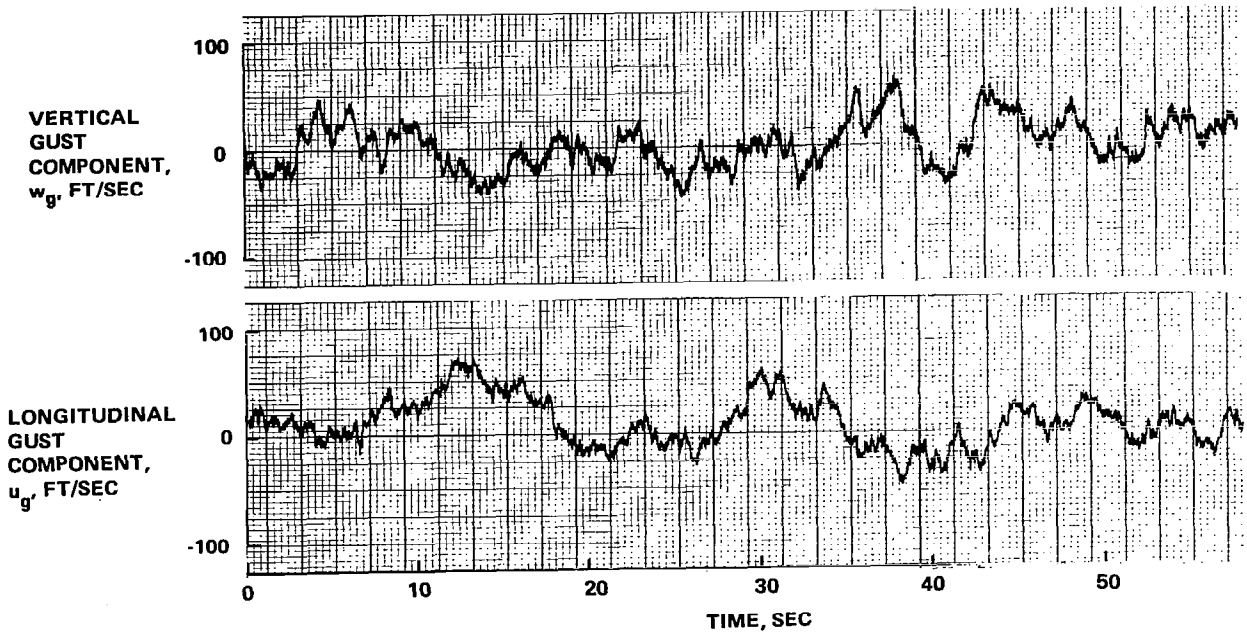

Figure 7-39. - Simulated gust field ("severe" turbulence intensity, σ = 22 ft/sec).

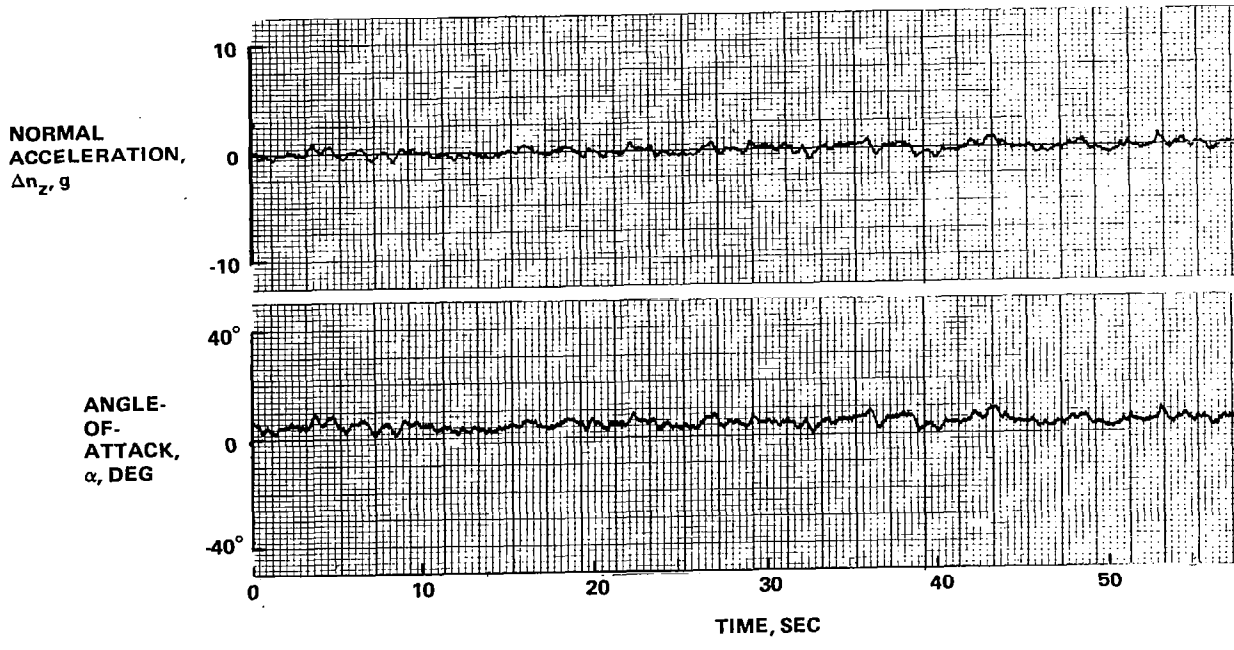

Figure 7-40. - STAC response to severe turbulence (sea level).

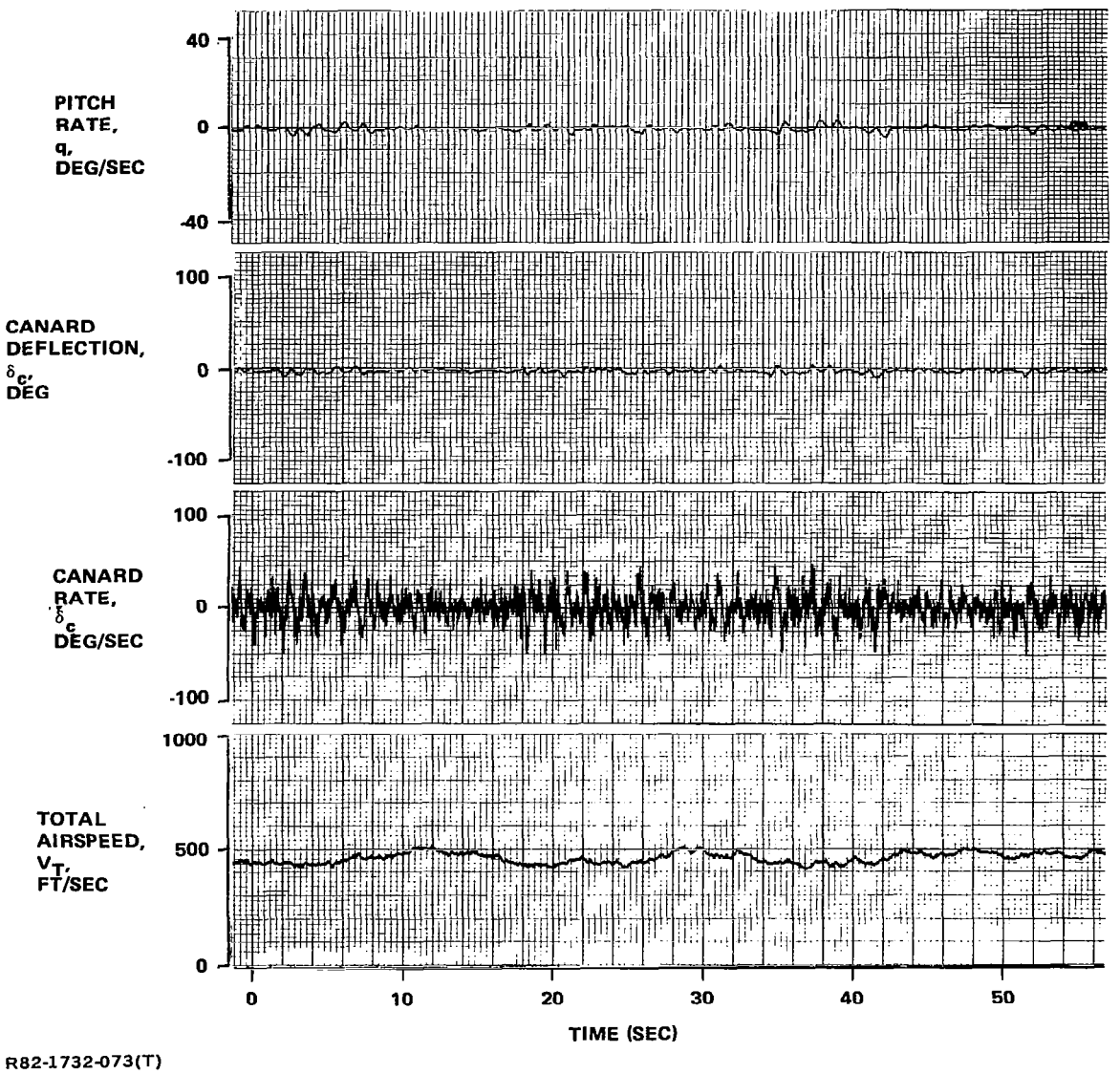

Figure 7-40. - Concluded.

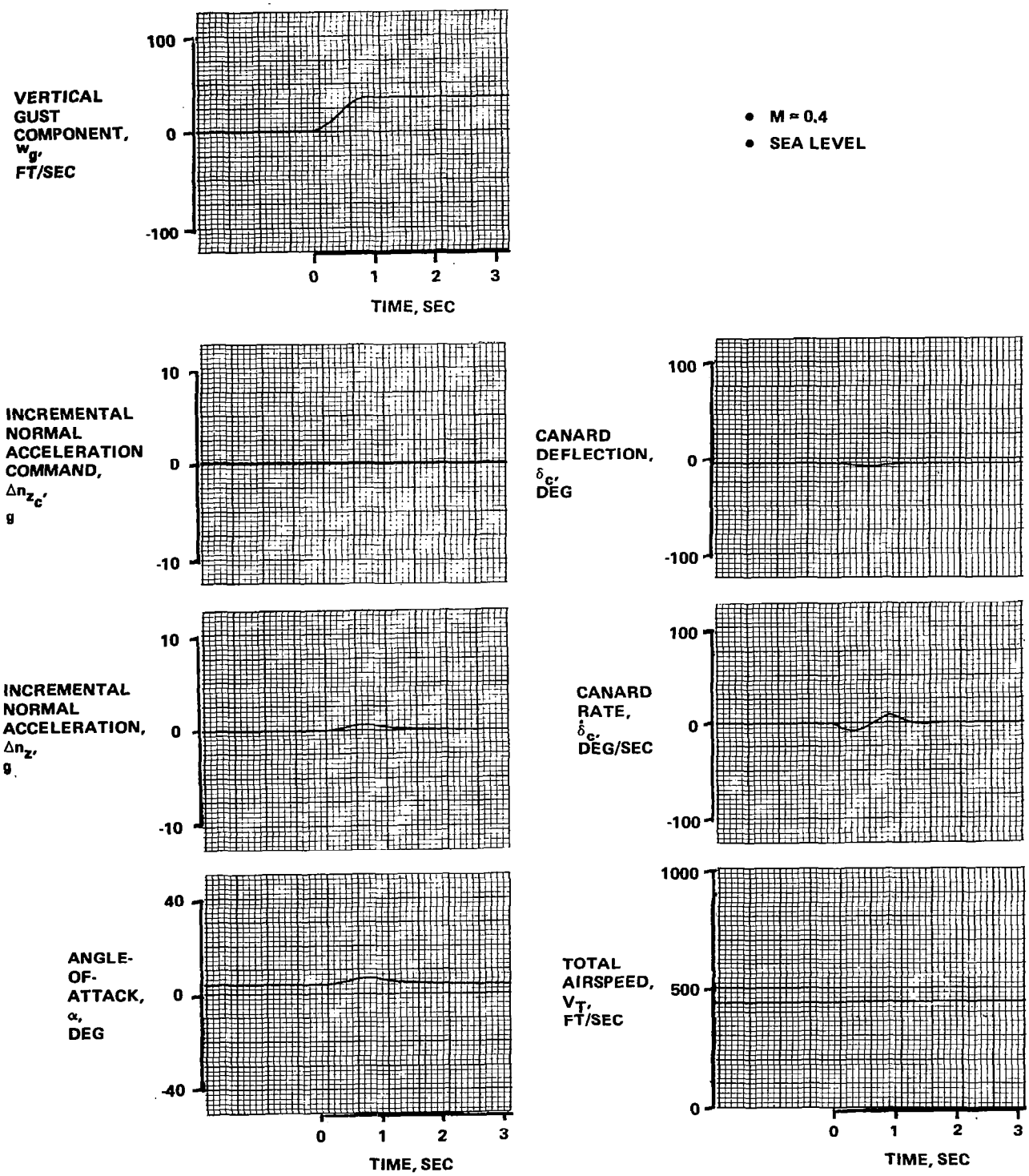

Figure 7-41. - STAC response to a discrete vertical gust.

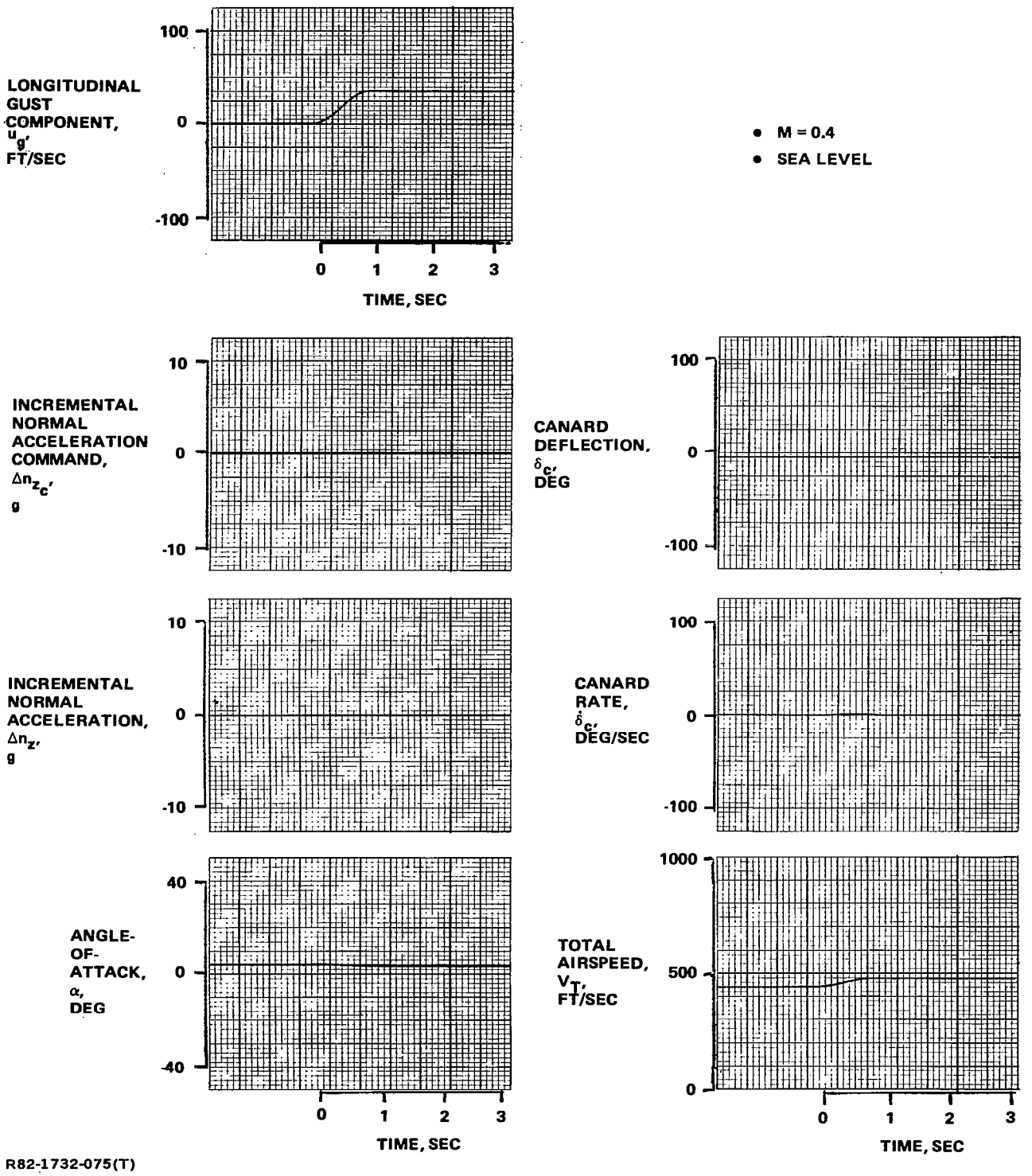

Figure 7-42. - STAC response to a discrete longitudinal gust.

8 - BASIC LATERAL/DIRECTIONAL CONTROL SYSTEM DESIGN AND EVALUATION

8.1 DESIGN PHILOSOPHY

It was recognized from the outset that the adverse effects of kinematic and dynamic coupling of lateral/directional motions into the pitch axis would be of major concern in the development of roll and yaw axis control laws (see Ref. 1 for a cogent discussion of these issues). These coupling phenomena become more pronounced with increasing angle-of-attack. Inertia coupling is particularly adverse for supersonic configurations because of their high pitch/yaw to roll inertias associated with the high fineness ratios mandated by wave-drag considerations. The fundamental control law issue is the selection of the desired roll mode for the aircraft. Rolling about the body x axis at high angle-of-attack invites nose-slice departures if the (augmented) directional stability is inadequate. Rolling about the stability axis leads to roll-pitch inertia coupling. For purposes of this study, a stability axis roll mode was selected mainly because this mode is typical of modern fighters. Furthermore, since the resulting inertia coupling would severely tax the available pitch control power, the generic control problems of RSS aircraft would be highlighted.

As with the longitudinal laws, the simplest possible lateral/directional control structure was implemented and classical design techniques were employed to determine control system gains. The reduced equations of motion were manipulated to yield gain computing algorithms that used stored stability derivative data to attain desired levels of handling qualities metrics over the flight regime.

Whereas the longitudinal control system provided both primary mode stabilization and command augmentation, only moderate compensation proved necessary in the lateral/directional systems. As shown in Figure 8-1, the directional stability of the basic STAC aircraft is excellent over the entire angle-of-attack range. Only in the area near $\alpha = 20°$ is C_{n_β} marginal; and then only for a limited β range near zero. Since the dihedral effect is also favorable ($C_{l_\beta} < 0$, Figure 8-1) for all angles-of-attack, $C_{n_{\beta\ dyn}}$ is highly positive (Figure 8-2). Past studies have shown that negative $C_{n_{\beta\ dyn}}$ indicates susceptibility to "nose-slice" departures. Another commonly used divergence metric, the Lateral Control Divergence Parameter (LCDP), is also shown for the unaugmented STAC aircraft in Figure 8-2. Since the STAC ailerons exhibit proverse yaw up to $\alpha = 44°$, LCDP remains positive out to $\alpha = 66°$ - indicating normal aileron response for the bare airframe. These excellent airframe characteristics provided a benign basis for achieving good lateral/directional flying qualities.

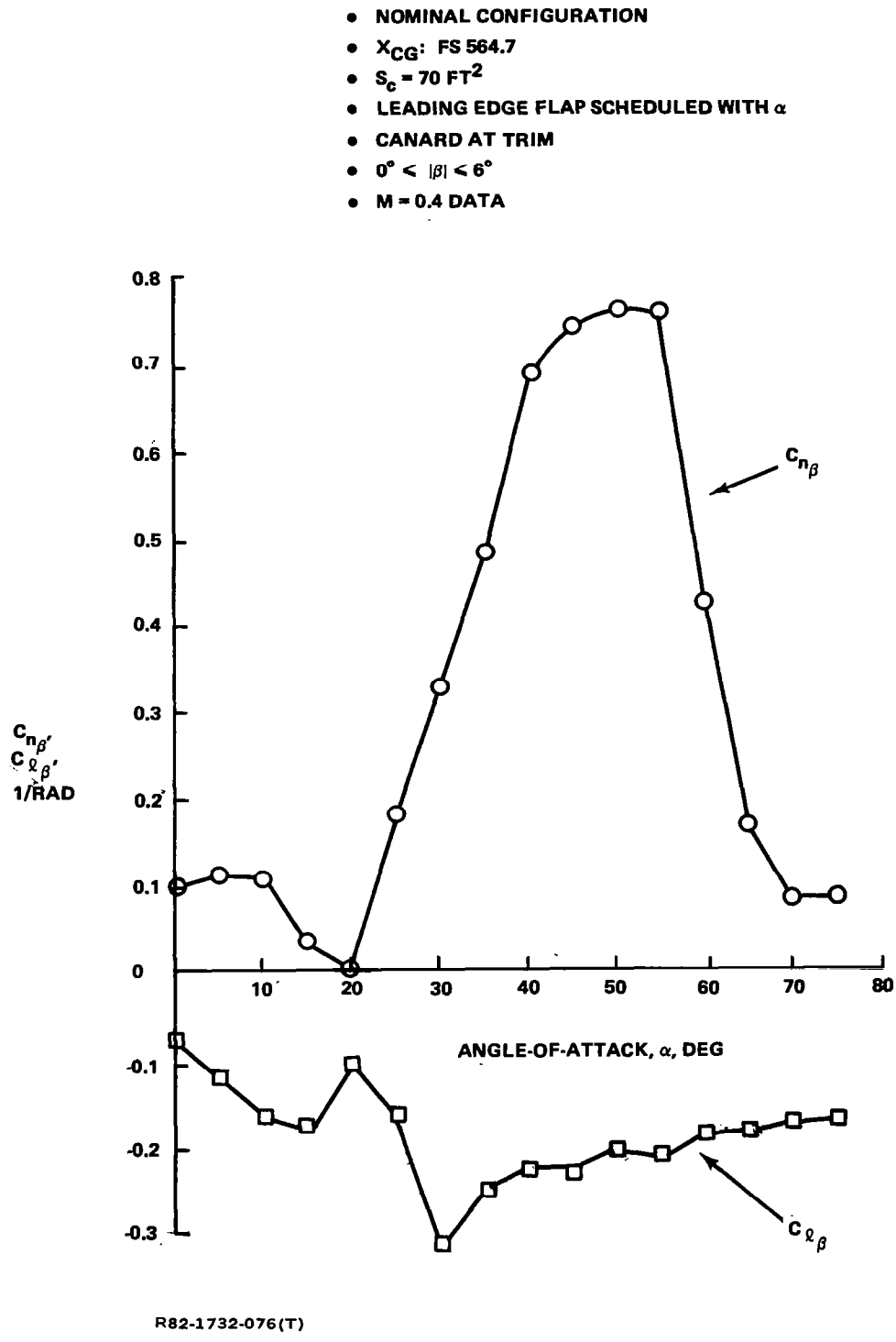

Figure 8-1. - STAC airframe static directional stability and dihedral effect (body axes) vs angle-of-attack.

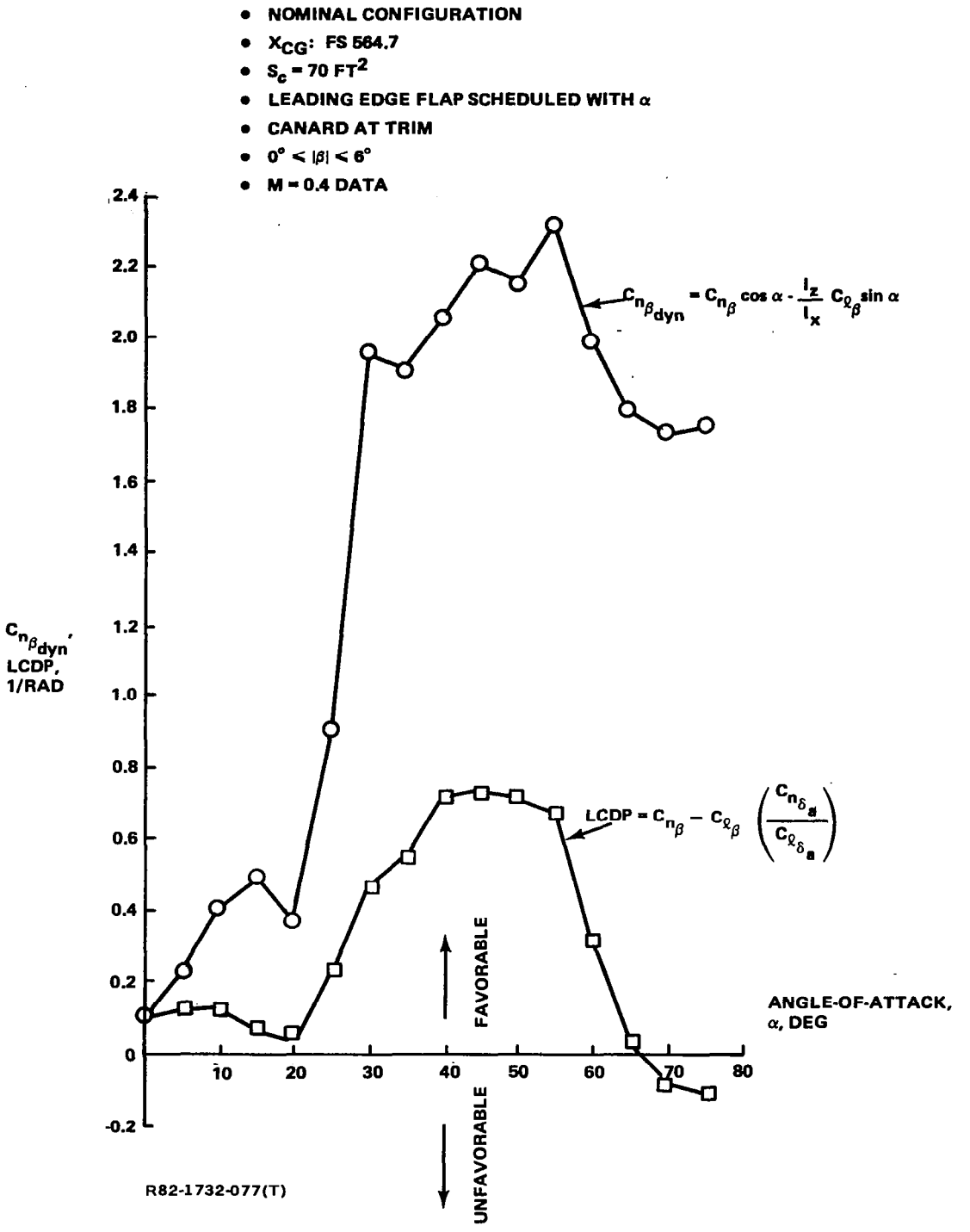

Figure 8-2. - STAC airframe dynamic directional stability derivative, $C_{n_{\beta_{dyn}}}$, and lateral control divergence parameter, LCDP, vs angle-of-attack.

8.2 LATERAL/DIRECTIONAL CONTROL LAW SYNTHESIS

Figure 8-3 illustrates the roll rate command system in block diagram form. The pilot commanded roll rate is modified by a roll rate limiter (discussed in Section 9) and a first-order lag prefilter. The prefilter lowers actuator rate demands for abrupt control inputs. The prefilter time constant was set to $\tau_p = 0.1$ sec. A forward-loop integrator was included to ensure zero steady-state roll rate error. This integrator also has the effect of reducing bank angle excursions due to disturbances. Thus it aids in maintaining constant bank angle in turbulence but, by partially decoupling the lateral and directional modes, inhibits the pilot's ability to roll the aircraft with slow rudder inputs. The desirability of this feature remains to be examined in piloted simulation. The aileron actuators are modelled with 100 deg/sec rate limits and appropriate deflection limits. The cross-feed gain, G_{DCAI}, can be used to partially compensate for the rolling moment that is generated by differential canard deflection. Differential canard actuation is used to provide yaw control power at high angle-of-attack (see below).

If the one degree-of-freedom approximation to the roll mode is used, and the stick prefilter is neglected, the roll rate to roll rate command transfer function is of the form:

$$\frac{p(s)}{p_c(s)} = \frac{K_p L'_{\delta_a} (s + K_{pI}/K_p)}{s^2 + s(K_p L'_{\delta_a} - L'_p) + K_{pI} L'_{\delta_a}} \tag{8.1}$$

If the term $(s + K_{pI}/K_p)$ is factored from the denominator, the transfer function reduces to a first-order lag of form:

$$\frac{p(s)}{p_c(s)} = \frac{K_p L'_{\delta_a}}{(s + 1/\tau_R)} \tag{8.2}$$

where

$$K_p = \frac{1}{\tau_R L'_{\delta_a}}, \tag{8.3}$$

and

$$K_{pI}/K_p = - L_p'. \tag{8.4}$$

The gains K_p and K_{pI} can be computed for any desired value of τ_R from stored stability derivatives C_{l_p} and $C_{l_{\delta_a}}$. For an unaugmented airframe,

$$\tau_R \cong - \frac{1}{L_p'}.$$

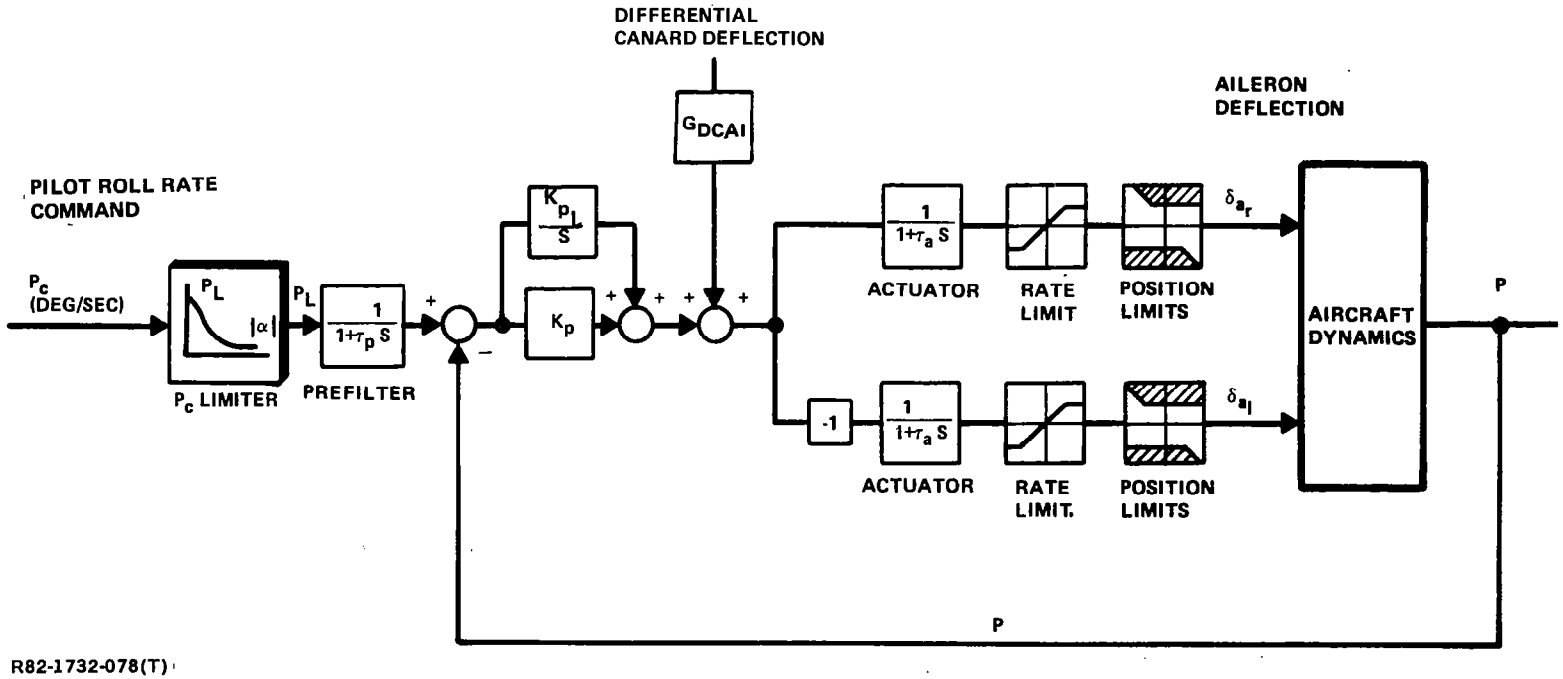

Figure 8-3. - Lateral control system.

Since L_p' is proportional to (ρV), the quickening of roll mode convergence with airspeed and density (typical of an unaugmented aircraft) can be emulated by programming $\tau_R = \frac{1}{\rho V}(\tau_{R_o})$. In this study, τ_{R_o} was set to 0.3 sec for M = 0.4 at sea level. As can be seen from Figure 8-4, the degree of augmentation required in the roll channel is moderate except at angles-of-attack in excess of 40 degrees.

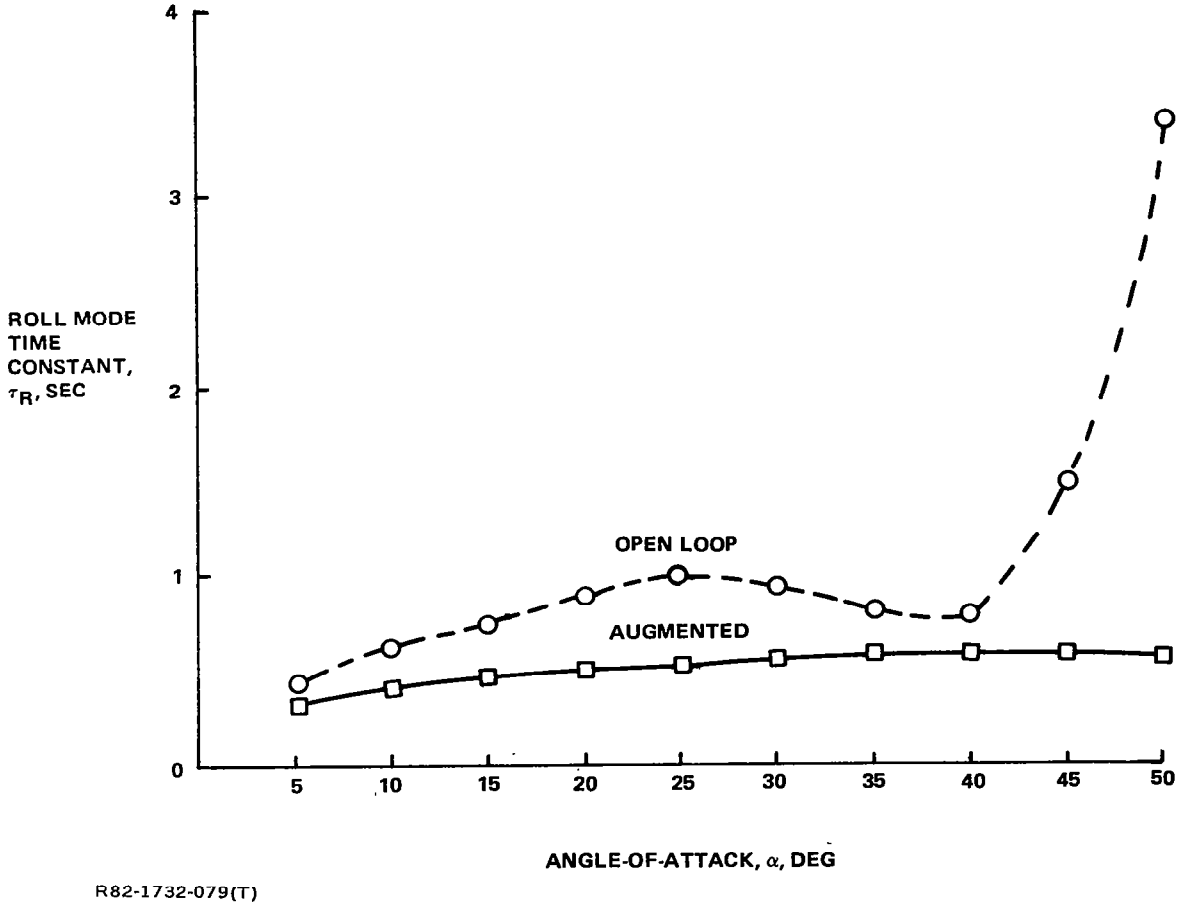

Figure 8-4. - Open loop and augmented roll mode time constant(1 g flight) vs angle-of-attack.

Figure 8-5 is a block diagram of the directional control system. The control law is a simple rudder command system. The rudder pedal input is modified by a limiter (see Section 9) and, as in the other channels, by a first-order lag prefilter (τ_r = 0.1 sec). The command signal actuates both the rudder and the port and starboard canard surfaces differentially. The rudder actuator is modelled as a first-order lag (τ_a = 0.05 sec) with 100 deg/sec rate limits; the differential canard command is summed with the sym-

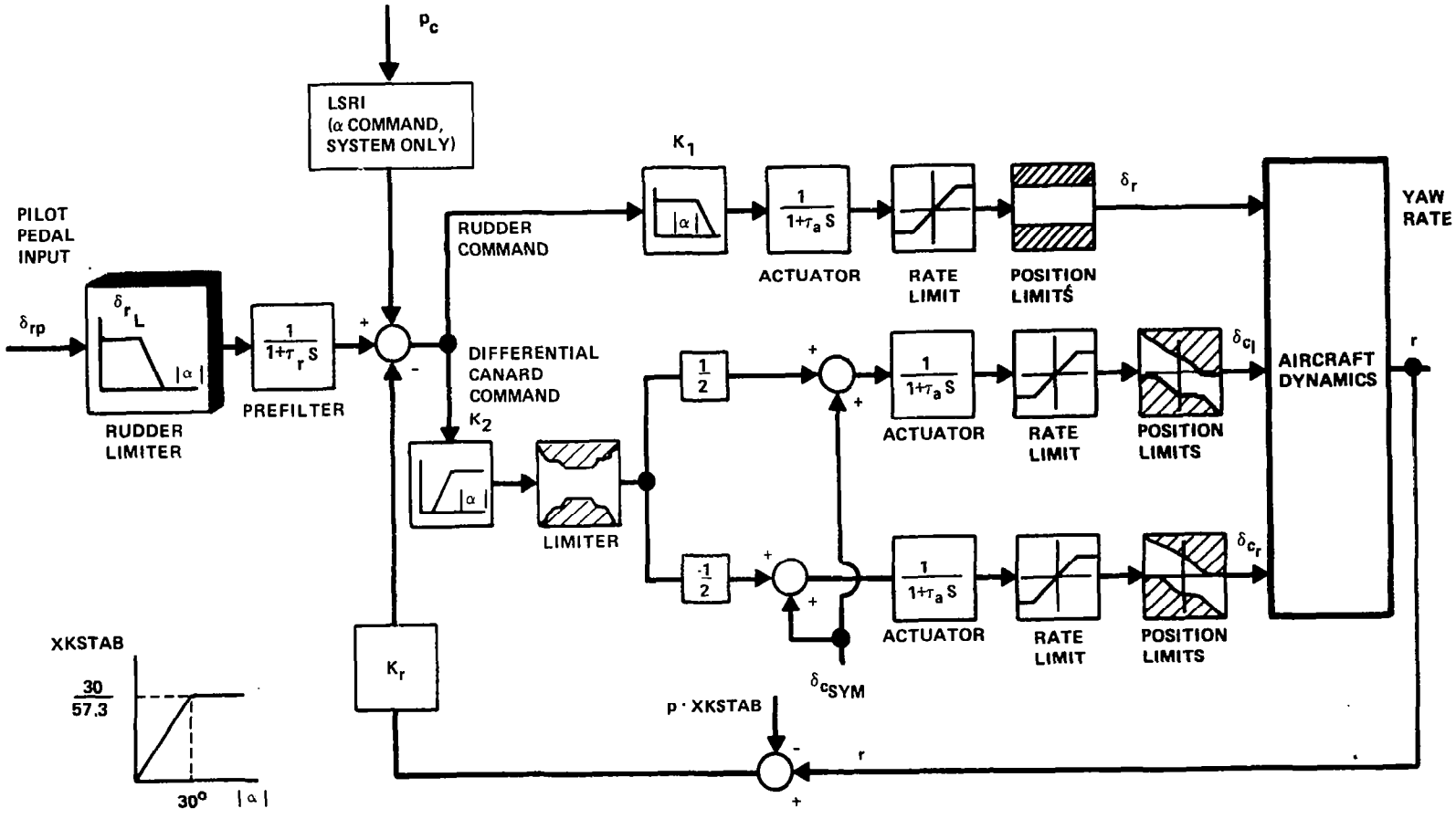

R82-1732-080(T)

Figure 8-5. - Directional control system.

metric longitudinal canard command signal $\delta_{c_{sym}}$. A lateral stick-to-rudder interconnect (LSRI) was implemented for use with the α command system only.

Note that only a single feedback loop is used. The body axis yaw rate feedback is modified by the term p.XKSTAB (p is the body axis roll rate) to provide coordination of the desired stability axis roll mode at low-to-moderate angle-of-attack. The function XKSTAB is a linear approximation to (sin α) up to $\alpha = 30°$. Beyond $\alpha = 30°$, XKSTAB is held constant, thus yielding a high angle-of-attack roll axis intermediate to the stability and body axes. In addition to providing roll coordination, yaw rate feedback also augments dutch roll damping. Dutch roll frequency could have been augmented by A_y or β feedback, but because of the favorable directional stability characteristics of the STAC configuration, dutch roll frequency augmentation proved unnecessary. Moreover, elimination of an A_y loop avoided the ambiguity introduced by the change in sign of C_{y_β} with angle-of-attack (see Figure 8-6).

The rudder/differential canard blending functions K_1 and K_2 shown in Figure 8-5 are complementary functions. The command to the rudder is reduced in proportion to the decay in rudder power with angle-of-attack, and the command signal causing differential canard deflection is proportionally increased. At high-angle-of-attack, differential canard deflection also causes significant rolling moments. In order to avoid aileron saturation, the maximum differential canard command was reduced to below the aerodynamically most effective deflection (in terms of yaw control power) as shown in Figure 8-7. The total yaw control power thus achieved is depicted in Figure 8-8.

An expression for the feedback gain K_r was developed from the two-degree-of-freedom approximation to the dutch roll mode:

$$K_r = \frac{2\zeta_d\omega_d - 2\zeta_1\omega_1}{K_1 N'_{\delta_r} + GK_2 N'_{\Delta\delta_c}} \tag{8.5}$$

where

$$2\zeta_1\omega_1 = - Y_v - N_r' \ . \tag{8.6}$$

Since only a single feedback is used, damping and frequency could not be adjusted independently. Thus the term $2\zeta_d\omega_d$ represents the combined, desired dutch roll characteristics. G represents the gearing between rudder and differential canard command. Since the rudder deflection was limited to $\pm 20°$ and the maximum differential canard deflection was $\pm 48°$, this gearing was set to G = 2.4. The baseline values for the closed-loop dutch roll characteristics were selected to be $2\zeta_d\omega_d = 1$ rad/sec. Figure 8-9 illustrates the dutch roll damping characteristics of the unaugmented and augmented aircraft.

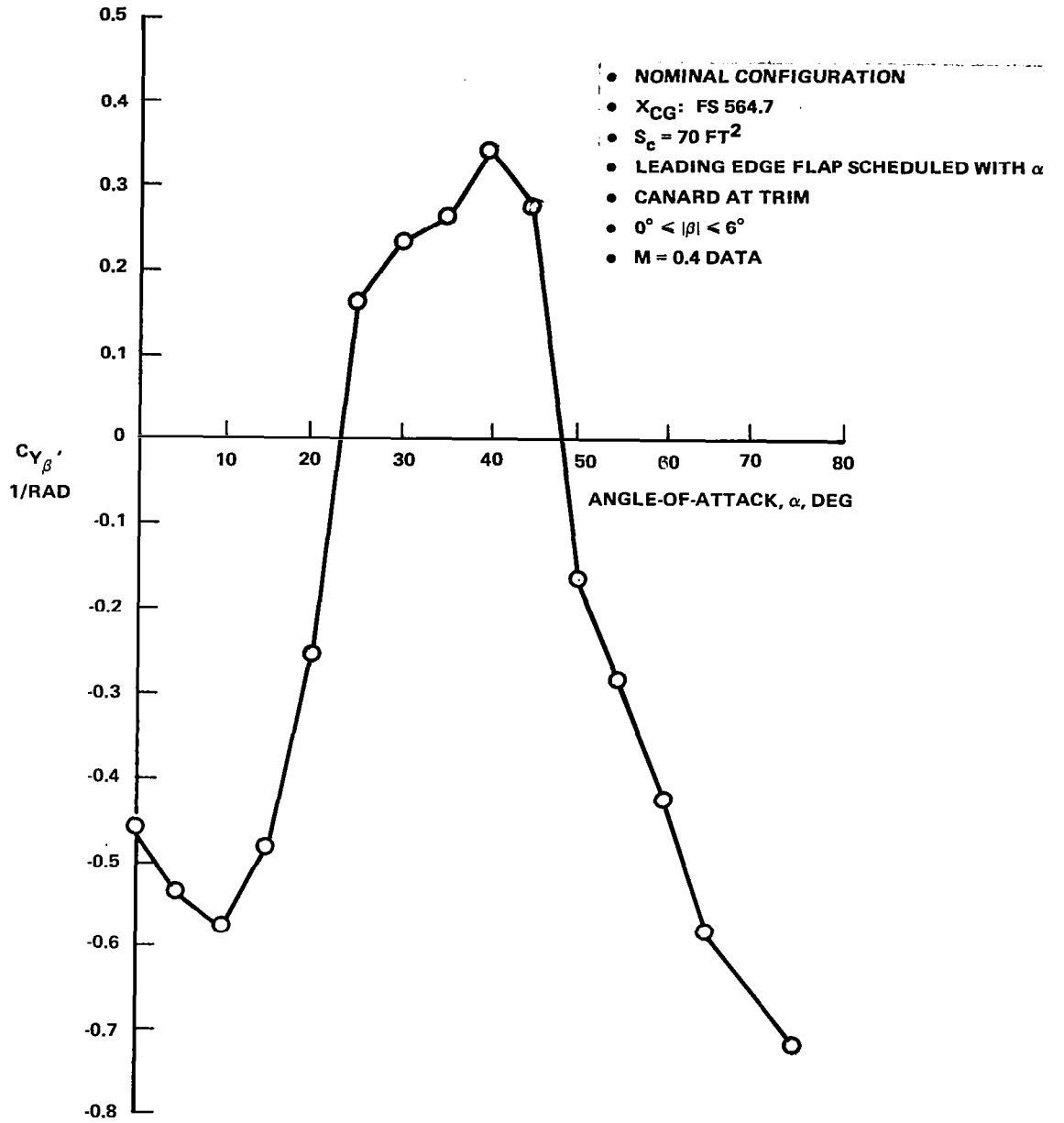

R82-1732-081(T)

Figure 8-6. - STAC airframe side force coefficient due to sideslip, C_{Y_β}, vs angle-of-attack.

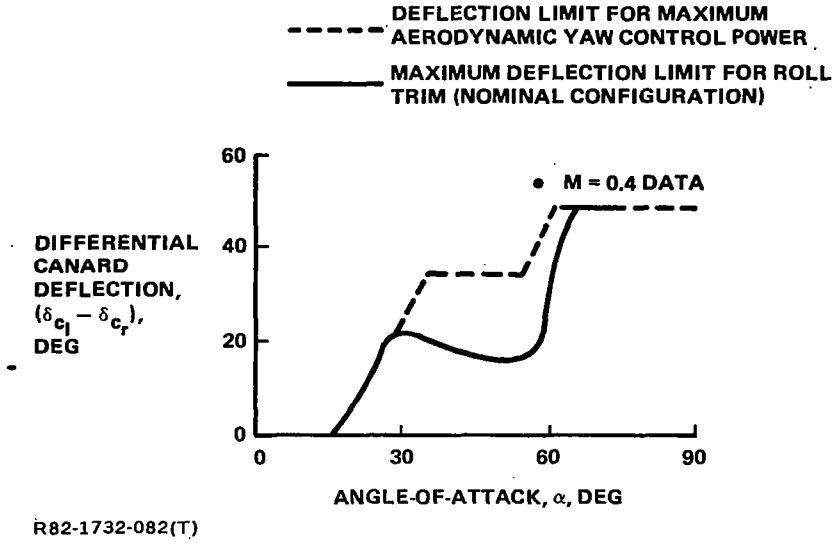

Figure 8-7. - Differential canard deflection limits vs angle-of-attack.

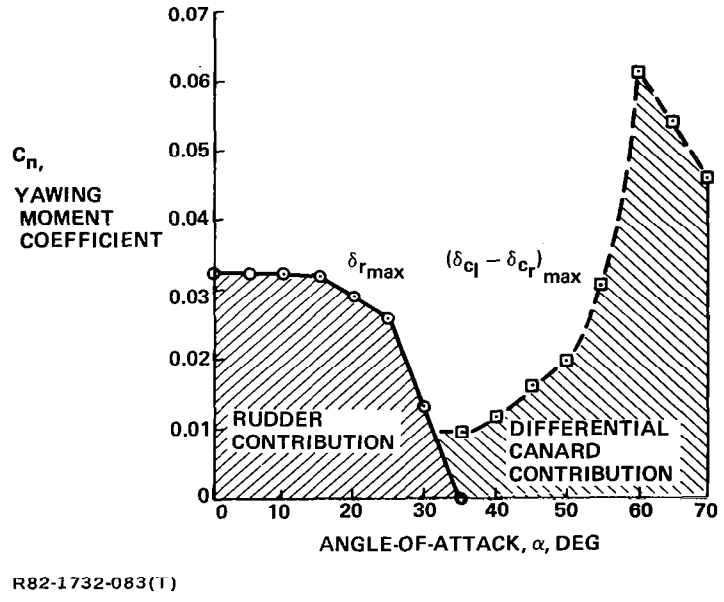

Figure 8-8 Total yaw control power (blending schedules K_1 and K_2) vs angle-of-attack.

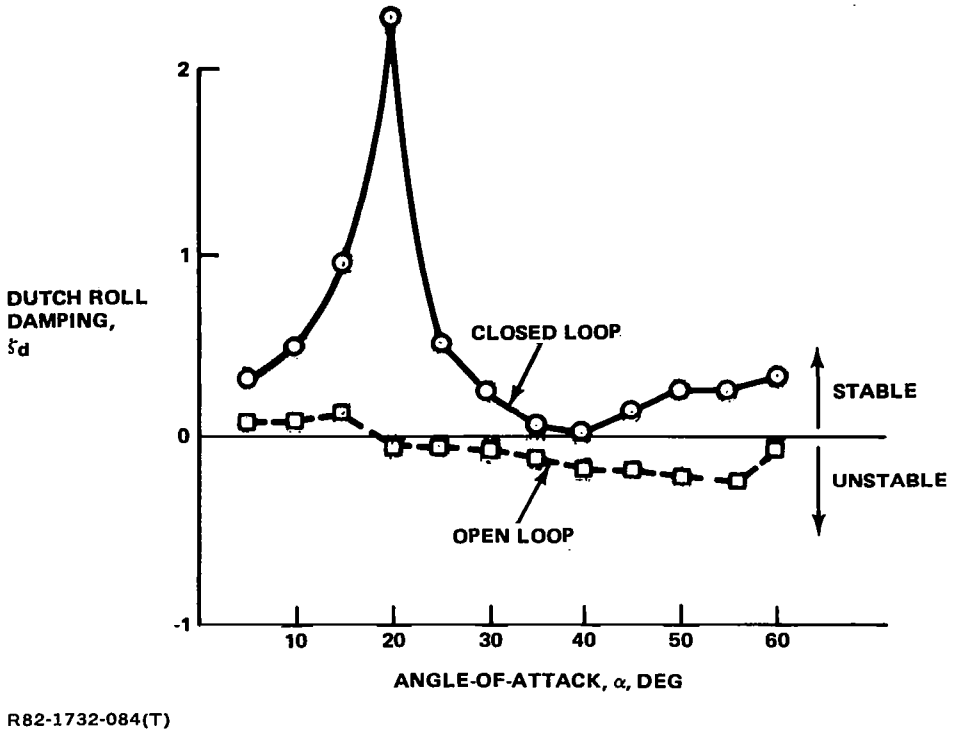

Figure 8-9. - Open loop and augmented dutch roll damping, ζ_d, vs angle-of-attack, α .

8.3 LATERAL/DIRECTIONAL CONTROL LAW EVALUATION

8.3.1 Basic Responses

Aircraft response to a lateral stick step input is shown in Figure 8-10 for an initial trim condition at M = 0.4, sea level ($\alpha_{trim} \approx 6°$). The response to a step rudder pedal command is shown in Figure 8-11. Note in particular the effect of the forward-loop integrator in maintaining bank angle following the roll rate transient.

There is a dichotomy associated with attempting a stability axis roll if the longitudinal control law is a pure "G" command system. Recall that, in the "G" system, the n_z feedback is biased by the signal ($\cos\theta\cos\phi$). Including this bias term avoided the necessity to retrim the longitudinal stick with attitude changes. As the aircraft is rolled to an inverted attitude, this "G" law will force the angle-of-attack negative ($\alpha \rightarrow 0$ at $\phi = 90°$). Thus, in the course of rapid sustained rolls through several cycles, the "G" system enforces a body axis roll mode (Figure 8-12). Note the oscillatory behavior of α and β.

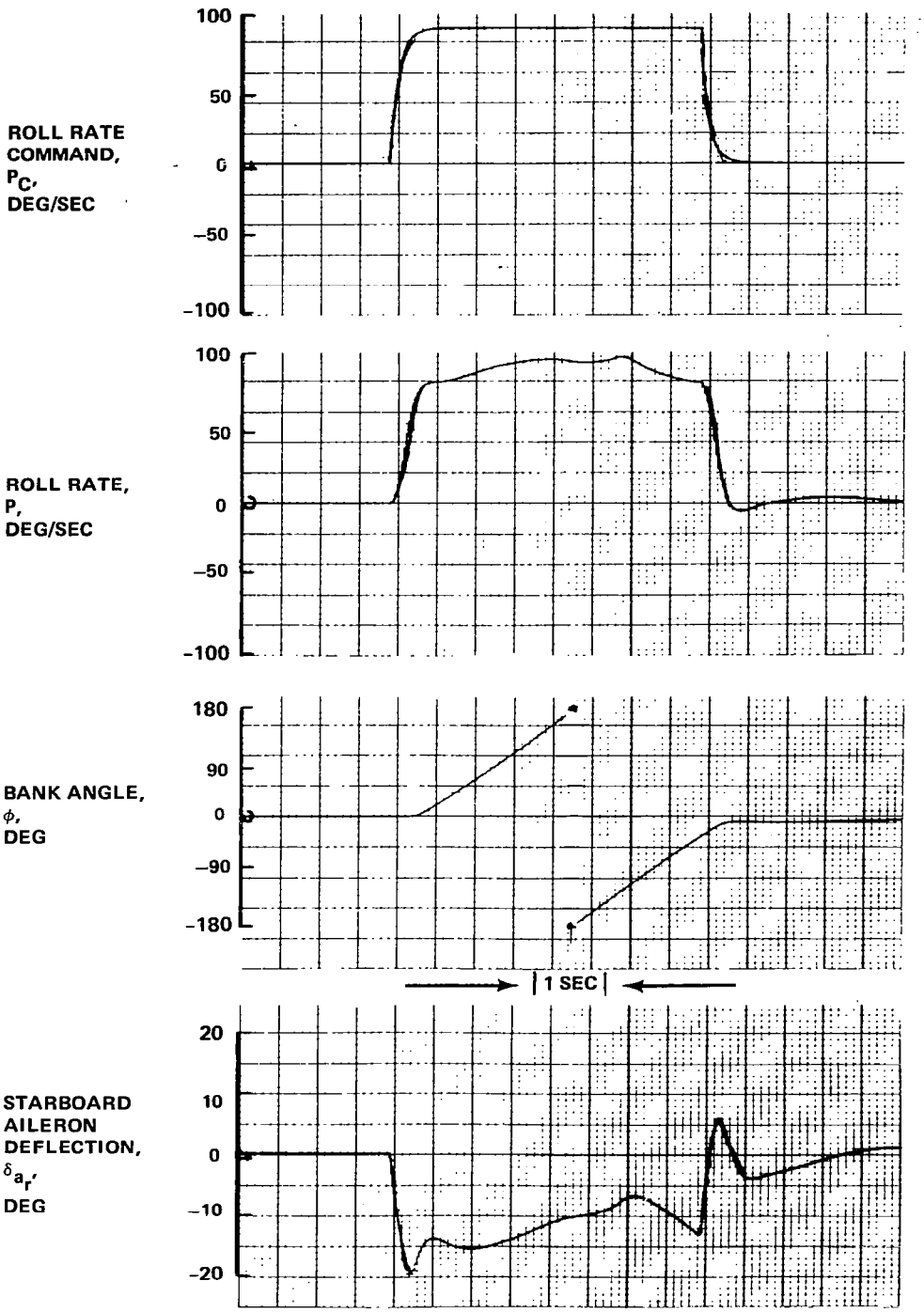

Figure 8-10. - Augmented airframe roll response to a step roll rate command (M = 0.4, sea level).

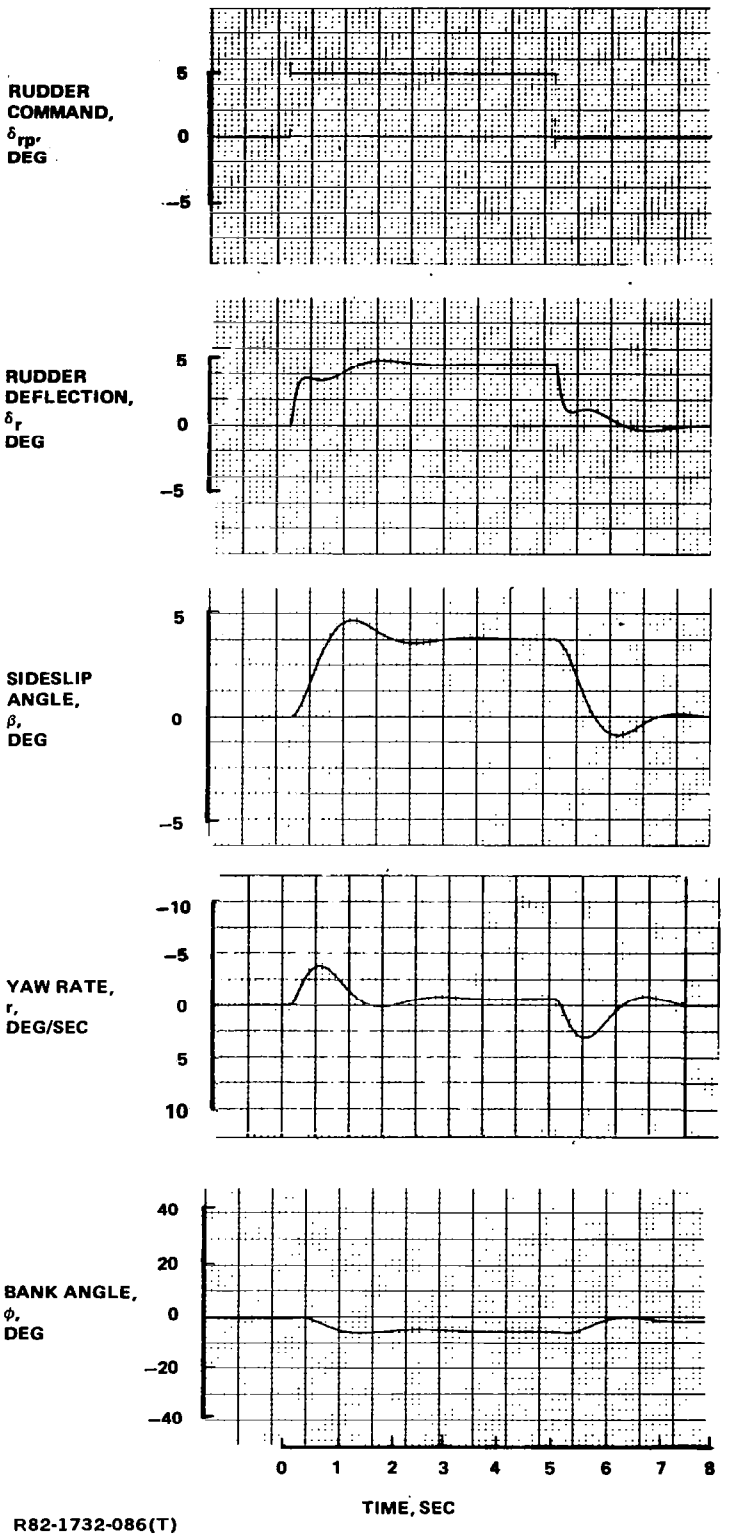

Figure 8-11. - Augmented airframe directional response to a step rudder pedal input (M = 0.4, sea level).

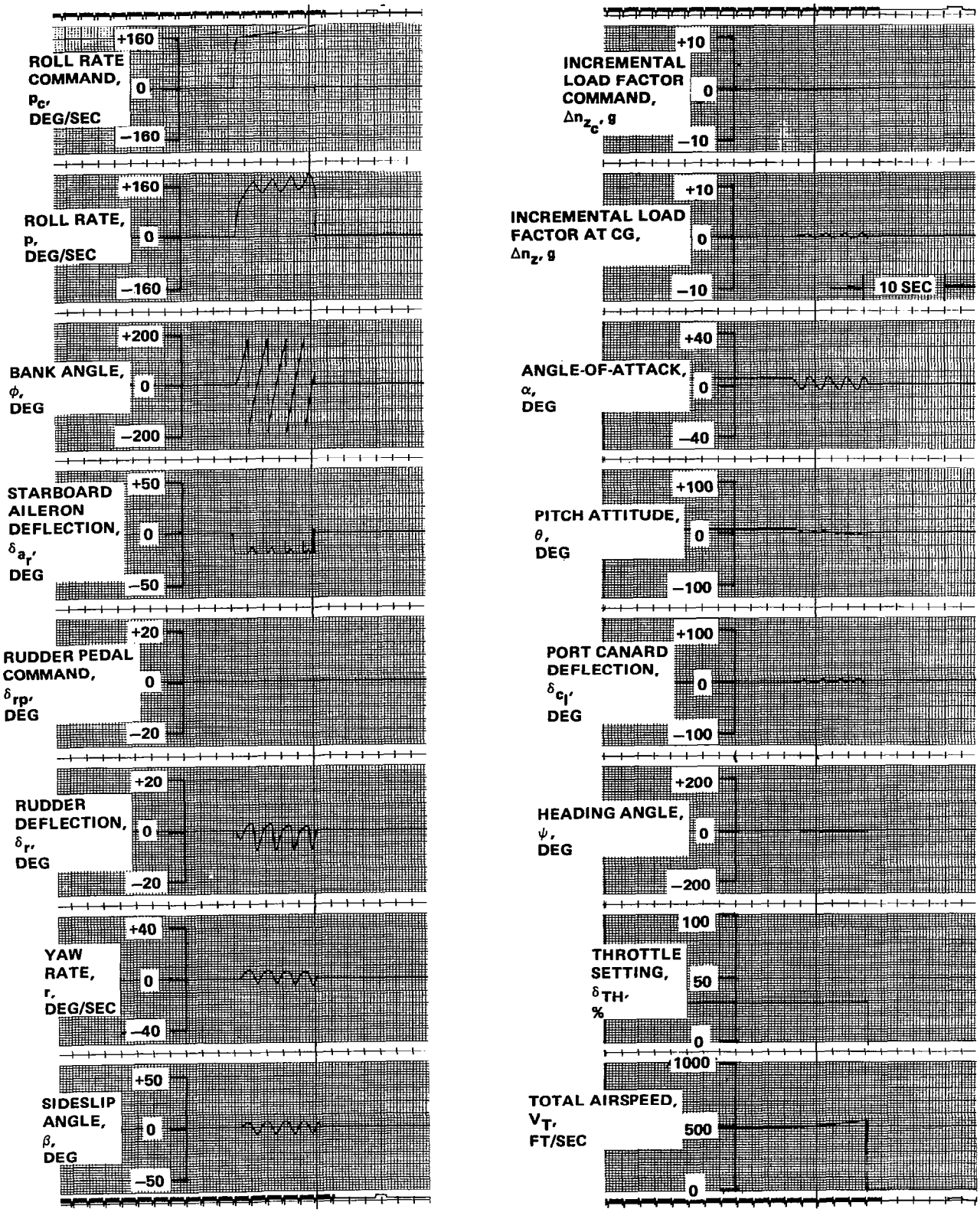

R82-1732-087(T)

Figure 8-12. Sustained rolling maneuver ("G" command longitudinal control law, nominal configuration).

A true stability axis roll mode was possible only with the "α" command longitudinal control law. When this law was developed, it became clear that simple stability axis yaw rate feedback to the rudder is inadequate to properly coordinate the motion during rapid roll entries. Recall that the STAC aircraft moment of inertia ratio is $I_z/I_x \simeq 10$. Substantial lead is therefore required for coordination. This requirement was met by using a lateral stick to rudder interconnect (LSRI). The LSRI mechanization is shown in Figure 8-13. First, the lateral stick deflection is sensed. If its magnitude exceeds the specified deadband, the signal is passed through a first-order lag and washout before being summed with the rudder command as was shown in Figure 8-5. Parameters of system, including the gain G_{LSRI}, the lag time constant, and the washout break frequency were determined empirically. Roll response of the aircraft configured for the α command system with and without the LSRI is shown in Figure 8-14.

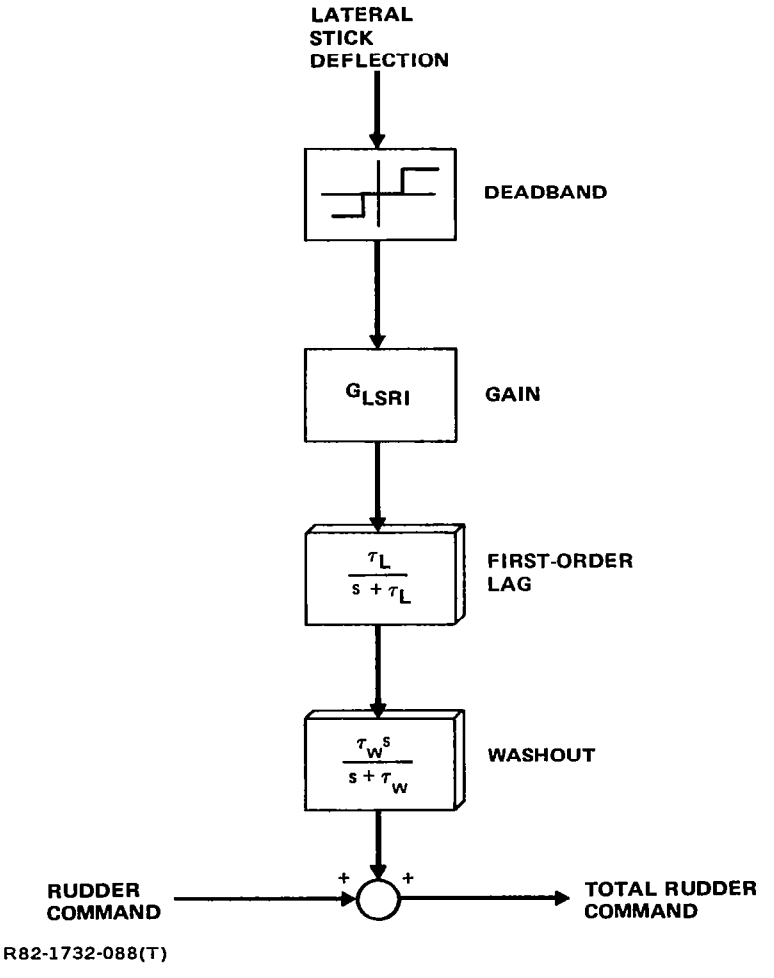

Figure 8-13. - Lateral stick-to-rudder interconnect (LSRI) mechanization.

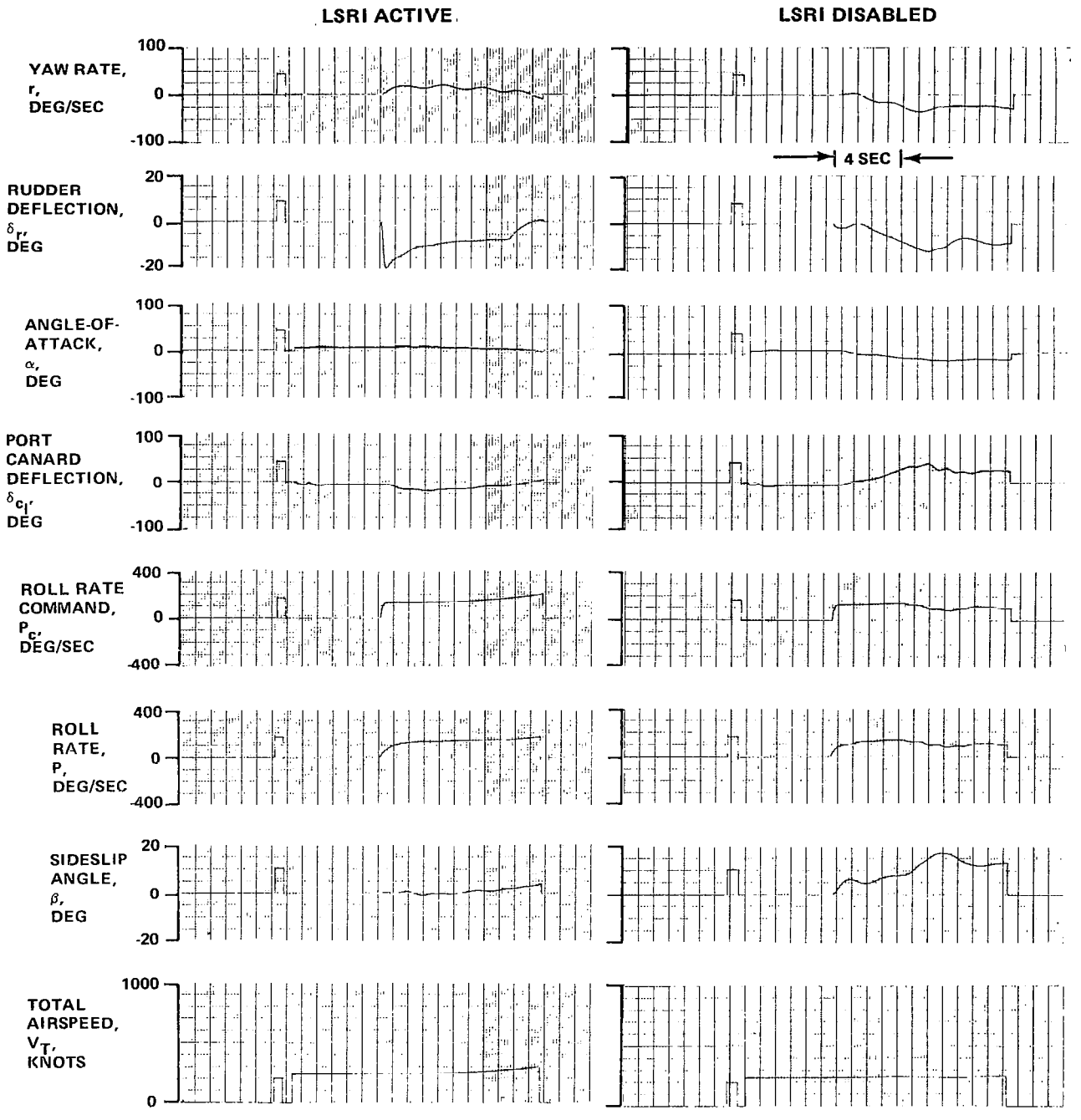

R82-1732-089(T)

Figure 8-14. - Roll response for α system with and without LSRI.

8.3.2 Sensitivity of the Lateral/Directional Control Laws to Plant Variations

The sensitivity of the lateral/directional control laws to plant variation was assessed emphasizing the aerodynamic parameters with the highest uncertainty levels. Figure 8-15 shows the nominal aircraft response to a 90 deg/sec, 4-sec roll rate command at M = 0.4. The figure also shows the system response with the roll damping derivative C_{l_p} set to zero. This derivative can be difficult to estimate, particularly at higher angles-of-attack. The lateral control system response with $C_{l_p} = 0$ shows a slight increase in roll rate overshoot, but the salient character of the basic response is preserved.

Figure 8-16 illustrates the directional control system sensitivity to aerodynamic plant variations. The significant directional control system aerodynamic parameters are damping in yaw, C_{n_r}, and directional stability, C_{n_β}. The nominal directional control system response for a 5° rudder input command is shown for M = 0.4. With damping in yaw, C_{n_r}, set equal to zero, there is a slight increase in sideslip angle overshoot. With C_{n_β} halved, the dutch roll frequency is reduced and steady state sideslip angle increased. None of the off-nominal runs, however, resulted in severely degraded responses.

8.3.3 Effects of Atmospheric Turbulence on the Lateral/Directional Control System

The effect of atmospheric disturbances, both discrete gusts and continuous turbulence, on the operation of the lateral/directional control system was investigated. As in the longitudinal control system turbulence investigation, white noise was filtered through Dryden filters and input to the simulation for aircraft turbulence response assessment. Figures 8-17 and 8-18 show the input gust field and the lateral/directional control system operation in severe turbulence (σ = 22 ft/sec) at M = 0.4. The aircraft penetrates the turbulence without excessive aileron or rudder deflections. Only 25% of aileron capability and 15% of rudder capability (peak) are used to moderate minor excursions in bank angle, roll rate, sideslip angle, and yaw rate.

Figure 8-19 shows the lateral/directional control system response to a severe (σ = 22 ft/sec) lateral discrete gust. The "1-cosine" shape gust was tuned to the frequency of the closed-loop, dutch-roll mode. The aircraft penetrates this discrete gust with only minor aileron and rudder deflection requirements.

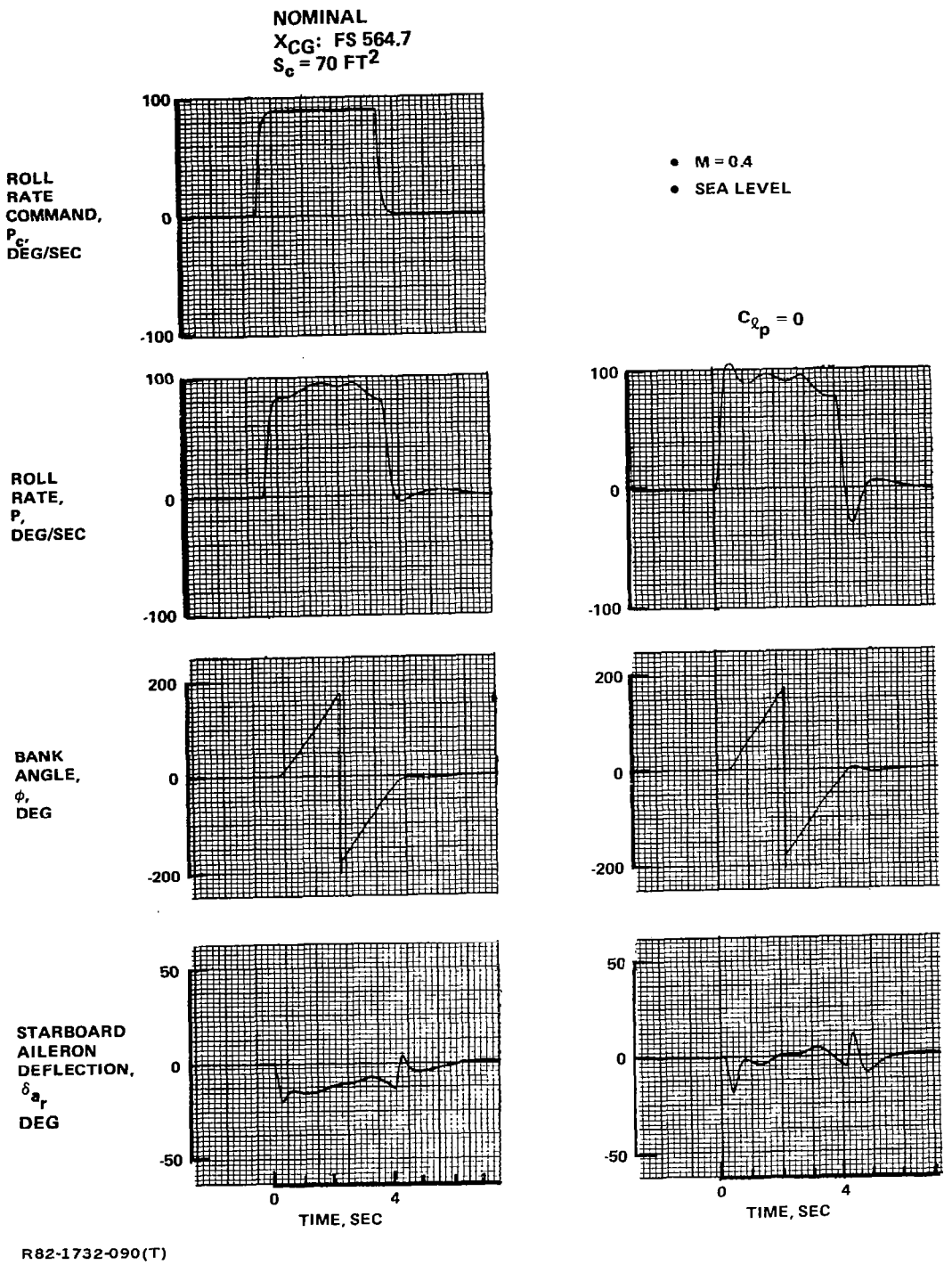

Figure 8-15. - Lateral control response sensitivity to the roll rate damping derivative, C_{l_p}.

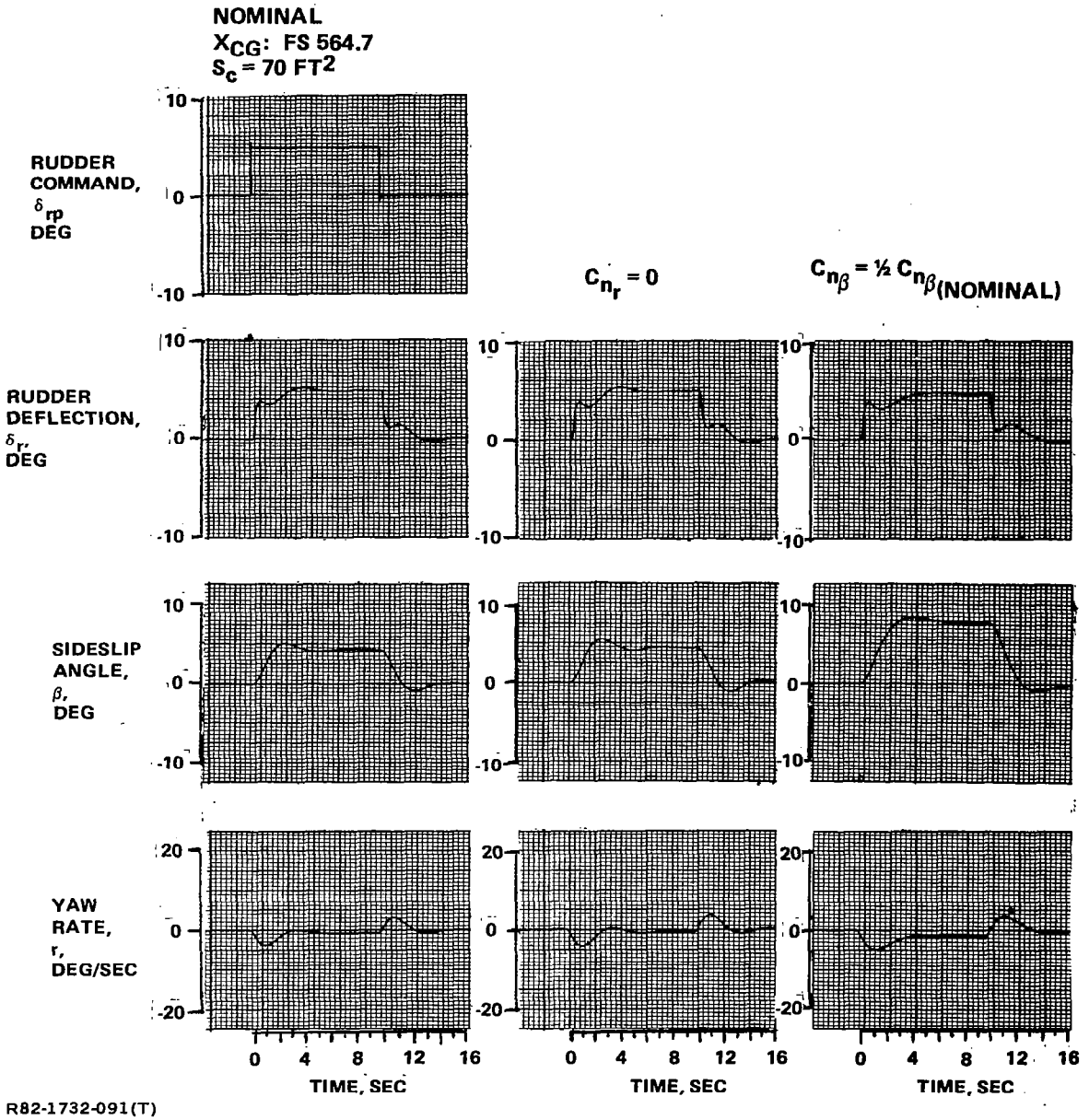

Figure 8-16. Directional control response sensitivity to the yaw damping derivative, C_{n_r}, and directional stability derivative, C_{n_β}.

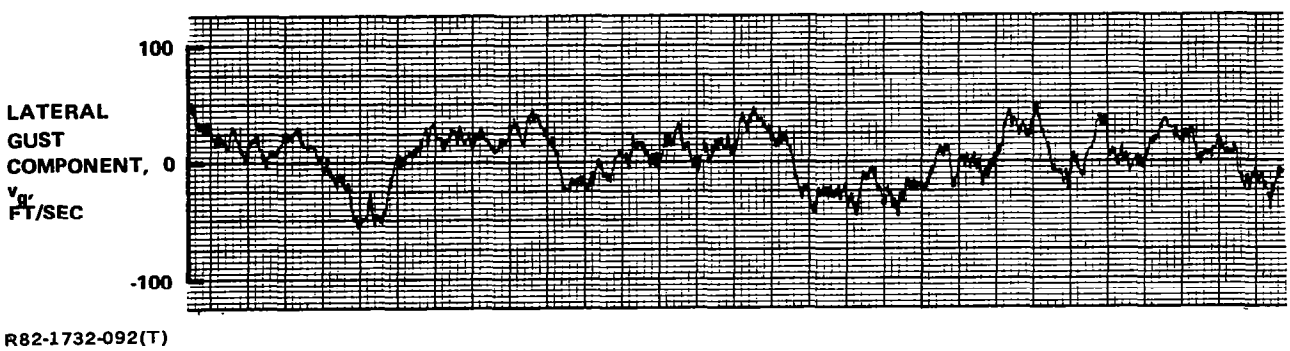

Figure 8-17. - Simulated lateral gust field ("severe" turbulence intensity, σ = 22 ft/sec).

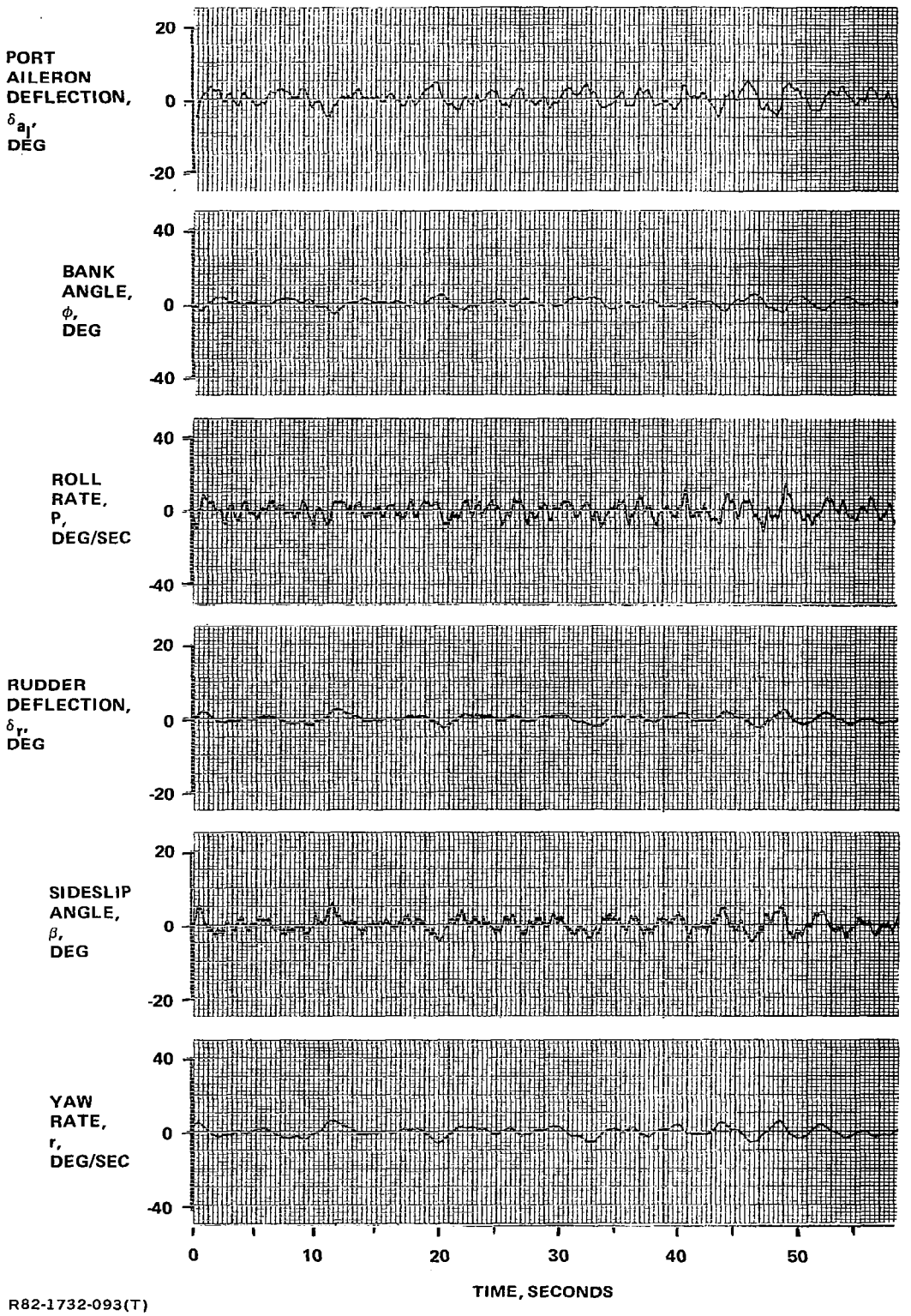

Figure 8-18. - STAC response to severe turbulence (sea level).

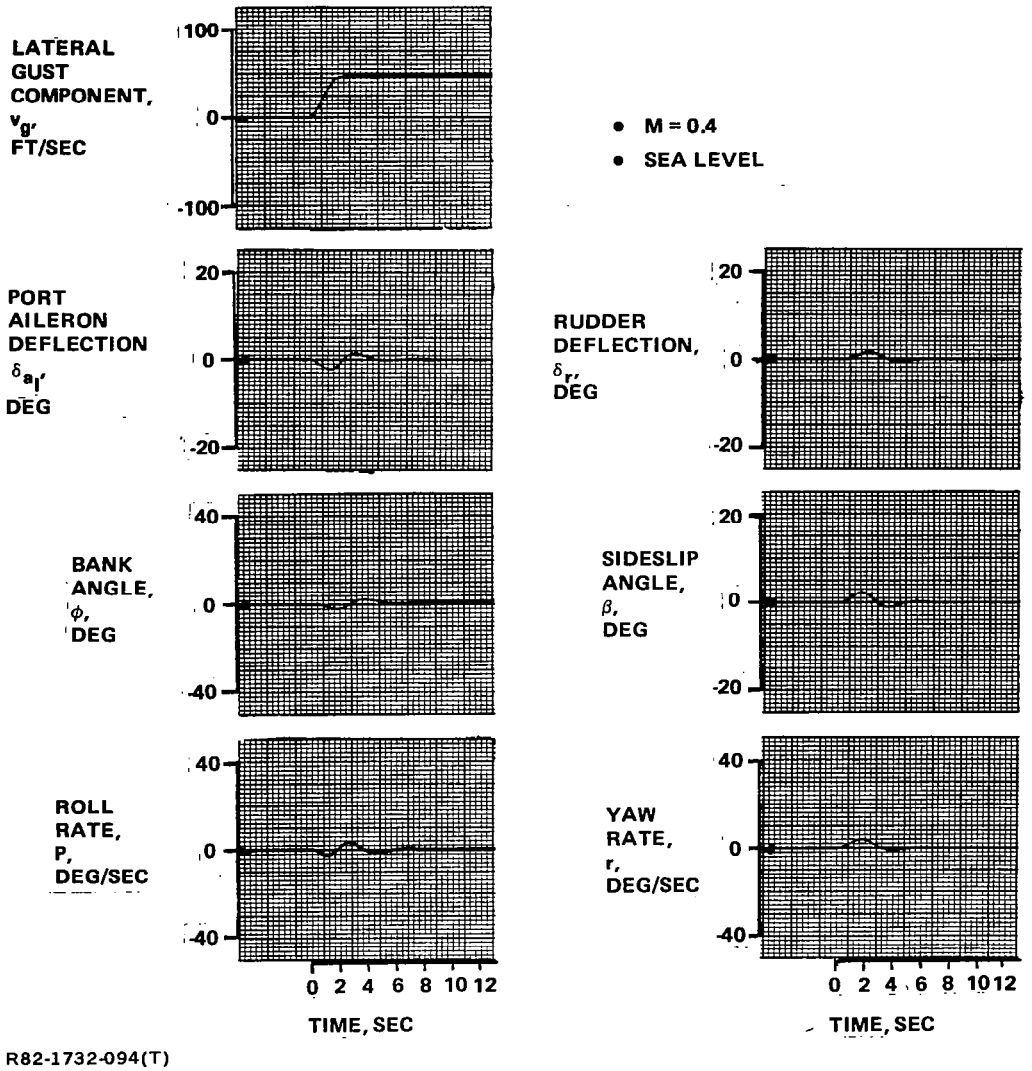

Figure 8-19. Response to a discrete lateral gust.

9 - COMMAND LIMITER DEVELOPMENT

9.1 APPROACH

The initial control system evaluation, reported in Sections 7 and 8, was, for the most part, conducted at low-angle-of-attack (M = 0.4, sea level, $\alpha_{trim} \simeq 6°$) with single-axis command inputs. Satisfactory response was demonstrated for large-amplitude lateral/directional inputs; all longitudinal inputs, however, were of small amplitude. It had always been clear that the critical control system design issue for Relaxed Static Stability (RSS) aircraft centered on control of large-amplitude, coupled multi-axis maneuvers. The impact of each term in the full nonlinear six-degree-of-freedom equations of motion needed to be evaluated relative to its effect on the adequacy of the primary pitch controller (canard). The next step in developing the control laws was to determine what, if any, command limiting would be required to prevent aircraft departure during aggressive maneuvering. A basic groundrule was that any such modifications to the control laws was to be made outside the basic feedback system structure so as not to impact the model-following algorithms.

That some form of pitch axis limiter for the "G" system would be required was a foregone conclusion. As noted previously, a pure "G" command longitudinal control law, in the absence of an autothrottle, causes loss of speed stability. Control limiter development was, therefore, initiated with a pitch axis investigation.

9.2 DEVELOPMENT OF THE $\Delta n_z/\alpha$ COMMAND LIMITER FOR THE "G" SYSTEM

Canard position and rate saturation concerns were crucial to command limiter development. If saturation occurs, the aircraft is effectively operating in an open-loop sense in terms of stability. In developing the pitch axis command limiter, the intent was to avoid long-term canard position saturation during aggressive maneuvering, since this would lead to departure. On the other hand, excessive command limiting can be expected to have an adverse impact on aircraft agility; short-term saturation was therefore permitted. In fact, the duration of canard saturation became a figure of merit for limiter design.

The results of the canard rate study showed that, if uniform handling qualities were to be maintained over the angle-of-attack range up to $C_{L_{max}}$, relatively high canard rates would be required. For instance, at M = 0.4, sea level, with $\tau_c = 0.1$ sec and $CAP_A = 1$, the peak canard rate would be in excess of 200 deg/sec for a maximum throw stick input. Such rates were considered to be too high, and the intent was to ultimately limit the canard actuator rate to ±100 deg/sec. Initially, however, no rate constraint was imposed, so that the effects of position saturation could be isolated.

The final $\Delta n_z/\alpha$ limiter, implemented in series with the pilot longitudinal stick input, is shown in Figure 9-1. This device, which acts to limit/augment the pilot command, is two-dimensional.

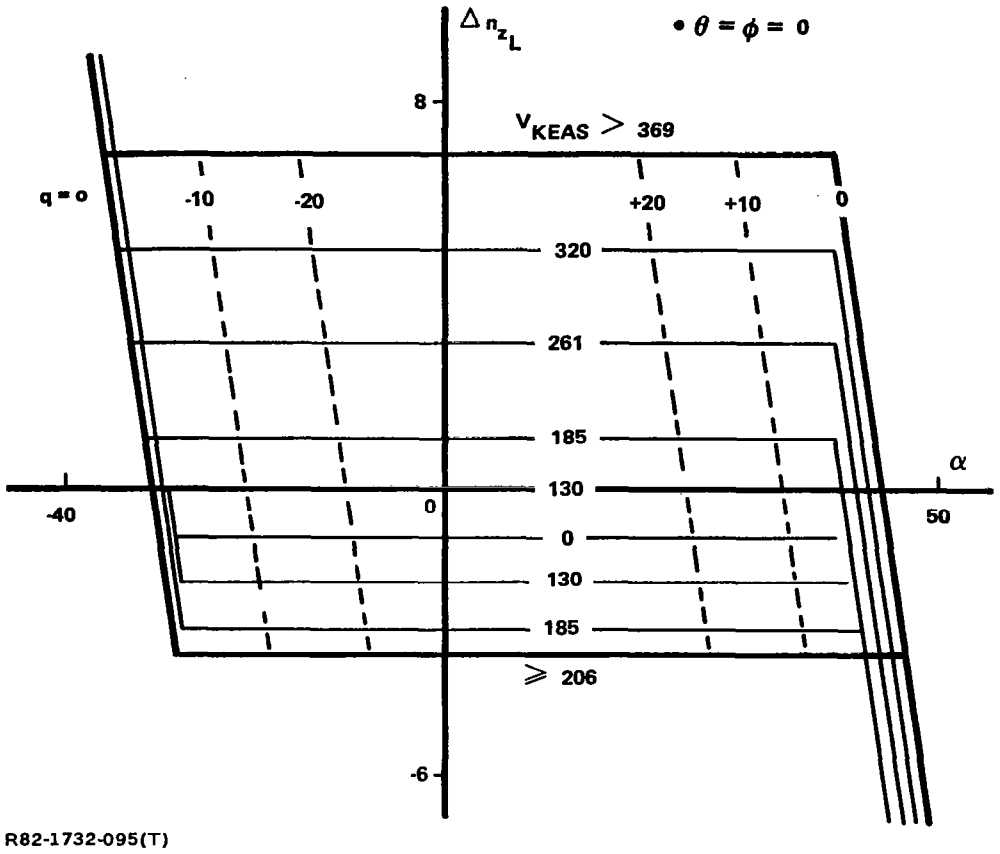

Figure 9-1. Load factor/angle-of-attack ($\Delta n_z/\alpha$) limiter.

The upper and lower bounds, which directly modify the commanded incremental load factor, were computed to ultimately constrain the aircraft within its maximum incremental structural load factor limits (+7 g, -3.5 g). These limits are progressively lowered with dynamic pressure, restricting the aircraft to incremental load factors commensurate with $C_{L_{max}}$. As the airspeed decays to zero, the limiter (for upright flight) causes unloading of the aircraft - in effect acting as a "stick pusher". The zero airspeed line is biased upwards as a function of attitude, $f(\cos\theta\cos\phi)$, such that if the aircraft is in inverted flight, a positive incremental load factor command causes the aircraft to pitch earthward as speed decays. A gain other than unity on the bias term was also investigated. For certain symmetric maneuvers, such as an inside loop, the magnitude of the bias gain will affect aircraft performance and energy level. As the gain is increased, a tighter loop results, but the aircraft exits the maneuver at a lower energy state.

Whereas the upper and lower bounds are quasi-static limits, the right and left limiter α boundaries are intended to prevent dynamic overshoot/ departure in angle-of-attack. Due to the limited nose-down pitch power available, rapid large-amplitude longitudinal stick inputs would, despite the prefilter and Δn_z limiting, cause large angle-of-attack excursions at low speed. An

example is shown on the left side of Figure 9-2. By limiting angle-of-attack in a dynamic sense such excursions were eliminated. For 1 g flight (Δn_{z_c} = 0), the absolute positive angle-of-attack limit was set slightly above α for $C_{L_{max}}$. This absolute positive α limit was reduced in proportion to pitch

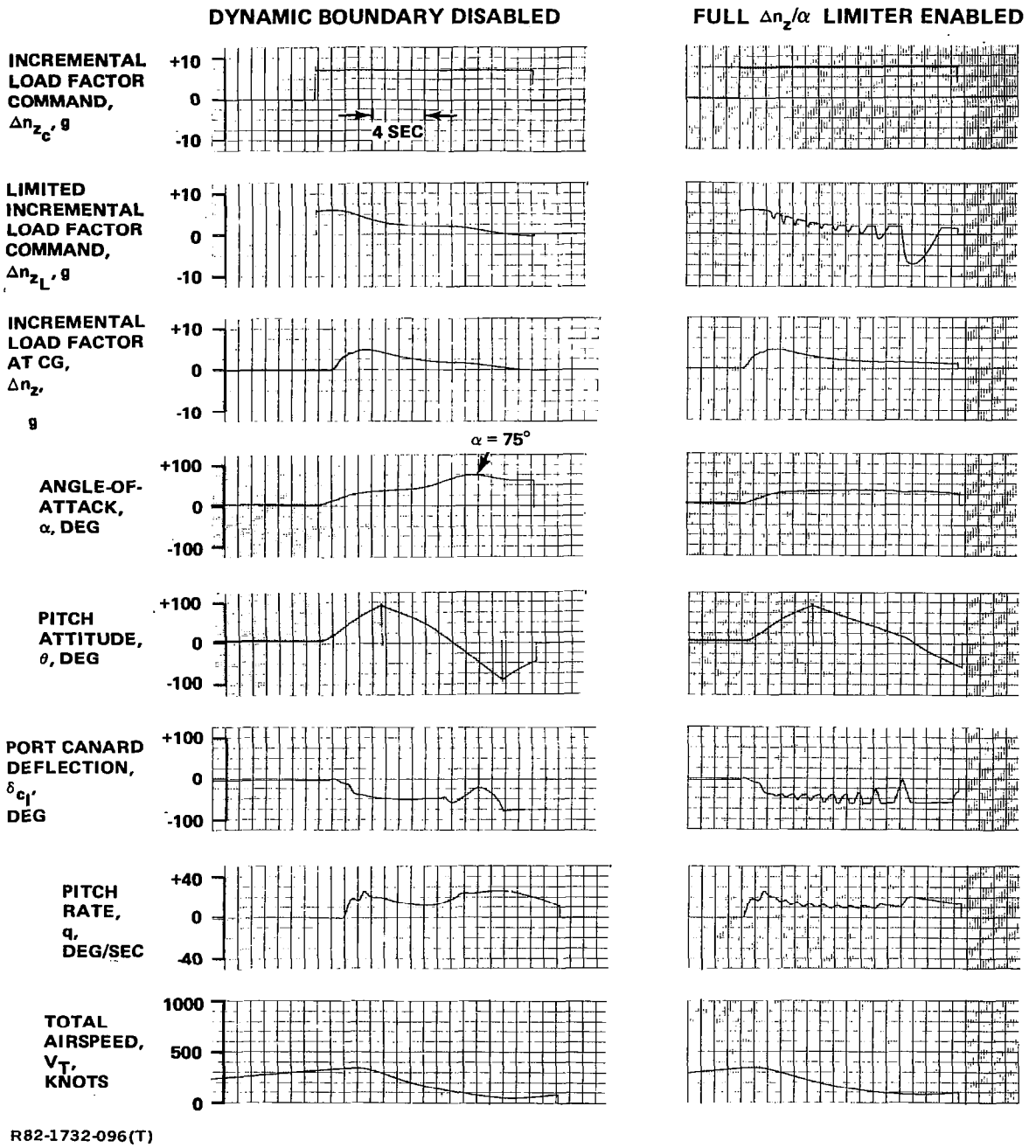

Figure 9-2. - Effect of dynamic boundary on n_z/α limiter operation.

rate ($\Delta\alpha/\Delta q$ = 1 sec). Note that the right and left α boundaries extend above and below the incremental load factor limits. This logic is intended to ensure that the canard drives to its aerodynamic limits, if necessary, to prevent departure.

The forward-loop integrator must be protected from overloading whenever the canard saturates. Logic was incorporated to break the error signal to the integrator if the sense of canard saturation was in the direction required to arrest a departure. The integrator signal was also interrupted during canard rate saturation. With these modifications in place, the results shown on the right side of Figure 9-2 were generated. The activation of the dynamic limiter boundary is clearly evident in the modified Δn_z command (limiter output, Δn_{z_L}) trace. Note that angle-of-attack is constrained to below $C_{L_{max}}$ throughout the loop maneuver and, as a result, the aircraft also maintains a higher average energy state.

It should be noted that the dynamic limiter boundaries are sensitive to canard rate limits. When rate limits of ±100 deg/sec were imposed, the canard tended to longer periods of saturation and departure prevention was adversely affected. Increasing either the slope of the dynamic boundary or the $\Delta\alpha/\Delta q$ ratio tended to yield satisfactory operation. Thus, it is clear that pitch controller actuator rate requirements for RSS aircraft are impacted not only by handling qualities issues, but by departure prevention considerations as well. Inadequate pitch control power/actuator rate capability lead to restrictive command limiters/reduced CAP levels with implications for both precision tracking and large-amplitude maneuvering. No limiter modifications were, however, immediately implemented, pending the results of a piloted simulator evaluation. The remainder of the study was conducted with unlimited canard rates.

9.3 DEVELOPMENT OF THE ROLL RATE COMMAND LIMITER

With an adequate pitch axis command limiter in place, the investigation next addressed multiple axis commands - the issue of pitch-roll inertia coupling in particular. The basic evaluation maneuver was a simulated rolling pull-out. One such run is shown in Figure 9-3. A full authority aileron roll command was followed 2.5 sec later by a full aft stick input. Initial conditions were M = 0.4 at sea level. Despite the $\Delta n_z/\alpha$ limiter, the aircraft departed to $\alpha = 90°$ (left side of Figure 9-3).

A roll rate command limiter was therefore developed to counter the effect of pitch-roll inertia coupling directly. The aircraft pitch acceleration is given by the equation:

$$\dot{q} = [(I_z - I_x)\, pr + I_{xz}\,(r^2 - p^2) + M]/I_y. \tag{9.1}$$

For a pure stability axis roll mode ($\beta = 0$):

$$p = p_s \cos\alpha,\ r = p_s \sin\alpha, \tag{9.2}$$

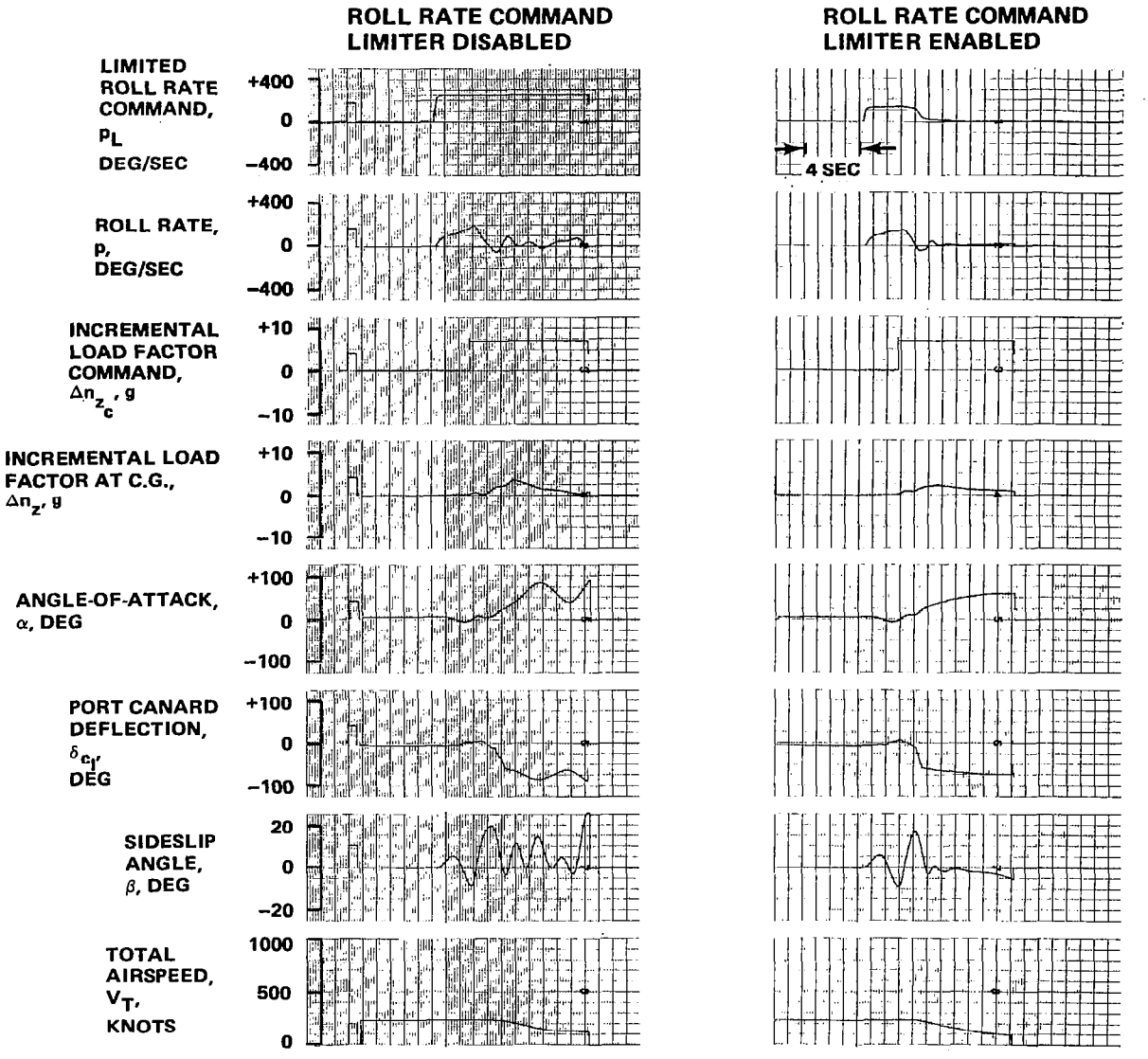

Figure 9-3. - Effect of roll rate command limiter.

where p_s is the stability axis roll rate.

If $I_{xz} = 0$:

$$\dot{q} = [(I_z - I_x)\, p_s^2 \sin 2\alpha + M]/I_y. \qquad (9.3)$$

By solving for p_s with $\dot{q} = 0$ at various trim 1-g angles-of-attack, a first estimate of the maximum roll rate that could be sustained with the available pitch control power was established. This steady-state boundary was incorporated as the angle-of-attack sensitive limit in the roll rate command limiter shown in Figure 9-4.

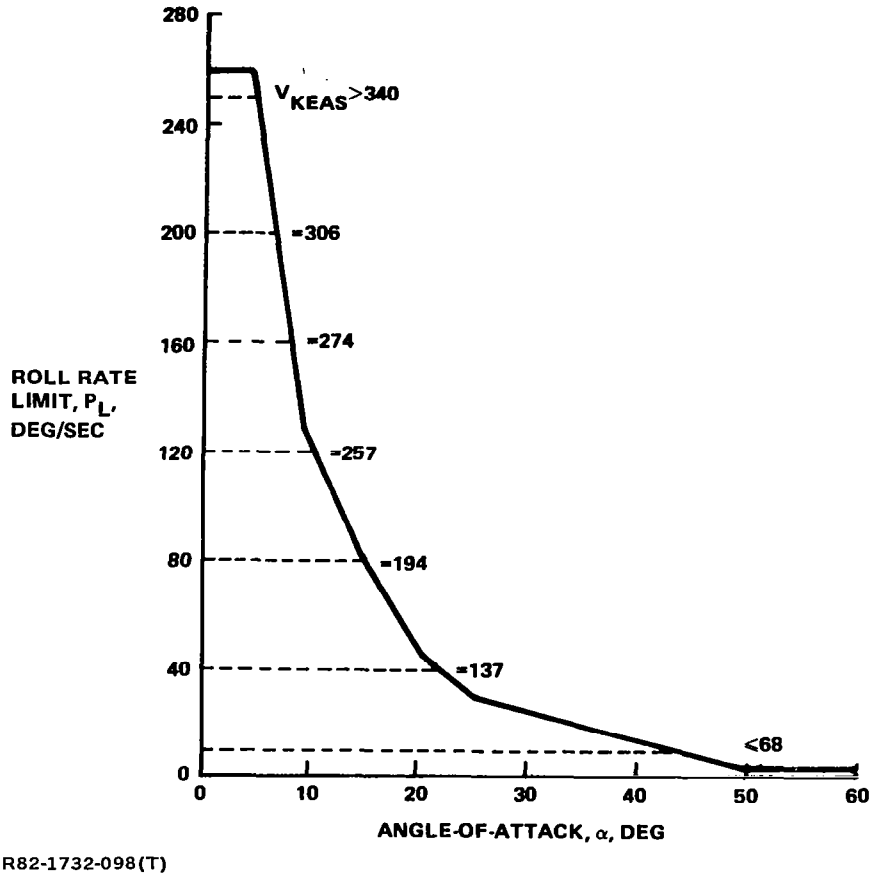

Figure 9-4. Roll rate limiter.

Even with the angle-of-attack sensitive roll rate limiter in place, certain combinations of command inputs still resulted in departures. For instance, a roll doublet at M = 0.3 in combination with a delayed (2.5 sec) full-aft stick command at idle power caused the aircraft to depart into an apparent slow flat spin (Figure 9-5).

Additional roll rate restrictions with angle-of-attack failed to solve the problem. Rather, it was determined that by limiting the initial roll rate command with dynamic pressure, pitch-up could be prevented. This additional roll rate command restriction, shown by the dashed lines of Figure 9-4, was implemented. The right side of Figure 9-3 illustrates the effect of this complete limiter in preventing roll-pitch inertia coupling from exceeding the capability of the airframe. Note, however, that the canard is at or close to the negative stop through much of the maneuver, indicating that any relaxation of the limiter constraints would invite departure. Entry into the flat-spin-type gyration shown in Figure 9-5 was also eliminated by this modification.

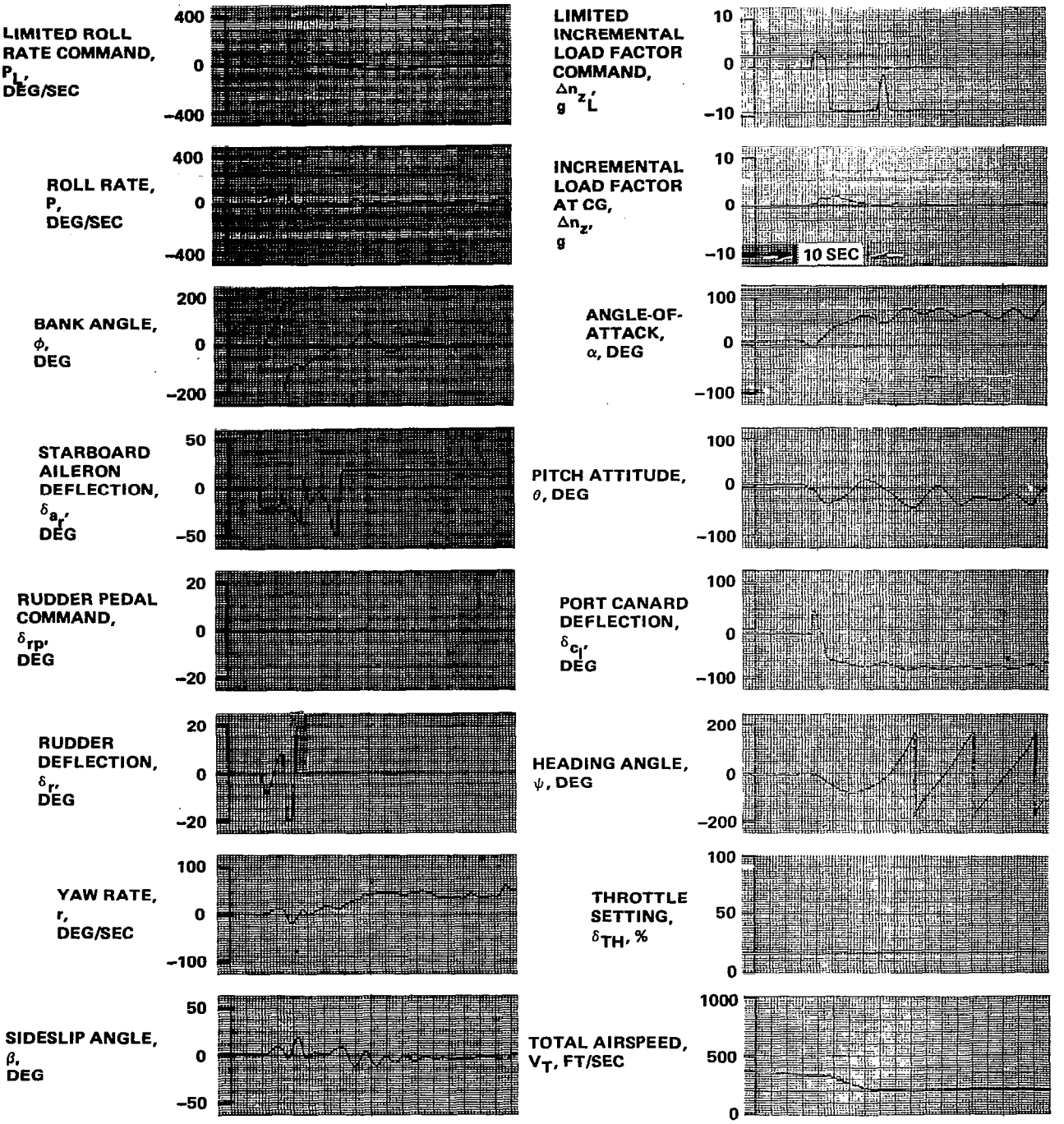

Figure 9-5. Power-off roll doublet with full aft stick command at Δt = 2.5 sec ("G" command longitudinal control law, nominal configuration).

9.4 DEVELOPMENT OF THE RUDDER COMMAND LIMITER

In the low-angle-of-attack range, full STAC rudder deflection yields approximately 20 degrees of steady-state sideslip. Aggressive use of rudder inputs during rolling maneuvers can, therefore, result in significant kinematic coupling. Consider the aircraft normal acceleration (heave) equation:

$$\dot{w} = qU - pv + g \cos\theta \cos\phi + F_z/m. \qquad (9.4)$$

If, at positive α, a positive body axis roll rate ($p > 0$) is achieved with positive sideslip ($v > 0$), angle-of-attack will be suppressed. Conversely, if excessive proverse rudder is carried, negative sideslip with positive roll will cause an increase in angle-of-attack.

These effects are illustrated in Figures 9-6 and 9-7. In both cases the aircraft was initially trimmed at M = 0.4, sea level. A full-lateral stick command ($\Delta n_z/\alpha$ and roll rate limiters operating) was input 5 sec following a full rudder command. In the case of an adverse rudder step (Figure 9-6), the angle-of-attack was depressed to negative values and the aircraft followed the roll rate command. A proverse rudder input resulted in an erratic bank angle response and an uncommanded buildup in angle-of-attack, accompanied by a decay in airspeed (Figure 9-7). A similar maneuver at M = 0.8 would have exceeded the aircraft structural limit (Figure 9-8). Reversing the sequence of inputs (full proverse rudder following a full stick roll after a 7-sec delay) resulted in an incipient departure at M = 0.4 as indicated by repeated canard position saturation (left side, Figure 9-9).

Pilot comments suggested that there is little need to maintain $\beta = 20°$ in up-and-away flight. For this reason the maximum pilot rudder authority was reduced to $\pm 10°$. It was also found that by restricting the pilot's rudder authority at $\alpha > 20°$, kinematically induced departures could be prevented. The final rudder command limiter is shown in Figure 9-10. The right side of Figure 9-9 demonstrates the effectiveness of the final rudder command limiter in suppressing uncommanded angle-of-attack buildup due to kinematic coupling.

9.5 DEVELOPMENT OF THE α COMMAND LIMITER

Although speed stability, per se, is not an issue with the angle-of-attack command longitudinal control law, the baseline aircraft still requires a command input limiter to prevent dynamic overshoot in angle-of-attack. The α command limiter is shown in Figure 9-11. The right and left angle-of-attack/pitch rate sensitive boundaries are identical to those of the "G" command limiter. The lower bound is set to a constant: $\alpha_{c_L} = -10°$. The upper bound of α_{c_L} is programmed with dynamic pressure, as shown in Figure 9-12.

In the region labeled "E", a limit angle-of-attack is imposed to help maintain aircraft operation below the limit load factor. Since the limiter uses precomputed data rather than an actual load factor feedback, this function

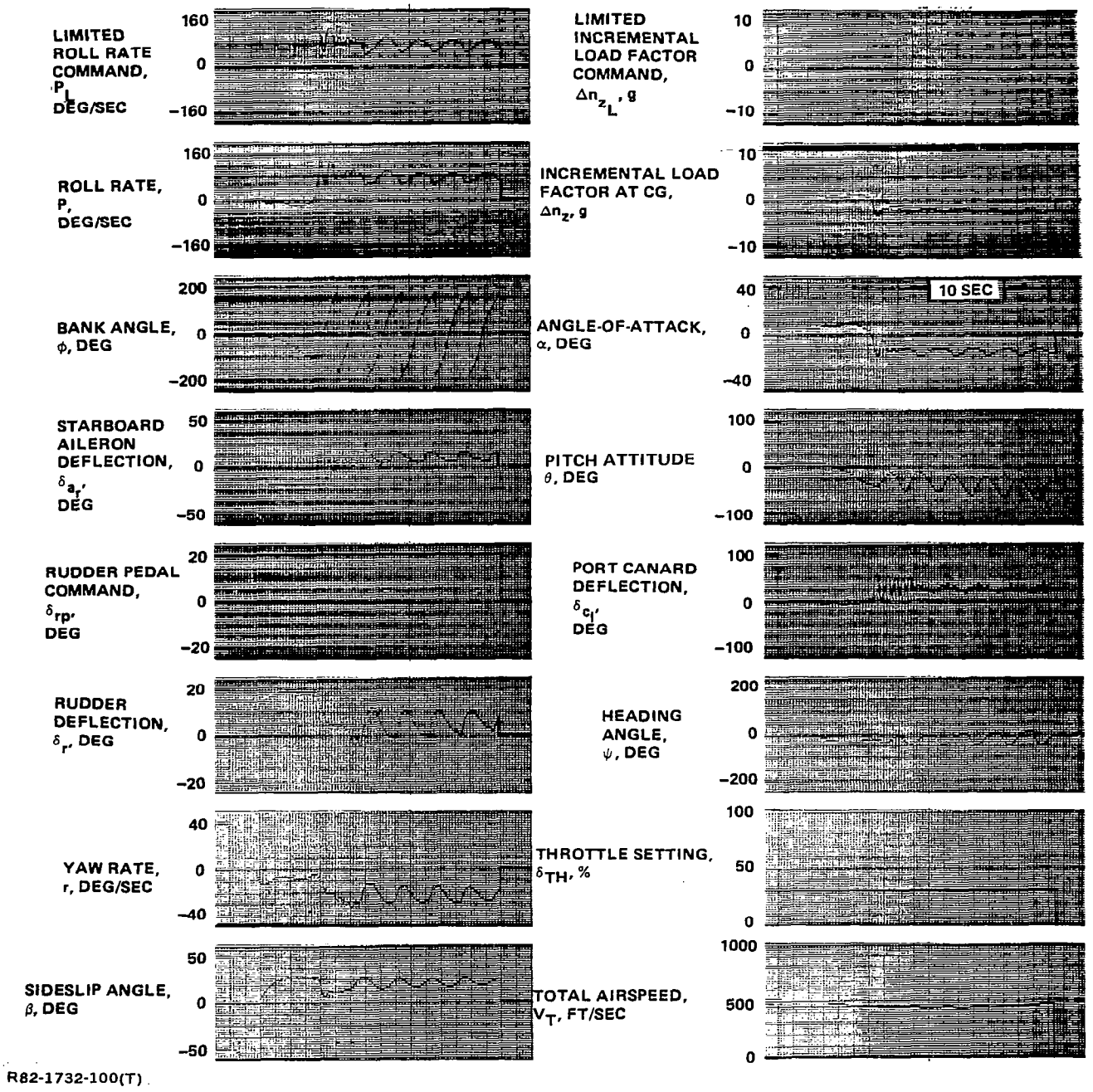

Figure 9-6. Full stick roll following full adverse rudder step (trim power, "G" command longitudinal control law, nominal configuration).

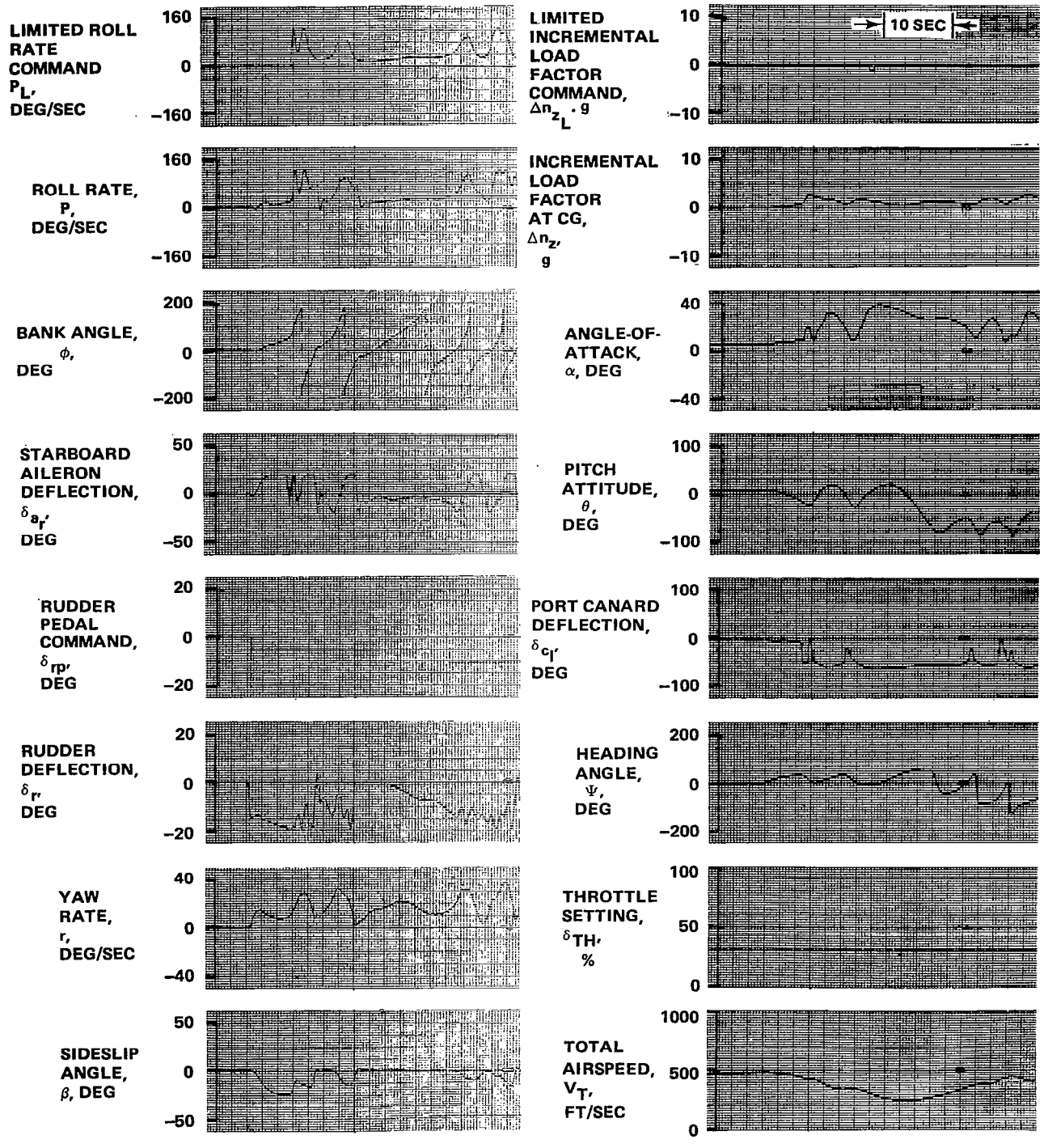

Figure 9-7. Full stick roll following full proverse rudder step (trim power, "G" command longitudinal control law, nominal configuration).

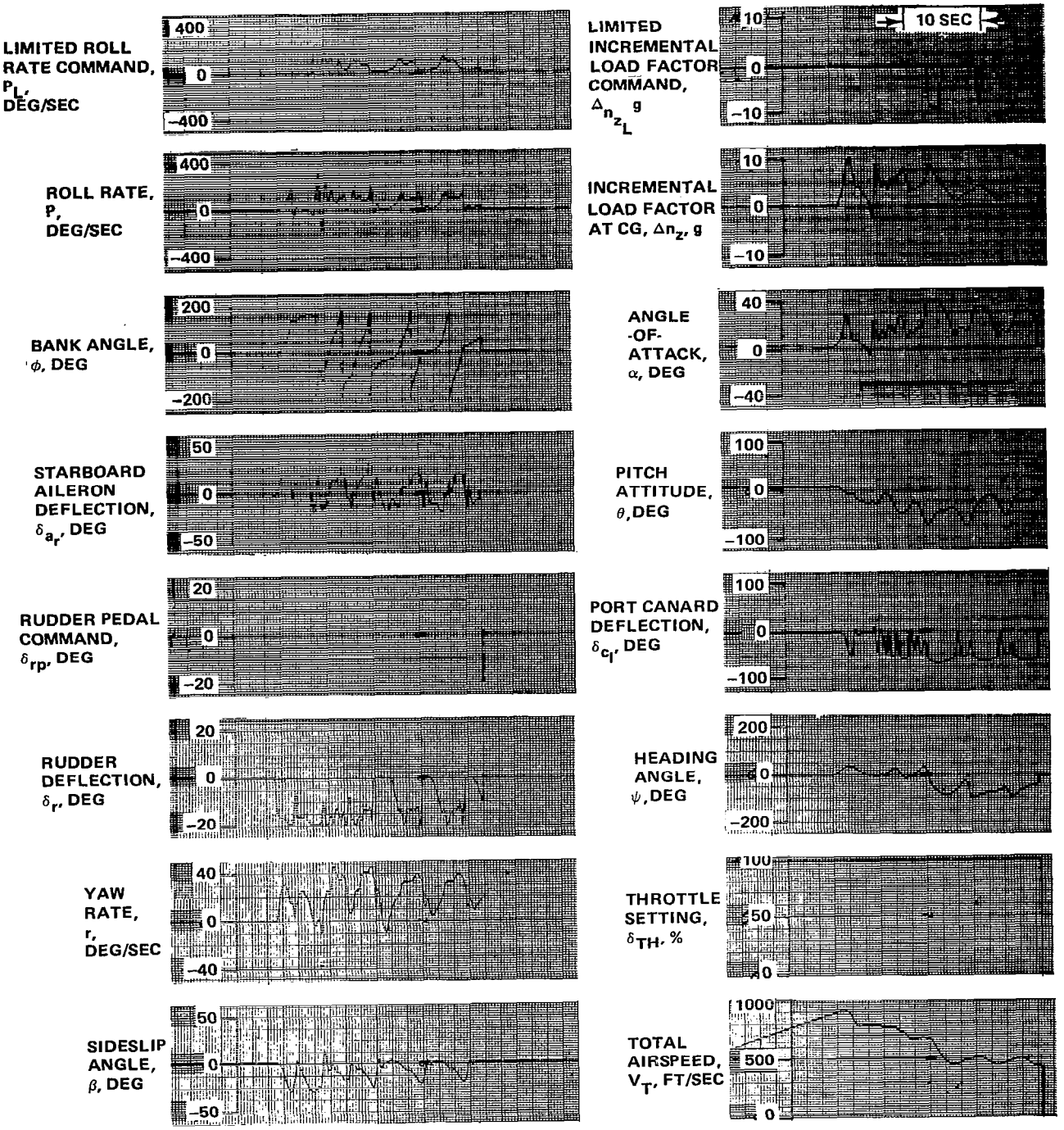

Figure 9-8. Full stick roll following full proverse rudder step (maximum afterburner power, "G" command longitudinal control law, nominal configuration).

only provides some pilot workload relief in a simulator task. In region "D", the limiter simply allows pilot commands to angle-of-attack near $C_{L_{max}}$.

Limiter development for region "C" proved most critical; here, trim dynamic pressure is low and a substantial incremental positive angle-of-attack command causes rapid speed decay. As airspeed decays, the ability of the canard to produce nose-down angular acceleration in opposition to a positive pitch rate is degraded. Furthermore, if the actual angle-of-attack excursion is substantial, the signal carried on the forward-loop integrator can become large,

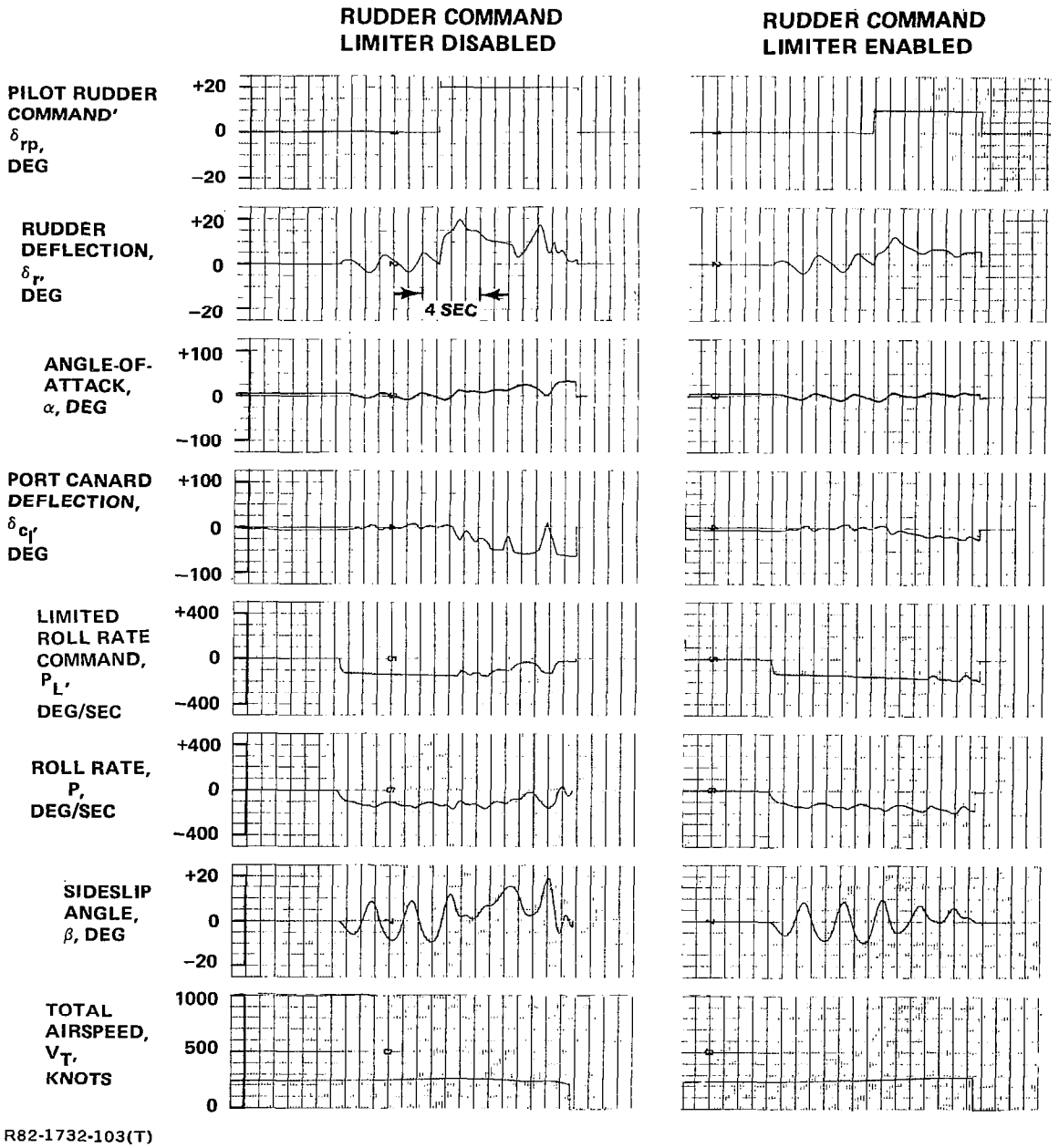

Figure 9-9. - Effect of rudder command limiter.

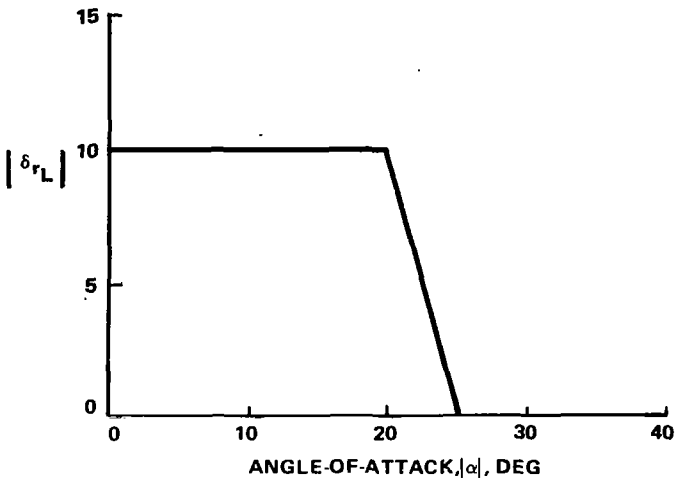

Figure 9-10. Rudder input limiter.

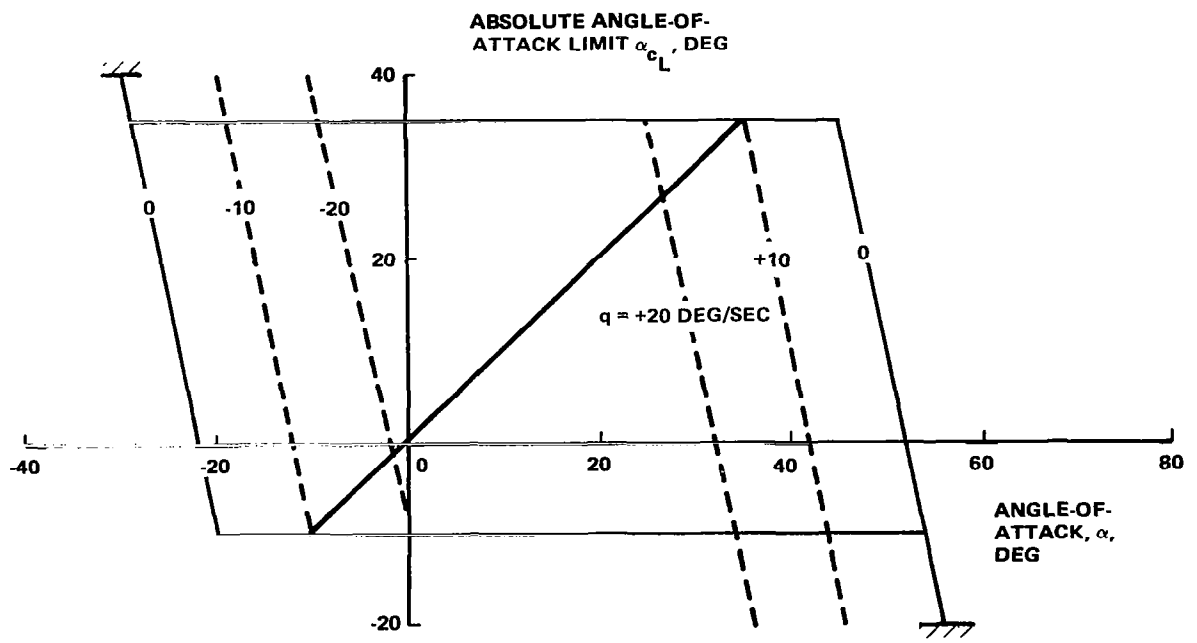

Figure 9-11. Angle-of-attack/angle-of-attack command limiter.

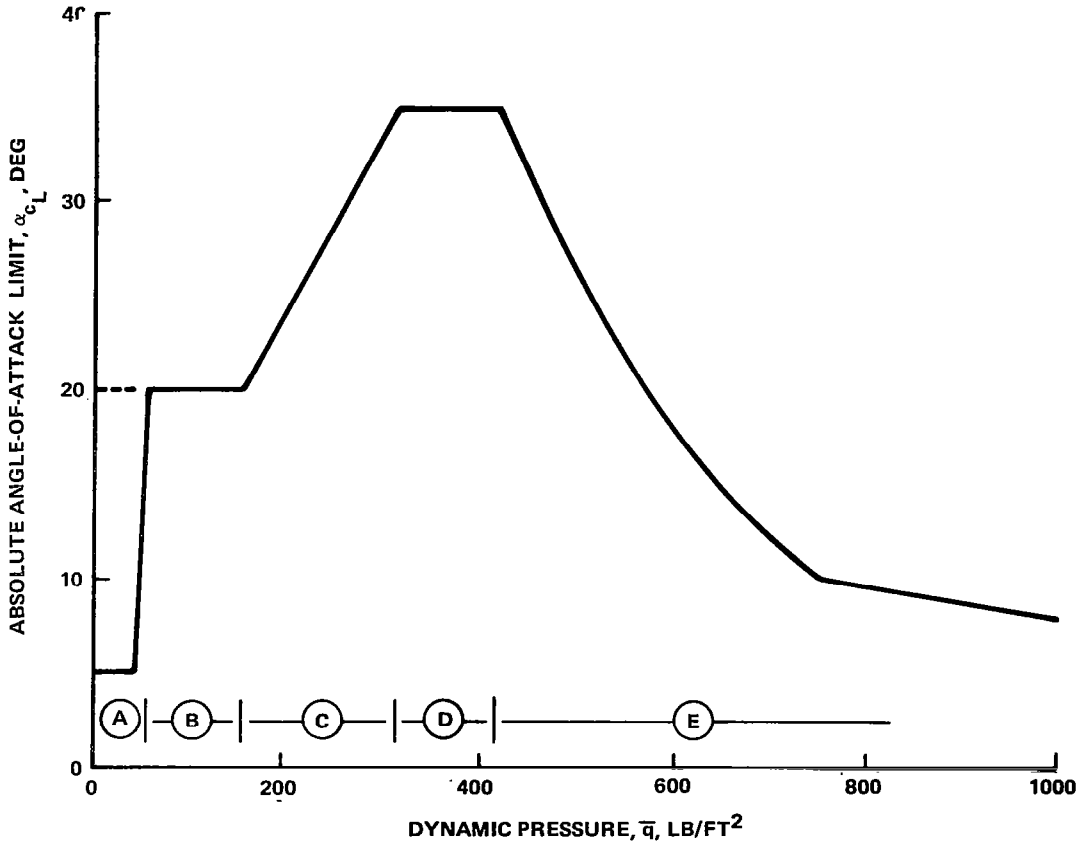

R82-1732-106(T)

Figure 9-12. Absolute angle-of-attack limit schedule with dynamic pressure.

causing large excursions below the commanded angle-of-attack during recovery. The region "C" limit angle-of-attack curve was developed by systematically lowering α_{c_L} until full-aft stick commands could be accommodated at low speed without long-term position saturation of the canard. For flight below 200 KEAS (region "B") aircraft dynamics are slow, and further command limiting with dynamic pressure was not needed. Region "A" represents a "stick-pusher"; this feature is used only in upright flight ($\cos\theta\cos\phi > 0$).

In developing the angle-of-attack command limiter, successively more severe symmetric maneuvers were attempted and the limiter "tightened" only to the extent required to avoid departure with briefly saturated longitudinal control. This work was also accomplished without regard for canard rates. Once the limiter had been defined, a 100 deg/sec canard rate limit was imposed. Rather than redefine the dynamic limiter boundaries, as had been considered previously, the lower canard rate was compensated with additional input signal conditioning for large stick deflections. The stick prefilter time constant was programmed with stick deflection, as shown in Figure 9-13. This modification was applied to the "G" system as well.

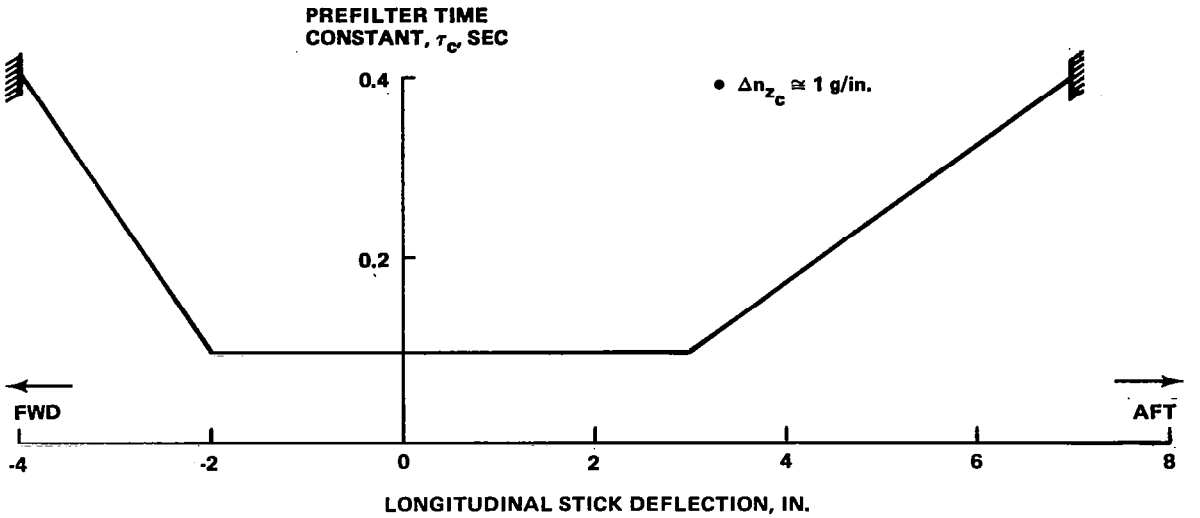

R82-1732-107(T)

Figure 9-13. Longitudinal stick input prefilter time constant

Figure 9-14 illustrates the operation of the angle-of-attack limiter. The aircraft was accelerated in afterburner from M = 0.4 at sea level. At time t = 15 sec, full-aft stick was commanded. As the aircraft entered as high-speed loop, the limiter held the incremental load factor at approximately 6.5 g. The oscillation in the angle-of-attack command trace some 4 sec into the maneuver reflects the dynamic pitch rate lead term in the limiter function. As airspeed decays (t > 20 sec), the limiter operates in region "C". Note that control was easily maintained to airspeeds as low as 120 KEAS.

9.6 COMMENTS ON LIMITER DEVELOPMENT

The developed command limiters represent but one set of many possible maneuver limiting functions/mechanizations. Those described herein were intended to prevent departure when the aircraft was subject to long-term full-authority control inputs. By addressing the fundamental mechanisms of departure (e.g., inertia coupling) directly, a relatively simple limiter structure was derived. Since the limiter parameters were defined for sustained maneuvers they may, however, overly restrict transient commands. For example, the roll rate limits with angle-of-attack might be made a function of roll rate in order to permit rapid initial roll acceleration. Similarly, additional lead information might be provided to the $\Delta n_z/\alpha$ and α_c/α limiters so that the dynamic boundaries are made sensitive to both pitch acceleration and rate. An additional relaxation of constraints could be accomplished if the rudder command limiter, intended to suppress kinematic coupling, were designed to respond to the product (pv) in a closed-loop sense.

Such added limiter sophistication may eventually prove desirable, or even necessary, once maneuver performance/agility issues are addressed in piloted

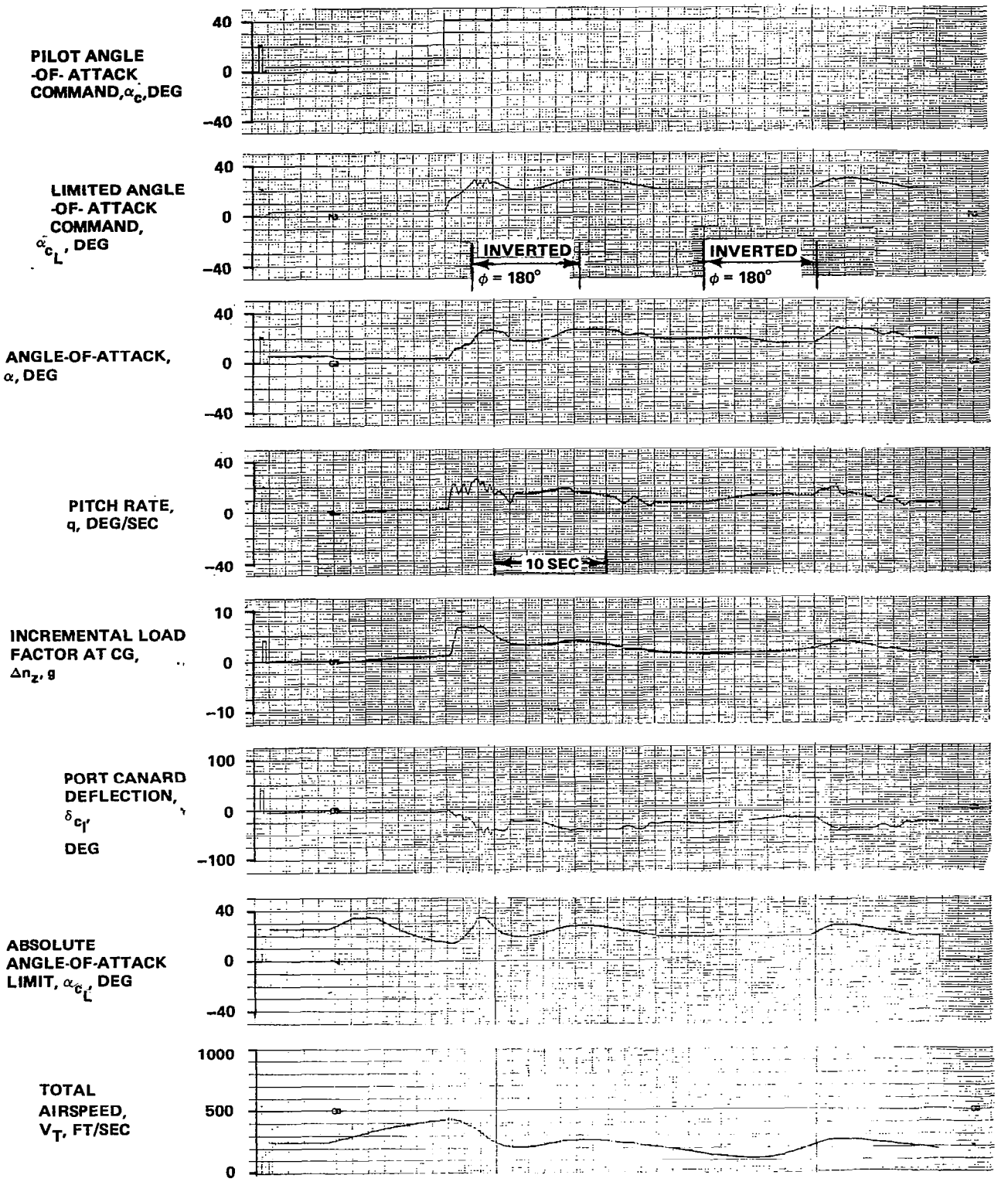

Figure 9-14. Angle-of-attack limiter operation ("α" command longitudinal control law).

simulation. Whereas conventional aircraft are limited in their agility only to the extent that the designer chooses to provide/deny angular acceleration capability, agility for Relaxed Static Stability aircraft is ultimately defined by the control system. For RSS aircraft, six-degree-of-freedom dynamic considerations will determine aerodynamic control power requirements; indeed, even in the conceptual design phase, the aircraft must be configured to reflect dynamic stability and control concerns. Command limiters are inherent to Relaxed Static Stability aircraft. One configuration design goal must, however, be to provide a balanced design with aircraft performance uncompromised by overly restrictive command limiters.

10 - CONCLUSIONS

The "Control Definition Study for Advanced Vehicles" was undertaken to examine the high-angle-of-attack flight mechanics of a representative, advanced, canard-configured, Relaxed Static Stability (RSS) tactical aircraft. The study vehicle was the Grumman Aerospace Corporation Supersonic Tactical Aircraft Configuration (STAC). The baseline aircraft is balanced 16% $\bar{c}_w$ unstable. The STAC pitching moment characteristics show a progressive degradation in nose-down pitch control power with angle-of-attack such that, near the angle-of-attack for $C_{L_{max}}$, the maximum nose-down pitching moment is $\Delta C_m \simeq -0.04$. This trend of decreasing available nose-down aerodynamic pitching moment with increasing angle-of-attack is characteristic of statically unstable aircraft.

The critical stability and control issue for STAC-class aircraft is departure prevention at high-angle-of-attack. In the low-angle-of-attack regime adequate artificial stability can be provided by simple control laws. As shown in this study, model-following gain computing algorithms can be developed by classical methods. These algorithms adjust the control system gains with flight condition and plant variations. As long as the primary pitch controller is not position/rate saturated, uniform and predictable flying qualities can be maintained. It is only when control power is inadequate that RSS becomes an issue, impacting aircraft performance, handling qualities, and, ultimately, safety of flight. With the pitch control saturated, the aircraft will depart at a rate associated with the time constant of the dominant (unstable) root of the open-loop "short-period" mode. Thus, matching of control laws to the aircraft's aerodynamic/mass/performance characteristics through appropriate command limiters becomes the major stability and control task. This nonlinear, six-degree-of-freedom problem is intractable by linear theory. A successful limiter development effort is possible only through exhaustive simulation. In the end, only piloted simulation can serve to adjudge the tactical effectiveness of the augmented airplane in Air Combat Maneuvering. If the required departure prevention command limiters overly restrict the aircraft's agility, the aircraft/airframe design must be revised.

Since a piloted simulator evaluation of the developed control laws is mandatory, the derived control systems were made simple, yet sufficiently flexible to facilitate parametric studies. In the absence of specific design guidelines applicable to canarded RSS aircraft, the gain computing algorithms were developed in a way that permits explicit control of familiar (MIL-F-8785C) handling qualities metrics. Two different longitudinal control laws were investigated: the Δn_z command and α command systems. A single set of lateral/directional laws was developed: stability axis roll rate and direct rudder command. It was shown that with a pure "G" command system the stability axis roll mode is inhibited. For the angle-of-attack system, additional lead to the yaw controller was required to coordinate roll entries.

The developed control laws were sufficiently robust to withstand significant variations in plant dynamics. Furthermore, the augmented aircraft was shown to be resistant to gust upsets.

A significant effort was dedicated to determining canard actuator rate requirements. For the "G" command system, operating in the linear aerodynamics range, canard rate/deflection requirements were higher for motion initiation than for recovery. Initiation rates in response to a step input were found to depend directly on the desired frequency of the short-period mode and to vary inversely with control power and the equivalent system lag time constant. Initial peak canard deflection did not depend on control system lags.

Achievable canard rates were also found to have a major impact on limiter design. Preventing dynamically/kinematically induced departures required rapid control actuation in opposition to uncommanded motion. Low control surface rates require more restrictive command limiters; this, in turn, may degrade ACM capability to unacceptable levels. Thus it is clear that the successful design of Relaxed Static Stability Aircraft demands early consideration of critical airframe stability and control issues during the conceptual design phase of the development cycle.

GRUMMAN AEROSPACE CORPORATION

Bethpage, New York 11714

15 February 1982

11 - REFERENCES

1. Nguyen, L.T., Ogburn, M.E., Gilbert, W.P., Kibler, K.S., Brown, P.W., and Deal, P.L., "Simulator Study of Stall/Post-Stall Characteristics of a Fighter Airplane with Relaxed Longitudinal Static Stability," NASA TP 1538, December 1979.

2. Nguyen, L.T., Gilbert, W.P., and Grafton, S.B., "Control Considerations for CCV Fighters at High Angles of Attack," Paper Presented at AGARD Fluid Mechanics Panel Meeting on Aerodynamic Characteristics of Controls, Naples, Italy, May 11-14, 1979.

3. Meyer, R. and Fields, W.D., "Configuration Development of a Supersonic Cruise Strike Fighter," AIAA 16th Aerospace Sciences Meeting, AIAA Preprint 78-148, January 1978.

4. Mason, W.H. and Miller, D.S., "Controlled Supercritical Cross-Flow on Supersonic Wings - An Experimental Validation," AIAA 13th Fluid & Plasma Dynamics Conference, AIAA Preprint 80-1421, July 1980.

5. Hendrickson, R., Grossman, R., and Sclafani, A.S., "Design Evolution of a Supersonic Cruise Strike-Fighter," AIAA Aircraft Systems & Technology Conference, AIAA Preprint 78-1452, August 1978.

6. Ferris, James C., "Wing Tunnel Investigation of a Variable Camber and Twist Wing," NASA TN D-8475, August 1977.

7. "MIL-F-8785C, Military Specification - Flying Qualities of Piloted Airplanes," February, 1980.

APPENDIX A

STAC PROPULSION MATH MODEL

TABLE A-1. - ENGINE MODEL: GROSS THRUST
(PER ENGINE, LB)

MACH \ ALT, FT	0	10K	20K	30K	36089	40K
MAXIMUM (100%)						
0	14588	10517	7220	–	–	–
0.2	16061	11423	7847	5196	–	–
0.4	18056	12828	8822	5848	4465	3680
0.6	20530	14957	10296	6852	5233	4322
0.8	23653	17858	12489	8330	6371	5265
0.9	25045	19480	13904	9283	7114	5881
1.0	25065	21135	15445	10386	7981	6601
MILITARY (50%)						
0	10362	7238	4817	–	–	–
0.2	11422	7867	5235	3371	–	–
0.4	12922	8904	5924	3813	2862	2375
0.6	14664	10514	6991	4497	3375	2800
0.8	16687	12693	8609	5534	4151	3443
0.9	17579	13747	9681	6221	4665	3871
1.0	17320	14789	10865	7043	5280	4379
45%						
0	9330	6517	4336	–	–	–
0.2	10344	7123	4739	3052	–	–
0.4	11795	8123	5403	3477	2611	2168
0.6	13650	9646	6413	4125	3096	2569
0.8	15602	11743	7942	5106	3830	3177
0.9	16550	12903	8949	5751	4311	3577
1.0	16568	13875	10054	6513	4881	4050
40%						
0	8136	5673	3773	–	–	–
0.2	9087	6254	4158	2678	–	–
0.4	10548	7170	4768	3068	2304	1916
0.6	12631	8630	5736	3688	2768	2298
0.8	14335	10844	7175	4611	3459	2871
0.9	15168	11995	8117	5213	3909	3244
1.0	15888	12873	9244	5922	4439	3683
37%						
0	7284	5159	3488	–	–	–
0.2	8128	5676	3832	2515	–	–
0.4	9043	6422	4343	2849	2167	1801
0.6	10034	7648	5161	3383	2568	2136
0.8	10376	8932	6386	4174	3168	2629
0.9	10411	9523	7185	4693	3559	2953
1.0	10418	9447	7838	5284	4005	3323
35%						
0	5273	3884	2763	–	–	–
0.2	5812	4225	2994	2077	–	–
0.4	6252	4724	3342	2315	1818	1510
0.6	6523	5561	3909	2682	2102	1746
0.8	5764	6059	4723	3229	2527	2098
0.9	5095	6093	5243	3572	2787	2314
1.0	4447	5444	5490	3949	3077	2554
30%						
0	1197	959	736	–	–	–
0.2	1245	986	761	610	–	–
0.4	1247	1035	805	683	592	494
0.6	896	969	788	691	648	540
0.8	58	466	630	581	626	524
0.9	−686	−25	465	488	554	464
1.0	−1509	−540	183	406	467	394

R82-1732-109(1/2)(T)

TABLE A-1. CONCLUDED.

ALT, FT / MACH	0	10K	20K	30K	36089	40K
25%						
0	377	307	241	–	–	–
0.2	380	306	242	193	–	–
0.4	352	293	237	190	167	138
0.6	–47	41	78	93	98	81
0.8	–1072	–639	–346	–165	–94	–78
0.9	–1927	–1209	–704	–387	–255	–211
1.0	–2814	–1802	–1090	–619	–422	–351
IDLE (20%)						
0	150	127	104	–	–	–
0.2	142	120	99	81	–	–
0.4	103	92	83	70	64	52
0.6	–355	–220	–120	–55	–28	–25
0.8	–1495	–993	–630	–375	–263	–219
0.9	–2319	–1600	–1050	–640	–459	–381
1.0	–3048	–2071	–1356	–859	–636	–524

R82-1732-109(2/2)(T)

TABLE A-2. ENGINE MODEL: RAM DRAG
(PER ENGINE, LB)

MACH \ ALT FT	0	10K	20K	30K	36089	40K
MAXIMUM (100%)						
0	0	0	0	–	–	–
0.2	880	605	404	261	–	–
0.4	1913	1320	882	570	428	355
0.6	3195	2230	1490	963	724	600
0.8	4840	3438	2318	1498	1126	933
0.9	5738	4190	2849	1840	1384	1147
1.0	6424	5021	3454	2242	1686	1397
MILITARY (50%)						
0	0	0	0	–	–	–
0.2	880	605	404	261	–	–
0.4	1913	1320	882	570	428	355
0.6	3195	2230	1490	963	724	600
0.8	4840	3438	2318	1498	1126	933
0.9	5738	4190	2849	1840	1384	1147
1.0	6424	5021	3454	2242	1686	1397
45%						
0	0	0	0	–	–	–
0.2	882	606	405	262	–	–
0.4	1917	1323	884	571	429	356
0.6	3201	2234	1493	964	725	601
0.8	4848	3445	2322	1500	1128	935
0.9	5816	4197	2854	1844	1386	1149
1.0	6607	5029	3461	2246	1689	1399
40%						
0	0	0	0	–	–	–
0.2	883	607	406	262	–	–
0.4	1919	1324	885	572	430	356
0.6	3205	2237	1495	966	726	602
0.8	4832	3449	2326	1502	1130	936
0.9	5747	4202	2858	1846	1388	1150
1.0	6718	5023	3466	2249	1691	1401
37%						
0	0	0	0	–	–	–
0.2	818	566	381	248	–	–
0.4	1741	1225	826	538	407	338
0.6	2776	2057	1386	904	684	567
0.8	3962	3060	2144	1399	1058	877
0.9	4613	3595	2628	1714	1297	1075
1.0	5268	4147	3126	2079	1573	1304
35%						
0	0	0	0	–	–	–
0.2	699	491	335	221	–	–
0.4	1463	1048	716	474	362	300
0.6	2277	1742	1191	789	603	500
0.8	3170	2535	1823	1207	923	765
0.9	3642	2931	2222	1472	1125	932
1.0	4100	3332	2611	1774	1356	1124
30%						
0	0	0	0	–	–	–
0.2	393	289	208	145	–	–
0.4	805	606	435	303	241	199
0.6	1228	983	706	493	390	323
0.8	1733	1381	1046	731	577	478
0.9	2012	1590	1252	874	691	572
1.0	2300	1821	1439	1033	817	677

R82-1732-110(1/2)(T)

TABLE A-2. CONCLUDED.

ALT, FT / MACH	0	10K	20K	30K	36089	40K
25%						
0	0	0	0	–	–	–
0.2	221	164	118	85	–	–
0.4	459	343	248	176	143	118
0.6	738	556	403	284	229	190
0.8	1084	813	596	420	334	277
0.9	1292	968	712	502	399	331
1.0	1519	1137	833	592	471	390
IDLE (20%)						
0	0	0	0	–	–	–
0.2	141	106	78	56	–	–
0.4	298	223	164	118	95	78
0.6	490	361	266	191	153	127
0.8	738	542	392	280	225	187
0.9	889	653	468	334	269	223
1.0	1051	772	554	392	315	261

R82-1732-110(2/2)(T)

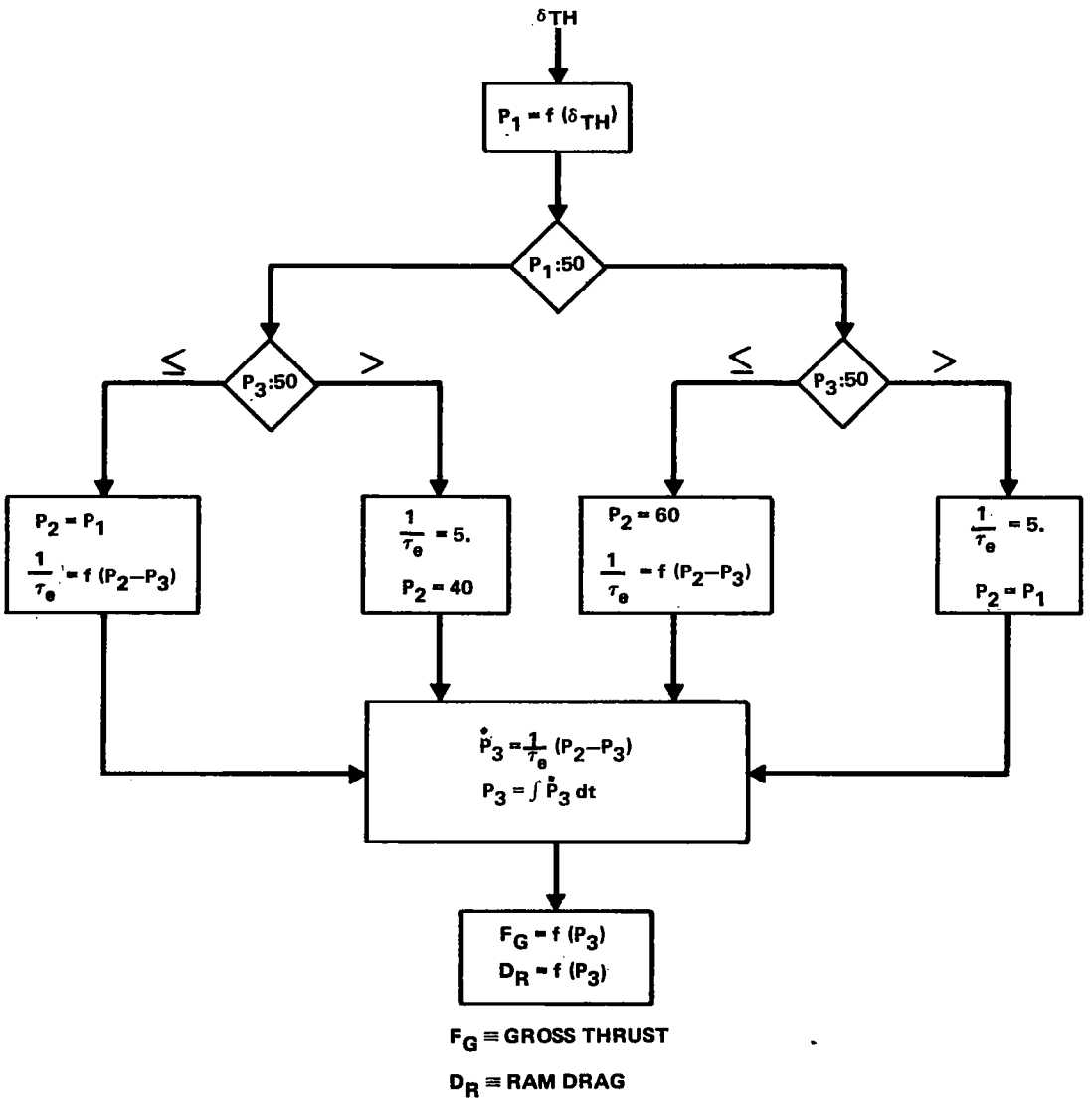

R82-1732-111(T)

Figure A-1. STAC simulation: Dynamic engine model.

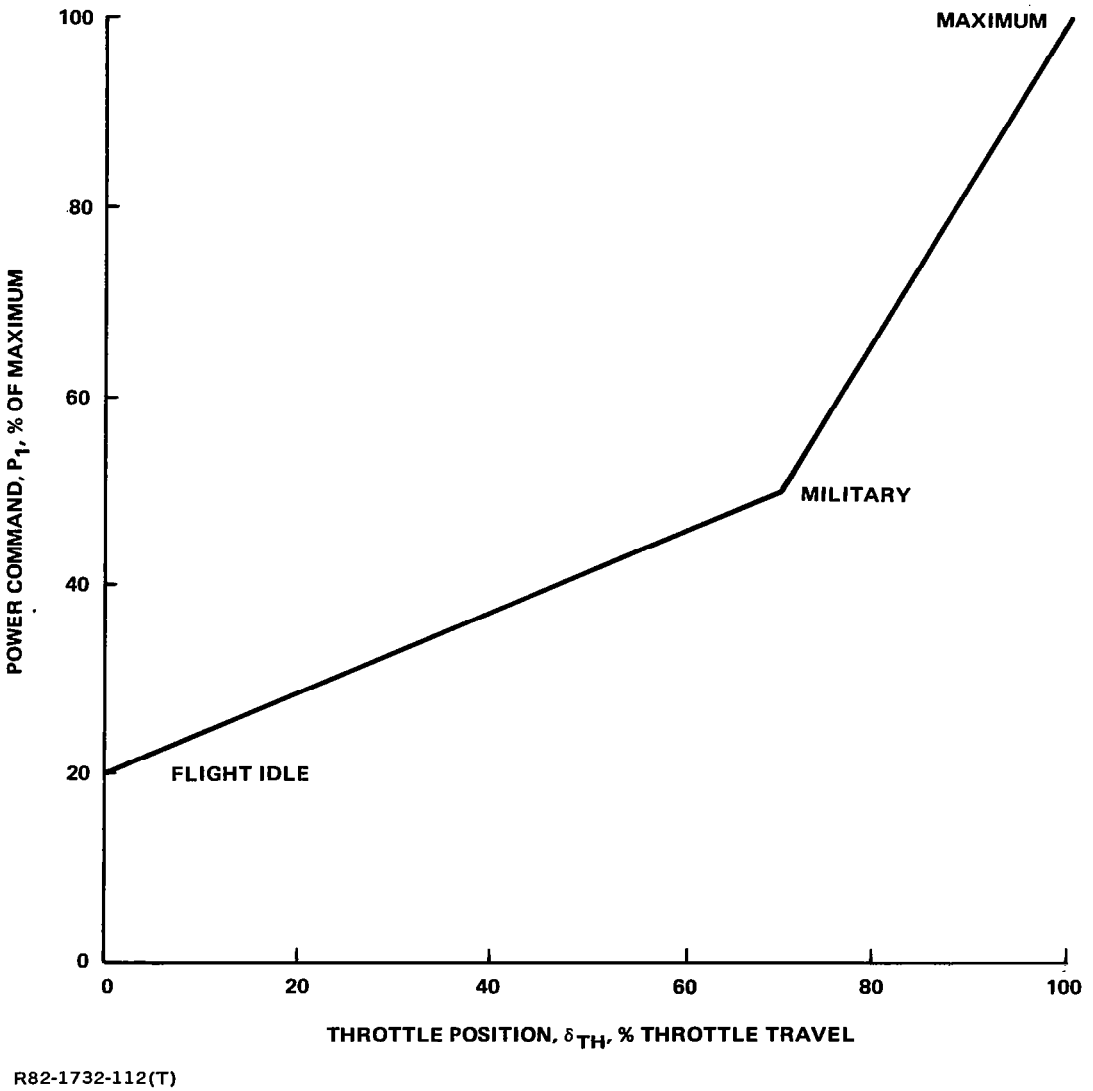

Figure A-2. Power command as a function of throttle position.

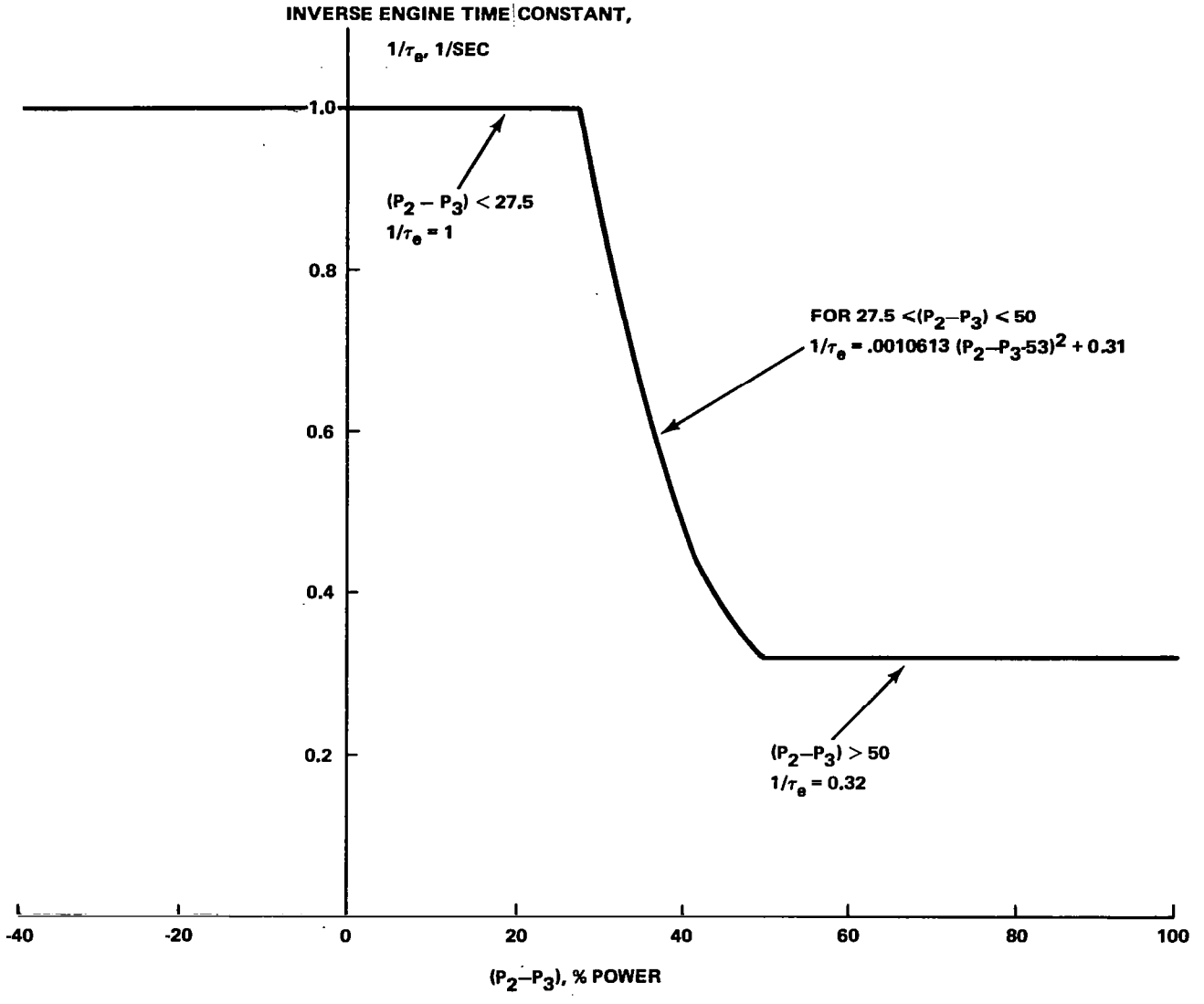

R82-1732-113(T)

Figure A-3. Variation of inverse of thrust time constant with incremental power command.

APPENDIX B

STAC AERODYNAMIC MATH MODEL

The aerodynamic data used in the simulation were derived from the previously described low-speed wind tunnel tests conducted with a 1/27-scale model of the STAC configuration. The longitudinal and lateral/directional force and moment coefficient equations generally consist of a summation of component, control surface and dynamic effects:

- Longitudinal Buildup
  - Wing-body configuration is basis for buildup
  - Separate canard, leading edge/trailing edge wing device effects, and control surface increments are additive contributions
  - Pitch damping contribution completes the buildup.
- Lateral/Directional Buildup
  - Wing/body/canard is basis for buildup
  - Separate vertical tail, rudder, differential canard, leading edge/trailing edge device, and control surface increments are additive contributions
  - Roll damping, yaw damping, roll due-to-yaw, yaw due-to-roll, and sideslip damping contributions complete the buildup.

The moment equations were coded so as to facilitate parametric center of gravity variations.

Table B-1 provides a brief description of the individual terms used to make up the total aerodynamic coefficients. Tables B-2 and B-3 follow, showing the total coefficient formulation. Table B-4 contains the aerodynamic data.

TABLE B-1. - AERODYNAMIC MATH MODEL COEFFICIENT SUMMARY

COEFFICIENT	INDEPENDENT VARIABLE INPUT α	β	δ_c	DESCRIPTION
$C_{N_{WB}}$	*			WING/BODY NORMAL FORCE
$C_{M_{WB}}$	*			PITCHING MOMENT
$C_{A_{WB}}$	*			AXIAL FORCE
$C_{N_{C_{L/R}}}$	*		*	LEFT/RIGHT CANARD NORMAL FORCE
F	*			CANARD DOWNWASH FACTOR
$C_{N_{TE_L}}$	*			TE FLAP NORMAL FORCE INCREMENT
$C_{M_{TE_L}}$	*			PITCHING MOMENT
$C_{A1_{TE_L}}$	*			AXIAL FORCE 1
$C_{A2_{TE_L}}$	*			AXIAL FORCE 2
$C_{M_{Q_{C_{L/R}}}}$	*		*	LEFT/RIGHT CANARD PITCH DAMPING
$C_{LN_{WB}}$	*	*	*	WING/BODY YAWING MOMENT
$C_{LL_{WB}}$	*	*	*	ROLLING MOMENT
$C_{LY_{WB}}$	*	*	*	SIDE FORCE
$C_{LL_{WB_0}}$		*	*	ROLLING MOMENT AT $\alpha = 0$
$C_{LN_{TE_L}}$	*			TE FLAP YAWING MOMENT INCREMENT
$C_{LL_{TE_L}}$	*			ROLLING MOMENT
$C_{LY_{TE_L}}$	*			SIDE FORCE
$C_{Y_{V2}}$	*	*		VERTICAL TAIL SIDE FORCE
$C_{Y_{\beta V2}}$	*			VERTICAL TAIL SIDE FORCE DERIVATIVE
$C_{Y_{\delta R}}$	*			RUDDER SIDE FORCE INCREMENT
$C_{L_{R_W}}$	*			WING ROLL DUE TO YAW
$C_{N_{R_F}}$	*		*	FUSELAGE YAW DAMPING
$C_{N_{LE}}$	*			LE FLAP NORMAL FORCE INCREMENT
$C_{M_{LE}}$	*			PITCHING MOMENT
$C_{A_{LE}}$	*			AXIAL FORCE
$C_{LL_{LE}}$	*	*	*	ROLLING MOMENT
$C_{LN_{DIF}}$	*	*		DIFFERENTIAL CANARD YAWING MOMENT
$C_{LL_{DIF}}$	*	*		ROLLING MOMENT
$C_{LY_{DIF}}$	*	*		SIDE FORCE
$(\Delta C_M)_\beta$	*	*	*	PITCHING MOMENT DUE-TO-YAW
$\Delta C_{N_{W2}}$	*			TRANSONIC WING NORMAL FORCE INCREMENT
$\Delta C_{M_{W2}}$	*			PITCHING MOMENT
$\Delta C_{A_{W2}}$	*			AXIAL FORCE

R82-1732-114(T)

TABLE B-2. LONGITUDINAL EQUATION FORMULATION

NORMAL FORCE :

$$C_N = C_{N_{WB}} + C_{N_{CAN}}\{1-F\} + C_{N_{TE_L}}\{\delta_{TE_L}+\delta_{TE_R}\}$$

$$+ C_{N_{LE}}\delta_{LE} + \Delta C_{N_{W2}} K_{W2}$$

$$\text{WHERE } C_{N_{CAN}} = S_{CAN}/S_{REF}\{C_{N_{C_L}} \cos\delta_{C_L} + C_{N_{C_R}} \cos\delta_{C_R}\}$$

AXIAL FORCE :

$$C_A = C_{A_{WB}} + C_{A_{CAN}} + C_{A1_{TE_L}}\{\delta_{TE_L}+\delta_{TE_R}\} + C_{A_{LE}}\delta_{LE}$$

$$+ \Delta C_{A_{W2}} K_{W2} + C_{A2_{TE_L}}\{|\delta_{TE_L}|+|\delta_{TE_R}|\}$$

$$\text{WHERE } C_{A_{CAN}} = S_{CAN}/S_{REF}\{C_{N_{C_L}} \sin\delta_{C_L} + C_{N_{C_R}} \sin\delta_{C_R}\}$$

PITCHING MOMENT :

$$C_M = C_{M_{WB}} + C_{N_{CAN}}\{l_C/\bar{c}\} + C_{M_{TE_L}}\{\delta_{TE_L}+\delta_{TE_R}\}$$

$$+ C_{M_{LE}}\delta_{LE} + \Delta C_{M_{W2}} K_{W2} + 1.2\, S_{CAN}/70.\{C_{M_{q_{C_L}}} + C_{M_{q_{C_R}}}\}$$

$$\{(X_{CG}-X_{CAN})/(X_{REF}-X_{CAN})\}^2\{(q\bar{c}/2V_T)\} + (\Delta C_M)_\beta$$

$$+ C_N\{(X_{CG}-X_{REF})/\bar{c}\}$$

R82-1732-115(T)

TABLE B-3. LATERAL/DIRECTIONAL EQUATION FORMULATION

SIDE FORCE :

$$C_{LY} = C_{LY_{WB}} + C_{Y_{V2}} + C_{LY_{DIF}}\{\delta_{C_L} - \delta_{C_R}\}K_{DIF} + C_{Y_{\delta_R}}\delta_R + C_{LY_{TE_L}}\{\delta_{TE_L} - \delta_{TE_R}\}$$

YAWING MOMENT :

$$C_{LN} = C_{LN_{WB}} - C_{Y_{V2}}(X_T - X_{REF})/b - C_{Y_{\delta_R}}\delta_R(X_R - X_{REF})/b + C_{LN_{DIF}}\{\delta_{C_L} - \delta_{C_R}\}K_{DIF} + C_{LN_{TE_L}}\{\delta_{TE_L} - \delta_{TE_R}\} + \{C_{N_{P_W}} - 2C_{Y_{\beta_{V2}}} Z_T(X_T - X_{CG})/b^2\}\{(pb/2V_T)\} + \{C_{N_{R_W}} + 2C_{Y_{\beta_{V2}}}[(X_T - X_{CG})/b]^2 + C_{N_{R_F}} + 4C_{LN_{\beta_{WB}}}(X_{CG} - X_{REF})/b + 2C_{LY_{\beta_{WB}}}[(X_{CG} - X_{REF})/b]^2\}\{(rb/2V_T)\} + C_{LY}\{(X_{CG} - X_{REF})/b\}$$

ROLLING MOMENT :

$$C_{LL} = C_{LL_{WB_0}} + C_{LL_{WB}} + C_{Y_{V2}}\{Z_T/b\} + C_{Y_{\delta_R}}\delta_R\{Z_R/b\} + C_{LL_{DIF}}\{\delta_{C_L} - \delta_{C_R}\}K_{DIF} + C_{LL_{TE_L}}\{\delta_{TE_L} - \delta_{TE_R}\} + C_{LL_{LE}}\delta_{LE} + \{C_{L_{P_W}} + 2C_{Y_{\beta_{V2}}}(Z_T{}_2/b^2)\}\{(pb/2V_T)\} + \{C_{L_{R_W}} - 2C_{Y_{\beta_{V2}}} Z_T(X_T - X_{CG})/b^2\}\{(rb/2V_T)\}$$

R82-1732-116(T)

TABLE B-4. AERODYNAMIC DATA

$C_{N_{WB}}$ — CN-WB

$\alpha\rightarrow$	0.	0.	12.	22.	39.	49.	55.	90.
	0.	0.	.76	1.20	1.75	1.75	1.75	1.86

$C_{M_{WB}}$ — CM-WB

$\alpha\rightarrow$	0.	0.	12.	22.	39.	49.	55.	90.
	0.	0.	0.	.11	.09	.07	.08	-.32

$C_{A_{WB}}$ — CA-WB

$\alpha\rightarrow$	0.	0.	12.	22.	39.	49.	55.	90.
	0.	.0136	.0060	.018	.018	.018	.015	0.

$C_{N_{C_L}}$ — CN-LEFT CAN

$\delta_c\rightarrow$ / $\alpha_c\downarrow$	0.	-90.	-48.	-24.	-12.	0.	12.	24.	48.	90.
-90.	-.56	-.56	-.67	-.77	-.82	-.47	-.70	-.56	-.56
-60.	-.56	-.56	-.83	-.88	-1.20	-1.36	-0.73	-.56	-.56
-55.	-.56	-.56	-.85	-.94	-1.54	-1.35	-0.72	-.56	-.56
-50.	-.56	-.56	-.84	-1.05	-1.64	-1.25	-.70	-.56	-.56
-45.	-.56	-.60	-.83	-1.15	-1.60	-1.10	-.68	-.56	-.56
-30.	-.56	-.56	-.61	-1.04	-.81	-.73	-.55	-.56	-.56
-10.	-.26	-.26	-.24	-.20	-.25	-.22	-.24	-.26	-.26
0.	0.	0.	0.	0.	0.	0.	0.	0.	0.
10.	.35	.38	.40	.20	.25	.22	.24	.26	.26
30.	.85	.85	.76	1.04	.81	.73	.55	.56	.56
45.	.56	.56	.83	1.15	1.60	1.10	.68	.56	.56
50.	.56	.56	.84	1.05	1.64	1.25	.70	.56	.56
55.	.56	.56	.85	.94	1.54	1.35	.72	.56	.56
60.	.56	.56	.83	.88	1.20	1.36	.73	.56	.56
90.	.56	.56	.67	.77	.82	.47	.70	.56	.56

$C_{N_{C_R}}$ — CN-RIGHT CAN

F — DOWN WASH F

$\alpha\rightarrow$	0.	-180.	-16.	0.	16.	180.
	0. 0.0	0.0	1.0000	0.0	0.0	

R82-1732-126(1/18)(T)

TABLE B-4. - CONTINUED.

$C_{N_{TE_L}}$ CN-TEL

α→	0.	0.	10.	20.	30.	40.	50.	60.	90.	180.
0.	0.	0.0023	0.0040	0.0037	0.0022	0.0017	0.0013	0.0010	0.0006	0.0006

$C_{M_{TE_L}}$ CM-TEL

α→	0.	0.	10.	20.	30.	40.	50.	60.	90.	180.
0.	-0.	-0.0009	-0.0011	-0.0010	-0.0014	-0.0014	-0.0011	-0.0010	-0.0007	-0.0007

$C_{A1_{TE_L}}$ CA1-TEL

α→	0.	0.	10.	20.	30.	40.	50.	60.	90.	180.
0.	0.	.00000	.00005	.00014	.00019	.00020	.00021	.00022	.00023	.00023

$C_{A2_{TE_L}}$ CA2-TEL

α→	0.	0.	10.	20.	30.	40.	50.	60.	90.	180.
0.	0.	.00007	.00009	.00011	.00014	.00015	.00016	.00017	.00020	.00020

$C_{M_{Q_{C_L}}}$, $C_{M_{Q_{C_R}}}$ CMQ-LEFT CAN

α→	0.	0.	10.	20.	30.	45.	60.	70.	80.	90.
δ_c ↓ -90.	0.0	0.0000	0.0000	0.0000	0.0000	0.0000	0.0000	0.0000	-0.0000	
-75.	0.0	0.0406	0.0799	-0.0217	0.0076	-0.0314	-0.0494	-0.0736	-0.0992	
-60.	0.0	0.0784	-0.1568	-0.1058	-0.1859	-0.2266	-0.2756	-0.2876	-0.3235	
-45.	-0.2293	-0.3582	-0.2835	-0.4324	-0.4546	-0.4535	-0.5199	-0.5845	-0.6381	
-30.	-0.5266	-0.4388	-0.7478	-0.7481	-0.6072	-0.7425	-0.8254	-0.7696	-0.7815	
-15.	-1.1887	-1.1343	-1.1404	-0.8934	-1.0825	-0.7170	-0.7588	-0.8878	-0.9015	
0.	-1.2857	-1.3148	-1.7160	-1.8954	-0.1363	-0.9552	-1.0364	-1.0862	-1.1030	
15.	-1.1887	-0.8939	-1.0310	-0.1297	-0.6374	-0.7807	-0.8471	-0.8878	-0.9015	
30.	-0.5266	-0.6382	-0.2673	-0.3908	-0.5526	-0.6768	-0.7344	-0.7696	-0.7815	
45.	-0.2293	-0.1108	-0.2182	-0.3191	-0.4512	-0.5526	-0.5996	-0.6284	-0.6381	
60.	0.0	-0.0784	-0.1543	-0.2266	-0.3191	-0.3908	-0.4164	-0.3497	-0.3235	
75.	0.0	-0.0406	-0.0799	-0.1168	-0.1652	-0.1241	-0.1244	-0.1159	-0.0992	
90.	0.0	-0.0000	-0.0000	-0.0000	-0.0000	-0.0000	-0.0000	-0.0000	0.0000	

R82-1732-126(2/18)(T)

TABLE B-4. - CONTINUED.

$C_{LN_{WB}}$ $\delta_c \downarrow$ $\alpha \rightarrow$ $\beta =$ [0.]

CLN-WB

	0.	12.	16.	20.	25.	30.	35.	40.	45.
-90.	0.0	0.0	0.0	0.0	0.0	0.0	0.0	0.0	0.0
-70.	0.0	0.0	0.0	0.0	0.0	0.0	0.0	0.0	0.0
-48.	0.0	0.0	0.0	0.0	0.0	0.0	0.0	0.0	0.0
-24.	0.0	0.0	0.0	0.0	0.0	0.0	0.0	0.0	0.0
-12.	0.0	0.0	0.0	0.0	0.0	0.0	0.0	0.0	0.0
0.	0.0	0.0	0.0	0.0	0.0	0.0	0.0	0.0	0.0
12.	0.0	0.0	0.0	0.0	0.0	0.0	0.0	0.0	0.0
24.	0.0	0.0	0.0	0.0	0.0	0.0	0.0	0.0	0.0
48.	0.0	0.0	0.0	0.0	0.0	0.0	0.0	0.0	0.0
70.	0.0	0.0	0.0	0.0	0.0	0.0	0.0	0.0	0.0
90.	0.0	0.0	0.0	0.0	0.0	0.0	0.0	0.0	0.0

	0.	50.	55.	60.	65.	70.	90.
-90.	0.0	0.0	0.0	0.0	0.0	0.0	
-70.	0.0	0.0	0.0	0.0	0.0	0.0	
-48.	0.0	0.0	0.0	0.0	0.0	0.0	
-24.	0.0	0.0	0.0	0.0	0.0	0.0	
-12.	0.0	0.0	0.0	0.0	0.0	0.0	
0.	0.0	0.0	0.0	0.0	0.0	0.0	
12.	0.0	0.0	0.0	0.0	0.0	0.0	
24.	0.0	0.0	0.0	0.0	0.0	0.0	
48.	0.0	0.0	0.0	0.0	0.0	0.0	
70.	0.0	0.0	0.0	0.0	0.0	0.0	
90.	0.0	0.0	0.0	0.0	0.0	0.0	

CLN-WB

[2.]	0.	12.	16.	20.	25.	30.	35.	40.	45.
-90.	-0.0028	0.0017	0.0026	0.0084	0.0099	0.0194	0.0235	0.0405	0.0342
-70.	-0.0033	0.0022	0.0025	0.0075	0.0104	0.0189	0.0241	0.0400	0.0358
-48.	-0.0044	-0.0005	-0.0015	0.0030	0.0075	0.0151	0.0228	0.0376	0.0423
-24.	-0.0054	-0.0045	-0.0045	-0.0080	-0.0015	0.0081	0.0198	0.0326	0.0473
-12.	-0.0034	-0.0035	-0.0025	-0.0060	-0.0065	0.0011	0.0118	0.0226	0.0273
0.	-0.0024	0.0015	0.0035	0.0	0.0025	0.0061	0.0058	0.0156	0.0203
12.	-0.0004	0.0058	0.0073	0.0055	0.0090	0.0136	0.0034	0.0154	0.0187
24.	-0.0004	0.0074	0.0093	0.0078	0.0113	0.0188	0.0083	0.0213	0.0207
48.	-0.0018	0.0040	0.0072	0.0074	0.0096	0.0207	0.0191	0.0348	0.0305
70.	-0.0036	0.0016	0.0035	0.0082	0.0091	0.0196	0.0230	0.0410	0.0354
90.	-0.0041	0.0021	0.0023	0.0084	0.0089	0.0194	0.0235	0.0405	0.0359

2.	50.	55.	60.	65.	70.	90.
-90.	0.0353	0.0344	0.0130	-0.0021	-0.0032	-0.0039
-70.	0.0348	0.0368	0.0178	0.0020	-0.0028	-0.0035
-48.	0.0370	0.0368	0.0215	0.0062	-0.0020	-0.0027
-24.	0.0470	0.0318	0.0195	0.0032	-0.0010	-0.0017
-12.	0.0360	0.0218	0.0095	0.0032	-0.0010	-0.0017
0.	0.0170	0.0118	0.0045	0.0012	0.0	-0.0007
12.	0.0118	0.0080	0.0011	-0.0008	0.0006	-0.0001
24.	0.0144	0.0132	0.0091	-0.0019	0.0002	-0.0005
48.	0.0279	0.0272	0.0039	-0.0027	-0.0012	-0.0019
70.	0.0348	0.0336	0.0096	-0.0028	-0.0027	-0.0034
90.	0.0346	0.0334	0.0127	-0.0027	-0.0029	-0.0036

R82-1732-126(3/18)(T)

TABLE B-4. - CONTINUED.

CLN-WB

6.	0.	12.	16.	20.	25.	30.	35.	40.	45.
-90.	-0.0109	0.0050	0.0079	0.0178	0.0208	0.0386	0.0209	0.0267	0.0338
-70.	-0.0114	0.0042	0.0064	0.0156	0.0216	0.0391	0.0237	0.0325	0.0383
-48.	-0.0121	-0.0024	-0.0024	0.0059	0.0176	0.0253	0.0345	0.0477	0.0559
-24.	-0.0101	-0.0094	-0.0104	-0.0151	-0.0054	0.0173	0.0535	0.0787	0.0869
-12.	-0.0091	-0.0084	-0.0084	-0.0181	-0.0084	0.0163	0.0285	0.0477	0.0919
0.	-0.0071	0.0006	0.0046	-0.0011	0.0076	0.0083	0.0115	0.0227	0.0459
12.	-0.0055	0.0081	0.0130	0.0096	0.0163	0.0052	0.0017	0.0135	0.0298
24.	-0.0048	0.0104	0.0146	0.0129	0.0199	0.0081	0.0	0.0144	0.0262
48.	-0.0062	0.0070	0.0142	0.0165	0.0201	0.0205	0.0129	0.0213	0.0288
70.	-0.0110	0.0052	0.0104	0.0180	0.0207	0.0326	0.0210	0.0248	0.0326
90.	-0.0115	0.0050	0.0079	0.0184	0.0211	0.0373	0.0215	0.0263	0.0348

6.	50.	55.	60.	65.	70.	90.
-90.	0.0528	0.0364	-0.0002	-0.0095	-0.0083	-0.0103
-70.	0.0523	0.0477	0.0071	-0.0052	-0.0069	-0.0089
-48.	0.0571	0.0553	0.0275	0.0007	-0.0050	-0.0070
-24.	0.0731	0.0463	0.0295	0.0047	-0.0060	-0.0080
-12.	0.0661	0.0343	0.0205	0.0037	-0.0030	-0.0050
0.	0.0371	0.0183	0.0085	-0.0013	-0.0040	-0.0060
12.	0.0231	0.0104	0.0014	-0.0060	-0.0047	-0.0067
24.	0.0264	0.0123	-0.0033	-0.0081	-0.0055	-0.0075
48.	0.0438	0.0263	-0.0054	-0.0091	-0.0069	-0.0089
70.	0.0513	0.0360	-0.0033	-0.0098	-0.0074	-0.0094
90.	0.0522	0.0357	-0.0006	-0.0092	-0.0083	-0.0103

CLN-WB

16.	0.	12.	16.	20.	25.	30.	35.	40.	45.
-90.	-0.0123	-0.0042	-0.0058	-0.0042	0.0133	0.0152	-0.0059	-0.0030	0.0028
-70.	-0.0128	-0.0051	-0.0059	-0.0044	0.0141	0.0104	-0.0034	-0.0002	0.0027
-48.	-0.0180	-0.0118	-0.0117	-0.0062	0.0082	0.0067	0.0066	0.0135	0.0124
-24.	-0.0250	-0.0218	-0.0177	-0.0092	-0.0048	0.0147	0.0306	0.0455	0.0534
-12.	-0.0250	-0.0178	-0.0117	-0.0082	-0.0058	0.0017	0.0056	0.0325	0.0384
0.	-0.0200	-0.0198	-0.0217	-0.0082	-0.0028	-0.0043	0.0006	0.0215	0.0274
12.	-0.0142	-0.0137	-0.0228	-0.0071	0.0013	-0.0061	0.0063	0.0095	0.0213
24.	-0.0106	-0.0085	-0.0129	-0.0058	0.0052	-0.0038	0.0046	0.0052	0.0163
48.	-0.0084	-0.0039	-0.0058	-0.0049	0.0127	0.0089	-0.0013	-0.0015	0.0080
70.	-0.0112	-0.0017	-0.0046	-0.0044	0.0135	0.0157	-0.0047	-0.0039	0.0033
90.	-0.0137	-0.0013	-0.0061	-0.0033	0.0140	0.0155	-0.0065	-0.0027	0.0018

16.	50.	55.	60.	65.	70.	90.
-90.	-0.0211	-0.0221	-0.0271	-0.0161	-0.0221	-0.0272
-70.	-0.0206	-0.0167	-0.0218	-0.0160	-0.0181	-0.0232
-48.	-0.0017	-0.0068	0.0051	-0.0190	-0.0191	-0.0242
-24.	0.0133	0.0012	-0.0019	-0.0150	-0.0251	-0.0302
-12.	0.0313	0.0092	-0.0049	-0.0140	-0.0171	-0.0222
0.	0.0203	-0.0058	-0.0149	-0.0180	-0.0211	-0.0262
12.	0.0113	-0.0133	-0.0226	-0.0208	-0.0232	-0.0283
24.	0.0020	-0.0179	-0.0271	-0.0218	-0.0239	-0.0290
48.	-0.0129	-0.0204	-0.0234	-0.0193	-0.0237	-0.0288
70.	-0.0200	-0.0222	-0.0281	-0.0172	-0.0226	-0.0277
90.	-0.0218	-0.0224	-0.0271	-0.0174	-0.0231	-0.0282

R82-1732-126(4/18)(T)

TABLE B-4. - CONTINUED.

CLN-WB

26.	0.	12.	16.	20.	25.	30.	35.	40.	45.
-90.	-.010	-.013	-.006	-.008	-.011	-.016	-.019	-.021	-.016
-70.	-.015	-.018	-.011	-.013	-.016	-.021	-.024	-.026	-.021
-48.	-.020	-.023	-.016	-.018	-.021	-.026	-.029	-.032	-.026
-24.	-.040	-.050	-.039	-.038	-.031	-.016	-.019	-.007	-.020
-12.	-.044	-.055	-.038	-.033	-.021	-.018	-.014	-.014	-.021
0.	-.042	-.055	-.039	-.036	-.027	-.025	-.015	-.016	-.022
12.	-.054	-.065	-.048	-.043	-.031	-.028	-.024	-.024	-.031
24.	-.037	-.044	-.032	-.031	-.026	-.027	-.027	-.028	-.029
48.	-.020	-.023	-.016	-.018	-.021	-.026	-.029	-.032	-.026
70.	-.015	-.018	-.011	-.013	-.016	-.021	-.024	-.026	-.021
90.	-.010	-.013	-.006	-.008	-.011	-.016	-.019	-.021	-.016
26.	50.	55.	60.	65.	70.	90.			
-90.	-.005	-.003	-.006	-.009	-.012	-.015			
-70.	-.010	-.008	-.011	-.014	-.017	-.020			
-48.	-.015	-.013	-.016	-.019	-.022	-.025			
-24.	-.029	-.037	-.034	-.039	-.042	-.045			
-12.	-.009	-.021	-.034	-.039	-.042	-.045			
0.	-.013	-.017	-.034	-.037	-.042	-.045			
12.	-.019	-.031	-.044	-.049	-.052	-.055			
24.	-.017	-.022	-.030	-.034	-.032	-.035			
48.	-.015	-.013	-.016	-.019	-.012	-.015			
70.	-.010	-.008	-.011	-.014	-.017	-.020			
90.	-.005	-.003	-.006	-.009	-.012	-.015			

CLN-WB

90.	0.	12.	16.	20.	25.	30.	35.	40.	45.
-90.	-.05	-.05	-.05	-.05	-.05	-.05	-.05	-.05	-.05
-70.	-.05	-.05	-.05	-.05	-.05	-.05	-.05	-.05	-.05
-48.	-.05	-.05	-.05	-.05	-.05	-.05	-.05	-.05	-.05
-24.	-.05	-.05	-.05	-.05	-.05	-.05	-.05	-.05	-.05
-12.	-.05	-.05	-.05	-.05	-.05	-.05	-.05	-.05	-.05
0.	-.05	-.05	-.05	-.05	-.05	-.05	-.05	-.05	-.05
12.	-.05	-.05	-.05	-.05	-.05	-.05	-.05	-.05	-.05
24.	-.05	-.05	-.05	-.05	-.05	-.05	-.05	-.05	-.05
48.	-.05	-.05	-.05	-.05	-.05	-.05	-.05	-.05	-.05
70.	-.05	-.05	-.05	-.05	-.05	-.05	-.05	-.05	-.05
90.	-.05	-.05	-.05	-.05	-.05	-.05	-.05	-.05	-.05
90.	50.	55.	60.	65.	70.	90.			
-90.	-.05	-.05	-.05	-.05	-.05	-.05			
-70.	-.05	-.05	-.05	-.05	-.05	-.05			
-48.	-.05	-.05	-.05	-.05	-.05	-.05			
-24.	-.05	-.05	-.05	-.05	-.05	-.05			
-12.	-.05	-.05	-.05	-.05	-.05	-.05			
0.	-.05	-.05	-.05	-.05	-.05	-.05			
12.	-.05	-.05	-.05	-.05	-.05	-.05			
24.	-.05	-.05	-.05	-.05	-.05	-.05			
48.	-.05	-.05	-.05	-.05	-.05	-.05			
70.	-.05	-.05	-.05	-.05	-.05	-.05			
90.	-.05	-.05	-.05	-.05	-.05	-.05			

R82-1732-126(5/18)(T)

TABLE B-4. - CONTINUED

β = [ ]

$C_{LL_{WB}}$

CLL-WB

$\alpha \rightarrow$ [0.] / $\delta_c \downarrow$	0.	12.	16.	20.	25.	30.	35.	40.	45.
-90.	0.0	0.0	0.0	0.0	0.0	0.0	0.0	0.0	0.0
-70.	0.0	0.0	0.0	0.0	0.0	0.0	0.0	0.0	0.0
-48.	0.0	0.0	0.0	0.0	0.0	0.0	0.0	0.0	0.0
-24.	0.0	0.0	0.0	0.0	0.0	0.0	0.0	0.0	0.0
-12.	0.0	0.0	0.0	0.0	0.0	0.0	0.0	0.0	0.0
0.	0.0	0.0	0.0	0.0	0.0	0.0	0.0	0.0	0.0
12.	0.0	0.0	0.0	0.0	0.0	0.0	0.0	0.0	0.0
24.	0.0	0.0	0.0	0.0	0.0	0.0	0.0	0.0	0.0
48.	0.0	0.0	0.0	0.0	0.0	0.0	0.0	0.0	0.0
70.	0.0	0.0	0.0	0.0	0.0	0.0	0.0	0.0	0.0
90.	0.0	0.0	0.0	0.0	0.0	0.0	0.0	0.0	0.0

0.	50.	55.	60.	65.	70.	90.
-90.	0.0	0.0	0.0	0.0	0.0	0.0
-70.	0.0	0.0	0.0	0.0	0.0	0.0
-48.	0.0	0.0	0.0	0.0	0.0	0.0
-24.	0.0	0.0	0.0	0.0	0.0	0.0
-12.	0.0	0.0	0.0	0.0	0.0	0.0
0.	0.0	0.0	0.0	0.0	0.0	0.0
12.	0.0	0.0	0.0	0.0	0.0	0.0
24.	0.0	0.0	0.0	0.0	0.0	0.0
48.	0.0	0.0	0.0	0.0	0.0	0.0
70.	0.0	0.0	0.0	0.0	0.0	0.0
90.	0.0	0.0	0.0	0.0	0.0	0.0

CLL-WB

[2.]	0.	12.	16.	20.	25.	30.	35.	40.	45.
-90.	0.0	-0.0082	-0.0020	-0.0090	-0.0195	-0.0266	-0.0070	-0.0045	-0.0114
-70.	0.0	-0.0068	-0.0013	-0.0093	-0.0147	-0.0225	-0.0105	-0.0070	-0.0114
-48.	0.0	-0.0049	-0.0026	-0.0067	-0.0069	-0.0151	-0.0120	-0.0089	-0.0068
-24.	0.0	-0.0029	-0.0046	-0.0007	0.0011	-0.0021	-0.0040	-0.0059	-0.0018
-12.	0.0	-0.0039	-0.0056	-0.0037	-0.0009	0.0019	0.0050	0.0031	0.0112
0.	0.0	-0.0049	-0.0056	-0.0037	-0.0039	-0.0081	0.0040	0.0001	0.0082
12.	0.0	-0.0071	-0.0055	-0.0074	-0.0069	-0.0084	0.0023	-0.0022	-0.0035
24.	0.0	-0.0108	-0.0059	-0.0076	-0.0092	-0.0130	-0.0010	-0.0026	-0.0078
48.	0.0	-0.0154	-0.0079	-0.0113	-0.0164	-0.0225	-0.0065	-0.0041	-0.0155
70.	0.0	-0.0144	-0.0056	-0.0123	-0.0202	-0.0257	-0.0080	-0.0046	-0.0172
90.	0.0	-0.0092	-0.0043	-0.0110	-0.0198	-0.0266	-0.0073	-0.0049	-0.0137

2.	60.	55.	60.	65.	70.	90.
-90.	-0.0055	-0.0096	-0.0043	-0.0058	-0.0044	-0.0042
-70.	-0.0072	-0.0094	-0.0058	-0.0064	-0.0059	-0.0057
-48.	-0.0068	-0.0057	-0.0056	-0.0055	-0.0054	-0.0052
-24.	-0.0048	-0.0037	-0.0036	-0.0045	-0.0044	-0.0042
-12.	0.0032	-0.0017	-0.0046	-0.0045	-0.0044	-0.0042
0.	0.0022	-0.0027	-0.0036	-0.0035	-0.0034	-0.0032
12.	0.0004	-0.0060	-0.0038	-0.0027	-0.0033	-0.0031
24.	-0.0020	-0.0074	-0.0045	-0.0034	-0.0033	-0.0031
48.	-0.0057	-0.0101	-0.0060	-0.0049	-0.0045	-0.0043
70.	-0.0071	-0.0112	-0.0066	-0.0062	-0.0061	-0.0059
90.	-0.0068	-0.0113	-0.0069	-0.0061	-0.0060	-0.0058

R82-1732-126(6/18)(T)

TABLE B-4. - CONTINUED.

CLL-WB

6.	0.	12.	16.	20.	25.	30.	35.	40.	45.
-90.	0.0	-0.0161	-0.0280	-0.0247	-0.0286	-0.0389	-0.0087	-0.0132	-0.0206
-70.	0.0	-0.0154	-0.0211	-0.0244	-0.0259	-0.0378	-0.0136	-0.0170	-0.0210
-48.	0.0	-0.0129	-0.0169	-0.0183	-0.0188	-0.0304	-0.0201	-0.0209	-0.0186
-24.	0.0	-0.0099	-0.0109	-0.0053	-0.0088	-0.0074	-0.0231	-0.0190	-0.0146
-12.	0.0	-0.0159	-0.0169	-0.0143	-0.0138	-0.0104	-0.0071	-0.0149	-0.0056
0.	0.0	-0.0149	-0.0189	-0.0143	-0.0128	-0.0054	0.0099	0.0051	0.0004
12.	0.0	-0.0164	-0.0207	-0.0148	-0.0138	-0.0078	0.0190	0.0123	-0.0020
24.	0.0	-0.0180	-0.0233	-0.0168	-0.0161	-0.0187	0.0138	0.0074	-0.0069
48.	0.0	-0.0220	-0.0289	-0.0237	-0.0239	-0.0341	-0.0006	-0.0034	-0.0191
70.	0.0	-0.0204	-0.0310	-0.0258	-0.0291	-0.0393	-0.0062	-0.0086	-0.0235
90.	0.0	-0.0164	-0.0293	-0.0254	-0.0293	-0.0382	-0.0071	-0.0132	-0.0216

6.	50.	55.	60.	65.	70.	90.
-90.	-0.0165	-0.0175	-0.0140	-0.0138	-0.0109	-0.0103
-70.	-0.0182	-0.0182	-0.0163	-0.0151	-0.0121	-0.0115
-48.	-0.0184	-0.0181	-0.0168	-0.0156	-0.0143	-0.0137
-24.	-0.0174	-0.0181	-0.0158	-0.0156	-0.0163	-0.0157
-12.	-0.0164	-0.0161	-0.0158	-0.0156	-0.0153	-0.0147
0.	-0.0094	-0.0121	-0.0118	-0.0116	-0.0113	-0.0107
12.	-0.0067	-0.0106	-0.0083	-0.0098	-0.0088	-0.0082
24.	-0.0070	-0.0116	-0.0076	-0.0084	-0.0081	-0.0075
48.	-0.0124	-0.0147	-0.0112	-0.0103	-0.0113	-0.0107
70.	-0.0171	-0.0174	-0.0128	-0.0126	-0.0129	-0.0123
90.	-0.0178	-0.0182	-0.0140	-0.0128	-0.0122	-0.0116

CLL-WB

16.	0.	12.	16.	20.	25.	30.	35.	40.	45.
-90.	0.0	-0.0387	-0.0296	-0.0206	-0.0510	-0.0448	-0.0328	-0.0428	-0.0348
-70.	0.0	-0.0374	-0.0231	-0.0150	-0.0473	-0.0447	-0.0417	-0.0447	-0.0379
-48.	0.0	-0.0368	-0.0269	-0.0221	-0.0465	-0.0529	-0.0542	-0.0496	-0.0429
-24.	0.0	-0.0378	-0.0359	-0.0381	-0.0375	-0.0659	-0.0632	-0.0516	-0.0459
-12.	0.0	-0.0438	-0.0429	-0.0471	-0.0405	-0.0329	-0.0542	-0.0446	-0.0449
0.	0.0	-0.0398	-0.0409	-0.0471	-0.0445	-0.0409	-0.0122	-0.0356	-0.0279
12.	0.0	-0.0391	-0.0373	-0.0441	-0.0379	-0.0310	0.0078	-0.0300	-0.0169
24.	0.0	-0.0364	-0.0343	-0.0388	-0.0391	-0.0319	0.0123	-0.0289	-0.0156
48.	0.0	-0.0371	-0.0340	-0.0335	-0.0456	-0.0381	-0.0042	-0.0345	-0.0252
70.	0.0	-0.0384	-0.0350	-0.0276	-0.0495	-0.0429	-0.0203	-0.0390	-0.0322
90.	0.0	-0.0400	-0.0309	-0.0203	-0.0507	-0.0451	-0.0321	-0.0428	-0.0362

16.	50.	55.	60.	65.	70.	90.
-90.	-0.0276	-0.0282	-0.0276	-0.0299	-0.0269	-0.0253
-70.	-0.0294	-0.0287	-0.0296	-0.0302	-0.0292	-0.0276
-48.	-0.0382	-0.0375	-0.0379	-0.0382	-0.0365	-0.0349
-24.	-0.0492	-0.0495	-0.0479	-0.0472	-0.0455	-0.0439
-12.	-0.0472	-0.0465	-0.0449	-0.0452	-0.0445	-0.0429
0.	-0.0342	-0.0335	-0.0329	-0.0322	-0.0315	-0.0299
12.	-0.0244	-0.0240	-0.0244	-0.0223	-0.0246	-0.0230
24.	-0.0191	-0.0207	-0.0203	-0.0186	-0.0202	-0.0186
48.	-0.0222	-0.0238	-0.0229	-0.0219	-0.0225	-0.0209
70.	-0.0253	-0.0268	-0.0261	-0.0260	-0.0254	-0.0238
90.	-0.0299	-0.0289	-0.0283	-0.0292	-0.0269	-0.0253

R82-1732-126(7/18)(T)

TABLE B-4. - CONTINUED.

CLL-WB

26.	0.	12.	16.	20.	25.	30.	35.	40.	45.
-90.	-.007	-.049	-.066	-.068	-.070	-.052	-.051	-.050	-.048
-70.	-.007	-.049	-.066	-.068	-.070	-.052	-.051	-.050	-.048
-48.	-.007	-.049	-.046	-.038	-.050	-.072	-.071	-.080	-.058
-24.	.003	-.029	-.046	-.050	-.055	-.069	-.081	-.070	-.058
-12.	.003	-.039	-.056	-.068	-.060	-.052	-.061	-.050	-.048
0.	-.007	-.049	-.066	-.068	-.070	-.052	-.051	-.050	-.048
12.	-.007	-.049	-.066	-.068	-.070	-.052	-.051	-.050	-.048
24.	-.007	-.049	-.066	-.068	-.070	-.052	-.051	-.050	-.048
48.	-.007	-.049	-.066	-.068	-.070	-.052	-.051	-.050	-.048
70.	-.007	-.049	-.066	-.068	-.070	-.052	-.051	-.050	-.048
90.	-.007	-.049	-.066	-.068	-.070	-.052	-.051	-.050	-.048

26.	50.	55.	60.	65.	70.	90.
-90.	-.047	-.046	-.045	-.044	-.043	-.042
-70.	-.047	-.046	-.045	-.044	-.043	-.042
-48.	-.057	-.056	-.055	-.054	-.053	-.052
-24.	-.057	-.056	-.055	-.054	-.053	-.052
-12.	-.047	-.046	-.045	-.044	-.043	-.042
0.	-.047	-.046	-.045	-.044	-.043	-.042
12.	-.047	-.046	-.045	-.044	-.043	-.042
24.	-.047	-.046	-.045	-.044	-.043	-.042
48.	-.047	-.046	-.045	-.044	-.043	-.042
70.	-.047	-.046	-.045	-.044	-.043	-.042
90.	-.047	-.046	-.045	-.044	-.043	-.042

CLL-WB

90.	0.	12.	16.	20.	25.	30.	35.	40.	45.
-90.	0.	0.	0.	0.	0.	0.	0.	0.	0.
-70.	0.	0.	0.	0.	0.	0.	0.	0.	0.
-48.	0.	0.	0.	0.	0.	0.	0.	0.	0.
-24.	0.	0.	0.	0.	0.	0.	0.	0.	0.
-12.	0.	0.	0.	0.	0.	0.	0.	0.	0.
0.	0.	0.	0.	0.	0.	0.	0.	0.	0.
12.	0.	0.	0.	0.	0.	0.	0.	0.	0.
24.	0.	0.	0.	0.	0.	0.	0.	0.	0.
48.	0.	0.	0.	0.	0.	0.	0.	0.	0.
70.	0.	0.	0.	0.	0.	0.	0.	0.	0.
90.	0.	0.	0.	0.	0.	0.	0.	0.	0.

90.	50.	55.	60.	65.	70.	90.
-90.	0.	0.	0.	0.	0.	0.
-70.	0.	0.	0.	0.	0.	0.
-48.	0.	0.	0.	0.	0.	0.
-24.	0.	0.	0.	0.	0.	0.
-12.	0.	0.	0.	0.	0.	0.
0.	0.	0.	0.	0.	0.	0.
12.	0.	0.	0.	0.	0.	0.
24.	0.	0.	0.	0.	0.	0.
48.	0.	0.	0.	0.	0.	0.
70.	0.	0.	0.	0.	0.	0.
90.	0.	0.	0.	0.	0.	0.

R82-1732-126(8/18)(T)

TABLE B-4. - CONTINUED.

$\beta = \square$

$C_{LY_{WB}}$

CLY-WB

$\delta_c \downarrow$ \ $\alpha \rightarrow$ [0.]	0.	12.	16.	20.	25.	30.	35.	40.	45.
-90.	0.0	0.0	0.0	0.0	0.0	0.0	0.0	0.0	0.0
-70.	0.0	0.0	0.0	0.0	0.0	0.0	0.0	0.0	0.0
-48.	0.0	0.0	0.0	0.0	0.0	0.0	0.0	0.0	0.0
-24.	0.0	0.0	0.0	0.0	0.0	0.0	0.0	0.0	0.0
-12.	0.0	0.0	0.0	0.0	0.0	0.0	0.0	0.0	0.0
0.	0.0	0.0	0.0	0.0	0.0	0.0	0.0	0.0	0.0
12.	0.0	0.0	0.0	0.0	0.0	0.0	0.0	0.0	0.0
24.	0.0	0.0	0.0	0.0	0.0	0.0	0.0	0.0	0.0
48.	0.0	0.0	0.0	0.0	0.0	0.0	0.0	0.0	0.0
70.	0.0	0.0	0.0	0.0	0.0	0.0	0.0	0.0	0.0
90.	0.0	0.0	0.0	0.0	0.0	0.0	0.0	0.0	0.0

0.	50.	55.	60.	65.	70.	90.
-90.	0.0	0.0	0.0	0.0	0.0	0.0
-70.	0.0	0.0	0.0	0.0	0.0	0.0
-48.	0.0	0.0	0.0	0.0	0.0	0.0
-24.	0.0	0.0	0.0	0.0	0.0	0.0
-12.	0.0	0.0	0.0	0.0	0.0	0.0
0.	0.0	0.0	0.0	0.0	0.0	0.0
12.	0.0	0.0	0.0	0.0	0.0	0.0
24.	0.0	0.0	0.0	0.0	0.0	0.0
48.	0.0	0.0	0.0	0.0	0.0	0.0
70.	0.0	0.0	0.0	0.0	0.0	0.0
90.	0.0	0.0	0.0	0.0	0.0	0.0

CLY-WB

[2.]	0.	12.	16.	20.	25.	30.	35.	40.	45.
-90.	-0.0082	-0.0005	-0.0041	-0.0093	0.0277	0.0373	0.0379	0.0508	0.0453
-70.	-0.0075	-0.0015	-0.0017	-0.0077	0.0267	0.0338	0.0377	0.0498	0.0492
-48.	-0.0082	-0.0030	-0.0024	-0.0034	0.0204	0.0242	0.0348	0.0453	0.0459
-24.	-0.0082	-0.0080	-0.0074	0.0016	0.0054	0.0092	0.0248	0.0353	0.0459
-12.	-0.0032	-0.0080	-0.0124	-0.0084	0.0104	0.0242	0.0448	0.0553	0.0459
0.	-0.0032	-0.0130	-0.0174	-0.0034	0.0054	0.0192	0.0348	0.0353	0.0259
12.	-0.0061	-0.0200	-0.0203	0.0011	0.0069	0.0140	0.0220	0.0284	0.0167
24.	-0.0081	-0.0204	-0.0207	0.0016	0.0098	0.0135	0.0150	0.0296	0.0138
48.	-0.0081	-0.0104	-0.0098	0.0	0.0147	0.0185	0.0224	0.0395	0.0277
70.	-0.0089	-0.0046	-0.0015	-0.0042	0.0212	0.0308	0.0339	0.0518	0.0390
90.	-0.0074	-0.0006	-0.0016	-0.0084	0.0268	0.0381	0.0378	0.0524	0.0428

2.	50.	55.	60.	65.	70.	90.
-90.	0.0178	0.0168	-0.0149	-0.0044	-0.0203	-0.0189
-70.	0.0266	0.0248	-0.0019	-0.0005	-0.0181	-0.0167
-48.	0.0415	0.0121	0.0126	-0.0018	-0.0162	-0.0148
-24.	0.0565	0.0321	0.0126	-0.0118	-0.0112	-0.0098
-12.	0.0315	0.0121	-0.0024	-0.0068	-0.0112	-0.0098
0.	-0.0085	-0.0079	-0.0074	-0.0068	-0.0062	-0.0048
12.	-0.0223	-0.0184	-0.0087	-0.0065	-0.0051	-0.0037
24.	-0.0244	-0.0230	-0.0101	-0.0054	-0.0073	-0.0059
48.	-0.0130	-0.0141	-0.0119	-0.0047	-0.0132	-0.0118
70.	0.0024	0.0047	-0.0138	-0.0033	-0.0176	-0.0162
90.	0.0162	0.0176	-0.0149	-0.0069	-0.0212	-0.0198

R82-1732-126(9/18)(T)

TABLE B-4. - CONTINUED.

CLY-WB

6.	0.	12.	16.	20.	25.	30.	35.	40.	45.
-90.	-0.0228	-0.0031	-0.0237	-0.0126	0.0567	0.0291	-0.0057	-0.0040	-0.0270
-70.	-0.0245	-0.0007	-0.0164	-0.0118	0.0557	0.0231	-0.0092	-0.0017	-0.0198
-48.	-0.0246	-0.0040	-0.0172	-0.0101	0.0412	0.0226	0.0143	0.0160	0.0178
-24.	-0.0246	-0.0190	-0.0172	-0.0101	0.0012	0.0326	0.0593	0.0560	0.0628
-12.	-0.0196	-0.0240	-0.0322	-0.0151	0.0162	0.0576	0.0743	0.1110	0.0378
0.	-0.0146	-0.0290	-0.0422	-0.0051	0.0062	0.0426	0.0693	0.0610	0.0128
12.	-0.0182	-0.0325	-0.0449	0.0020	0.0061	0.0357	0.0639	0.0440	0.0064
24.	-0.0194	-0.0288	-0.0459	0.0024	0.0123	0.0294	0.0519	0.0270	0.0001
48.	-0.0218	-0.0146	-0.0369	0.0	0.0404	0.0219	0.0261	0.0021	-0.0100
70.	-0.0227	-0.0055	-0.0311	-0.0067	0.0536	0.0243	0.0019	-0.0063	-0.0226
90.	-0.0228	-0.0014	-0.0238	-0.0126	0.0559	0.0282	-0.0099	-0.0057	-0.0295

6.	50.	55.	60.	65.	70.	90.
-90.	-0.0533	-0.0401	-0.0491	-0.0523	-0.0390	-0.0348
-70.	-0.0487	-0.0470	-0.0486	-0.0534	-0.0443	-0.0401
-48.	-0.0105	-0.0288	-0.0371	-0.0503	-0.0486	-0.0444
-24.	0.0395	0.0212	-0.0171	-0.0453	-0.0536	-0.0494
-12.	0.0345	-0.0288	-0.0321	-0.0503	-0.0436	-0.0394
0.	-0.0255	-0.0438	-0.0470	-0.0453	-0.0436	-0.0394
12.	-0.0373	-0.0505	-0.0545	-0.0445	-0.0420	-0.0378
24.	-0.0453	-0.0535	-0.0584	-0.0458	-0.0417	-0.0375
48.	-0.0520	-0.0487	-0.0594	-0.0518	-0.0402	-0.0360
70.	-0.0523	-0.0481	-0.0530	-0.0545	-0.0396	-0.0354
90.	-0.0550	-0.0434	-0.0499	-0.0540	-0.0399	-0.0357

CLY-WB

16.	0.	12.	16.	20.	25.	30.	35.	40.	45.
-90.	-0.0608	-0.0766	-0.0048	-0.0217	-0.0397	-0.0660	-0.0623	-0.0859	-0.1130
-70.	-0.0642	-0.0784	-0.0149	-0.0384	-0.0698	-0.0886	-0.0948	-0.0968	-0.1182
-48.	-0.0656	-0.0390	-0.0342	-0.0220	-0.0667	-0.0714	-0.0868	-0.0772	-0.0976
-24.	-0.0656	-0.0540	-0.0492	-0.0370	-0.0317	-0.0164	-0.0218	-0.0372	-0.0426
-12.	-0.0556	-0.0490	-0.0392	-0.0320	-0.0117	0.0086	0.0182	-0.0322	-0.0476
0.	-0.0506	-0.0390	-0.0192	0.0080	0.0233	0.0236	0.0332	0.0278	-0.0776
12.	-0.0479	-0.0330	-0.0044	0.0309	0.0423	0.0235	0.0065	0.0020	-0.0953
24.	-0.0500	-0.0351	0.0010	0.0339	0.0361	0.0156	-0.0030	-0.0017	-0.1090
48.	-0.0549	-0.0516	0.0003	0.0090	0.0053	-0.0110	-0.0213	-0.0391	-0.1207
70.	-0.0599	-0.0699	-0.0056	-0.0150	-0.0205	-0.0393	-0.0422	-0.0716	-0.1209
90.	-0.0600	-0.0775	-0.0048	-0.0251	-0.0431	-0.0661	-0.0614	-0.0892	-0.1146

16.	50.	55.	60.	65.	70.	90.
-90.	-0.1306	-0.1277	-0.1231	-0.1110	-0.1048	-0.0936
-70.	-0.1408	-0.1197	-0.1134	-0.1080	-0.1026	-0.0914
-48.	-0.1280	-0.1034	-0.0938	-0.1092	-0.1046	-0.0934
-24.	-0.0880	-0.0834	-0.0888	-0.1192	-0.1146	-0.1034
-12.	-0.0480	-0.0934	-0.0888	-0.1092	-0.1046	-0.0934
0.	-0.0780	-0.0804	-0.1088	-0.1142	-0.1096	-0.0984
12.	-0.0981	-0.1208	-0.1170	-0.1190	-0.1119	-0.1007
24.	-0.1110	-0.1270	-0.1224	-0.1203	-0.1124	-0.1012
48.	-0.1211	-0.1338	-0.1267	-0.1155	-0.1093	-0.0981
70.	-0.1287	-0.1332	-0.1245	-0.1116	-0.1078	-0.0966
90.	-0.1323	-0.1260	-0.1231	-0.1119	-0.1032	-0.0920

R82-1732-126(10/18)(T)

TABLE B-4. - CONTINUED.

CLY-WB

26.	0.	12.	16.	20.	25.	30.	35.	40.	45.
-90.	-.12	-.12	-.11	-.10	-.16	-.24	-.22	-.15	-.12
-70.	-.12	-.12	-.11	-.10	-.16	-.24	-.22	-.15	-.12
-48.	-.12	-.12	-.11	-.10	-.16	-.24	-.22	-.15	-.12
-24.	-.14	-.12	-.12	-.13	-.10	-.10	-.11	-.10	-.13
-12.	-.10	-.09	-.10	-.09	-.05	-.07	-.06	-.13	-.15
0.	-.09	-.07	-.07	-.06	-.04	-.05	-.03	-.02	-.13
12.	-.10	-.09	-.10	-.09	-.05	-.07	-.06	-.13	-.15
24.	-.14	-.12	-.12	-.10	-.16	-.24	-.22	-.15	-.12
48.	-.12	-.12	-.11	-.10	-.16	-.24	-.22	-.15	-.12
70.	-.12	-.12	-.11	-.10	-.16	-.24	-.22	-.15	-.12
90.	-.12	-.12	-.11	-.10	-.16	-.24	-.22	-.15	-.12

26.	50.	55.	60.	65.	70.	90.
-90.	-.11	-.11	-.10	-.09	-.08	-.07
-70.	-.11	-.11	-.10	-.09	-.08	-.07
-48.	-.11	-.11	-.10	-.09	-.08	-.07
-24.	-.14	-.14	-.13	-.12	-.11	-.10
-12.	-.11	-.15	-.14	-.13	-.12	-.11
0.	-.10	-.13	-.16	-.17	-.17	-.17
12.	-.11	-.15	-.14	-.13	-.12	-.11
24.	-.14	-.14	-.13	-.12	-.11	-.10
48.	-.11	-.11	-.10	-.09	-.08	-.07
70.	-.11	-.11	-.10	-.09	-.08	-.07
90.	-.11	-.11	-.10	-.09	-.08	-.07

CLY-WB

90.	0.	12.	16.	20.	25.	30.	35.	40.	45.
-90.	-.25	-.25	-.25	-.25	-.25	-.25	-.25	-.25	-.25
-70.	-.25	-.25	-.25	-.25	-.25	-.25	-.25	-.25	-.25
-48.	-.25	-.25	-.25	-.25	-.25	-.25	-.25	-.25	-.25
-24.	-.25	-.25	-.25	-.25	-.25	-.25	-.25	-.25	-.25
-12.	-.25	-.25	-.25	-.25	-.25	-.25	-.25	-.25	-.25
0.	-.25	-.25	-.25	-.25	-.25	-.25	-.25	-.25	-.25
12.	-.25	-.25	-.25	-.25	-.25	-.25	-.25	-.25	-.25
24.	-.25	-.25	-.25	-.25	-.25	-.25	-.25	-.25	-.25
48.	-.25	-.25	-.25	-.25	-.25	-.25	-.25	-.25	-.25
70.	-.25	-.25	-.25	-.25	-.25	-.25	-.25	-.25	-.25
90.	-.25	-.25	-.25	-.25	-.25	-.25	-.25	-.25	-.25

90.	50.	55.	60.	65.	70.	90.
-90.	-.25	-.25	-.25	-.25	-.25	-.25
-70.	-.25	-.25	-.25	-.25	-.25	-.25
-48.	-.25	-.25	-.25	-.25	-.25	-.25
-24.	-.25	-.25	-.25	-.25	-.25	-.25
-12.	-.25	-.25	-.25	-.25	-.25	-.25
0.	-.25	-.25	-.25	-.25	-.25	-.25
12.	-.25	-.25	-.25	-.25	-.25	-.25
24.	-.25	-.25	-.25	-.25	-.25	-.25
48.	-.25	-.25	-.25	-.25	-.25	-.25
70.	-.25	-.25	-.25	-.25	-.25	-.25
90.	-.25	-.25	-.25	-.25	-.25	-.25

R82-1732-126(11/18)(T)

TABLE B-4. - CONTINUED.

$C_{LL_{WB_0}}$ — CLL-WB'ALF=0

β ↓ \ δ_c →	-90.	-70.	-48.	-24.	-12.	0.	12.	24.	48.
0.	0.0	0.0	0.0	0.0	0.0	0.0	0.0	0.0	0.0
2.	0.0	0.0008	0.0007	0.0007	-0.0003	-0.0013	-0.0008	-0.0003	0.0019
6.	-0.0025	-0.0013	0.0002	0.0012	0.0012	-0.0028	-0.0052	-0.0061	-0.0029
16.	-0.0111	-0.0102	-0.0022	0.0078	0.0048	-0.0062	-0.0134	-0.0173	-0.0154
26.	-0.0111	-0.0102	-0.0022	0.0078	0.0048	-0.0062	-0.0134	-0.0173	-0.0154
90.	-0.0111	-0.0102	-0.0022	0.0078	0.0048	-0.0062	-0.0134	-0.0173	-0.0154

β ↓ \ δ_c →	0.	80.	90.
0.	0.0	0.0	
2.	0.0021	0.0013	
6.	-0.0020	-0.0028	
16.	-0.0129	-0.0111	
26.	-0.0129	-0.0111	
90.	-0.0129	-0.0111	

$C_{LN_{TE_L}}$ — CLN-TEL

α →	0.	10.	20.	30.	40.	50.	60.	90.	180.
0.0.0	0.00009	0.00018	0.00020	0.00004	-.00009	-.00016	-.00035	-.00035	

$C_{LL_{TE_L}}$ — CLL-TEL

α →	0.	10.	20.	30.	40.	50.	60.	90.	180.
0.0.00093	0.00093	0.00068	0.00045	0.00037	0.00031	0.00027	0.00017	0.00017	

$C_{LY_{TE_L}}$ — CLY-TEL

α →	0.	10.	20.	30.	40.	50.	60.	90.	180.
0.0.0	0.0	0.00020	0.00057	0.00120	0.00133	0.00115	0.00072	0.00072	

$C_{Y_{V2}}$ — CY-V2

β ↓ \ α →	-180.	-90.	0.	12.	16.	30.	70.	90.	180.
0.	0.0	0.0	0.0	0.0	0.0	0.0	0.0	0.0	0.0
30.	-0.177	-0.153	-0.177	-0.180	-0.114	-0.063	-0.132	-0.153	-0.177
90.	-0.1	-0.1	-0.1	-0.1	-0.1	-0.1	-0.1	-0.1	-0.1

$C_{Y_{\beta_{V2}}}$ — CYB-V2

α →	-180.	-90.	0.	12.	16.	30.	70.	90.	180.
0.	-0.3381	-0.2922	-0.3381	-0.3438	-0.2177	-0.1203	-0.2521	-0.2922	-0.3381

$C_{Y_{\delta_R}}$ — CY-DELR

α →	-180.	-35.	-25.	-15.	0.	14.	25.	35.	180.
	0.	0.	.0026	.0032	.0032	.0032	.0026	0.	0.

R82-1732-126(12/18)(T)

TABLE B-4. - CONTINUED.

$C_{L_{RN}}$ CLR-WING

α→	0.	40.	90.
	0.0	0.2400	0.0

$C_{N_{RF}}$ CNR-FUS

δ_c ↓ \ α→	0.	0.	12.	16.	20.	25.	30.	35.	40.	45.
-90.	-0.0587	-0.3371	-0.0963	-0.3724	0.1921	0.5756	0.8531	1.8700	1.4926	
-70.	-0.0651	-0.1522	-0.1965	-0.2800	0.2826	0.6063	0.7873	1.7322	1.6000	
-48.	-0.1680	-0.0798	-0.0978	0.0500	0.0718	0.5897	0.7500	1.6300	1.9500	
-24.	-0.1969	-0.0569	-0.0601	0.2500	0.0489	0.1750	0.6045	1.2620	2.0193	
-12.	-0.1630	-0.0672	-0.0746	0.3000	0.1651	0.1394	0.2860	0.7695	1.4916	
0.	-0.1078	-0.0883	-0.1016	0.3500	0.3323	0.3369	0.0888	0.4815	1.1504	
12.	-0.0471	-0.1112	-0.1381	0.4000	0.5011	0.7352	0.0857	0.5022	1.1402	
24.	0.0013	-0.1230	-0.1866	0.2700	0.6167	1.0100	0.2721	0.8153	1.4365	
48.	0.0051	-0.0784	-0.3347	0.0	0.5285	1.1000	0.8474	1.7293	1.6500	
70.	-0.0992	-0.1555	-0.4570	-0.2400	0.3000	0.6243	0.9464	1.8881	1.7596	
90.	-0.1266	-0.4183	-0.1907	-0.3900	0.1846	0.5823	0.8256	1.7870	1.7381	

δ_c ↓ \ α→	0.	50.	55.	60.	65.	70.	90.
-90.	3.0386	3.0219	-0.6391	-0.0281	-0.0289	-0.0462	
-70.	2.4058	3.0025	-0.5500	-0.6073	-0.0256	-0.0410	
-48.	2.3385	2.7343	1.1854	-0.9037	-0.0128	-0.0296	
-24.	1.7177	1.4027	1.4071	-0.3967	-0.0060	-0.0182	
-12.	1.1213	0.5971	0.8454	-0.0948	-0.0042	-0.0124	
0.	0.4444	-0.0865	0.2590	0.0876	-0.0025	-0.0069	
12.	-0.1687	-0.5189	-0.1143	0.1075	-0.0010	-0.0028	
24.	-0.5579	-0.6275	-0.1904	-0.0061	-0.0003	-0.0021	
48.	-0.1574	0.1025	-0.0664	-0.2549	-0.0070	-0.0161	
70.	1.6055	1.4793	-0.3398	-0.0950	-0.0234	-0.0421	
90.	2.9763	3.0007	-0.6157	-0.0818	-0.0231	-0.0378	

$C_{N_{LE}}$ CN-LEF

α→	-180.	-40.	-20.	0.	20.	40.	60.	180.
	0.	0.	.0013	.0020	.0040	.0010	0.	0.

$C_{M_{LE}}$ CM-LEF

α→	-180.	-40.	-20.	0.	20.	40.	60.	180.
	0.	0.	0.	0.	-.0010	-.0017	0.	0.

$C_{A_{LE}}$ CA-LEF

α→	-180.	-40.	-20.	0.	20.	40.	60.	180.
	0.	-.0010	-.0013	-.0007	.0020	.0030	.0020	0.

R82-1732-126(13/18)(T)

TABLE B-4. - CONTINUED.

$C_{LL_{LE}}$

β = □

$\alpha \rightarrow$ | $\delta_c \downarrow$

CLL-LEF

□	0.	12.	20.	35.	50.	60.	90.
-90.	0.	0.	0.	0.	0.	0.	0.
-48.	0.	0.	0.	0.	0.	0.	0.
-24.	0.	0.	0.	0.	0.	0.	0.
-12.	0.	0.	0.	0.	0.	0.	0.
0.	0.	0.	0.	0.	0.	0.	0.
12.	0.	0.	0.	0.	0.	0.	0.
90.	0.	0.	0.	0.	0.	0.	0.

CLL-LEF

2.	0.	12.	20.	35.	50.	60.	90.
-90.	0.	0.	0.	0.	0.	0.	0.
-48.	0.	0.	0.	0.	0.	0.	0.
-24.	0.	0.	0.	.00018	0.	0.	0.
-12.	0.	.00010	.00010	.00037	.00016	0.	0.
0.	0.	0.	0.	.00023	.00012	0.	0.
12.	0.	0.	0.	0.	0.	0.	0.
90.	0.	0.	0.	0.	0.	0.	0.

CLL-LEF

6.	0.	12.	20.	35.	50.	60.	90.
-90.	0.	0.	0.	0.	0.	0.	0.
-48.	0.	0.	0.	0.	0.	0.	0.
-24.	0.	0.	0.	.00040	0.	0.	0.
-12.	0.	.00027	.00023	.00040	0.	0.	0.
0.	0.	0.	0.	.00067	0.	0.	0.
12.	0.	0.	0.	0.	0.	0.	0.
90.	0.	0.	0.	0.	0.	0.	0.

CLL-LEF

16.	0.	12.	20.	35.	50.	60.	90.
-90.	0.	0.	0.	0.	0.	0.	0.
-48.	0.	0.	0.	0.	0.	0.	0.
-24.	0.	0.	0.	0.	0.	0.	0.
-12.	0.	.00027	.00060	0.	0.	0.	0.
0.	0.	0.	0.	.0004	0.	0.	0.
12.	0.	0.	0.	0.	0.	0.	0.
90.	0.	0.	0.	0.	0.	0.	0.

CLL-LEF

26.	0.	12.	20.	35.	50.	60.	90.
-90.	0.	0.	0.	0.	0.	0.	0.
-48.	0.	0.	0.	0.	0.	0.	0.
-24.	0.	0.	0.	0.	0.	0.	0.
-12.	0.	0.	0.	0.	0.	0.	0.
0.	0.	0.	0.	0.	0.	0.	0.
12.	0.	0.	0.	0.	0.	0.	0.
90.	0.	0.	0.	0.	0.	0.	0.

CLL-LEF

90.	0.	12.	20.	35.	50.	60.	90.
-90.	0.	0.	0.	0.	0.	0.	0.
-48.	0.	0.	0.	0.	0.	0.	0.
-24.	0.	0.	0.	0.	0.	0.	0.
-12.	0.	0.	0.	0.	0.	0.	0.
0.	0.	0.	0.	0.	0.	0.	0.
12.	0.	0.	0.	0.	0.	0.	0.
90.	0.	0.	0.	0.	0.	0.	0.

R82-1732-126(14/18)(1)

TABLE B-4. - CONTINUED.

$C_{LN_{DIF}}$

CLN-DIF

α ↓ \ β →	0.	6.	16.	26.	90.
0.	.000000	.000000	.000000	.000000	0.
7.	.000792	.000750	.000250	.000250	0.
11.	.000875	.000750	.000250	.000250	0.
19.	.000646	.000646	.000417	.000417	0.
24.	.000208	.000542	.000313	.000313	0.
30.	.000458	.000542	.000542	.000542	0.
35.	.000292	.000292	.000635	.000635	0.
40.	.000365	.000313	.000750	.000750	0.
50.	.000396	.001521	.001479	.001479	0.
60.	.001271	.001229	.001188	.001188	0.
70.	.000958	.000927	.000896	.000896	0.
90.	.000260	.000260	.000208	.000208	0.

$C_{LL_{DIF}}$

CLL-DIF

α ↓ \ β →	0.	6.	16.	26.	90.
0.	-.00013	-.00013	-.00010	-.00010	0.
7.	-.00013	-.00013	-.00008	-.00008	0.
11.	0.	.000420	0.	0.	0.
19.	.000333	.000333	.000063	.000063	0.
24.	.000500	.000563	0.	0.	0.
30.	.000229	.000479	.000521	.000521	0.
35.	.000375	.000583	.000750	.000750	0.
40.	.000313	.000573	.000594	.000594	0.
50.	.000229	.000417	.000354	.000354	0.
60.	.000177	.000167	.000167	.000167	0.
70.	.000177	.000177	.000177	.000177	0.
90.	.000083	.000083	.000083	.000083	0.

$C_{LY_{DIF}}$

CLY-DIF

α ↓ \ β →	0.	6.	16.	26.	90.
0.	.000000	.000000	.000000	.000000	0.
7.	.000729	.000896	.001042	.001042	0.
11.	.001042	.001000	.001438	.001438	0.
19.	.002417	.001979	.001625	.001625	0.
24.	.001979	.001688	.001563	.001563	0.
30.	.002135	.002365	.001979	.001979	0.
35.	.002229	.002323	.002552	.002552	0.
40.	.002260	.002990	.002781	.002781	0.
50.	.001667	.002708	.002760	.002760	0.
60.	.002208	.002208	.002208	.002208	0.
70.	.001833	.001750	.001656	.001656	0.
90.	.000438	.000438	.000344	.000344	0.

R82-1732-126(15/18)(T)

TABLE B-4. - CONTINUED.

$(\Delta C_M)_\beta$ β= □ $\delta_c \rightarrow$ $\alpha \downarrow$

(DCM)B

	-90.	-48.	-24.	-12.	0.	12.	90.
0.	0.	0.	0.	0.	0.	0.	0.
10.	0.	0.	0.	0.	0.	0.	0.
20.	0.	0.	0.	0.	0.	0.	0.
25.	0.	0.	0.	0.	0.	0.	0.
30.	0.	0.	0.	0.	0.	0.	0.
35.	0.	0.	0.	0.	0.	0.	0.
40.	0.	0.	0.	0.	0.	0.	0.
45.	0.	0.	0.	0.	0.	0.	0.
50.	0.	0.	0.	0.	0.	0.	0.
55.	0.	0.	0.	0.	0.	0.	0.
60.	0.	0.	0.	0.	0.	0.	0.
70.	0.	0.	0.	0.	0.	0.	0.
90.	0.	0.	0.	0.	0.	0.	0.

(DCM)B

	-90.	-48.	-24.	-12.	0.	12.	90.
4.							
0.	0.	0.	0.	0.	0.	0.	0.
10.	0.	0.	0.	0.	-.007	0.	0.
20.	0.	0.	-.008	0.	-.005	0.	0.
25.	0.	0.	-.020	-.016	0.	0.	0.
30.	0.	0.	-.020	-.031	-.040	0.	0.
35.	0.	0.	0.	-.021	-.130	-.100	-.100
40.	0.	0.	0.	-.017	-.140	-.150	-.150
45.	.070	.070	0.	0.	-.110	-.170	-.170
50.	.050	.050	0.	0.	-.032	-.050	-.050
55.	-.024	-.024	0.	0.	-.024	-.050	-.050
60.	0.	0.	0.	0.	-.017	-.050	-.050
70.	0.	0.	0.	0.	-.013	-.050	-.050
90.	0.	0.	0.	0.	-.013	-.050	-.050

(DCM)B

	-90.	-48.	-24.	-12.	0.	12.	90.
30.							
0.	0.	0.	0.	0.	0.	0.	0.
10.	0.	0.	0.	0.	-.050	0.	0.
20.	0.	0.	-.060	0.	-.040	0.	0.
25.	0.	0.	-.150	-.120	-.150	0.	0.
30.	0.	0.	-.150	-.230	-.180	-.460	-.460
35.	0.	0.	-.120	-.160	-.280	-.460	-.460
40.	0.	0.	-.120	-.130	-.200	-.300	-.300
45.	-.130	-.130	-.080	-.110	-.110	-.170	-.170
50.	-.170	-.170	-.080	-.230	-.240	-.050	-.050
55.	-.180	-.180	-.080	-.230	-.180	-.050	-.050
60.	-.080	-.080	-.080	-.230	-.130	-.050	-.050
70.	-.080	-.080	-.080	-.230	-.100	-.050	-.050
90.	-.080	-.080	-.080	-.230	-.100	-.050	-.050

R82-1732-126(17/18)(T)

TABLE B-4. - CONCLUDED.

						(DCM)B	
	90.	-90.	-48.	-24.	-12.	0.	12.	90.
	0.	0.	0.	0.	0.	0.	0.	0.
	10.	0.	0.	0.	0.	0.	0.	0.
	20.	0.	0.	0.	0.	0.	0.	0.
	25.	0.	0.	0.	0.	0.	0.	0.
	30.	0.	0.	0.	0.	0.	0.	0.
	35.	0.	0.	0.	0.	0.	0.	0.
	40.	0.	0.	0.	0.	0.	0.	0.
	45.	0.	0.	0.	0.	0.	0.	0.
	50.	0.	0.	0.	0.	0.	0.	0.
	55.	0.	0.	0.	0.	0.	0.	0.
	60.	0.	0.	0.	0.	0.	0.	0.
	70.	0.	0.	0.	0.	0.	0.	0.
	90.	0.	0.	0.	0.	0.	0.	0.

						DCN-W2	
$\Delta C_{N_{W2}}$	α→	0.	3.	16.	20.	24.	90.
		.185	.185	.185	.178	0.	0.

						DCM-W2	
$\Delta C_{M_{W2}}$	α→	0.	8.	16.	20.	24.	90.
		-.085	-.085	-.085	-.043	0.	0.

						DCA-W2	
$\Delta C_{A_{W2}}$	α→	0.	8.	16.	20.	24.	90.
		0.	-.018	-.010	-.005	0.	0.

R82-1732-126(18/18)(T)

APPENDIX C

AN APPROACH TO CONTROL LAW DEVELOPMENT FOR RELAXED STATIC STABILITY AIRCRAFT

R. Paul Martorella

The advent of Relaxed Static Stability (RSS) tactical aircraft would, at first, seem to require that a totally new approach be developed for synthesizing control laws. Modern optimal control techniques can certainly be used to compute control system forward loop and feedback gains (once a response model and figure of merit are defined), and will yield control laws that possess excellent feedback control properties (e.g., robustness). The present maturity of these methods is, however, such that the underlying physics of the problem tend to be obscured. Classical techniques, properly applied, can be used to develop an insight into control requirements for RSS aircraft, to design the essential control laws, and to provide a link between classical and modern approaches. The foregoing study used this philosophy; the central ideas of this approach are discussed here in more detail.

Since RSS vehicles lack inherent aerodynamic stability, the control system must provide both static stability and maneuver augmentation. Canarded RSS aircraft introduce some additional problems for control designers. Unstable aircraft stall characteristics are quite different from those of conventional airplanes. For example, when a stable aft-tail aircraft is slowed in level flight (as in an approach to stall), the tail deflection tends toward saturation in a sense opposite to that required for (nose-down) recovery. For an unstable vehicle, the high angle-of-attack trim requirements drive the canard/tail surface toward saturation in the same direction as would be necessary to recover the aircraft. Therefore, a dynamic criterion for recovery is required in the definition of minimum control speed (V_{min}). For a RSS aircraft this is an aft center of gravity problem, whereas for a stable airplane V_{min} is usually defined by a critical forward center of gravity limit. Examples of other differences could be cited.

Nevertheless, successful design of a RSS aircraft flight control system still requires the following basic approach:

- The flight characteristics of the aircraft must be well-understood
- Generic control laws for global maneuvering and precision tracking must be subject to the considerations of
  - Handling qualities criteria
  - Protection of the aircraft from
    * Deep stall
    * Departure
    * Spin
- Definition of control power requirements must be subject to consideration of
  - Control saturation
  - Actuator rate limits.

Before the flight characteristics and control power of the vehicle can be assessed, a control law configuration must first be developed since the airplane will be controlled and stabilized by these laws. The control law fundamentally affects the aircraft's flight characteristics and, hence, the airframe and control system cannot be considered as separate entities when discussing handling qualities. The overall design goal should be to achieve Level I (as per MIL-F-8785C) flying qualities with the fully augmented vehicle, and Level II with a degraded augmented mode. Several control laws were developed during the present investigation and are discussed in the body of the report. For the purpose of discussing a general philosophy of gain determination for RSS aircraft, a longitudinal channel Δn_z ("G") command system will be used. The same general philosophy was used in developing the lateral and directional channel control laws and the α command longitudinal control system.

C.1 LONGITUDINAL CONTROL SYSTEM (Δn_z AND PITCH RATE FEEDBACK) EXAMPLE

The design technique consisted of the following steps:

- Development of expressions for approximating airplane dynamics
- Selection of handling qualities requirements from MIL-F-8785C
- Determination of gains for simple control loops
- Modification of the control laws/gains to account for actuators, integrators, and other higher-order dynamic elements
- Final verification of system performance in the time domain.

C.2 AIRPLANE DYNAMICS

Airplane dynamics are approximated using an expression which is easily manageable, yet perfectly suitable and adequate for developing a gain-computing algorithm. For the Δn_z system, the airframe dynamics are approximated by the short-period mode. Even further simplifications are often possible (e.g., assuming negligible lift due to canard deflection, $Z_\delta = 0$), since the gain algorithm is required only to augment the short-period frequency and damping and not the total response. If other parts of the trajectory are to be altered, then the same philosophy can be used to augment the pertinent aerodynamic derivatives. The approximate airframe dynamics are given by:

$$\frac{\Delta n_z}{\Delta \delta_c} \simeq \frac{A}{s^2 + 2\zeta_A \omega_A s + \omega_A^2} ,$$

$$A = \frac{\bar{q}\, S_w\, \bar{c}_w}{I_y} \frac{C_{L_\alpha}}{W/\bar{q}\, S_w} C_{m_{\delta_c}} ,$$

$$2\zeta_A \omega_A \simeq C_{L_\alpha} \frac{\bar{q} S_w}{m V_T} - C_{m_q} \left(\frac{\bar{q}\, S_w\, \bar{c}_w}{I_y} \right) \frac{\bar{c}_w}{2V_T} ,$$

$$\omega_A^2 \cong -\left[C_{m_\alpha} \frac{\bar{q}\, S_w\, \bar{c}_w}{I_y} + \frac{C_{L_\alpha}\, C_{m_q}\, S_w^2\, \bar{c}_w^2}{2m} \left(\frac{\bar{q}}{V_T} \right)^2 \right] .$$

C.3 SELECTION OF FLYING QUALITIES REQUIREMENTS

Flying qualities requirements are taken from Paragraph 3.2.2 of MIL-F-8785C. They are expressed in terms of the equivalent short-period undamped natural frequency, $\omega_{n_{sp}}$, as a function of n_{z_α} (together implying CAP), and the equivalent short-period damping ratio. Level I, II, and III requirements are thus defined. An implicit assumption is that the short-period response will be of a quasi-second-order nature.

C.4 GAIN DETERMINATION

With the airplane dynamics modeled, initial gains are determined subject to consideration of MIL-F-8785C specifications for Level I flying qualities. The basic control configuration to be analyzed in this case is shown below.

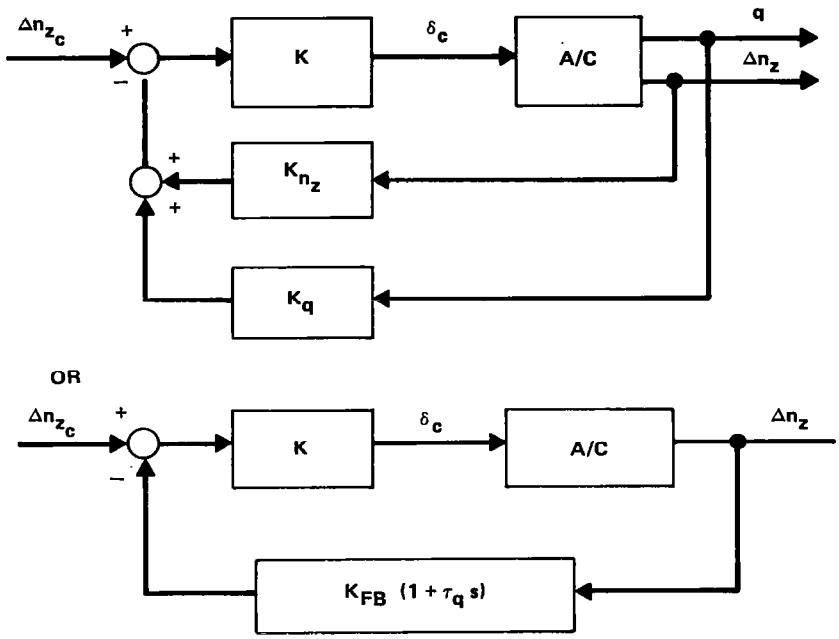

WHERE: $K_{FB} = K_{n_z}\left(1 + \frac{K_q}{K_{n_z}}\ \frac{g}{V_T}\right)$ AND $\tau_q = \frac{(K_q/K_{n_z})\ (1/n_{z_\alpha})}{1 + (K_q/K_{n_z})\ (g/V_T)}$

R82-1732-117(T)

Given the specification requirements for a desired level of short-period frequency or CAP and an equivalent short-period damping ratio ζ_n, equations for the gains are determined as follows:

$$n_{z_\alpha} = \frac{C_{L_\alpha}}{W/\bar{q}\, S_w},$$

$$CAP \cong \frac{\omega_n^2}{n_{z_\alpha}},$$

$$KK_{FB} = \frac{1}{A}\left(\omega_n^2 - \omega_A^2\right),$$

$$\tau_q = \frac{2\zeta_n\omega_n - 2\zeta_A\,\omega_A}{KK_{FB}A},$$

$$\frac{K_q}{K_{FB}} = \tau_q\, n_{z_\alpha}.$$

Note that the gains K, K_{FB}, and K_q are functions of the open-loop aircraft dynamics (ζ_A, ω_A) and the desired handling qualities metrics (ζ_n, ω_n).

Since one parameter must be selected, let $K_{FB} = 1.0$. The remaining gains are then defined explicitly. These gains can be computed continuously with an on-board computer as a function of Mach Number, altitude, and angle-of-attack, if necessary. The requisite aerodynamic parameters are input as part of the software comprising the algorithm. Typical gain variations are shown in Figure C-1. System performance for the STAC airframe at M = 0.4, sea level is shown by the curve labeled (A/C + n_z + q) in Figure C-2 (Nichols Chart) for the input values: CAP = 1.0, $\zeta_n = 1.2$. A high damping ratio was selected because it was known that phase margin will be reduced with the subsequent addition of an actuator and inclusion of a forward-loop integrator.

Since the closed-loop transfer function is second order, no interpretation is necessary as to the meaning of ω_n and ζ_n as is the case for higher-order systems. The Nichols Chart locus for the aircraft with the addition of n_z and q feedback will remain the same for all flight conditions if the gains are varied appropriately. Hence, for selected algorithm input values of CAP and ζ_n, the open-loop phase and gain margins will always be the same.

Any loss of phase or gain margin due to unmodelled control system elements (e.g., non-ideal actuators) will be a constant value independent of flight condition for a fixed open-loop bandwidth. If CAP requirements are selected such that the crossover frequency is increasing (e.g., with dynamic pressure), then the analysis should be done at the critical flight condition. By not initially including the actuator and integrator, the lowest possible gains (K_{n_z}, K_q) for stabilization of the airframe will be determined.

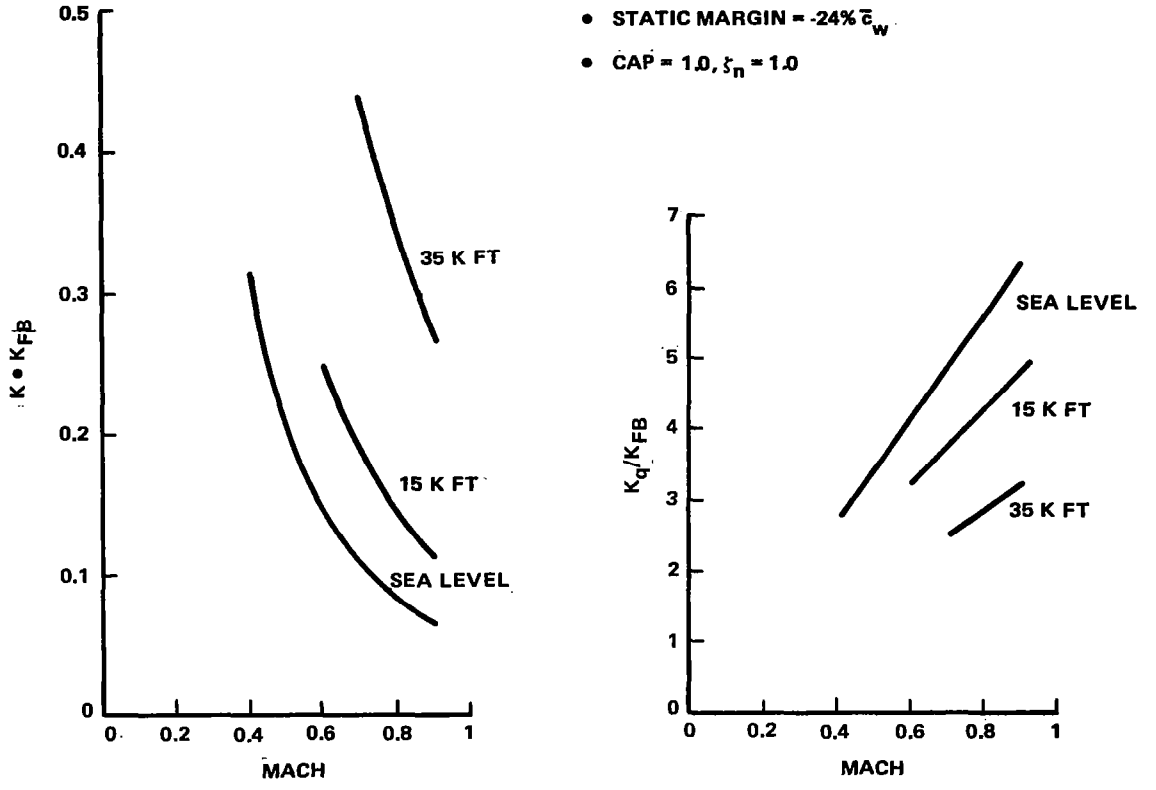

R82-1732-122(T)

Figure C-1. Longitudinal gain variations as a function of Mach Number and altitude

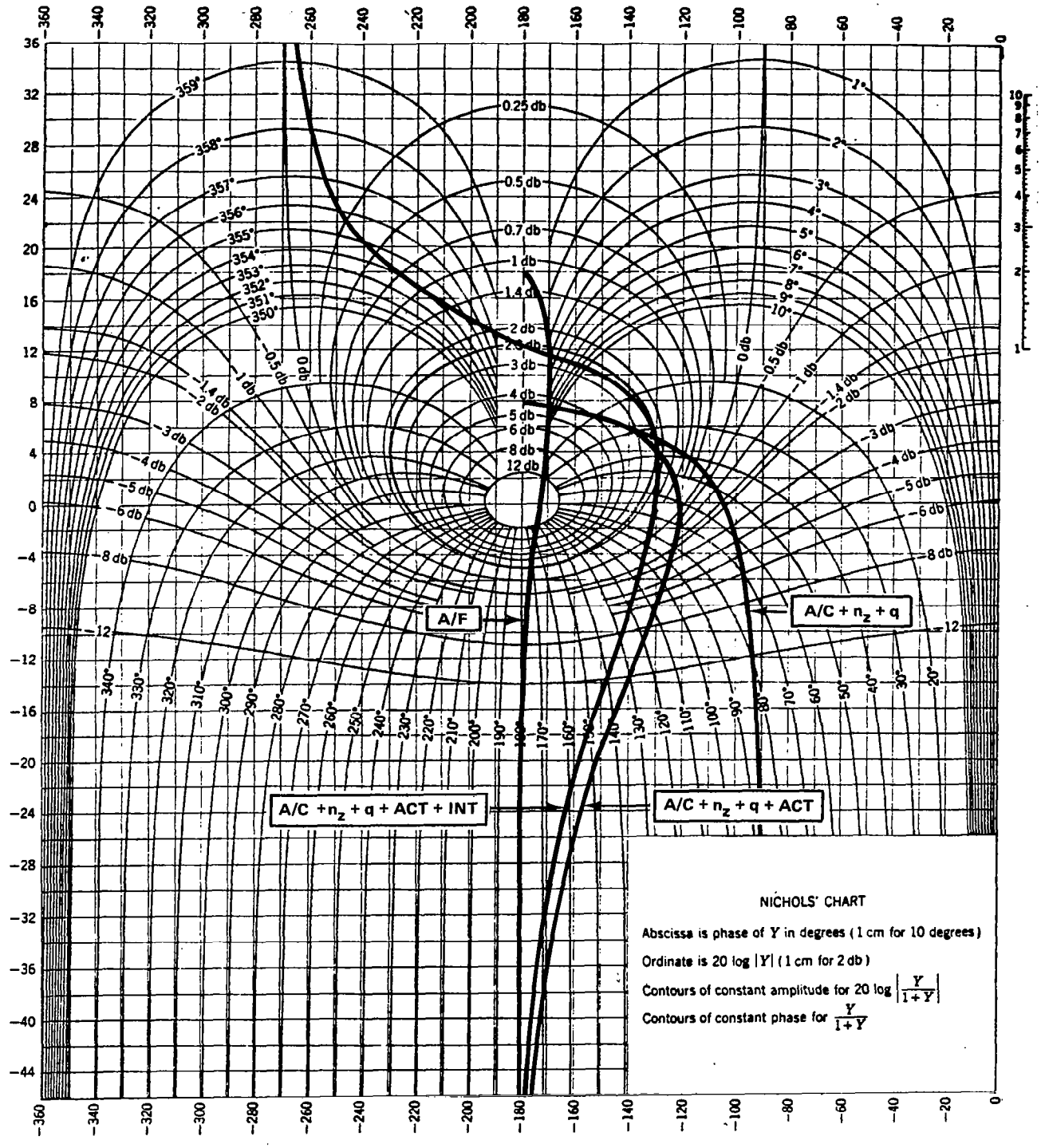

R82-1732-123(T)

Figure C-2. - Nichols chart plot for STAC configuration at M = 0.4, sea level.

The phase margin loss due to the actuator is 15 degrees, and the loss due to the integrator is 10 degrees. The crossover frequency is approximately 10 rad/sec. The gain margin for the full system is 12 dB at low frequency and infinite at high frequency. If higher-order dynamics are present in the control loop, such as an actuator with high-order terms, then these dynamic characteristics should be included when determining the compensation factors K_1 and K_2. Forward-loop compensation can also be used to obtain additional phase margin. Note that such higher-order terms will cause the gain margin at high frequency to become a finite number.

C.6 SPECIAL CASE FOR SECOND-ORDER RESPONSE

One interesting solution results if the value of $K_2\left(\frac{K_I}{K_F}\right)$ is selected equal to the airframe stable real root. In this case, a second-order response is possible even with the inclusion of the integrator, as seen below.

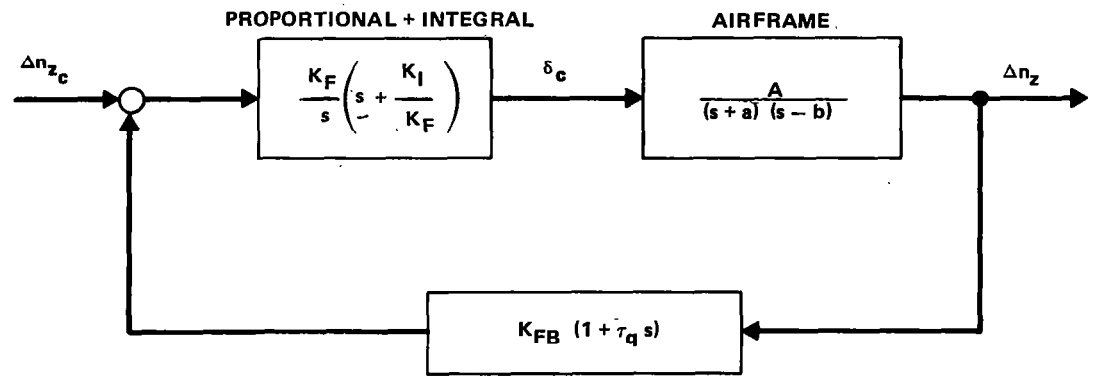

R82-1732-119(T)

$$\frac{\Delta n_z}{\Delta n_{z_c}} = \frac{K_F K_{FB} A (1+\tau_q s)/(s-b)}{s\left[1 + \frac{K_F}{s} A \cdot K_{FB} \frac{(1+\tau_q s)}{(s-b)}\right]},$$

$$= \frac{K_F K_{FB} A (1+\tau_q s)}{s^2 + (K_F K_{FB} A \tau_q - b)s + K_F K_{FB} A}.$$

As before, the effect of the actuator is assessed by Bode and Nichols Chart analyses, and appropriate input CAP and ζ_n values selected. This special case solution will always yield less phase margin than can be attained by locating the $\left(\frac{K_I}{K_F}\right)$ root closer to the origin in the s-plane. The additional phase margin, however, is attained at the expense of a response characteristic higher than second order. Note that similar low-order algorithms can be developed for the lateral and directional channels.

C.7 VERIFICATION OF SYSTEM PERFORMANCE

Verification of algorithm performance is accomplished in the time domain. It is then that final adjustments are made to the algorithm input CAP and ζ_n values as necessary. This time domain investigation must include both an engineering and piloted evaluation of aircraft response to:

- Single axis control inputs
- Multiple axis control inputs
- Air combat maneuvers.

Large-amplitude maneuvers are critical for testing the linear design in a non-linear aerodynamic regime. Simulation of realistic air combat maneuvers further helps to refine the control system where application of theory is cumbersome or impractical.

Piloted simulation is also necessary to fully develop another important feature of the vehicle control system: the command limiter. Depending on available control margin in pitch (since this is the unstable axis), this limiter configuration can become very complex and involve limiting in all three axes. The command limiters will usually become dependent on several state variables. Those used in this study are discussed in the body of the report.

C.8 EXAMPLE OF AUGMENTATION BY THE ADDITION OF $\dot{q}$ FEEDBACK

In theory, the addition of $\dot{q}$ feedback to the (n_z+q) feedback control law adds 90 degrees of phase lead at infinite gain. The control system is as follows:

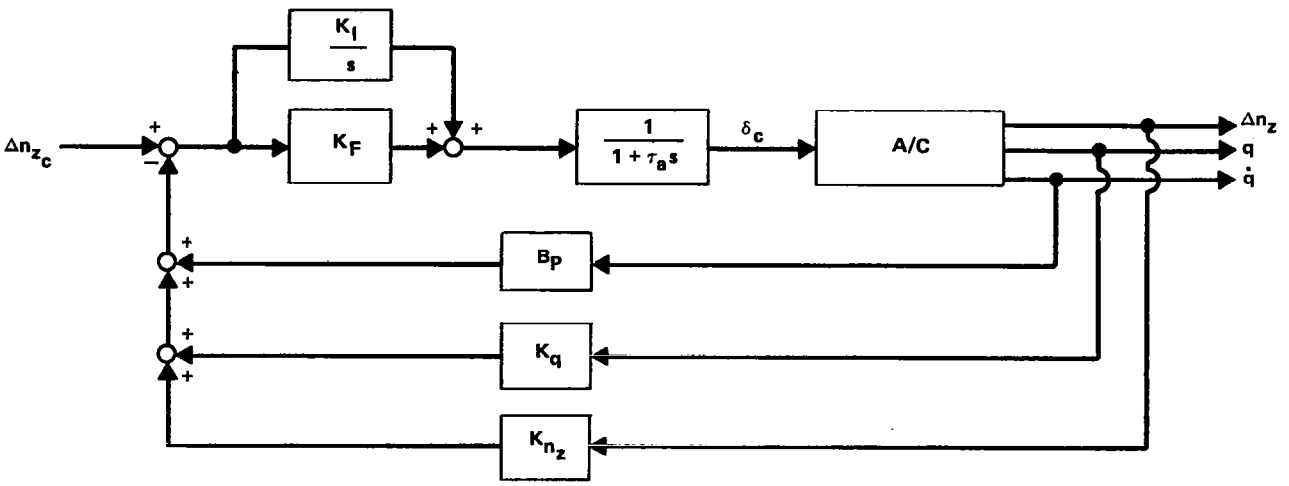

R82-1732-120(T)

For analysis this system can be reduced to the form:

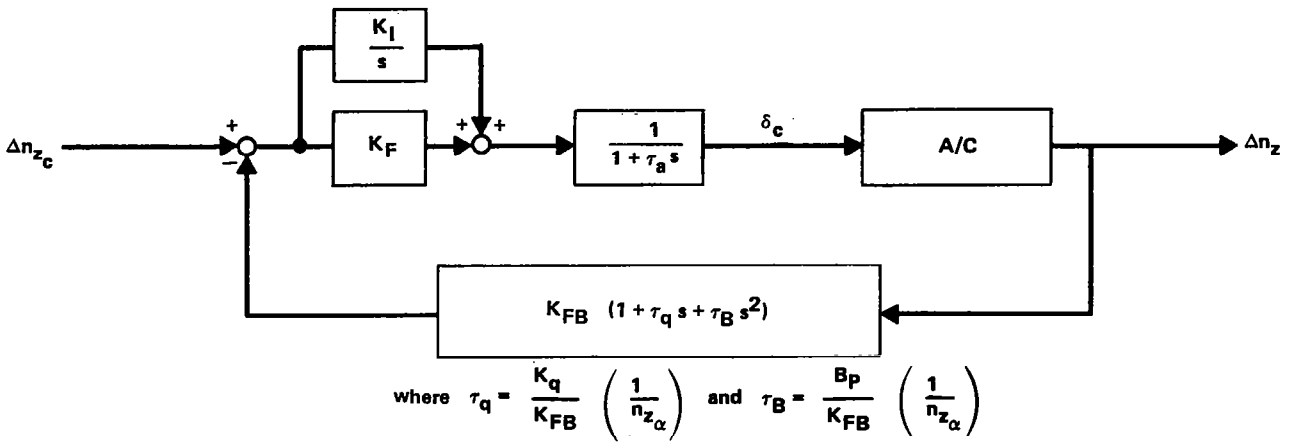

R82-1732-121(T)

The procedure for gain determination is similar to that discussed previously. Given the aircraft aerodynamics and handling qualities specifications, the forward-loop gain K_F and feedback gain K_q are determined without the integrator and actuator using input values for CAP, ζ_n and a selected τ_B. The selection of τ_B is guided by consideration of the feedback filter natural frequency relative to the ω_n requirement arising from the selected value of CAP. Care must be exercised in that raising τ_B leads to gain amplification at high frequency. The relationship between the variables is given by:

$$n_{z_\alpha} = \frac{C_{L_\alpha}}{W/\bar{q}S_w},$$

$$K_F K_{nz} = \frac{1}{A}\ \frac{(\omega_n^2 - \omega_A^2)}{(1 + \tau_B \omega_n^2)},$$

$$\tau_B = \frac{B_P}{K_{FB}}\ \frac{1}{n_{z_\alpha}},$$

$$\tau_q = \frac{(1+K_F K_{n_z} A\tau_B)\ (2\zeta_n \omega_n) - 2\zeta_A \omega_A}{K_F K_{n_z} A},$$

$$K_q = \tau_q n_{z_\alpha},$$

$$K_{FB} = 1.0 \text{ (selected)}.$$

As before, open- and closed-loop frequency response analyses are used to determine the compensation factors K_1 and K_2 as well as to guide a selection of τ_B. These choices then finalize gains K_F and K_I. With this feedback configuration it is much easier to attain a desired ω_n and maintain adequate system phase margin than was possible with the previous system.

A comparison in system performance using a first-order actuator representation is shown in Figures C-3 and C-4. The quadratic feedback compensator frequency is at 6.5 rad/sec and the closed-loop -90 degree phase occurs at 2.8 rad/sec. The $\dot{q}$ feedback can be obtained by locating the n_z sensor forward of the aircraft center of gravity, using two n_z sensors and some additional calculations, or measuring $\dot{q}$ directly. Ease of implementation and the adverse effects of sensor noise are the overriding considerations in this selection.

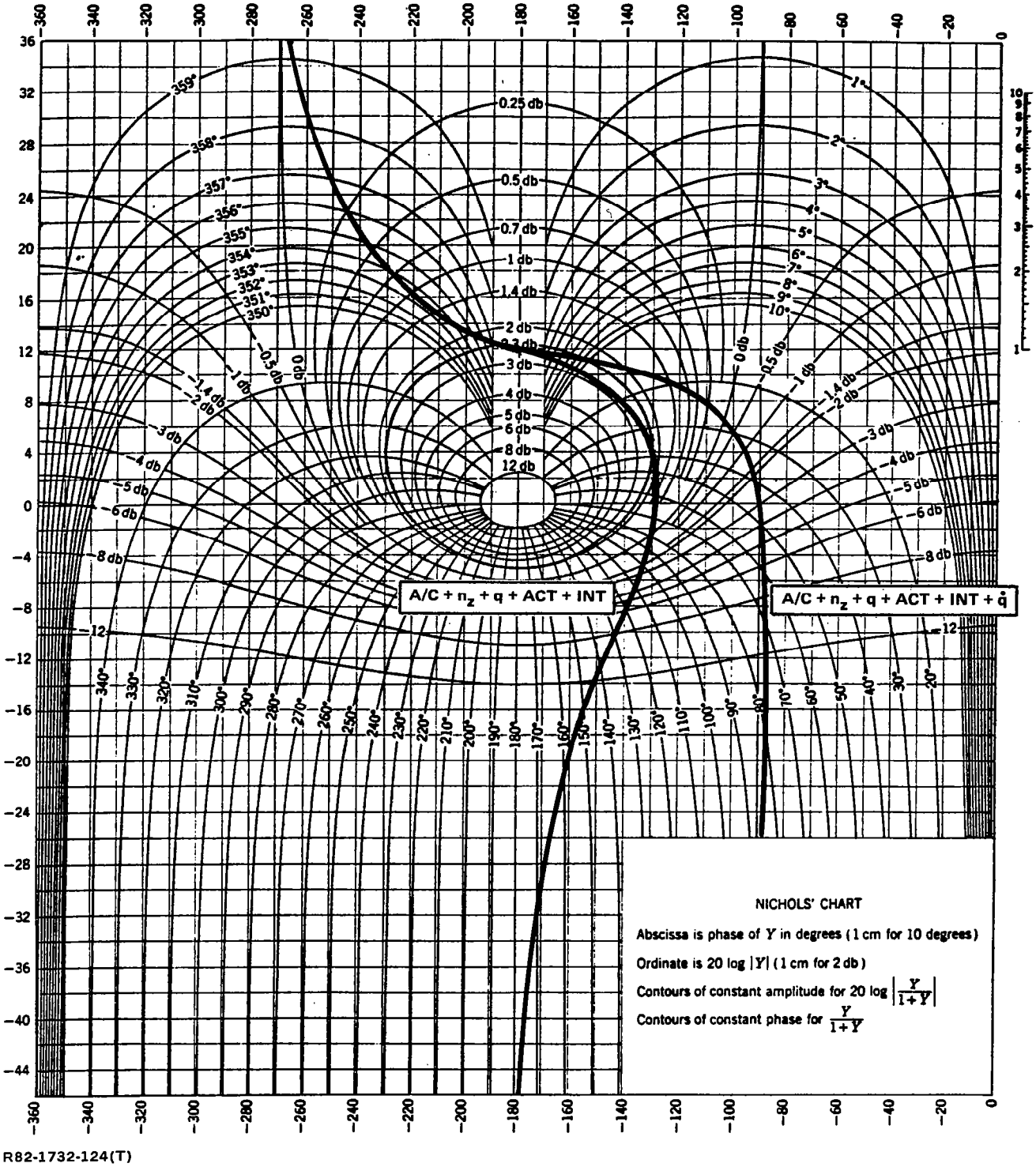

R82-1732-124(T)

Figure C-3. Nichols chart plot for STAC configuration at M = 0.4, sea level.

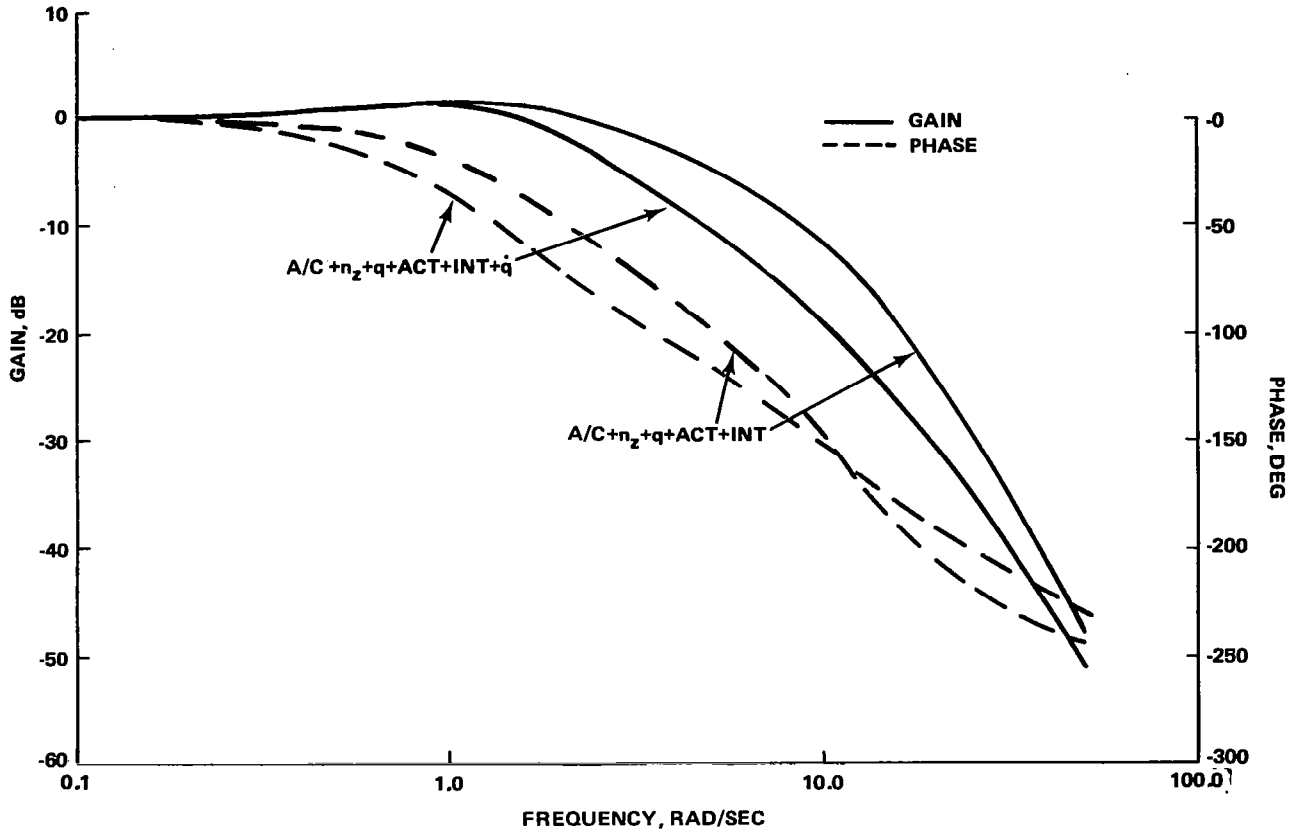

Figure C-4. Closed-loop performance, n_z/n_{z_c}.

APPENDIX D

CANARD RATE/DEFLECTION REQUIREMENT DATA

TABLE D-1. NOMENCLATURE.

ABBREVIATION	DESCRIPTION	UNITS
RUN	RUN NUMBER	
CAP	INPUT CONTROL ANTICIPATION PARAMETER VALUE (CAP_c)	RAD/SEC^2
ZETA	INPUT CLOSED LOOP SHORT PERIOD DAMPING RATIO (ζ_{SP})	
NZMAX	PEAK Δn_z VALUE	G's
ZETAC	COMPUTED (ACHIEVED) DAMPING RATIO (ζ_A)	
CAPC	COMPUTED (ACHIEVED) CAP VALUE (CAP_A)	$RAD/SEC^2/G$
CANDT1	CANARD INITIATION RATE	DEG/SEC
CANDT2	CANARD RECOVERY RATE	DEG/SEC
CNMX1	MAXIMUM CANARD DEFLECTION	DEG
CNMX2	MINIMUM CANARD DEFLECTION	DEG
NOTE: RUN 1 DATA IN EACH SERIES UNRELIABLE		

3016-5-127(T)

TABLE D-2. CANARD RATE/DEFLECTION REQUIREMENT DATA.

- X_{CG}: FS 558.2
- S_c = 40 FT^2

RUN	CAP	ZETA	NZMAX	NZSS	ZETAC	CAPC	CANDT1	CANDT2	CNMX1	CNMX2
PREFILTER TIME CONSTANT= 0.000										
~~1.000~~	~~0.400~~	~~0.300~~	0.519	0.250	-0.023	0.550	164.112	-43.500	0.142	-5.159
2.000	0.600	0.300	0.353	0.250	0.271	0.596	231.199	-6.402	0.315	-4.924
3.000	0.800	0.300	0.355	0.250	0.265	0.810	323.178	-10.007	1.505	-5.414
4.000	1.000	0.300	0.351	0.250	0.277	1.009	408.619	-15.484	2.613	-5.865
5.000	0.400	0.500	0.317	0.250	0.386	0.396	155.605	-3.336	-0.742	-3.987
6.000	0.600	0.500	0.306	0.250	0.431	0.599	236.416	-6.393	0.339	-4.212
7.000	0.800	0.500	0.302	0.250	0.449	0.797	319.704	-10.912	1.435	-4.475
8.000	1.000	0.500	0.299	0.250	0.462	0.997	404.753	-18.357	2.544	-4.752
9.000	0.400	0.700	0.289	0.250	0.509	0.396	155.231	-4.213	-0.745	-3.897
10.000	0.600	0.700	0.278	0.250	0.572	0.596	235.460	-9.023	0.326	-3.845
11.000	0.800	0.700	0.273	0.250	0.604	0.793	317.696	-15.564	1.410	-3.953
12.000	1.000	0.700	0.270	0.250	0.623	0.990	402.009	-23.521	2.508	-4.126
PREFILTER TIME CONSTANT= 0.050										
13.000	0.400	0.300	0.362	0.250	0.247	0.344	33.292	-3.578	-1.009	-4.487
14.000	0.600	0.300	0.353	0.250	0.273	0.514	51.079	-6.347	-0.096	-4.916
15.000	0.800	0.300	0.355	0.250	0.267	0.675	69.286	-9.683	0.800	-5.396
16.000	1.000	0.300	0.350	0.250	0.280	0.813	87.377	-13.293	1.571	-5.833
17.000	0.400	0.500	0.317	0.250	0.386	0.331	33.556	-3.346	-1.070	-3.985
18.000	0.600	0.500	0.306	0.250	0.432	0.477	50.899	-6.003	-0.290	-4.206
19.000	0.800	0.500	0.301	0.250	0.451	0.614	68.636	-9.169	0.457	-4.464
20.000	1.000	0.500	0.298	0.250	0.464	0.742	86.684	-12.851	1.169	-4.734
21.000	0.400	0.700	0.289	0.250	0.510	0.312	33.459	-3.528	-1.170	-3.892
22.000	0.600	0.700	0.278	0.250	0.573	0.446	50.529	-6.303	-0.452	-3.841
23.000	0.800	0.700	0.273	0.250	0.605	0.573	68.191	-9.521	0.227	-3.948
24.000	1.000	0.700	0.270	0.250	0.624	0.690	86.065	-13.105	0.879	-4.117
PREFILTER TIME CONSTANT= 0.100										
25.000	0.400	0.300	0.361	0.250	0.251	0.310	18.081	-3.495	-1.189	-4.471
26.000	0.600	0.300	0.351	0.250	0.278	0.454	27.895	-6.148	-0.411	-4.883
27.000	0.800	0.300	0.352	0.250	0.275	0.586	38.045	-9.324	0.315	-5.335
28.000	1.000	0.300	0.346	0.250	0.290	0.695	47.913	-12.549	0.919	-5.737
29.000	1.500	0.300	0.332	0.250	0.334	0.949	73.983	-21.168	2.336	-6.711
30.000	2.000	0.300	0.325	0.250	0.359	1.191	101.448	-30.925	3.702	-7.687
31.000	0.400	0.500	0.316	0.250	0.389	0.289	18.323	-3.163	-1.290	-3.978
32.000	0.600	0.500	0.305	0.250	0.436	0.406	27.842	-5.461	-0.662	-4.187
33.000	0.800	0.500	0.300	0.250	0.457	0.515	37.588	-8.046	-0.079	-4.428
34.000	1.000	0.500	0.296	0.250	0.473	0.614	47.493	-10.868	0.465	-4.676
35.000	1.500	0.500	0.290	0.250	0.503	0.839	73.226	-18.404	1.719	-5.294
36.000	2.000	0.500	0.286	0.250	0.525	1.045	100.384	-26.736	2.869	-5.895
37.000	0.400	0.700	0.288	0.250	0.512	0.265	18.294	-3.015	-1.416	-3.887
38.000	0.600	0.700	0.278	0.250	0.574	0.369	27.716	-5.145	-0.857	-3.837
39.000	0.800	0.700	0.273	0.250	0.607	0.466	37.338	-7.518	-0.343	-3.928
40.000	1.000	0.700	0.270	0.250	0.628	0.555	47.142	-10.004	0.137	-4.082
41.000	1.500	0.700	0.266	0.250	0.660	0.755	72.584	-16.546	1.247	-4.480
42.000	2.000	0.700	0.264	0.250	0.679	0.937	99.364	-23.294	2.258	-4.873
PREFILTER TIME CONSTANT= 0.250										
43.000	0.400	0.300	0.351	0.250	0.277	0.242	7.885	-2.933	-1.567	-4.370
44.000	0.600	0.300	0.337	0.250	0.318	0.340	12.106	-4.909	-1.022	-4.679
45.000	0.800	0.300	0.334	0.250	0.328	0.425	16.229	-6.835	-0.558	-4.988
46.000	1.000	0.300	0.326	0.250	0.355	0.492	20.321	-8.694	-0.202	-5.236
47.000	1.500	0.300	0.307	0.250	0.427	0.643	31.275	-13.580	0.627	-5.799
48.000	2.000	0.300	0.296	0.250	0.476	0.780	42.917	-18.697	1.397	-6.320
49.000	0.400	0.500	0.312	0.250	0.406	0.216	7.917	-2.445	-1.687	-3.925
50.000	0.600	0.500	0.297	0.250	0.468	0.290	11.939	-3.852	-1.284	-4.064
51.000	0.800	0.500	0.290	0.250	0.502	0.356	15.924	-5.250	-0.925	-4.213
52.000	1.000	0.500	0.285	0.250	0.531	0.416	20.090	-6.689	-0.607	-4.357
53.000	1.500	0.500	0.275	0.250	0.590	0.547	31.008	-10.400	0.096	-4.683
54.000	2.000	0.500	0.268	0.250	0.639	0.659	42.553	-14.177	0.717	-4.971
55.000	0.400	0.700	0.285	0.250	0.529	0.191	7.894	-2.067	-1.817	-3.872
56.000	0.600	0.700	0.276	0.250	0.586	0.254	11.836	-3.223	-1.473	-3.824
57.000	0.800	0.700	0.270	0.250	0.629	0.310	15.808	-4.382	-1.169	-3.803
58.000	1.000	0.700	0.266	0.250	0.660	0.361	19.942	-5.578	-0.895	-3.883
59.000	1.500	0.700	0.260	0.250	0.716	0.474	30.734	-8.405	-0.292	-4.074
60.000	2.000	0.700	0.256	0.250	0.758	0.572	42.324	-11.363	0.235	-4.243

R82-1732-128(1/9)(T)

TABLE D-2. - CONTINUED.

- X_{CG}: FS 576.2
- S_c = 40 FT^2

RUN	CAP	ZETA	NZMAX	NZSS	ZETAC	CAPC	CANDT1	CANDT2	CNMX1	CNMX2
PREFILTER TIME CONSTANT= 0.000										
1.000	0.400	0.300	0.306	0.250	0.431	0.330	135.125	-4.559	-6.961	-11.849
2.000	0.600	0.300	0.367	0.250	0.235	0.608	224.437	-8.624	-5.389	-12.733
3.000	0.800	0.300	0.360	0.250	0.254	0.820	303.326	-12.109	-4.347	-13.121
4.000	1.000	0.300	0.353	0.250	0.272	1.032	383.267	-15.857	-3.321	-13.518
5.000	0.400	0.500	0.322	0.250	0.368	0.396	146.777	-4.645	-6.437	-11.463
6.000	0.600	0.500	0.310	0.250	0.413	0.601	223.012	-7.489	-5.420	-11.594
7.000	0.800	0.500	0.304	0.250	0.437	0.812	301.140	-10.928	-4.389	-11.795
8.000	1.000	0.500	0.301	0.250	0.453	1.026	381.076	-17.238	-3.346	-12.028
9.000	0.400	0.700	0.293	0.250	0.488	0.394	146.263	-4.359	-6.444	-11.283
10.000	0.600	0.700	0.281	0.250	0.556	0.598	221.873	-8.387	-5.433	-11.096
11.000	0.800	0.700	0.275	0.250	0.591	0.807	299.339	-14.727	-4.410	-11.043
12.000	1.000	0.700	0.272	0.250	0.613	1.020	378.689	-22.522	-3.375	-11.161
PREFILTER TIME CONSTANT= 0.050										
13.000	0.400	0.300	0.378	0.250	0.209	0.357	31.864	-5.497	-6.648	-12.375
14.000	0.600	0.300	0.366	0.250	0.236	0.523	48.661	-8.534	-5.807	-12.719
15.000	0.800	0.300	0.359	0.250	0.256	0.678	65.300	-11.732	-5.039	-13.095
16.000	1.000	0.300	0.352	0.250	0.275	0.825	82.450	-15.321	-4.320	-13.479
17.000	0.400	0.500	0.322	0.250	0.369	0.332	31.764	-4.611	-6.758	-11.460
18.000	0.600	0.500	0.310	0.250	0.414	0.479	48.073	-7.414	-6.020	-11.587
19.000	0.800	0.500	0.304	0.250	0.439	0.620	64.852	-10.563	-5.322	-11.783
20.000	1.000	0.500	0.300	0.250	0.456	0.756	81.932	-14.120	-4.653	-12.008
21.000	0.400	0.700	0.293	0.250	0.490	0.312	31.629	-4.253	-6.852	-11.276
22.000	0.600	0.700	0.281	0.250	0.556	0.447	47.881	-7.092	-6.173	-11.091
23.000	0.800	0.700	0.275	0.250	0.592	0.577	64.459	-10.302	-5.531	-11.038
24.000	1.000	0.700	0.272	0.250	0.614	0.701	81.379	-13.782	-4.917	-11.153
PREFILTER TIME CONSTANT= 0.100										
25.000	0.400	0.300	0.376	0.250	0.212	0.324	17.433	-5.440	-6.843	-12.353
26.000	0.600	0.300	0.364	0.250	0.242	0.462	26.590	-8.169	-6.142	-12.673
27.000	0.800	0.300	0.356	0.250	0.264	0.587	35.803	-11.257	-5.522	-13.017
28.000	1.000	0.300	0.348	0.250	0.285	0.702	45.175	-14.384	-4.954	-13.364
29.000	1.500	0.300	0.336	0.250	0.321	0.982	69.949	-23.506	-3.579	-14.304
30.000	2.000	0.300	0.328	0.250	0.346	1.241	96.065	-32.940	-2.323	-15.248
31.000	0.400	0.500	0.321	0.250	0.371	0.291	17.391	-4.509	-6.984	-11.451
32.000	0.600	0.500	0.309	0.250	0.418	0.409	26.369	-6.838	-6.391	-11.565
33.000	0.800	0.500	0.302	0.250	0.445	0.518	35.535	-9.436	-5.843	-11.743
34.000	1.000	0.500	0.298	0.250	0.464	0.621	44.910	-12.172	-5.332	-11.946
35.000	1.500	0.500	0.292	0.250	0.496	0.861	69.307	-19.471	-4.150	-12.493
36.000	2.000	0.500	0.287	0.250	0.519	1.081	95.445	-27.202	-3.077	-13.047
37.000	0.400	0.700	0.292	0.250	0.494	0.266	17.319	-3.975	-7.098	-11.269
38.000	0.600	0.700	0.280	0.250	0.557	0.371	26.223	-6.156	-6.568	-11.086
39.000	0.800	0.700	0.275	0.250	0.594	0.468	35.317	-8.507	-6.081	-11.023
40.000	1.000	0.700	0.271	0.250	0.618	0.560	44.546	-10.959	-5.623	-11.125
41.000	1.500	0.700	0.267	0.250	0.654	0.771	68.713	-17.389	-4.579	-11.440
42.000	2.000	0.700	0.264	0.250	0.676	0.964	94.175	-24.749	-3.635	-11.781
PREFILTER TIME CONSTANT= 0.250										
43.000	0.400	0.300	0.367	0.250	0.235	0.256	7.562	-4.787	-7.241	-12.204
44.000	0.600	0.300	0.351	0.250	0.278	0.347	11.354	-6.798	-6.770	-12.390
45.000	0.800	0.300	0.339	0.250	0.314	0.424	15.208	-8.778	-6.379	-12.580
46.000	1.000	0.300	0.328	0.250	0.348	0.494	19.106	-10.746	-6.031	-12.761
47.000	1.500	0.300	0.311	0.250	0.411	0.658	29.660	-16.144	-5.203	-13.245
48.000	2.000	0.300	0.299	0.250	0.460	0.802	40.726	-21.453	-4.484	-13.687
49.000	0.400	0.500	0.317	0.250	0.386	0.219	7.493	-3.808	-7.386	-11.379
50.000	0.600	0.500	0.302	0.250	0.447	0.293	11.266	-5.348	-7.006	-11.413
51.000	0.800	0.500	0.293	0.250	0.487	0.359	15.055	-6.841	-6.670	-11.494
52.000	1.000	0.500	0.287	0.250	0.518	0.419	19.017	-8.342	-6.364	-11.588
53.000	1.500	0.500	0.277	0.250	0.578	0.555	29.539	-12.172	-5.685	-11.827
54.000	2.000	0.500	0.270	0.250	0.627	0.673	40.326	-16.051	-5.092	-12.049
55.000	0.400	0.700	0.288	0.250	0.516	0.192	7.454	-3.168	-7.497	-11.247
56.000	0.600	0.700	0.279	0.250	0.567	0.256	11.194	-4.400	-7.170	-11.070
57.000	0.800	0.700	0.272	0.250	0.614	0.313	14.962	-5.609	-6.880	-10.980
58.000	1.000	0.700	0.267	0.250	0.646	0.365	18.886	-6.807	-6.617	-10.946
59.000	1.500	0.700	0.261	0.250	0.704	0.480	29.108	-9.804	-6.035	-11.055
60.000	2.000	0.700	0.257	0.250	0.747	0.581	39.928	-12.751	-5.528	-11.167

TABLE D-2. - CONTINUED.

- X_{CG}: FS 594.2
- S_c = 40 FT^2

RUN	CAP	ZETA	NZMAX	NZSS	ZETAC	CAPC	CANDT1	CANDT2	CNMX1	CNMX2
PREFILTER TIME CONSTANT= 0.000										
1.000	0.400	0.300	0.388	0.250	0.185	0.455	165.351	-8.519	-11.359	-20.526
2.000	0.600	0.300	0.372	0.250	0.222	0.693	251.807	-12.485	-10.230	-20.828
3.000	0.800	0.300	0.364	0.250	0.242	0.944	333.898	-16.905	-9.048	-21.276
4.000	1.000	0.300	0.359	0.250	0.256	1.201	434.875	-21.736	-7.860	-21.787
5.000	0.400	0.500	0.321	0.250	0.373	0.451	164.641	-6.998	-11.363	-18.861
6.000	0.600	0.500	0.309	0.250	0.419	0.689	250.388	-10.395	-10.245	-18.957
7.000	0.800	0.500	0.303	0.250	0.443	0.936	331.406	-14.706	-9.085	-19.164
8.000	1.000	0.500	0.300	0.250	0.458	1.193	431.526	-23.284	-7.897	-19.421
9.000	0.400	0.700	0.289	0.250	0.509	0.450	164.162	-6.324	-11.355	-18.538
10.000	0.600	0.700	0.277	0.250	0.577	0.685	249.043	-10.630	-10.252	-18.179
11.000	0.800	0.700	0.272	0.250	0.614	0.930	337.085	-18.781	-9.108	-18.016
12.000	1.000	0.700	0.269	0.250	0.636	1.183	428.231	-29.057	-7.936	-18.116
PREFILTER TIME CONSTANT= 0.050										
13.000	0.400	0.300	0.388	0.250	0.187	0.405	35.673	-8.407	-11.635	-20.508
14.000	0.600	0.300	0.371	0.250	0.225	0.588	54.061	-12.363	-10.759	-20.799
15.000	0.800	0.300	0.363	0.250	0.246	0.766	73.224	-16.474	-9.916	-21.230
16.000	1.000	0.300	0.357	0.250	0.260	0.940	93.023	-21.004	-9.096	-21.719
17.000	0.400	0.500	0.320	0.250	0.374	0.373	35.510	-6.880	-11.762	-18.855
18.000	0.600	0.500	0.308	0.250	0.421	0.538	53.729	-10.420	-10.978	-18.945
19.000	0.800	0.500	0.302	0.250	0.445	0.698	72.675	-14.433	-10.217	-19.144
20.000	1.000	0.500	0.299	0.250	0.461	0.853	92.239	-18.691	-9.486	-19.390
21.000	0.400	0.700	0.289	0.250	0.512	0.350	35.146	-6.225	-11.852	-18.527
22.000	0.600	0.700	0.277	0.250	0.578	0.501	53.401	-9.576	-11.141	-18.173
23.000	0.800	0.700	0.272	0.250	0.615	0.646	72.142	-13.494	-10.450	-18.010
24.000	1.000	0.700	0.269	0.250	0.637	0.786	91.454	-17.936	-9.786	-18.105
PREFILTER TIME CONSTANT= 0.100										
25.000	0.400	0.300	0.386	0.250	0.191	0.365	19.463	-8.321	-11.886	-20.460
26.000	0.600	0.300	0.368	0.250	0.232	0.515	29.606	-11.965	-11.168	-20.713
27.000	0.800	0.300	0.359	0.250	0.256	0.656	40.355	-15.559	-10.494	-21.093
28.000	1.000	0.300	0.352	0.250	0.273	0.792	50.973	-19.504	-9.850	-21.521
29.000	1.500	0.300	0.341	0.250	0.306	1.112	79.824	-30.207	-8.346	-22.679
30.000	2.000	0.300	0.332	0.250	0.334	1.408	111.130	-41.573	-6.977	-23.867
31.000	0.400	0.500	0.320	0.250	0.377	0.324	19.373	-6.784	-12.038	-18.836
32.000	0.600	0.500	0.307	0.250	0.426	0.454	29.427	-9.685	-11.418	-18.905
33.000	0.800	0.500	0.301	0.250	0.453	0.576	39.808	-12.830	-10.833	-19.078
34.000	1.000	0.500	0.297	0.250	0.471	0.692	50.542	-16.167	-10.279	-19.291
35.000	1.500	0.500	0.290	0.250	0.503	0.963	78.935	-24.998	-8.999	-19.889
36.000	2.000	0.500	0.285	0.250	0.528	1.213	109.704	-34.118	-7.835	-20.519
37.000	0.400	0.700	0.288	0.250	0.516	0.295	19.337	-5.867	-12.146	-18.515
38.000	0.600	0.700	0.277	0.250	0.579	0.410	29.260	-8.506	-11.605	-18.166
39.000	0.800	0.700	0.271	0.250	0.618	0.517	39.517	-11.354	-11.090	-17.994
40.000	1.000	0.700	0.268	0.250	0.641	0.619	50.107	-14.408	-10.604	-18.070
41.000	1.500	0.700	0.264	0.250	0.677	0.855	78.087	-22.224	-9.480	-18.359
42.000	2.000	0.700	0.261	0.250	0.700	1.073	108.311	-30.527	-8.464	-18.700
PREFILTER TIME CONSTANT= 0.250										
43.000	0.400	0.300	0.373	0.250	0.220	0.282	8.358	-7.358	-12.366	-20.158
44.000	0.600	0.300	0.351	0.250	0.276	0.379	12.633	-9.867	-11.899	-20.209
45.000	0.800	0.300	0.338	0.250	0.315	0.466	16.976	-12.260	-11.475	-20.364
46.000	1.000	0.300	0.328	0.250	0.346	0.547	21.584	-14.699	-11.081	-20.546
47.000	1.500	0.300	0.311	0.250	0.410	0.730	33.817	-21.077	-10.195	-21.018
48.000	2.000	0.300	0.298	0.250	0.467	0.891	47.131	-27.301	-9.422	-21.452
49.000	0.400	0.500	0.314	0.250	0.397	0.239	8.293	-5.719	-12.509	-18.701
50.000	0.600	0.500	0.299	0.250	0.461	0.320	12.530	-7.616	-12.125	-18.654
51.000	0.800	0.500	0.290	0.250	0.502	0.392	16.861	-9.379	-11.772	-18.693
52.000	1.000	0.500	0.284	0.250	0.533	0.459	21.406	-11.195	-11.447	-18.756
53.000	1.500	0.500	0.274	0.250	0.596	0.607	33.437	-15.622	-10.719	-18.937
54.000	2.000	0.500	0.267	0.250	0.650	0.739	46.508	-19.939	-10.085	-19.110
55.000	0.400	0.700	0.283	0.250	0.544	0.209	8.261	-4.691	-12.608	-18.482
56.000	0.600	0.700	0.275	0.250	0.591	0.277	12.417	-6.251	-12.288	-18.145
57.000	0.800	0.700	0.268	0.250	0.639	0.339	16.742	-7.666	-11.990	-17.980
58.000	1.000	0.700	0.264	0.250	0.672	0.395	21.220	-9.058	-11.714	-17.888
59.000	1.500	0.700	0.259	0.250	0.730	0.521	33.083	-12.466	-11.100	-17.895
60.000	2.000	0.700	0.255	0.250	0.773	0.632	45.912	-15.776	-10.561	-17.956

R82-1732-128(3/9)(T)

TABLE D-2. - CONTINUED.

- X_{CG}: FS 540.2
- S_c = 70 FT^2

RUN	CAP	ZETA	NZMAX	NZSS	ZETAC	CAPC	CANDT1	CANDT2	CNMX1	CNMX2
PREFILTER TIME CONSTANT= 0.000										
1.000	0.400	0.300	0.358	0.250	0.258	0.453	107.147	-2.594	0.498	-1.806
2.000	0.600	0.300	0.330	0.250	0.343	0.622	159.067	-4.197	1.087	-2.035
3.000	0.800	0.300	0.327	0.250	0.349	0.832	216.216	-6.504	1.825	-2.326
4.000	1.000	0.300	0.327	0.250	0.352	1.053	276.508	-13.221	2.609	-2.632
5.000	0.400	0.500	0.276	0.250	0.582	0.411	100.897	-2.123	0.344	-1.450
6.000	0.600	0.500	0.280	0.250	0.559	0.616	157.508	-4.199	1.062	-1.618
7.000	0.800	0.500	0.281	0.250	0.553	0.826	214.214	-7.781	1.804	-1.795
8.000	1.000	0.500	0.281	0.250	0.551	1.042	273.546	-15.075	2.571	-1.979
9.000	0.400	0.700	0.250	0.250	1.000	0.408	102.347	-2.910	0.334	-1.327
10.000	0.600	0.700	0.253	0.250	0.823	0.610	156.039	-6.237	1.042	-1.391
11.000	0.800	0.700	0.254	0.250	0.792	0.818	211.899	-11.038	1.776	-1.502
12.000	1.000	0.700	0.255	0.250	0.777	1.031	270.276	-17.007	2.531	-1.619
PREFILTER TIME CONSTANT= 0.050										
13.000	0.400	0.300	0.326	0.250	0.355	0.372	22.468	-2.340	0.246	-1.744
14.000	0.600	0.300	0.329	0.250	0.345	0.529	34.196	-4.241	0.804	-2.027
15.000	0.800	0.300	0.326	0.250	0.353	0.680	46.407	-6.427	1.341	-2.311
16.000	1.000	0.300	0.326	0.250	0.356	0.832	59.006	-9.022	1.887	-2.608
17.000	0.400	0.500	0.276	0.250	0.584	0.341	22.221	-2.132	0.127	-1.448
18.000	0.600	0.500	0.280	0.250	0.562	0.486	33.861	-3.998	0.639	-1.613
19.000	0.800	0.500	0.281	0.250	0.556	0.624	45.938	-6.183	1.132	-1.786
20.000	1.000	0.500	0.281	0.250	0.555	0.759	58.459	-8.527	1.612	-1.965
21.000	0.400	0.700	0.249	0.250	1.000	0.320	22.051	-2.246	0.046	-1.325
22.000	0.600	0.700	0.253	0.250	0.826	0.452	33.539	-4.140	0.515	-1.389
23.000	0.800	0.700	0.254	0.250	0.795	0.579	45.439	-6.317	0.966	-1.497
24.000	1.000	0.700	0.255	0.250	0.780	0.702	57.775	-8.808	1.402	-1.610
PREFILTER TIME CONSTANT= 0.100										
25.000	0.400	0.300	0.324	0.250	0.360	0.335	12.372	-2.309	0.126	-1.733
26.000	0.600	0.300	0.326	0.250	0.354	0.463	18.765	-3.953	0.584	-2.001
27.000	0.800	0.300	0.323	0.250	0.364	0.584	25.587	-5.885	1.017	-2.266
28.000	1.000	0.300	0.322	0.250	0.370	0.704	32.490	-8.081	1.446	-2.539
29.000	1.500	0.300	0.316	0.250	0.389	0.983	51.374	-14.257	2.450	-3.207
30.000	2.000	0.300	0.309	0.250	0.417	1.245	72.348	-21.261	3.396	-3.848
31.000	0.400	0.500	0.275	0.250	0.590	0.297	12.202	-1.938	-0.019	-1.442
32.000	0.600	0.500	0.278	0.250	0.569	0.412	18.576	-3.434	0.389	-1.598
33.000	0.800	0.500	0.279	0.250	0.566	0.519	25.191	-5.138	0.770	-1.759
34.000	1.000	0.500	0.279	0.250	0.567	0.621	32.084	-6.973	1.134	-1.921
35.000	1.500	0.500	0.277	0.250	0.577	0.860	50.562	-12.108	1.988	-2.322
36.000	2.000	0.500	0.275	0.250	0.593	1.082	70.995	-17.825	2.785	-2.708
37.000	0.400	0.700	0.249	0.250	1.000	0.270	12.106	-1.849	-0.117	-1.322
38.000	0.600	0.700	0.252	0.250	0.835	0.373	18.394	-3.227	0.244	-1.380
39.000	0.800	0.700	0.254	0.250	0.804	0.468	24.919	-4.779	0.582	-1.479
40.000	1.000	0.700	0.254	0.250	0.790	0.558	31.838	-6.412	0.902	-1.581
41.000	1.500	0.700	0.255	0.250	0.779	0.768	49.768	-10.900	1.648	-1.835
42.000	2.000	0.700	0.255	0.250	0.780	0.963	69.680	-15.805	2.344	-2.081
PREFILTER TIME CONSTANT= 0.250										
43.000	0.400	0.300	0.313	0.250	0.402	0.259	5.327	-1.858	-0.131	-1.659
44.000	0.600	0.300	0.311	0.250	0.411	0.342	7.987	-3.047	0.161	-1.853
45.000	0.800	0.300	0.305	0.250	0.436	0.418	10.771	-4.314	0.430	-2.032
46.000	1.000	0.300	0.300	0.250	0.454	0.491	13.857	-5.642	0.692	-2.204
47.000	1.500	0.300	0.290	0.250	0.504	0.652	21.772	-8.933	1.268	-2.586
48.000	2.000	0.300	0.280	0.250	0.560	0.797	30.688	-12.567	1.787	-2.913
49.000	0.400	0.500	0.269	0.250	0.632	0.218	5.211	-1.426	-0.280	-1.398
50.000	0.600	0.500	0.270	0.250	0.627	0.292	7.901	-2.353	-0.028	-1.506
51.000	0.800	0.500	0.268	0.250	0.638	0.356	10.692	-3.294	0.199	-1.607
52.000	1.000	0.500	0.267	0.250	0.654	0.415	13.607	-4.290	0.410	-1.700
53.000	1.500	0.500	0.262	0.250	0.699	0.548	21.431	-6.723	0.884	-1.909
54.000	2.000	0.500	0.257	0.250	0.749	0.667	30.110	-9.373	1.306	-2.086
55.000	0.400	0.700	0.247	0.250	1.000	0.191	5.168	-1.178	-0.380	-1.316
56.000	0.600	0.700	0.249	0.250	1.000	0.254	7.821	-1.928	-0.164	-1.326
57.000	0.800	0.700	0.250	0.250	1.000	0.311	10.578	-2.690	0.029	-1.381
58.000	1.000	0.700	0.250	0.250	1.000	0.361	13.438	-3.483	0.208	-1.435
59.000	1.500	0.700	0.249	0.250	1.000	0.474	21.090	-5.549	0.610	-1.555
60.000	2.000	0.700	0.249	0.250	1.000	0.574	29.549	-7.794	0.964	-1.656

R82-1732-128(4/9)(T)

TABLE D-2. - CONTINUED.

- X_{CG}: FS 558.2
- S_e = 70 FT^2

RUN	CAP	ZETA	NZMAX	NZSS	ZETAC	CAPC	CANDT1	CANDT2	CNMX1	CNMX2
PREFILTER TIME CONSTANT=										
0.000										
1.000	0.400	0.300	0.337	0.250	0.318	0.400	92.077	-3.252	-3.588	-6.771
2.000	0.600	0.300	0.348	0.250	0.286	0.629	143.851	-5.350	-2.865	-7.077
3.000	0.800	0.300	0.343	0.250	0.299	0.851	195.631	-7.497	-2.188	-7.340
4.000	1.000	0.300	0.340	0.250	0.311	1.079	249.433	-11.217	-1.495	-7.609
5.000	0.400	0.500	0.298	0.250	0.463	0.409	93.361	-2.829	-3.537	-6.309
6.000	0.600	0.500	0.294	0.250	0.482	0.622	142.654	-4.686	-2.884	-6.433
7.000	0.800	0.500	0.292	0.250	0.494	0.843	193.785	-6.879	-2.212	-6.576
8.000	1.000	0.500	0.290	0.250	0.503	1.070	247.099	-13.014	-1.523	-6.730
9.000	0.400	0.700	0.270	0.250	0.627	0.406	92.800	-2.741	-3.546	-6.157
10.000	0.600	0.700	0.266	0.250	0.660	0.618	141.554	-5.544	-2.897	-6.114
11.000	0.800	0.700	0.264	0.250	0.677	0.836	192.088	-9.873	-2.233	-6.141
12.000	1.000	0.700	0.263	0.250	0.688	1.059	238.784	-15.265	-1.554	-6.224
PREFILTER TIME CONSTANT=										
0.050										
13.000	0.400	0.300	0.352	0.250	0.275	0.369	20.283	-3.382	-3.652	-6.817
14.000	0.600	0.300	0.347	0.250	0.289	0.537	30.987	-5.223	-3.129	-7.068
15.000	0.800	0.300	0.342	0.250	0.302	0.697	42.047	-7.410	-2.633	-7.323
16.000	1.000	0.300	0.338	0.250	0.315	0.853	53.517	-9.852	-2.152	-7.584
17.000	0.400	0.500	0.298	0.250	0.464	0.340	20.156	-2.834	-3.738	-6.307
18.000	0.600	0.500	0.294	0.250	0.484	0.491	30.719	-4.567	-3.270	-6.428
19.000	0.800	0.500	0.291	0.250	0.496	0.636	41.647	-6.597	-2.821	-6.568
20.000	1.000	0.500	0.289	0.250	0.507	0.776	52.963	-8.911	-2.388	-6.716
21.000	0.400	0.700	0.270	0.250	0.627	0.319	20.029	-2.633	-3.804	-6.154
22.000	0.600	0.700	0.266	0.250	0.661	0.457	30.477	-4.480	-3.375	-6.111
23.000	0.800	0.700	0.264	0.250	0.678	0.589	41.263	-6.526	-2.965	-6.138
24.000	1.000	0.700	0.263	0.250	0.690	0.717	52.414	-8.820	-2.571	-6.219
PREFILTER TIME CONSTANT=										
0.100										
25.000	0.400	0.300	0.350	0.250	0.280	0.333	11.099	-3.297	-3.775	-6.802
26.000	0.600	0.300	0.345	0.250	0.296	0.471	16.982	-5.110	-3.341	-7.037
27.000	0.800	0.300	0.339	0.250	0.312	0.599	23.041	-7.150	-2.943	-7.271
28.000	1.000	0.300	0.334	0.250	0.327	0.722	29.333	-9.316	-2.564	-7.507
29.000	1.500	0.300	0.325	0.250	0.358	1.013	46.228	-15.349	-1.661	-8.105
30.000	2.000	0.300	0.317	0.250	0.388	1.285	64.775	-22.027	-0.828	-8.680
31.000	0.400	0.500	0.298	0.250	0.467	0.297	11.037	-2.687	-3.880	-6.300
32.000	0.600	0.500	0.293	0.250	0.489	0.416	16.825	-4.292	-3.505	-6.413
33.000	0.800	0.500	0.290	0.250	0.504	0.528	22.818	-6.011	-3.157	-6.540
34.000	1.000	0.500	0.288	0.250	0.516	0.634	29.031	-7.785	-2.827	-6.674
35.000	1.500	0.500	0.283	0.250	0.542	0.882	45.594	-12.804	-2.061	-7.015
36.000	2.000	0.500	0.279	0.250	0.565	1.113	63.751	-17.945	-1.355	-7.352
37.000	0.400	0.700	0.270	0.250	0.628	0.270	10.965	-2.392	-3.959	-6.150
38.000	0.600	0.700	0.265	0.250	0.663	0.376	16.692	-3.818	-3.626	-6.109
39.000	0.800	0.700	0.263	0.250	0.682	0.475	22.608	-5.297	-3.318	-6.127
40.000	1.000	0.700	0.262	0.250	0.695	0.569	28.727	-6.856	-3.028	-6.198
41.000	1.500	0.700	0.260	0.250	0.717	0.787	45.177	-11.069	-2.356	-6.397
42.000	2.000	0.700	0.258	0.250	0.734	0.987	62.754	-15.568	-1.741	-6.601
PREFILTER TIME CONSTANT=										
0.250										
43.000	0.400	0.300	0.340	0.250	0.310	0.260	4.788	-2.841	-4.030	-6.702
44.000	0.600	0.300	0.330	0.250	0.341	0.350	7.237	-4.164	-3.743	-6.853
45.000	0.800	0.300	0.321	0.250	0.372	0.429	9.757	-5.358	-3.492	-6.991
46.000	1.000	0.300	0.313	0.250	0.400	0.503	12.413	-6.638	-3.260	-7.121
47.000	1.500	0.300	0.299	0.250	0.461	0.671	19.592	-9.958	-2.729	-7.425
48.000	2.000	0.300	0.287	0.250	0.519	0.821	27.413	-13.443	-2.264	-7.685
49.000	0.400	0.500	0.292	0.250	0.492	0.221	4.748	-2.244	-4.134	-6.248
50.000	0.600	0.500	0.285	0.250	0.529	0.295	7.171	-3.222	-3.897	-6.311
51.000	0.800	0.500	0.280	0.250	0.558	0.362	9.661	-4.133	-3.686	-6.377
52.000	1.000	0.500	0.276	0.250	0.584	0.424	12.369	-5.082	-3.492	-6.441
53.000	1.500	0.500	0.268	0.250	0.642	0.561	19.317	-7.515	-3.059	-6.589
54.000	2.000	0.500	0.262	0.250	0.695	0.684	27.036	-9.969	-2.677	-6.716
55.000	0.400	0.700	0.268	0.250	0.642	0.193	4.712	-1.849	-4.211	-6.141
56.000	0.600	0.700	0.263	0.250	0.683	0.257	7.112	-2.639	-4.008	-6.100
57.000	0.800	0.700	0.260	0.250	0.713	0.314	9.573	-3.392	-3.827	-6.077
58.000	1.000	0.700	0.258	0.250	0.737	0.367	12.165	-4.155	-3.662	-6.077
59.000	1.500	0.700	0.255	0.250	0.787	0.484	19.056	-5.988	-3.295	-6.148
60.000	2.000	0.700	0.252	0.250	0.829	0.587	26.613	-7.877	-2.973	-6.211

R82-1732-128(5/9)(T)

TABLE D-2. - CONTINUED.

- X_{CG}: FS 676.2
- S_e = 70 FT^2

RUN	CAP	ZETA	NZMAX	NZSS	ZETAC	CAPC	CAMDIL	CAMDIP	CNMX1	CNMX2
PREFILTER TIME CONSTANT= 0.000										
1.000	0.400	0.300	0.353	0.250	0.272	0.409	87.317	-4.491	-6.893	-11.363
2.000	0.600	0.300	0.344	0.250	0.296	0.616	131.559	-6.381	-6.342	-11.604
3.000	0.800	0.300	0.342	0.250	0.304	0.855	178.254	-8.583	-5.723	-11.851
4.000	1.000	0.300	0.339	0.250	0.312	1.060	227.280	-11.037	-5.088	-12.104
5.000	0.400	0.500	0.295	0.250	0.479	0.404	85.887	-3.629	-6.952	-10.653
6.000	0.600	0.500	0.292	0.250	0.495	0.613	130.586	-5.458	-6.348	-10.766
7.000	0.800	0.500	0.290	0.250	0.504	0.829	177.101	-7.479	-5.738	-10.892
8.000	1.000	0.500	0.289	0.250	0.510	1.052	225.375	-10.501	-5.110	-11.028
9.000	0.400	0.700	0.267	0.250	0.650	0.402	85.622	-3.201	-6.928	-10.394
10.000	0.600	0.700	0.263	0.250	0.683	0.609	129.851	-5.162	-6.353	-10.332
11.000	0.800	0.700	0.262	0.250	0.697	0.823	175.808	-8.590	-5.752	-10.346
12.000	1.000	0.700	0.261	0.250	0.706	1.043	223.487	-13.340	-5.133	-10.409
PREFILTER TIME CONSTANT= 0.050										
13.000	0.400	0.300	0.348	0.250	0.285	0.365	18.622	-4.408	-7.060	-11.360
14.000	0.600	0.300	0.344	0.250	0.298	0.529	28.357	-6.382	-6.591	-11.591
15.000	0.800	0.300	0.341	0.250	0.307	0.689	38.439	-8.654	-6.132	-11.832
16.000	1.000	0.300	0.338	0.250	0.316	0.846	48.719	-11.092	-5.686	-12.076
17.000	0.400	0.500	0.295	0.250	0.480	0.338	18.542	-3.643	-7.124	-10.650
18.000	0.600	0.500	0.291	0.250	0.497	0.487	28.170	-5.337	-6.703	-10.760
19.000	0.800	0.500	0.290	0.250	0.506	0.630	38.134	-7.274	-6.292	-10.883
20.000	1.000	0.500	0.288	0.250	0.513	0.770	48.430	-9.464	-5.892	-11.014
21.000	0.400	0.700	0.267	0.250	0.650	0.318	18.463	-3.172	-7.171	-10.390
22.000	0.600	0.700	0.263	0.250	0.684	0.454	27.989	-4.975	-6.790	-10.329
23.000	0.800	0.700	0.262	0.250	0.699	0.585	37.837	-6.963	-6.416	-10.343
24.000	1.000	0.700	0.261	0.250	0.707	0.713	47.999	-9.025	-6.052	-10.404
PREFILTER TIME CONSTANT= 0.100										
25.000	0.400	0.300	0.347	0.250	0.290	0.330	10.212	-4.299	-7.187	-11.340
26.000	0.600	0.300	0.341	0.250	0.305	0.466	15.537	-6.242	-6.798	-11.554
27.000	0.800	0.300	0.338	0.250	0.317	0.595	21.066	-8.298	-6.428	-11.773
28.000	1.000	0.300	0.334	0.250	0.328	0.718	26.795	-10.450	-6.075	-11.992
29.000	1.500	0.300	0.326	0.250	0.355	1.009	42.048	-16.041	-5.242	-12.535
30.000	2.000	0.300	0.318	0.250	0.382	1.281	58.690	-22.200	-4.468	-13.059
31.000	0.400	0.500	0.294	0.250	0.483	0.295	10.175	-3.485	-7.264	-10.640
32.000	0.600	0.500	0.290	0.250	0.502	0.414	15.439	-5.142	-6.929	-10.742
33.000	0.800	0.500	0.288	0.250	0.514	0.526	20.898	-6.857	-6.609	-10.853
34.000	1.000	0.500	0.286	0.250	0.523	0.632	26.549	-8.646	-6.304	-10.970
35.000	1.500	0.500	0.283	0.250	0.544	0.880	41.552	-13.476	-5.591	-11.268
36.000	2.000	0.500	0.279	0.250	0.564	1.111	57.898	-18.412	-4.933	-11.564
37.000	0.400	0.700	0.267	0.250	0.651	0.270	10.145	-3.013	-7.321	-10.386
38.000	0.600	0.700	0.263	0.250	0.687	0.375	15.346	-4.432	-7.028	-10.326
39.000	0.800	0.700	0.261	0.250	0.705	0.474	20.738	-5.884	-6.747	-10.333
40.000	1.000	0.700	0.260	0.250	0.715	0.568	26.314	-7.426	-6.478	-10.386
41.000	1.500	0.700	0.259	0.250	0.729	0.786	41.072	-11.479	-5.852	-10.541
42.000	2.000	0.700	0.258	0.250	0.742	0.987	57.101	-15.733	-5.277	-10.709
PREFILTER TIME CONSTANT= 0.250										
43.000	0.400	0.300	0.336	0.250	0.320	0.258	4.379	-3.782	-7.438	-11.205
44.000	0.600	0.300	0.327	0.250	0.350	0.348	6.633	-5.210	-7.183	-11.328
45.000	0.800	0.300	0.320	0.250	0.375	0.429	8.924	-6.563	-6.947	-11.445
46.000	1.000	0.300	0.314	0.250	0.399	0.504	11.352	-7.860	-6.729	-11.555
47.000	1.500	0.300	0.300	0.250	0.454	0.673	17.821	-11.022	-6.234	-11.800
48.000	2.000	0.300	0.289	0.250	0.507	0.823	24.883	-14.276	-5.796	-12.011
49.000	0.400	0.500	0.289	0.250	0.509	0.220	4.345	-3.000	-7.512	-10.571
50.000	0.600	0.500	0.283	0.250	0.542	0.295	6.577	-4.078	-7.302	-10.619
51.000	0.800	0.500	0.279	0.250	0.567	0.362	8.865	-5.131	-7.107	-10.668
52.000	1.000	0.500	0.275	0.250	0.590	0.424	11.248	-6.127	-6.926	-10.716
53.000	1.500	0.500	0.268	0.250	0.641	0.564	17.604	-8.418	-6.519	-10.822
54.000	2.000	0.500	0.263	0.250	0.689	0.687	24.544	-10.779	-6.159	-10.912
55.000	0.400	0.700	0.265	0.250	0.668	0.193	4.340	-2.487	-7.565	-10.373
56.000	0.600	0.700	0.261	0.250	0.709	0.257	6.517	-3.318	-7.390	-10.318
57.000	0.800	0.700	0.258	0.250	0.738	0.315	8.791	-4.154	-7.225	-10.284
58.000	1.000	0.700	0.256	0.250	0.759	0.368	11.147	-4.953	-7.071	-10.271
59.000	1.500	0.700	0.254	0.250	0.804	0.486	17.402	-6.928	-6.726	-10.310
60.000	2.000	0.700	0.252	0.250	0.845	0.591	24.206	-8.851	-6.421	-10.346

R82-1732-128(6/9)(T)

TABLE D-2. - CONTINUED.

- X_{CG}: FS 528.2
- S_c = 120 FT^2

RUN	CAP	ZETA	NZMAX	NZSS	ZETAC	CAPC	CANDT1	CANDT2	CNMX1	CNMX2
PREFILTER TIME CONSTANT=										
0.000										
1.000	0.400	0.300	0.386	0.250	0.191	0.441	65.276	-1.716	-0.935	-2.578
2.000	0.600	0.300	0.362	0.250	0.247	0.629	100.715	-2.824	-0.523	-2.717
3.000	0.800	0.300	0.356	0.250	0.263	0.854	137.492	-4.683	-0.038	-2.902
4.000	1.000	0.300	0.348	0.250	0.286	1.070	175.120	-9.417	0.440	-3.085
5.000	0.400	0.500	0.322	0.250	0.368	0.407	65.113	-1.399	-0.998	-2.314
6.000	0.600	0.500	0.309	0.250	0.419	0.622	99.730	-2.613	-0.537	-2.400
7.000	0.800	0.500	0.303	0.250	0.445	0.842	135.750	-5.462	-0.064	-2.502
8.000	1.000	0.500	0.298	0.250	0.464	1.060	173.227	-10.511	0.417	-2.611
9.000	0.400	0.700	0.295	0.250	0.481	0.407	64.862	-1.699	-0.999	-2.285
10.000	0.600	0.700	0.280	0.250	0.557	0.617	96.565	-3.973	-0.546	-2.265
11.000	0.800	0.700	0.274	0.250	0.596	0.834	134.348	-7.133	-0.082	-2.285
12.000	1.000	0.700	0.271	0.250	0.621	1.049	171.161	-11.549	0.393	-2.349
PREFILTER TIME CONSTANT=										
0.050										
13.000	0.400	0.300	0.364	0.250	0.243	0.352	13.934	-1.532	-1.093	-2.523
14.000	0.600	0.300	0.361	0.250	0.249	0.535	21.666	-2.859	-0.683	-2.712
15.000	0.800	0.300	0.355	0.250	0.266	0.694	29.429	-4.259	-0.334	-2.893
16.000	1.000	0.300	0.347	0.250	0.290	0.843	37.448	-5.881	-0.008	-3.070
17.000	0.400	0.500	0.322	0.250	0.369	0.337	14.015	-1.389	-1.126	-2.313
18.000	0.600	0.500	0.308	0.250	0.421	0.487	21.435	-2.556	-0.796	-2.398
19.000	0.800	0.500	0.302	0.250	0.447	0.629	29.089	-3.946	-0.484	-2.497
20.000	1.000	0.500	0.298	0.250	0.467	0.766	37.009	-5.573	-0.187	-2.602
21.000	0.400	0.700	0.295	0.250	0.481	0.317	13.962	-1.416	-1.174	-2.283
22.000	0.600	0.700	0.280	0.250	0.557	0.452	21.248	-2.616	-0.876	-2.263
23.000	0.800	0.700	0.274	0.250	0.596	0.582	28.777	-4.008	-0.594	-2.283
24.000	1.000	0.700	0.271	0.250	0.622	0.706	36.567	-5.550	-0.323	-2.345
PREFILTER TIME CONSTANT=										
0.100										
25.000	0.400	0.300	0.362	0.250	0.247	0.317	7.582	-1.528	-1.163	-2.516
26.000	0.600	0.300	0.359	0.250	0.256	0.470	11.876	-2.725	-0.817	-2.696
27.000	0.800	0.300	0.352	0.250	0.275	0.596	16.137	-4.083	-0.537	-2.863
28.000	1.000	0.300	0.342	0.250	0.302	0.712	20.526	-5.506	-0.283	-3.023
29.000	1.500	0.300	0.329	0.250	0.346	0.988	32.285	-9.458	0.334	-3.433
30.000	2.000	0.300	0.317	0.250	0.385	1.239	45.458	-13.838	0.904	-3.822
31.000	0.400	0.500	0.321	0.250	0.371	0.293	7.664	-1.317	-1.216	-2.310
32.000	0.600	0.500	0.307	0.250	0.425	0.412	11.733	-2.314	-0.952	-2.389
33.000	0.800	0.500	0.300	0.250	0.454	0.521	15.937	-3.422	-0.710	-2.481
34.000	1.000	0.500	0.296	0.250	0.476	0.624	20.285	-4.627	-0.485	-2.575
35.000	1.500	0.500	0.287	0.250	0.517	0.862	31.898	-7.865	0.037	-2.815
36.000	2.000	0.500	0.282	0.250	0.548	1.075	44.639	-11.576	0.517	-3.048
37.000	0.400	0.700	0.295	0.250	0.481	0.268	7.641	-1.233	-1.276	-2.282
38.000	0.600	0.700	0.280	0.250	0.559	0.371	11.629	-2.115	-1.045	-2.261
39.000	0.800	0.700	0.274	0.250	0.599	0.468	15.761	-3.122	-0.833	-2.275
40.000	1.000	0.700	0.270	0.250	0.626	0.558	20.038	-4.205	-0.635	-2.330
41.000	1.500	0.700	0.265	0.250	0.669	0.767	31.416	-7.065	-0.180	-2.476
42.000	2.000	0.700	0.262	0.250	0.696	0.955	43.852	-9.883	0.235	-2.621
PREFILTER TIME CONSTANT=										
0.250										
43.000	0.400	0.300	0.352	0.250	0.275	0.248	3.320	-1.282	-1.317	-2.472
44.000	0.600	0.300	0.343	0.250	0.299	0.349	5.075	-2.144	-1.080	-2.601
45.000	0.800	0.300	0.332	0.250	0.334	0.425	6.846	-2.935	-0.910	-2.705
46.000	1.000	0.300	0.320	0.250	0.375	0.493	8.684	-3.755	-0.758	-2.799
47.000	1.500	0.300	0.301	0.250	0.451	0.653	13.726	-6.085	-0.404	-3.019
48.000	2.000	0.300	0.287	0.250	0.520	0.794	19.301	-8.451	-0.096	-3.206
49.000	0.400	0.500	0.316	0.250	0.390	0.218	3.304	-1.029	-1.380	-2.287
50.000	0.600	0.500	0.299	0.250	0.460	0.291	5.002	-1.604	-1.213	-2.336
51.000	0.800	0.500	0.290	0.250	0.503	0.356	6.744	-2.209	-1.068	-2.388
52.000	1.000	0.500	0.283	0.250	0.540	0.415	8.587	-2.816	-0.938	-2.437
53.000	1.500	0.500	0.272	0.250	0.614	0.546	13.520	-4.385	-0.650	-2.551
54.000	2.000	0.500	0.264	0.250	0.676	0.661	18.937	-6.002	-0.397	-2.649
55.000	0.400	0.700	0.292	0.250	0.492	0.191	3.281	-0.839	-1.442	-2.276
56.000	0.600	0.700	0.278	0.250	0.571	0.253	4.951	-1.320	-1.302	-2.256
57.000	0.800	0.700	0.271	0.250	0.621	0.308	6.668	-1.800	-1.179	-2.246
58.000	1.000	0.700	0.266	0.250	0.658	0.358	8.481	-2.290	-1.068	-2.250
59.000	1.500	0.700	0.259	0.250	0.724	0.469	13.310	-3.465	-0.823	-2.310
60.000	2.000	0.700	0.256	0.250	0.766	0.567	18.601	-4.686	-0.610	-2.363

R82-1732-128(7/9)(T)

TABLE D-2. - CONTINUED.

- X_{CG}: FS 540.2
- S_c = 120 FT^2

RUN	CAP	ZETA	NZMAX	NZSS	ZETAC	CAPC	CANDT1	CANDT2	CNMX1	CNMX2
PREFILTER TIME CONSTANT=										
0.000										
1.000	0.400	0.300	0.256	0.250	0.762	0.265	49.730	-1.477	-3.193	-4.627
2.000	0.600	0.300	0.361	0.250	0.251	0.628	93.042	-3.483	-2.345	-5.104
3.000	0.800	0.300	0.352	0.250	0.274	0.845	126.592	-5.009	-1.913	-5.258
4.000	1.000	0.300	0.346	0.250	0.292	1.070	161.398	-8.031	-1.467	-5.422
5.000	0.400	0.500	0.314	0.250	0.397	0.406	60.250	-1.853	-2.791	-4.616
6.000	0.600	0.500	0.305	0.250	0.436	0.619	92.192	-2.966	-2.365	-4.676
7.000	0.800	0.500	0.299	0.250	0.459	0.837	125.325	-4.619	-1.930	-4.756
8.000	1.000	0.500	0.296	0.250	0.476	1.061	159.783	-9.160	-1.484	-4.846
9.000	0.400	0.700	0.285	0.250	0.532	0.403	59.824	-1.728	-2.799	-4.541
10.000	0.600	0.700	0.275	0.250	0.589	0.614	91.419	-3.463	-2.375	-4.491
11.000	0.800	0.700	0.271	0.250	0.621	0.829	124.085	-6.380	-1.945	-4.476
12.000	1.000	0.700	0.268	0.250	0.642	1.050	158.095	-10.194	-1.505	-4.520
PREFILTER TIME CONSTANT=										
0.050										
13.000	0.400	0.300	0.369	0.250	0.230	0.366	13.166	-2.192	-2.855	-4.951
14.000	0.600	0.300	0.360	0.250	0.253	0.534	20.064	-3.530	-2.506	-5.097
15.000	0.800	0.300	0.351	0.250	0.277	0.690	27.206	-4.910	-2.190	-5.247
16.000	1.000	0.300	0.344	0.250	0.296	0.842	34.638	-6.464	-1.881	-5.405
17.000	0.400	0.500	0.314	0.250	0.398	0.338	13.086	-1.819	-2.913	-4.614
18.000	0.600	0.500	0.304	0.250	0.437	0.486	19.867	-2.988	-2.607	-4.673
19.000	0.800	0.500	0.299	0.250	0.462	0.628	26.939	-4.350	-2.318	-4.751
20.000	1.000	0.500	0.295	0.250	0.479	0.765	34.262	-5.857	-2.040	-4.838
21.000	0.400	0.700	0.285	0.250	0.532	0.315	12.992	-1.678	-2.961	-4.539
22.000	0.600	0.700	0.275	0.250	0.589	0.452	19.697	-2.831	-2.680	-4.490
23.000	0.800	0.700	0.271	0.250	0.622	0.581	26.678	-4.172	-2.416	-4.474
24.000	1.000	0.700	0.268	0.250	0.643	0.706	33.889	-5.648	-2.163	-4.517
PREFILTER TIME CONSTANT=										
0.100										
25.000	0.400	0.300	0.368	0.250	0.233	0.331	7.168	-2.191	-2.931	-4.941
26.000	0.600	0.300	0.357	0.250	0.259	0.470	11.004	-3.348	-2.641	-5.077
27.000	0.800	0.300	0.348	0.250	0.286	0.593	14.913	-4.608	-2.388	-5.213
28.000	1.000	0.300	0.340	0.250	0.308	0.713	18.992	-5.977	-2.143	-5.355
29.000	1.500	0.300	0.328	0.250	0.348	0.996	29.943	-9.788	-1.565	-5.722
30.000	2.000	0.300	0.318	0.250	0.384	1.258	41.964	-13.944	-1.035	-6.075
31.000	0.400	0.500	0.313	0.250	0.400	0.295	7.131	-1.786	-3.003	-4.610
32.000	0.600	0.500	0.303	0.250	0.442	0.412	10.883	-2.735	-2.758	-4.663
33.000	0.800	0.500	0.297	0.250	0.469	0.521	14.763	-3.812	-2.534	-4.733
34.000	1.000	0.500	0.293	0.250	0.489	0.625	18.786	-4.965	-2.322	-4.811
35.000	1.500	0.500	0.286	0.250	0.525	0.866	29.517	-8.083	-1.832	-5.015
36.000	2.000	0.500	0.281	0.250	0.554	1.088	41.265	-11.436	-1.383	-5.219
37.000	0.400	0.700	0.285	0.250	0.533	0.267	7.073	-1.545	-3.060	-4.537
38.000	0.600	0.700	0.275	0.250	0.591	0.372	10.786	-2.426	-2.842	-4.488
39.000	0.800	0.700	0.270	0.250	0.625	0.468	14.618	-3.386	-2.643	-4.467
40.000	1.000	0.700	0.267	0.250	0.647	0.559	18.549	-4.399	-2.456	-4.505
41.000	1.500	0.700	0.263	0.250	0.685	0.770	29.098	-7.090	-2.028	-4.618
42.000	2.000	0.700	0.261	0.250	0.710	0.965	40.587	-9.958	-1.635	-4.738
PREFILTER TIME CONSTANT=										
0.250										
43.000	0.400	0.300	0.357	0.250	0.261	0.260	3.104	-1.904	-3.094	-4.878
44.000	0.600	0.300	0.342	0.250	0.303	0.349	4.676	-2.763	-2.902	-4.957
45.000	0.800	0.300	0.329	0.250	0.344	0.425	6.313	-3.598	-2.744	-5.029
46.000	1.000	0.300	0.319	0.250	0.381	0.496	8.036	-4.412	-2.595	-5.102
47.000	1.500	0.300	0.301	0.250	0.451	0.658	12.758	-6.498	-2.257	-5.279
48.000	2.000	0.300	0.288	0.250	0.516	0.802	17.803	-8.658	-1.963	-5.431
49.000	0.400	0.500	0.308	0.250	0.421	0.220	3.071	-1.459	-3.166	-4.579
50.000	0.600	0.500	0.295	0.250	0.478	0.293	4.633	-2.117	-3.011	-4.599
51.000	0.800	0.500	0.287	0.250	0.519	0.357	6.252	-2.746	-2.875	-4.629
52.000	1.000	0.500	0.281	0.250	0.552	0.417	7.954	-3.387	-2.751	-4.662
53.000	1.500	0.500	0.271	0.250	0.621	0.550	12.510	-4.875	-2.476	-4.741
54.000	2.000	0.500	0.264	0.250	0.680	0.667	17.506	-6.410	-2.235	-4.812
55.000	0.400	0.700	0.283	0.250	0.544	0.191	3.048	-1.189	-3.221	-4.530
56.000	0.600	0.700	0.273	0.250	0.605	0.254	4.593	-1.701	-3.088	-4.483
57.000	0.800	0.700	0.267	0.250	0.648	0.309	6.189	-2.212	-2.971	-4.458
58.000	1.000	0.700	0.263	0.250	0.681	0.360	7.867	-2.713	-2.866	-4.443
59.000	1.500	0.700	0.258	0.250	0.742	0.473	12.329	-3.942	-2.633	-4.463
60.000	2.000	0.700	0.255	0.250	0.783	0.572	17.214	-5.144	-2.429	-4.495

TABLE D-2. - CONCLUDED.

- X_{CG}: FS 558.2
- S_c = 120 FT^2

RUN	CAP	ZETA	NZMAX	NZSS	ZETAC	CAPC	CANDT1	CANDT2	CNMX1	CNMX2
PREFILTER TIME CONSTANT=										
0.000										
1.000	0.400	0.300	0.571	0.250	-0.079	0.647	50.880	-4.826	-4.601	-9.340
2.000	0.600	0.300	0.355	0.250	0.265	0.619	84.065	-4.405	-4.783	-8.291
3.000	0.800	0.300	0.349	0.250	0.282	0.834	113.881	-5.883	-4.393	-8.427
4.000	1.000	0.300	0.345	0.250	0.296	1.055	144.658	-7.466	-3.994	-8.572
5.000	0.400	0.500	0.306	0.250	0.428	0.406	54.849	-2.482	-5.172	-7.680
6.000	0.600	0.500	0.300	0.250	0.457	0.615	83.602	-3.570	-4.790	-7.723
7.000	0.800	0.500	0.296	0.250	0.474	0.829	113.149	-4.920	-4.401	-7.787
8.000	1.000	0.500	0.293	0.250	0.487	1.048	143.608	-7.173	-4.006	-7.861
9.000	0.400	0.700	0.276	0.250	0.584	0.404	54.631	-2.140	-5.177	-7.521
10.000	0.600	0.700	0.270	0.250	0.627	0.612	83.099	-3.301	-4.796	-7.450
11.000	0.800	0.700	0.267	0.250	0.650	0.824	112.398	-5.432	-4.410	-7.428
12.000	1.000	0.700	0.265	0.250	0.666	1.041	142.424	-8.433	-4.019	-7.457
PREFILTER TIME CONSTANT=										
0.050										
13.000	0.400	0.300	0.365	0.250	0.241	0.369	11.930	-3.028	-5.236	-8.173
14.000	0.600	0.300	0.355	0.250	0.267	0.532	18.207	-4.363	-4.932	-8.283
15.000	0.800	0.300	0.348	0.250	0.285	0.688	24.511	-5.688	-4.643	-8.414
16.000	1.000	0.300	0.343	0.250	0.299	0.840	31.065	-7.204	-4.362	-8.554
17.000	0.400	0.500	0.306	0.250	0.429	0.339	11.867	-2.444	-5.287	-7.678
18.000	0.600	0.500	0.299	0.250	0.458	0.487	18.098	-3.601	-5.011	-7.719
19.000	0.800	0.500	0.296	0.250	0.477	0.629	24.340	-4.904	-4.749	-7.781
20.000	1.000	0.500	0.293	0.250	0.490	0.765	30.823	-6.320	-4.496	-7.852
21.000	0.400	0.700	0.276	0.250	0.584	0.318	11.807	-2.131	-5.327	-7.519
22.000	0.600	0.700	0.270	0.250	0.628	0.454	17.990	-3.192	-5.072	-7.448
23.000	0.800	0.700	0.267	0.250	0.651	0.583	24.168	-4.450	-4.832	-7.426
24.000	1.000	0.700	0.265	0.250	0.667	0.707	30.581	-5.816	-4.602	-7.454
PREFILTER TIME CONSTANT=										
0.100										
25.000	0.400	0.300	0.363	0.250	0.245	0.334	6.534	-3.000	-5.316	-8.159
26.000	0.600	0.300	0.352	0.250	0.274	0.469	9.936	-4.158	-5.064	-8.258
27.000	0.800	0.300	0.345	0.250	0.294	0.594	13.434	-5.444	-4.831	-8.375
28.000	1.000	0.300	0.339	0.250	0.311	0.714	17.033	-6.784	-4.608	-8.498
29.000	1.500	0.300	0.329	0.250	0.345	0.992	26.502	-10.484	-4.092	-8.811
30.000	2.000	0.300	0.320	0.250	0.376	1.246	36.647	-14.211	-3.622	-9.111
31.000	0.400	0.500	0.306	0.250	0.432	0.297	6.496	-2.411	-5.376	-7.672
32.000	0.600	0.500	0.298	0.250	0.463	0.415	9.879	-3.378	-5.155	-7.707
33.000	0.800	0.500	0.294	0.250	0.484	0.524	13.338	-4.448	-4.950	-7.761
34.000	1.000	0.500	0.291	0.250	0.499	0.627	16.898	-5.559	-4.759	-7.823
35.000	1.500	0.500	0.285	0.250	0.529	0.865	26.237	-8.477	-4.317	-7.989
36.000	2.000	0.500	0.281	0.250	0.552	1.082	36.305	-11.525	-3.916	-8.158
37.000	0.400	0.700	0.276	0.250	0.585	0.269	6.462	-2.041	-5.422	-7.516
38.000	0.600	0.700	0.270	0.250	0.630	0.375	9.815	-2.911	-5.224	-7.446
39.000	0.800	0.700	0.266	0.250	0.655	0.472	13.242	-3.859	-5.042	-7.420
40.000	1.000	0.700	0.264	0.250	0.672	0.563	16.762	-4.830	-4.873	-7.443
41.000	1.500	0.700	0.262	0.250	0.699	0.772	25.974	-7.353	-4.485	-7.522
42.000	2.000	0.700	0.260	0.250	0.718	0.962	35.799	-9.952	-4.134	-7.614
PREFILTER TIME CONSTANT=										
0.250										
43.000	0.400	0.300	0.352	0.250	0.274	0.262	2.811	-2.639	-5.478	-8.068
44.000	0.600	0.300	0.337	0.250	0.317	0.350	4.236	-3.535	-5.312	-8.105
45.000	0.800	0.300	0.327	0.250	0.352	0.428	5.689	-4.425	-5.164	-8.155
46.000	1.000	0.300	0.318	0.250	0.381	0.500	7.213	-5.275	-5.027	-8.208
47.000	1.500	0.300	0.303	0.250	0.444	0.661	11.216	-7.218	-4.721	-8.334
48.000	2.000	0.300	0.291	0.250	0.501	0.802	15.545	-9.215	-4.455	-8.444
49.000	0.400	0.500	0.300	0.250	0.454	0.222	2.798	-2.061	-5.535	-7.627
50.000	0.600	0.500	0.291	0.250	0.501	0.295	4.209	-2.740	-5.394	-7.626
51.000	0.800	0.500	0.284	0.250	0.535	0.361	5.649	-3.375	-5.270	-7.639
52.000	1.000	0.500	0.279	0.250	0.563	0.421	7.158	-4.020	-5.156	-7.657
53.000	1.500	0.500	0.271	0.250	0.623	0.553	11.115	-5.625	-4.905	-7.703
54.000	2.000	0.500	0.264	0.250	0.674	0.670	15.363	-7.125	-4.685	-7.746
55.000	0.400	0.700	0.274	0.250	0.598	0.193	2.782	-1.693	-5.577	-7.508
56.000	0.600	0.700	0.267	0.250	0.647	0.257	4.180	-2.193	-5.455	-7.440
57.000	0.800	0.700	0.263	0.250	0.682	0.313	5.606	-2.696	-5.348	-7.403
58.000	1.000	0.700	0.261	0.250	0.709	0.364	7.099	-3.183	-5.251	-7.382
59.000	1.500	0.700	0.256	0.250	0.761	0.477	11.008	-4.463	-5.038	-7.380
60.000	2.000	0.700	0.254	0.250	0.802	0.576	15.178	-5.656	-4.851	-7.392

R82-1732-128(9/9)(T)

☆U.S. GOVERNMENT PRINTING OFFICE:1983 639 008/41 REGION NO. 4

1. Report No.	2. Government Accession No.	3. Recipient's Catalog No.
CR-3738		

4. Title and Subtitle	5. Report Date
CONTROL DEFINITION STUDY FOR ADVANCED VEHICLES	November 1983
	6. Performing Organization Code

7. Author(s)	8. Performing Organization Report No.
Maris Lapins, R. Paul Martorella, Robert W. Klein, Rudolph C. Meyer, and Michael J. Sturm	
	10. Work Unit No.

9. Performing Organization Name and Address	11. Contract or Grant No.
Grumman Aerospace Corporation Bethpage, New York 11714	NAS1-16636
	13. Type of Report and Period Covered
12. Sponsoring Agency Name and Address	Contractor Report
National Aeronautics and Space Administration Washington, DC 20546	14. Sponsoring Agency Code

15. Supplementary Notes

Langley Technical Monitor: Luat T. Nguyen

16. Abstract

A study was conducted to investigate the low-speed, high angle-of-attack flight mechanics of an advanced, canard-configured, supersonic tactical aircraft designed with moderate longitudinal Relaxed Static Stability (Static Margin, SM = 16%$\bar{c}_w$ at M = 0.4). Control laws were developed for the longitudinal axis ("G" or maneuver and angle-of-attack command systems) and for the lateral/directional axes. The performance of these control laws was examined in engineering simulation. A canard deflection/rate requirement study was performed as part of the "G" command law evaluation at low angles-of-attack. Simulated coupled maneuvers revealed the need for command limiters in all three aircraft axes to prevent departure from controlled flight. When modified with command/maneuver limiters, the control laws were shown to be adequate to prevent aircraft departure during aggressive Air Combat Maneuvering.

17. Key Words (Suggested by Author(s))	18. Distribution Statement
Relaxed static stability Canard configured fighter aircraft Control laws High angle of attack Departure prevention Command/maneuver limiters	Unclassified - Unlimited Subject Category 08

19. Security Classif. (of this report)	20. Security Classif. (of this page)	21. No. of Pages	22. Price
Unclassified	Unclassified	218	A10

N-305
R82-1732-130(T)

For sale by the National Technical Information Service, Springfield, Virginia 22161